Analysis of novel pathways in neurodegeneration using mouse and fly model organisms

Leigh Catherine Paton

St John's College

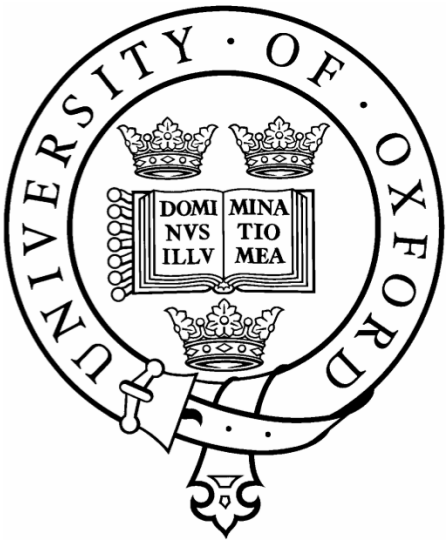

Supervisor: Professor Dame Kay E. Davies

Department of Physiology, Anatomy and Genetics

University of Oxford

Thesis submitted for the degree Doctor of Philosophy

Hilary Term 2015

Abstract

Analysis of novel pathways in neurodegeneration using mouse and fly model organisms

Leigh C. Paton, St John's College, University of Oxford

Submitted for the degree of Doctor of Philosophy, Hilary Term 2015

The aim of this project was to understand the molecular mechanisms underlying movement disorders and to identify new genes involved in neurodegeneration. By genetic crossing two mutations identified in the Shakin' Stevens mouse, were separated into individual mouse strains. Both have provided important new insights into two pathways characteristic of neurodegeneration: The autophagy-lysosome pathway, a protein degradation pathway in the Nymphe mouse (*nym/nym*), and lipid metabolism defects in the Jabber mouse (*jab*/+).

The *nym* homozygous mouse was identified as a novel mouse model of the lysosomal storage disorder mucolipidosis II (MLII) homozygous for a patient mutation in the *GNPTAB* gene. The novel mouse model of MLII more fully recapitulates the human pathology than the previously described *Gnptab* knock-out mouse. Histological analysis of the brain revealed for the first time progressive neurodegeneration in the cerebellum with severe Purkinje cell loss. In addition, based on similar features between Niemann-Pick type C disease and MLII, the *nym* homozygous mice were treated with 2-hydroxypropyl-β-cyclodextrin, a drug previously reported to rescue Purkinje cell death in a mouse model of NPC disease. No improvement in brain pathology was observed, demonstrating that cerebellar degeneration is not primarily triggered by loss of Npc2 function.

The *jab* mouse model, harbouring a mutation in the small GTPase Arl1, was characterised as a novel model of chylomicron retention disease, a lipoprotein deficiency, and offered the opportunity to study a novel gene involved in the maintenance of lipid homeostasis and neurodegeneration, specifically demyelination in the peripheral nervous system. The *jab* mutation in *Drosophila* presented with characteristic features of the *jab* mouse, highlighting the functional conservation of Arl1 and validated the use of *Drosophila* for further studies. Interestingly, together with constitutively active and inactive mutants, pathology in lipid droplet formation and defective insulin signalling was associated with defective Arl1 function. Using *Drosophila* will enable further studies into Arl1's role in tissue specific function and help elucidate molecular pathway leading to demyelination.

Thus, this work has highlighted the value of a phenotype-driven approach to investigate novel neurodegenerative pathways and their amenability to therapy.

Declaration

The work presented in this thesis was performed in the MRC Functional Genomics Unit, Department of Physiology, Anatomy and Genetics, University of Oxford, from 2011-2015. All work was funded by the Medical Research Council. Except where acknowledgement is made, all of the work presented is my own and has not been submitted for any other degree in this or any other University or institute of learning.

Acknowledgements

First and foremost, I would like to thank Professor Dame Kay Davies for giving me this unique learning opportunity in such an energetic research environment. I am incredibly grateful for her support and guidance throughout the years which have enabled me to grow intellectually and personally. These skills will be invaluable for my future career.

Secondly, I would like to thank Dr Janet Kenyon and Dr Emmanuelle Bitoun for giving me exceptional training from the start of my DPhil and always providing me with encouragement and expertise throughout. I am equally in debt to the supervision by Dr Stuart Grice on the *Drosophila* project of my thesis. I especially would like to thank him for introducing me to the range of *Drosophila* techniques, discussing scientific concepts and being of invaluable help during my thesis write-up. Furthermore, I would like to thank Dr Jilong Liu for supporting me to conduct my *Drosophila* research project in his laboratory. I am also incredibly grateful for his expertise and guidance. My thanks is also directed to Dr Clive Wilson and his group for advice on further research efforts regarding the *Drosophila* project.

Next, I would also like to thank all the past and present members of the Davies and Liu Lab for teaching me novel techniques, for discussions on trouble-shooting of experiments and for their friendship and support. Special thanks goes to: Dr Mattéa Finelli, Dr Peter Oliver, Dr Rebecca Fairclough, Benjamin Edwards, Arran Babbs, Sarah Squire, Dr Esther Becker, Allyson Potter, Dave Powell, Nandini Shah, Friederike Winter, Yixing Wu, Dr Kevin Liu, Gauri Ang, William Pembroke, Dr Anna Dulneva, Stephanie Hoekstra, Dr Achilleas Livieratos, Dr James Sleigh, Dr Amy Reddington, Dr David Burns, Dr Simon Guiraud, Dr Katie Richardson, Dr Huijia Chen, Dr Andrew Bassett, Dr Gabriel Aughey, Jenna Schwarz, Dr Charlotte Tibbit, Dr Omur Tastan, Mayte Siswick, Dr Lydia Hulme and Dr Sanjay Ghosh.

In addition, I would like to thank Professor Fran Platt for an inspirational collaboration on the mucolipidosis II mouse model. Special thanks goes to Dr. David Priestman for teaching me novel techniques but also Dr Nada Al Eisa, James Gray, Allie Colaco, Dave Smith, Joanna Cross, Dr Oscar Chen and Dr Paul Fineran for their help and support.

I must also acknowledge the MRC for funding my three year DPhil and the grants from St John's College in support of my career and research development. Furthermore, I want to thank Professor Zoltan Molnar for providing advice and support as my college advisor.

Next, I want to thank some great friends from St John's College, DPAG and beyond, who have supported me throughout and made my time in Oxford unique. Thank you, Dr Barbara, Andreas B, Matthias, Anna CS, Dr Michael, Dr Gaëlle and Dr Ian, Marta, Melissa, Dr Madu, Dr

Richard, Ross, Ant, Adam, Dr Ben, Andreas G, Stefano, Kieran, Maria, Dr David, Dr Alberto, Dr Mimi, Jan, Dr Struan, Dr Sven, Dr Justine, Anna M, Gauri, Nick, Emma, Dr Katherine, Tim, Gizem, Vicki, Klara, Caitlin, Flora, James, Dr Ed, Annette, Katherine, Paul, Dr Carole, Pri, Eden, Pirada, Dr Eddy, Tom, John and Jon, Rita, Theresa, Hazel, Dave and Penny, Dr Max, Dr Ellie, Dr Hugo, Dr Laura, Friederike, Julian, Siamak, James, Luiz, Kim, Rozzy, Dr Matt, Dr Kevin, Annika and Timo, Suvi, Dr Anneke and Dr Jochen, Dr Rasmus, Ronja, Diana, Vlada, Dr Claudia, Jess, Kelly, Ella, Ewelina, Lucy, Anke and Chris, Anna-Cara, Jens, Jocelyn, Birte, Elena, Daniela, Sophie, Céline, Kerstin, Lea, Stephanie, and Nettie.

Most of all, I want to thank my family for always being there for me and just being absolutely fantastic throughout my whole DPhil - with its ups and downs. Mum and Dad, thank you for your patience, unconditional support and encouragement. To the best sister, Vivienne, thanks so much for your constant support and love.

Table of contents

List of Figures and Tables

Figures

Tables

List of abbreviations

Aβ: Amyloid-β
AD: Alzheimer's disease
ADRP: Adipocyte differentiation-related protein
AED: After egg deposition
Akt: Protein kinase B
ALP: Autophagy-lysosome pathway
ALS: Amyotrophic lateral sclerosis
APO: Apolipoprotein
APP: Amyloid precursor protein
ARF: ADP-ribosylation factor
ARL: ADP-ribosylation factor like
ARFRP1: Arf related protein 1
ATGL: Adipose triglyceride lipase
BOS: Base of support
BSA: Bovine serum albumin
CA: constitutively active
CA1: Cornu ammonis 1
CA3: Cornu ammonis 3
CD: 2-hydroxypropyl-β-cyclodextrin
C/EBP-α: CCAAT/enhancer-binding protein alpha
CI: constitutively inactive
CIP: calf intestinal alkaline phosphatase
***cis*-Golgi:** *cis*-Golgi Network
CNS: Central nervous system
COPII: Coat protein II
CRD: chylomicron retention disease
Dilps: *Drosophila* insulin like peptides
DGAT: diacylglycerol acyltransferase
DMEM: Dulbecco's Modified Eagle's Medium
E: embryonic day
4E-BP: eukaryotic initiation factor 4E (eIF-4E) binding protein-1
ENU: N-ethyl-N-nitrosourea
ER: Endoplasmic reticulum
FCS: foetal calf serum
FRDA: Friedreich's ataxia
GAP: GTPase-activating proteins
Gapdh: glyceraldehyde-3-phosphate dehydrogenase
GBA: β-glucocerebrosidase
GDP: Guanosine diphosphate
GFAP: Glial fibrillary acid protein
GEF: guanine-nucleotide exchange factors
GLUT: Glucose transporter
GM2: Ganglioside monosialic 2
GNPTA: N-acetylglucosamine-1-phosphotransferase
Golgi: Golgi apparatus
GRIP: golgin-97, **R**anBP2alpha, **I**mh1p and **p**230/golgin-245
GTP: Guanosine-5'-triphosphate
HD: Huntington's disease
HEK cells: Human embryonic kidney cells
IGF: Insulin-like growth factor
InR: Insulin receptor
iPS cells: Induced pluripotent stem cells
jab: Jabber mouse
L2: 2nd instar larval stage
L3: 3rd instar larval stage
Lamp: Lysosomal-associated membrane marker
LB: Luria-Bertani
LD: Lipid droplet
LF: Left front
LH: Left hind
LSD: Lysosomal storage disease
MBP: Myelin basic protein
MCS: Multiple cloning site
MEF: Mouse embryonic fibroblast
MGAT: Monoacylglycerol acyltransferase
MLII/III: Mucolipidosis II/III
M6P: Mannose 6-phosphate
MPTP: 1-methyl-4-phenyl-1,2,3,6-tetrahydropyridine
mRNA: messenger RNA
mTOR: Mammalian target of rapamycin

NMJ: Neuromuscular junction
NPC: Niemann-Pick disease type C
nym: Nymphe mouse
OPA1: Optic atrophy 1
OS: Oxidative stress
OXR1: Oxidation resistance 1
P: Postnatal day
PARK2: Parkinson disease 2
PARK7: Parkinson disease 7
PAS: Periodic acid-Schiff
PCR: Polymerase chain reaction
PC: Purkinje cell
PD: Parkinson's disease
PET: Positron emission tomography
PFA: Paraformaldehyde
PI3K: Phosphoinositide-3 kinase
PINK1: PTEN induced putative kinase 1
PIP2: Phosphatidylinositol 4,5-bisphosphate
PIP3: Phosphatidylinositol 3,4,5-triphosphate
Pmp22: Peripheral myelin protein 22
PNS: Peripheral nervous system
PPARγ: Peroxisome proliferator-activated receptor gamma
PPD: p-Phylenediamine
PTEN: Phosphatase and tensin homolog deleted on chromosome 10
qRT-PCR: Quantitative real-time polymerase chain reaction
RF: Right front
RH: Right hind
RNAi: RNA interference
Rp49: Ribosomal protein 49
RT: Room temperature
SAR: Secretion-associated and Ras-related
SC: Schwann cells
SHIRPA: SmithKline Beecham, Harwell, Imperial College, Royal London Hospital, phenotype assessment
siRNA: Small interfering RNA
S6K: Ribosomal protein S6 kinase beta-1
SNAP: Soluble NSF Attachment Protein
SNARE: SNAP (Soluble NSF Attachment Protein) Receptor
SOD1: Cu,Zn-superoxide dismutase
stv: Stevens mouse
TAG: Triacylglyceride
TBS: Tris-Buffered Saline
TDP-43: Transactive response DNA-binding protein 43
TEMED: Tetramethylethylenediamine
TIP47: Tail-interacting protein of 47 kDa
TM: Transmembrane
***trans*-Golgi:** *trans*-Golgi network
TRPC3: Transient receptor potential cation channel C3
UAS: Upstream activated sequences
UPS: Ubiquitin-proteasome system
WT: Wild-type

1. Introduction

The prevalence of neurological diseases is growing at an alarming rate in aging populations. The World Health Organisation reported that the incidence of deaths in the world from Alzheimer's disease (AD) and other dementias rose three-fold, and deaths from Parkinson's disease (PD) rose two-fold in the last 20 years (Lozano et al. 2011). Not only the lives of patients and their families are affected, but also a huge burden is placed on society and the health care system. The costs of these diseases are staggering. The European Brain Council published that the total direct health care cost of diseases of the brain constituted 24% of the total healthcare expenditure in 2010 in Europe (Gustavsson et al. 2011), a 9% increase in comparison to the past study in 2005 (Andlin-Sobocki et al. 2005). To improve prevention, treatment and health care, it is crucial to intensify research efforts to more fully understand the pathogenesis and underlying molecular mechanisms of neurological diseases.

1.1. Neurodegenerative diseases are caused by common mechanisms

Neurodegenerative diseases are characterised by progressive loss of function and degeneration of a specific population of neurons. These pathologies lead to symptoms such as impairment in sensation, cognitive decline and motor coordination. The precise molecular mechanisms leading to neuronal cell death are still unknown. However, immense research efforts have made progress in deciphering the primary triggers of neurodegenerative diseases. Common mechanisms have emerged from these studies, providing insights into the genetic mechanisms and/or type of protein aggregate that cause cell death (Jellinger 2010, Ramanan and Saykin 2013). Specifically, processes important for cell homeostasis such as protein degradation pathways, mitochondrial, Golgi apparatus (Golgi from here onwards) and endoplasmic reticulum (ER) function, but also energy homeostasis including lipid metabolism need to be tightly controlled. Deregulation of these processes can contribute to neuronal dysfunction and cell death (Taylor et al. 2002, Forman et al. 2005, Ramanan and Saykin 2013, Jellinger 2010). Some of the main pathways associated with onset and progression of neuronal cell death are discussed below (Figure 1.1).

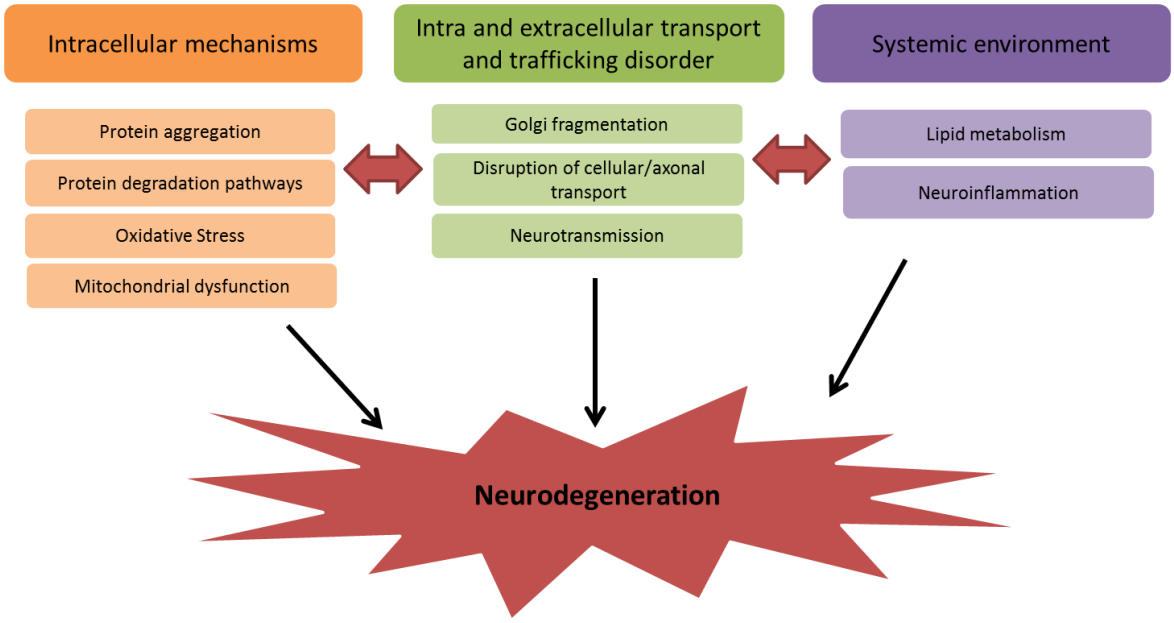

Figure 1.1. Molecular pathways leading to neurodegeneration
Displayed are pathways influencing the balance of neuronal survival and degeneration within broader functional groups based on their major site or mode of action (Intracellular mechanisms, intra- and extracellular transport and trafficking disorder and systemic environment). The pathways in this model are highly related and can have overlapping or interacting components which can collectively modulate processes. Adapted from (Ramanan and Saykin 2013).

1.1.1. Intracellular mechanisms

1.1.1.1. Protein aggregation

Post-mortem studies have identified aggregation of misfolded protein visualised as inclusions or plaques. These findings led to studying disease specific hallmarks in more detail such as α-synuclein in PD (Taylor et al. 2002), amyloid-β (Aβ) in AD (Hardy and Higgins 1992, Karran et al. 2011), huntingtin protein in Huntington's disease (HD) (McMurray 2001) and transactive response DNA-binding protein 43 (TDP-43) in frontotemporal dementia and amyotrophic lateral sclerosis (ALS) (Rademakers et al. 2012). Aberrant proteins can be generated due to production errors as, for example, mutations in the amyloid precursor protein (APP) gene, encoding for the Aβ peptide in AD, leading to more amyloidogenic species of Aβ. However, also cellular stress and overproduction of proteins have been implicated in the generation of aggregation prone proteins (Taylor et al. 2002). These aberrant proteins are also able to interact with other proteins and lipids resulting in abnormal deposition and aggregation

(Bauer and Nukina 2009). However, some controversies exist, as to what extent aggregation of proteins trigger cell death. In fact, inclusions have also been reported to act as a cellular protective mechanisms and therefore question the approach of targeting aggregated proteins or their synthesis for drug development (Ross and Poirier 2005). Yet, misfolded proteins can have deleterious effects on cellular health therefore quality control and repair systems are crucial to maintain cellular homeostasis. Molecular chaperones and intracellular proteases belong to the quality control system in the ER. These components assist in protein folding and correct potential stress induced misfolded proteins (Frydman 2001). Indeed, reduced activity of molecular chaperones and intracellular proteases have been identified in neurodegenerative diseases (Scheper and Hoozemans 2009). Therefore, to reduce protein aggregation the functioning of protein degradation pathways is crucial.

1.1.1.2. Protein degradation pathways

Two degradation pathways are currently known to remove damaged cellular components. Both of them control the quality of cellular components and maintain cell homeostasis. These are the ubiquitin-proteasome system (UPS) and the autophagy-lysosome pathway (ALP).

The UPS is able to target proteins selectively for degradation through a defined cascade of enzymes that connect chains of ubiquitin onto the misfolded, aggregated or else abnormal protein (Glickman and Ciechanover 2002, Pickart and Fushman 2004, Kraft et al. 2010). The 26S proteasome, a large catalytic protease complex, recognises the ubiquitin tag and enables the degradation of the protein into small peptides (Baumeister et al. 1998). Genes involved in the UPS system have already been implicated in neurodegenerative diseases, such as parkin (PARK2; a ubiquitin-protein ligase), leading to monogenetic forms of PD (Um et al. 2010). In modest quantities, protein degradation via the UPS may be neuroprotective as parkin overexpression was shown to increase Aβ clearance in AD cell culture models and ameliorate

levels of defective proteins and mitochondria in aging *Drosophila* brains (Khandelwal et al. 2011, Rana et al. 2013).

The ALP is a tightly regulated mechanism to degrade unwanted or dysfunctional cellular components (Krainc 2010). In macroautophagy (termed autophagy from this point) proteins or entire organelles are engulfed in a double membrane vesicle called an autophagosome and fuse with lysosomes which contain lysosomal enzymes and degrade waste material collected by the autophagosome. The lysosomes play a crucial role in the ALP and it has been suggested that dysfunction of lysosomal function may form part of the pathogenesis of neurodegenerative diseases such as PD, AD, ALS and HD (Nixon 2013, Tofaris 2012). Moreover, an increasing number of mutations in genes from the ALP have been identified in adult-onset neurodegeneration (Sidransky et al. 2009, Nixon 2013, Lesage and Brice 2009). Indeed, it has been shown that selective knock-out of autophagy genes in neurons of mice led to ubiquitinated intracellular inclusions and cell death (Hara et al. 2006, Komatsu et al. 2006, Komatsu et al. 2007). Heterozygosity for a single mutant β-glucocerebrosidase (GBA) allele, which is the gene that encodes a specific lysosomal hydrolase and when dysfunctional causes the lysosomal storage disease (LSD) Gaucher's disease, is a significant risk factor for PD and for dementia with Lewy bodies (Goker-Alpan et al. 2004, Sidransky et al. 2009, Aharon-Peretz et al. 2004). LSDs are caused by loss of a lysosomal hydrolase and lead to accumulation of undegraded macromolecules, lysosomal and autophagic dysfunction and, ultimately, cell death. Conversely, patients with Gauchers's disease, despite presenting symptoms different to PD, may show PD pathology such as tremor, bradykinesia, rigidity, α-synuclein-immunoreactive Lewy bodies and degeneration of dopaminergic neurons (Aharon-Peretz et al. 2004, Wong et al. 2004). Disruption of the ALP in AD causes striking neuronal autophagy pathology similar to that in the LSDs. Inhibiting the ALP produces similar neuropathology in wild-type mice and exacerbates Aβ and autophagy pathology in mouse models of AD (Nixon and Yang 2011). Novel therapies are already being developed that enhance autophagy to foster the degradation

of protein aggregates (Rubinsztein et al. 2012, Rubinsztein et al. 2007). The study of chapter 4 highlights the need to better understand the ALP leading to neurodegeneration.

1.1.1.3. Oxidative stress

Oxidative stress (OS) refers to an increase in toxic reactive oxygen species and reduced antioxidant capacity which in turn leads to the inability to protect from reactive oxygen species-induced cellular damage (Lin and Beal 2006, Turner et al. 2009, Keller et al. 2005). Dysfunctional mitochondria and/or glutamate excitotoxicity can lead to the generation of OS. OS has been found to precede symptoms associated with neurodegenerative disease and may damage DNA, protein and lipid peroxidation (Reed 2011, Wang and Michaelis 2010, Xie et al. 2013). Proteins which have been damaged can oxidise reduced glutathione, making glutathione reactive, and cause imbalances in calcium homeostasis, a characteristic of many neurodegenerative diseases (Ballatori et al. 2009). The link between OS and cell death is still unclear, although there is some debate as to whether reactive oxygen species are the main cause or simply a result of neurodegeneration (Halliwell 2006). However, studies have shown that OS can affect α-synuclein and Aβ's cellular localisation and aggregation (Henchcliffe and Beal 2008, Squier 2001). Furthermore, *PARK2*, *PARK7*, and *PINK1*, genes associated with PD, have shown to be involved in the regulation of OS. For example, mouse and *Drosophila* brains have shown increased sensitivity to OS in response to *PARK7* knockdown (Kim et al. 2005) and, interestingly, to ameliorate the loss of *PARK7*, reactive oxygen species scavengers, *PINK1* and *PARK2* overexpression were effective (Irrcher et al. 2010). Especially due to OS being a pre-symptomatic biomarker of neurodegeneration, increased research has focused on potential genetic modulators of OS and how these might affect susceptibility to neurodegeneration.

1.1.1.4. Mitochondrial dysfunction

Mitochondria are the energy power houses for the cell. In addition, to being the major producer of reactive oxygen species in the cell, mitochondria also play important roles in endocytic and cell death pathways. Interestingly, many AD and PD disease proteins are located to the mitochondria. Therefore, the resulting divergence of multiple disease pathways to the

mitochondria makes the mitochondria an interesting target to understand and combat neurodegeneration (De Strooper and Scorrano 2012). Mitochondrial fission and fusion defects have already been linked to neurodegeneration (Chen and Chan 2009) and the disruption in mitochondrial function and mitochondrial DNA damage are pathologies detected in many neurodegenerative diseases (Mancuso et al. 2008). For example, the classic PD model, induced by the chemical neurotoxin MPTP, highlights the role of mitochondria and OS. MPTP inhibits the mitochondrial complex I leading to parkinsonism (Langston et al. 1983, Nistico et al. 2011). In addition, α-synuclein overexpression models of PD lead to surplus α-synuclein localising to the mitochondria and causing cytochrome c release and OS (Henchcliffe and Beal 2008).

1.1.2. Intra- and extracellular trafficking mechanisms

1.1.2.1. Fragmentation of the Golgi apparatus

The Golgi is part of the endomembrane system and responsible for packaging proteins into vesicles for their travel to the cell membrane, to other vesicles for secretion or to a different final destination. Newly synthesised proteins travel from the ER to the Golgi and then through the Golgi, encountering multiple modifications and packaging processes that need to be tightly regulated. This is a very dynamic process including multiple membrane fusion and fission events. Due to the Golgi's important role in protein handling it has been of interest to more fully understand the Golgi's role in neurodegenerative diseases. Interestingly Golgi fragmentation has already been associated with ALS, AD and PD (Fan et al. 2008). For example, Golgi fragmentation has been shown to be an early hallmark of neurodegeneration in nigral neurons associated with α-synuclein aggregation in PD. This is most probably brought about by α-synuclein and other misfolded proteins causing defective ER to Golgi trafficking (Fujita et al. 2006). Multiple neurodegenerative diseases that present with Golgi fragmentation also present with defective axonal transport. The *trans*-Golgi network (*trans*-Golgi), the exit site of the Golgi, is important for protein sorting, membrane trafficking and ultimately determines the final destination or secretion of a protein. Therefore a defect in the Golgi, especially the *trans*-Golgi,

could lead to serious perturbations in axonal transport and presynaptic function (Fan et al. 2008).

1.1.2.2. Cellular/axonal transport

Defective neuronal and axonal transport has been shown to play a crucial role in disease mechanisms in neurodegenerative diseases (Vickers et al. 2009, De Vos et al. 2008, Morfini et al. 2009). For example in ALS, early axonal degeneration in Cu,Zn-superoxide dismutase (SOD1) mouse models has been linked to axonal transport and neurofillament defects (Pun et al. 2006). Furthermore, in AD abnormal proteins such as tau and APP, have shown to cause axonopathy prior to hallmark pathologies of neurofibrillary tangles and Aβ plaques (Gotz et al. 2006). However, further studies are needed to define if defective cellular/axonal transport is a consequence of neurodegeneration or actually causes neurodegeneration.

1.1.2.3. Neurotransmission

Neurotransmitters are endogenous chemicals that release signals from neuron to neuron into the synaptic cleft. Current therapies for AD and PD are indeed based on perturbations of neurotransmitter transmission in these diseases. For example, cholinergic modulation, leading to increased acetylcholine neurotransmission, is one form of therapy for AD because of the finding that selective loss of cholinergic signalling neurons in the brain, important for learning and memory, is causative for disease (Davies and Maloney 1976, Corbett et al. 2012). Similarly, dopaminergic modulation, leading to an increase in the neurotransmitter dopamine, is a current therapy for PD because of the main pathology found in PD of loss of dopaminergic neurons from the substantia nigra, important for motor function (Hoehn and Yahr 1967, Antonini and Albin 2013).

1.1.3. Systemic environment

1.1.3.1. Lipid metabolism deregulation

Lipid deregulation and therefore loss of lipid homeostasis has been shown to have a pivotal effect in the pathophysiology of multiple neurodegenerative diseases, including motor neuron disease, AD, PD and HD (Adibhatla and Hatcher 2008, Schmitt et al. 2014). For example, apolipoprotein (APO) E ε4 which transports lipoproteins, fat-soluble vitamins and cholesterol into the circulatory system has been shown to increase the risk of AD (Martins et al. 2006). Interestingly, the use of statins to lower circulating cholesterol, has been proposed to have a modest reduction in AD and PD risk (Sparks 2011, Gao et al. 2012). Lipids are crucial as building blocks for neuronal membranes, but are also involved in signalling cascades and therefore disruption of lipid pathways may have detrimental effects on synaptic signalling, neuronal plasticity and degeneration (Karasinska and Hayden 2011, Proitsi et al. 2015, Anchisi et al. 2013, Wood 2012). Altered levels of lipids, as for example in obesity, can alter disease progression and cause increased inflammation and exacerbate neurodegeneration, and thereby, promote cognitive decline and increase vulnerability to brain injury (Awada et al. 2013, Bruce-Keller et al. 2009). However, lipids and nutrients are also needed to maintain health state and improve prognosis. For example in ALS patients, it has been highlighted that there is an imbalance between food intake and energy (Braun et al. 2012). They often present with reduced body mass and increased resting energy expenditure (Desport et al. 2001, Dupuis et al. 2011). Energetic alterations are similarly found in transgenic animal models of ALS, the SOD1 mice. These mice are leaner than controls, show an increased metabolic rate, a reduced lipid profile and present increased fatty acid uptake in muscles (Dupuis et al. 2004, Fergani et al. 2007). Therefore, it is crucial to maintain lipid homeostasis; too much or too little can lead to disease.

Lipid metabolism is crucial, not only, in regards to maintaining lipid homeostasis as a source of energy but also in signalling cascades and building blocks for the structure of cells (Wymann and Schneiter 2008, Schmitt et al. 2014). Interestingly, a link between diabetes, a major metabolic disease, and AD has been evolving. Type 2 diabetes patients have double the

risk of also being affected by AD in their lifetime (Kroner 2009). Indeed, also in early AD metabolic dysfunction can be detected including loss of insulin signalling detected in the phosphoinositide-3 kinase (PI3K) and protein kinase B (AKT) pathways (Liu et al. 2011). Furthermore, in support of this new relationship, insulin resistance or deficiency mouse models present with Aβ plaques in the brain whereas Aβ toxicity mouse models present with reduced levels of insulin signalling activity (Vignini et al. 2013). Therefore, both diseases, diabetes and AD, may share common signalling pathways and hence also therapies. For example, medicines for diabetes may be effective in AD, including insulin and insulin-like growth factor (IGF) stimulation (de la Monte 2012) and glycogen synthase kinase 3 (GSK3) inhibition (Gao et al. 2011). This relationship is supported by the secondary pathology of diabetes, peripheral diabetic neuropathy. Symptoms of diabetic neuropathy have been suggested to result from sensory axon degeneration and metabolic changes, such as abnormal nutrients and lipid metabolism, in Schwann cells (Said 2007, Chowdhury et al. 2013). The study of Chapter 5 highlights the need for a better understanding of lipid deregulation leading to neurodegeneration.

1.1.3.2. Neuroinflammatory process

Neuroinflammatory processes have been implicated in many neurodegenerative diseases, from commonly found pathologies, such as glial cell activation, T-cell infiltration and blood-brain barrier dysfunction (Stolp and Dziegielewska 2009). For example, activated microglia in AD and PD brains have been detected in post-mortem tissue, but also in *in-vivo* PET imaging of patients (Prinz et al. 2011). In support of this finding, Aβ and α-synuclein pathologies in AD and PD have shown to activate microglia. In turn, these activated microglia release inflammatory cytokines and activating inflammatory-mediating enzymes leading to an increased inflammatory response and resulting cell damage (Prinz et al. 2011, Lucin and Wyss-Coray 2009, Lee et al. 2010). Furthermore, activated microglia and astrocytes have shown to contribute to ALS motor degeneration (Ilieva et al. 2009, Ferraiuolo et al. 2011, Bowerman et al. 2013). Interestingly, the transplantation of ALS diseased glial progenitors into spinal cord of wild-type rats caused astrogliosis, microgliosis as well as abnormal motor function and motor

neuron degeneration (Papadeas et al. 2011). Finally, also metabolic diseases such as obesity and type 2 diabetes have been linked to the onset of inflammation in the brain (Cai 2013).

In response to these potential neurodegenerative pathways, neurons undergo cell death via one of three major mechanisms: apoptosis (gene-directed programmed cell death), necrosis (passive killing of the cell) or cell death with autophagy (Jellinger 2010).

Whereas neurodegenerative diseases are very heterogenous, it is still clearly apparent that there are common pathways. However, major questions remain in neurodegenerative disease research. For example, it is specifically of interest why only a subset of neurons - different subsets of neurons in different diseases - are affected, despite ubiquitous expression of the disease protein. Furthermore, a long pre-clinical phase exists in many neurodegenerative diseases despite mutations being present from birth. Therefore, it is of interest to understand which pathologies occur during these early phases and identify early biomarkers that can help us to intervene at the earliest time point in disease. Finally, the starting trigger of neurodegenerative diseases, fundamental for early therapeutic intervention, is in many cases still unknown (Ribe et al. 2008, Gorman 2008).

Consequently, to help the understanding of individual roles of genes in neurodegeneration, cell and animal models are frequently used. These models allow for the investigation of disease mechanisms and can reveal much needed insights into disease pathogenesis which is crucial for the development of novel treatment options.

1.2. Model systems in the study of neurodegenerative diseases

Post-mortem brain tissue cultures yield insights into end-stage disease pathology. Humans can be used to study disease progression with other technologies such as MRI and Positron Emission Tomography studies but are rather costly. Therefore, human stem cell technology has been employed to derive neuronal cells from embryonic stem cells into which mutations can be engineered (Aubry et al. 2008, Cooper et al. 2010, Reinhardt et al. 2013). These, however, do not carry disease-associated genetic variants in addition to a specific mutation. A new

technology has been developed by Takahashi and Yamanaka in 2006 in which patient fibroblasts could be reprogrammed into patient-specific induced pluripotent stem (iPS) cells (Takahashi and Yamanaka 2006). This technology shows important progress towards modelling neurodegenerative diseases using human cell-based systems (Soldner et al. 2011, Hargus et al. 2014). Currently, huge variations are still present in the differentiation protocols and need to be adapted to reduce variability. Cellular studies still need to be interpreted with caution, despite iPS cells promising to be a "human disease model in a dish", since they can be prone to experimental artefacts. For instance, some cellular processes can be specific to a given cell line/type or a certain condition of culture and cellular stress. In addition, a given stage of cell differentiation or the number of passages can lead to artefacts and may affect experimental conclusion (Badger et al. 2014, Devine et al. 2011, Hargus et al. 2014). Therefore, when modelling diseases that rely on functional neuronal networks or behaviour, cellular processes should be complemented by studies in a whole organism (Dawson et al. 2010).

Drug discovery studies are highly dependent on animal models that recapitulate human disease to investigate potential therapeutic strategies and allow for the investigation of disease progression. These studies are not possible in humans. Unfortunately, animal models recapitulating human disease are needed for most neurodegenerative diseases - even those diseases with a known genetic cause. Possible model organisms with nervous systems that can be used and genetically manipulated have included worms (*Caenorhabditis elegans*) (Xu and Kim 2011), flies (*Drosophila melanogaster*) (Jaiswal et al. 2012, Bellen et al. 2010), zebrafish (*Danio rerio*) *(Cheng et al. 2011)* and mice (*Mus musculus*) (Heintz and Zoghbi 2000, Gama Sosa et al. 2012, Beckers et al. 2009).

1.2.1. Invertebrate model organisms

The arthropod fruit fly *Drosophila melanogaster* (*Drosophila* from here onwards) and the nematode worm, *Caenorhabditis elegans*, have belonged to the most popular invertebrate systems (Jeibmann and Paulus 2009, Lu and Vogel 2009, Thompson and Marsh 2003, Wang et al. 2009, Hamamichi et al. 2008). The powerful genetic toolset available for invertebrate

models has been of great advantage. For example, forward genetic screens can be conducted to analyse genes that modulate disease progression. In addition, their small size and short generation time allows fast and cheap production facilitating investigation of multiple disease-associated transgenic lines at the same time in comparison to the mammalian system (Link 2001). *Drosophila* is used as a model organism in Chapter 5.

Drosophila has been investigated by Thomas Hunt Morgan in his seminal genetic experiments in 1908 leading to the chromosome theory of inheritance and since then used in biological and medical research (Morgan 1915). Huge impact was made by studies using *Drosophila* in many areas of biology ranging from developmental biology, genetics, cell biology to neuroscience, biochemistry and, specifically, as human disease models. Indeed, *Drosophila* is an ideal model organism for human disease not only because 60% of genes are conserved between *Drosophila* and human genes, but more importantly, 77% of human disease genes have orthologues in *Drosophila* (Adams et al. 2000, Reiter et al. 2001).

Drosophila offers lots of advantages as a model organism. Importantly, they are of small size, allowing a large number of individual cultures to be stored in a small space, and due to their fast generation time experiments can be conducted in a very short time frame – all in all making this a very cost effective model. More importantly, a number of genetic tools have been generated to produce *Drosophila* models and maintain the stocks. Common tools include: balancer chromosomes (used to maintain heterozygous mutant *Drosophila* with detrimental mutations by abolishing homologous recombination), gene knock-down by RNA interference (RNAi), transposon mediated mutagenesis (Venken and Bellen 2012), and tissue-specific expression systems (for example using the UAS-GAL4 system, also allowing expression/knock-down of genes at different times of development). In addition, a large amount of resources are publically available such as stock centres (where specific genotypes are maintained and distributed), cDNA clones, cell lines and expression vectors.

The GAL4/UAS system has really expanded the *Drosophila*'s tool box and raised attention to the most tractable metazoan organisms. The *S. cerevisiae Gal4* gene encodes a transcriptional regulator that controls gene expression by binding upstream activated sequences

(UAS) (del Valle Rodriguez et al. 2011). This system has been incorporated in to *Drosophila*, in which GAL4 can also induce expression of genes including a UAS site within their promoters (Brand and Perrimon 1993) (Figure 1.2). The *Gal4* gene randomly inserted in to the genome and often is coordinated by the endogenous enhancer, leading to cell- or tissue specific expression. In addition, the transcription of the target gene, located downstream of the UAS site, is restricted to the expression pattern of the *Gal4* gene. The GAL4 driver and the target gene are kept as individual parental lines, allowing for spatial and temporal regulation by crossing the target transgene to distinct GAL4 drivers. The GAL4/UAS system is commonly employed to overexpress or knock-down target genes ubiquitously or in any tissue of choice using tissue-specific GAL4-driver.

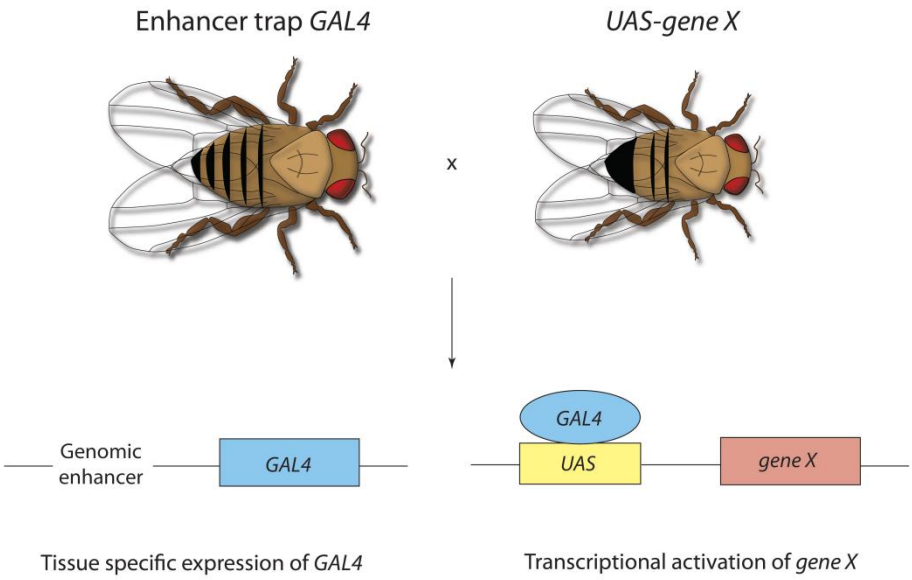

Figure 1.2. The Gal4/UAS (upstream activating sequence) system
This GAL4/UAS system allows tissue-specific expression of transgenes. To achieve this, the enhancer trap GAL4 flies are crossed to the flies harbouring the UAS site in their promoter, upstream of the gene of interest (gene X). Binding of GAL4 to UAS will enable tissue-specific expression of the gene of interest. Taken from (Davies 2012).

The *Drosophila* life cycle entails many discrete stages. After egg deposition (AED) the larvae hatch into the first of three larval moults or instars. During the larval stages, most time is spent on feeding and a rapid increase in size is observed. At this stage, the basic fly body plan is

established through the development of imaginal precursors (adult precursors). A crucial developmental stage at early third instar is called the "critical size" when larvae have acquired sufficient nutrients to complete development without further food source. Following this stage, larvae search for a pupariation site (De Moed et al. 1999, Beadle et al. 1938). The larvae pupariate 5-6 days after hatching (Figure 1.3) and during the pupal stage larval metamorphosis occurs. Larval metamorphosis incorporates tissue break-down and imaginal precursor differentiation into adult appendages. Four to five days later, the adult flies hatch from their pupal cases (called eclosion), have fully developed appendages and become sexually mature within 6-8 hours. The timing of these developmental stages is dependent on nutritional and environmental factors and coordinated by systemic signals such as steroid hormones (Mirth and Riddiford 2007, Tennessen and Thummel 2011, Gebhardt and Stearns 1993, Botella et al. 1985). The entire life cycle takes around 10-12 days at optimum culturing conditions (25°C).

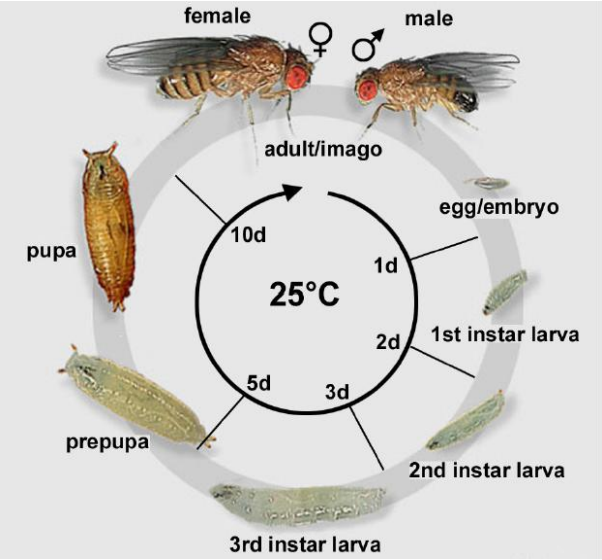

Figure 1.3. The life cycle of *Drosophila*
Fertilised females lay hundreds of eggs over several days. At 25°C embryonic development lasts for ~21hr. The hatched larvae (1st instar) take 2 days to molt into 2nd then 3rd instar larvae. 3rd instar larvae continue feeding (foraging stage) before they leave their food source and migrate away searching for a pupariation site (wandering stage) and eventually pupariate (prepupa then pupa). 10-12 days after egg-laying, adult flies hatch from the pupal case (eclosion). Taken from (Roote and Prokop 2013).

The embryonic central nervous system (CNS) in *Drosophila* contains both neurons and glial cells. Despite not containing myelin, glial cells are crucial in the ensheathing of neurons, such as the wrapping glia in the peripheral nervous system (PNS). Glial cells of *Drosophila* are grouped into four main types: cortex, neuropil, surface and peripheral glia, which all carry out

similar functions to mammalian glial cells. Cortex glia function very similarly to astrocytes. Cortex glia extend their membrane around neuronal cell bodies providing trophic and structural support. Neuropil glia function very similarly to oligodendrocytes by extending their membranes and insulating neurons but also providing trophic support. Surface glia form the blood-brain-barrier of the *Drosophila* CNS. Finally, peripheral glia are made up of wrapping or ensheathing glia which extend their membranes around axonal profiles very much resembling non-myelinating Schwann cells in Remak bundles of vertebrates (Stork et al. 2012, Freeman and Doherty 2006).

One advantage of *Drosophila* lies in the possibility to dissect cellular signalling pathways by conducting large-scale unbiased genetic screens. Forward genetic screens (from mutant phenotype to causative gene) use chemical mutagenesis, insertional mutagenesis, or RNAi to dissect mutations associated with a specific pathology. For example, these screens can test for enhancers and suppressors of a larval lethal phenotype found in a *Drosophila smn* mutant (Chang et al. 2008). In addition, to help in the understanding of the molecular players involved in polyQ-induced degeneration, as in HD or spinocerebellar ataxia, modifier screens in *Drosophila* have revealed several UPS-related proteins, ultimately showing that ubiquitin mediated degradation is neuroprotective (Bilen and Bonini 2007, Fernandez-Funez et al. 2000, Mallik and Lakhotia 2010).

Recently, *Drosophila* have also been used as a tool to provide key insights into conserved metabolic processes (Rajan and Perrimon 2013, Baker and Thummel 2007). The metabolism of *Drosophila* is carried out by a well-balanced network of organs, many of which are analogous to those of their vertebrate counterparts: the gut absorbs nutrients and the fat body, equivalent in function to white adipose tissue and liver in mammals, stores nutrients and is a primary regulator of energy metabolism. The study of Chapter 5 employs *Drosophila* to better understand lipid deregulation leading to neurodegeneration.

1.2.2. Vertebrate model organisms

The low cost vertebrate system zebrafish ***Danio rerio*** has shown an increased use as an experimental organism because of its close evolutionary relationship with mammals, but also the ability to exploit the power of forward and reverse genetic screens otherwise only limited to invertebrates. In addition due to transparency of zebrafish, imaging during development is very easy. Furthermore zebrafish present with many advanced behaviours including memory, conditioned responses, and social behaviours like schooling (Lieschke and Currie 2007).

Mus musculus (mouse from here onwards) is the most widely used organism to model human neurodegenerative disease and has helped reveal healthy and mutated gene function (Trancikova et al. 2011, Rosenthal and Brown 2007). The mouse is used as a model organism in Chapter 3 and 4. The mouse has proven itself as model organism due to its many advantages such as small size, relatively short generation time, large litter size, relatively short life span, 85% conserved genes with human, similar development to humans and the ability to perform behavioural tasks, undertake drug treatment studies and the availability of genetic tools readily available (Muller and Grossniklaus 2010, Denny et al. 2001). Neurodegenerative diseases are late onset and therefore modelling these diseases in mice can be challenging due to different lifespan and development profile in mice compared to humans. Furthermore, aging studies in mice take up a large amount of time and are expensive. However, early markers of neurodegeneration are becoming more important and can be studied in mice. The ability to study pre-symptomatic markers in mice is a major advantage in comparison to humans in which more invasive studies may be more difficult.

The majority of human neurodegenerative diseases are sporadic and of unknown etiology. Interestingly, most idiopathic AD, PD and ALS cases are clinically and neuropathologically very similar to their most common familial forms (Ryan and Rossor 2010, Turner and Talbot 2008, Gasser 2009). As idiopathic and genetic forms of neurodegenerative diseases are phenotypically very similar and taking into account, that naturally occurring mouse models of neurodegeneration are missing, the generation of transgenic mouse models has been driven by familial disease mutations. For example, the *SOD1* overexpressing mutants,

modelling ALS, have been very successful in resembling key pathologies of the human disease (Turner and Talbot 2008, Gurney et al. 1994). However, limitations in this mouse model exist, as TDP43 inclusions, present in the idiopathic form of ALS and resembling the majority of ALS cases, are absent in the familial mouse mutants. This finding highlights the involvement of different disease mechanisms in familial ALS mouse mutants and the ALS patients. Therefore, it is questionable if treatments that prove successful in the familial mouse model are also promising for the idiopathic form. This touches upon a larger problem, in which it is unknown if a mouse model can ever "perfectly" model the complex human-specific neurodegenerative diseases. Indeed, a large amount of transgenic mouse models harbouring a single gene mutation have not yet fully recapitulated human neurodegenerative disease pathology. Hence, a diverse set of transgenic mice incorporating mutations in human genes or even a combination of human genes are needed to better understand the function of those genes in the complex pathology of neurodegenerative diseases (Dawson et al. 2010, Kokjohn and Roher 2009). More importantly, once transgenic models have shown to recapitulate the characteristics of neurodegenerative diseases, they can be employed to test potential genetic and pharmacological therapies.

1.2.2.1. ENU mutant mice can model disease and elucidate novel gene function

Gene knock-outs in mouse models have been a common strategy to understand physiological function of genes. While this aids in the understanding of gene function, most neurodegenerative diseases do not present as homozygous loss of function mutations. In addition, such strategies can cause more severe phenotypes leading to embryonic lethality in which the mutant cannot be studied or compensatory mechanisms step-in, which are not relevant to the disease in question (Elsea and Lucas 2002). Hence, to compensate for this 'phenotype-genotype gap' caused by lethal gene knock-out mutants, several groups set-up random mutagenesis programmes in the late 1990s to generate large numbers of novel mouse mutants. Initial broad-based phenotyping screens, called SHIRPA (**S**mithKline Beecham, **H**arwell, **I**mperial College, **R**oyal London Hospital, **p**henotype **a**ssessment) were conducted (Nolan et al. 2000, Brown and Balling 2001). SHIRPA includes three major screens which

increase in complexity. The first screen tests for general observational abnormalities in the mice. The second screen involves more complex behavioural tests and pathological investigations. The third screen focuses on specific tests for identifying neurological mouse models, such as movement disorders which display clearly observable phenotypes and are features of many neurodegenerative diseases (Nolan et al. 2000, Rogers et al. 1997, Rogers et al. 2001).

The MRC Harwell initiated a mouse mutagenesis programme using the alkylating agent N-ethyl N-nitrosourea (ENU) to induce germ line single random point mutations in male mice. These males are then bred to wild-type females to generate offspring that are subsequently analysed directly for dominant mutations. Furthermore, the offspring can be used for a second or third generation of breeding to dissect an inherited recessive trait (Nolan et al. 2000). The offspring are screened to dissect neurological and behavioural phenotypes using the SHIRPA screen including parameters such as gait, motor control and coordination (Rogers et al. 1997). Next, Mendelian inheritance and penetrance of the trait of interest are determined followed by identification of the mutation using genetic mapping and sequencing of candidate genes (Acevedo-Arozena et al. 2008). A huge advantage of ENU mutagenesis is that the mutation generated by ENU, is located in the endogenous copy of the gene. Therefore, endogenous levels of the gene will be expressed being physiologically relevant and excluding any non-physiological effects of protein expression levels. Finally, this strategy permits the identification of novel human disease-causing genes and offers invaluable insights into the molecular and pathogenic mechanisms of many neurodegenerative diseases (Oliver and Davies 2005). One of the main disadvantages of the ENU strategy used to be the time consuming dissection of the causative mutation based on genetic mapping followed by sequencing of candidate genes. However, this can now be completed more efficiently with affordable next-generation sequencing technology (Boles et al. 2009, Sheridan et al. 2011). Also, potentially, only severe, early onset and easily recognisable phenotypes will be identified using this strategy, therefore missing out more subtle or variable traits (Oliver and Davies 2012, Oliver et al. 2007, Acevedo-Arozena et al. 2008). Late-onset phenotypes, modelling human

neurodegenerative diseases better might also be missed. To tackle this problem, a small cohort of aging ENU mutants are tested at multiple time points up to 18 months (Johnson et al. 2005). These studies, despite being challenging and time consuming, will be able to dissect novel genes and pathways involved in age-related diseases.

An advantage of ENU mutants is that a range of mutations can potentially be generated in a single gene allele, including hypomorphic (reduced amount of gene product), hypermorphic (increased amount of gene product) and neomorphic (altered function) alleles, in addition to loss of function mutations. Interestingly, as thousands of mutant mice are generated, multiple individual mice could harbour different mutations in the same gene, which will more likely provide insights into gene dosage. In addition, different mutations can help understand multiple functions of a gene, as identifying functionally important protein interacting domains, but also model human disease more closely (Oliver and Davies 2005, Keays et al. 2006, Oliver and Davies 2012). A growing number of potential genetic variants leading to disease susceptibility, including novel SNPs or de novo copy number variants as well as epigenetic and environmental factors will drive further mouse modelling experiments (Lewis 2012).

The identification of new models of movement disorders has been the focus in the Davies' group. To date the Davies' laboratory has identified a new allelic series of mutants in *peripheral myelin protein 22* (*Pmp22*), a constituent of the peripheral nerve myelin sheath, identified due to resting tremor (Isaacs et al. 2000, Isaacs et al. 2002, Oliver and Davies 2005). These mice modelled human peripheral neuropathy, leading to hypomyelination, caused by autosomal dominant mutations in *Pmp22* and resulting in varying degrees of pathology. This allelic series of *Pmp22* allowed dissection of genotype-phenotype correlations, such as modelling Dejerine-Sottas syndrome, which presents with a more severe phenotype, characterised by early onset pathology, than Charcot Marie Tooth disease type 1A (Nelis et al. 1999). Furthermore, a novel function for AF4 was elucidated. AF4 is a transcription factor and was only known to be implicated in leukaemia studying the AF4 knock-out. However, in the novel ENU mouse model, AF4 was associated with a novel role in Purkinje cell (PC) survival. The mutation led to accumulation of mutant protein in PCs being detrimental to PC survival

(Oliver et al. 2004). A gain-of-function mechanism was proposed, identifying AF4 as part of a large complex co-ordinating RNA polymerase II and chromatin remodelling via histone methylation (Bitoun et al. 2007). In addition, IGF1 was identified as a target of AF4 revealing the pathogenic mechanism in mutant cerebellum. Indeed, the IGF1 pathway is a recurrent finding in mouse and human ataxias and may be targeted for treatment (Bitoun et al. 2009, Croci et al. 2011). In addition, the Davies laboratory demonstrated that transient receptor potential cation channel C3 (TRPC3) is involved in ataxia. Mutation caused altered gating and increased activity of the channel as a gain of function mechanism. Trpc3 is expressed at high levels in PCs and was shown to be crucial for survival and development of PCs (Becker et al. 2009). Insights were also gained from a mutant linking circadian rhythm disruptions (Pritchett et al. 2012, Oliver et al. 2012) and schizophrenia (Fanous et al. 2010, Thompson et al. 2003). It was shown that missense mutations in SNAP25, a component of the SNARE complex and essential for exocytosis, led to increased binding affinity to the SNARE complex and defective vesicle recycling *in vivo* during exocytosis. This malfunction limits neurotransmission under continued stimulation (Jeans et al. 2007) which is observed in schizophrenia. Limitations in the study of SNARE proteins exist, as knock-outs are lethal, therefore the ENU mouse model offers novel insights (Johnson et al. 2008). Finally, also novel insights were gained on a protein Oxr1, the exact mechanism of which is unknown, but loss caused neurodegeneration and showed the crucial role of Oxr1 in OS-related neurodegeneration (Oliver et al. 2011). Unexpectedly, the Oxr1 ENU mutant mouse was caused by a spontaneous deletion, uncertain if ENU related or not, but small deletions can occur occasionally (Shibuya and Morimoto 1993). These ENU mutants characterised by the Davies laboratory have highlighted the value of a phenotype-driven approach to investigate novel neurodegenerative pathways. The work in this thesis focuses on two ENU mutant models of movement disorders derived from the ENU mutant Shakin' Stevens in which two single base pair mutations were identified.

1.3. Novel mouse model of neurodegenerative disease: The Shakin' Steven's Mouse

The Shakin' Stevens mouse (Stevens (*stv*) mouse from here onwards) presents with growth retardation, tremor, hind limb clasping, reduced muscle strength, demyelination, neuromuscular junction disorganisation, muscle pathology, 2-3 fold increase in hydrolase activity in the blood sera and a normal lifespan. The *stv* mouse has a movement disorder, including tremor, and offered to elucidate novel pathways in neurodegeneration providing insights into mechanisms of neurodegeneration. This complex disease was inherited in a dominant fashion. The mutations were mapped by Dr Janet Kenyon using microsatellite markers. Further fine mapping was carried out to reduce the critical region to 6 Mb between SNPs 86559223 and 92592980 (NCBI build 37) on chromosome 10. PCR and direct sequencing of the coding and exon-intron boundaries of the 6Mb region led to the discovery of two single base pair mutations, each causing an amino acid change in their corresponding proteins. A mutation in the *Gnptab* gene, involved in lysosomal function, and a mutation in the *Arl1* gene, a GTPase, which is involved in trafficking of proteins, were detected in the *stv* mouse. Both proteins are Golgi localised, the protein product of *Gnptab* at the *cis*-Golgi network (*cis*-Golgi) and Arl1 at the *trans*-Golgi. The Golgi is an immensely dynamic cellular organelle composed of cisternal stacks. Its organisation is maintained by a proteinaceous matrix, cytoskeletal components, and inositol phospholipids. The Golgi is structured in stacks as an interconnected network close to the nucleus and is made up of three main compartments, the *cis*-Golgi, which receives cargo from the ER, the medial cisterna, which is the path of travel for proteins to get to the *trans*-Golgi, which serves as a key sorting station, directing cargo to multiple intracellular and extracellular destinations (Farquhar and Palade 1998, Allan and Balch 1999). Newly synthesised proteins and membrane components are processed and sorted at the Golgi arriving from the ER and directed to lysosomes, secretory vesicles or the cell surface for excretion or the cell membrane as crucial building components (Glick and Nakano 2009). Furthermore, post-translational modifications of proteins and lipids are also processes conducted by the Golgi. Finally, the Golgi has received increased attention for being a hub for

cellular signalling molecules and playing an important role in the physiological outcome of signal transduction due to its function in spatially organising signalling pathways (Baschieri and Farhan 2012, Goud and Gleeson 2010). Therefore, Golgi dysfunction could have significant functional implications.

It was possible to separate out the individual gene mutations by genetic crossing, leading to two novel heterozygote mouse models the Nymphe (*nym*) mouse (*nym/+*) (harbouring a mutation in *Gnptab*) and the Jabber (*jab*) mouse (*jab/+*) (harbouring a mutation in *Arl1*).

Therefore, the aims for the *stv* mouse were to:

- **Investigate which gene, *Gnptab* or *Arl1*, or both, caused the peripheral neuropathology observed in the *stv* mouse. The parameters investigated in the *stv* mouse, such as growth retardation, hind limb clasping, reduced muscle strength, demyelination, neuromuscular junction disorganisation, muscle pathology and hydrolase activity in the blood sera were investigated in the *nym* and *jab* mouse (Chapter 3).**

1.3.1. The Nymphe mouse

The gene mutated in the Nymphe (*nym*) mouse (*nym*/+) is *Gnptab (GNPTAB* in human) which contains 21 exons encoding for a 1256 amino acid precursor protein of a 144kDa molecular mass that is subsequently cleaved by the site-1 protease (Marschner et al. 2011) to form a mature α- and β- subunit (Kudo et al. 2005, Tiede et al. 2005). Together with the γ subunit that is encoded by *GNPTG*, α^2-, β^2- and γ^2-subunits form the heterohexameric lysosomal enzyme N-acetylglucosamine-1-phosphotransferase (GNPTA) (Figure 1.4). It has been shown that the α- and β- subunits are sufficient for the activity of GNPTA and recognition of the substrate. However, the γ subunit facilitates this recognition. GNPTA catalyses the first step in the biosynthesis of the mannose 6-phosphate (M6P) recognition marker in lysosomal hydrolases in the *cis*-Golgi (Figure 1.4). This signal leads to recognition by the M6P receptors at the *trans*-Golgi and transport of hydrolases to the lysosomes where they can degrade waste material from the cell. Most lysosomal hydrolases are targeted to the lysosome via the M6P dependent pathway, but there are also M6P-independent pathways utilised by different cell types (Coutinho et al. 2012).

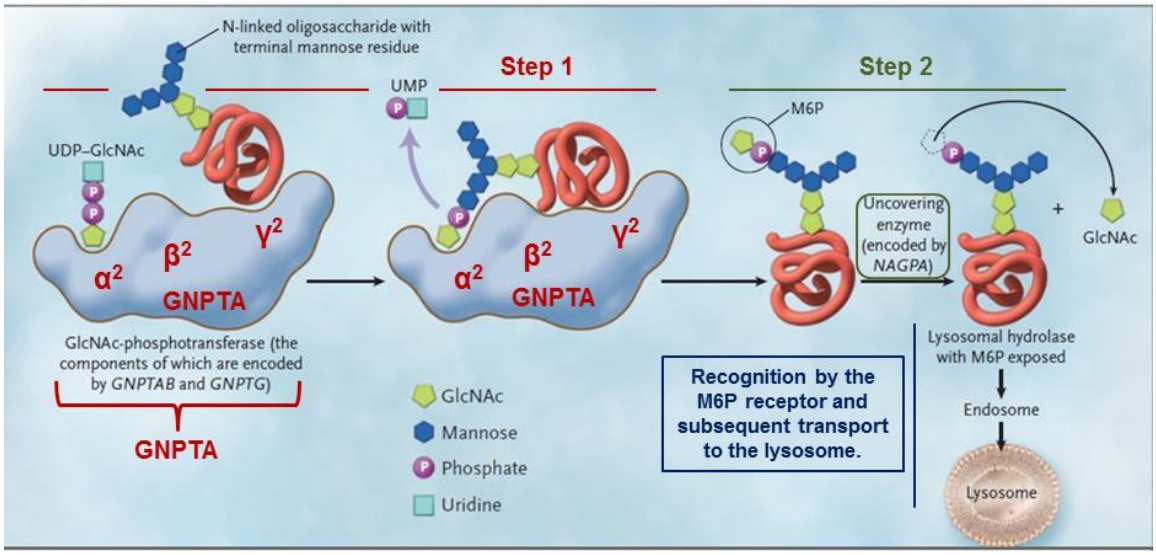

Figure 1.4.The N-acetyl-glucosamine-1-phosphotransferase enzyme is involved in the mannose -6-phosphate targeting pathway
The α and β subunits are encoded by *GNPTAB* and the γ subunit is encoded by *GNPTG*. Together with the γ subunit, α^2-, β^2- and γ^2-subunits form the heterohexameric enzyme N-acetyl-glucosamine-1-phosphotransferase (GNPTA). The mannose-6 phosphate (M6P) targeting pathway is a two-step pathway with GNPTA catalysing the first step **(Step 1)** that involves the transfer of GlcNAc-1-phosphate from UDP-GlcNAc to the C6 position of selected mannose of the hydrolase. The second step **(Step 2)** is catalysed by the uncovering enzyme that is encoded by the NAGPA gene and involves the removal of the glucosamine group (GlcNAc) to reveal the M6P recognition signal. Adapted from (Kang et al. 2010). Reproduced with permission from (Kang et al. 2010). Copyright Massachusetts Medical Society

1.3.1.1. Lysosomal storage diseases

Lysosomal storage diseases (LSDs) are inherited metabolic diseases that are caused by either loss of one of the 80 lysosomal hydrolases, the transporters that normally reside within the lysosomal compartment and are responsible for delivery of lysosomal hydrolases or even loss of the majority of all lysosomal enzymes (Ballabio and Gieselmann 2009, Coutinho et al. 2015, Neufeld 1991, Platt et al. 2012). A reduction or loss of function of one or more of these enzymes leads to progressive accumulation of undegraded macromolecules, lysosomal and autophagic dysfunction and, ultimately, cell death. LSDs are heterogeneous and severity is dependent on the level of residual activity. The less active the affected enzyme is the more aggressive and severe will the disease be manifested. However, the exact mechanistic link between these altered biochemical and cellular states and disease pathophysiology and pathogenesis is unclear. These progressive diseases are characterised by various defects including craniofacial, skeletal and cardiac abnormalities, variable neurological deficits and

ocular problems, as described in table 1.1 (Platt et al. 2012). All these diseases combined have an incidence of approximately 1 per 7500 live births (Meikle et al. 1999, Poupětová et al. 2010).

The lysosomes play a crucial role in the autophagic-lysosomal pathway (ALP) (see Section 1.1.1.2.) which has been shown to be involved in the majority of neurodegenerative diseases. Hence studying lysosomal function is very important as it can be applied to many other diseases. Insights into the ALP dysfunction in LSD can, in theory, shed light on the pathogenesis seen in more general neurodegenerative diseases. The ALP is investigated in many LSDs, as we will do in this study, and neurodegenerative diseases.

Table 1.1. The causes of lysosomal storage diseases, the organelles affected and major sites of pathology

Mechanism of lysosomal storage	Disease	Lysosomal protein defect (gene symbol)	Substrate(s) stored	Major peripheral organ systems affected	CNS pathology
Lysosomal enzyme deficiencies	Aspartylglucosamin-uria	Aspartylglucosaminidase (glycosylasparaginase, AGA)	Aspartylglucosamine (N-acetylglucosaminyl-asparigine)	Skeleton, connective tissue	+
	Fabry	α-Galactosidase (GLA)	(Lyso-) Globotriaosylceramide	Kidney, Heart	-
	Gaucher types 1, 2, and 3	β-Glucocerebrosidase (GBA)	Glucosylceramide, glucosylsphingosine	Spleen/liver, bone marrow	+[a,b]
	GM1-gangliosidosis	β-Galactosidase (GLB1)	GM1-ganglioside, oligosaccharides	Skeleton, Heart	+[b]
	Krabbe	Galactocerebrosidase (GALC)	Galactosylceramide	Heart	+[b]
	Mucopolysaccharidoses	Enzymes involved in mucopolysaccharide catabolism	Mucopolysaccharides	Cartiladge, bone, heart, lungs	+
	Multiple sulfatase deficiency	SUMF1 (Formylglycine generating enzyme needed to activate sulfatase)	Multiple, including sulphated glycosaminoglycans	Spleen/liver, bone, skin	+[b]
	Pompe	α-Glucosidase (GAA)	Glycogen	Skeletal muscle	-
	Sandhoff	β-Hexosaminidase A and B (HEXB)	GM2-gangliosides		+[b]
Trafficking defect of lysosomal enzymes	Mucolipidosis type II (I-cell disease)	N-acetyl glucosamine 1-phosphotransferase α/β (GNPTAB)	Carbohydrates, lipids, proteins	Skeleton, heart	+
	Mucolipidosis type IIIA (pseudo-Hurler polydystrophy)	N-acetyl glucosamine 1-phosphotransferase α/β (GNPTAB)	Carbohydrates, lipids, proteins	Skeleton, heart	+/-
Defects in soluble non-enzymatic lysosomal proteins	Niemann-Pick disease type C2	NPC2 (soluble cholesterol binding protein)	Cholesterol and sphingolipids	Liver	+
Defects in lysosomal membrane proteins	Cystinosis	Cystonosin (cysteine transporter, CTNS)	Cystine	Kidney, eye	+/-
	Free sialic acid storage disorder	Sialin (sialic acid transporter, SLC 17A5)	Free sialic acid	Liver/spleen, skeleton	+
	Mucolipidosis IV	Mucolipin-I (MCOLN1)	Mucopolysaccharides and lipids	Eye	+
	Niemann-Pick disease type C1	NPC1 (membrane protein involved in lipid transport)	Cholesterol and sphingolipids	Liver	+

[a]Types 2 and 3, [b]including cerebellar ataxia (Cerebellar Disorders: A Practical Approach to Diagnosis and Management (Mario Ubaldo Manto)). Adapted from (Platt et al. 2012).

1.3.1.2. Mucolipidosis II

Homozygous or compound heterozygous nonsense or frameshift mutations in *GNPTAB* are causative for mucolipidosis (ML) II, in which GNPTA enzymatic activity is completely lost, or MLIIIα/β, caused by missense mutations in which residual activity of GNPTA is still present. Both cases lead to defects in the biosynthesis of M6P residues, which is the recognition signal targeting soluble acid hydrolases to the lysosome (Reitman et al. 1981, Raas-Rothschild et al. 2000, Cathey et al. 2010, Kornfeld 1987, Kudo et al. 2005). MLII (the focus of this study) and MLIIIα/β are autosomal recessively inherited metabolic diseases that affect cellular homeostasis that is responsible for normal turnover of various materials within the cells. MLII (GNPTA deficiency, originally called I-cell disease) is a rare, debilitating paediatric LSD belonging to the group of inherited metabolic diseases. The prevalence of MLII is 0.16 in 100,000 (Poorthuis et al. 1999). In MLII, unlike many other LSDs in which only one specific hydrolase is defective, hydrolases are still produced but many are secreted into the extracellular space due to impaired lysosomal targeting (Kornfeld and Sly 2001).

- **Cellular and biochemical pathology of mucolipidosis II**

Patients affected by MLII exhibit defective lysosomal targeting of enzymes due to defects in the biosynthesis of the M6P marker. The disease is caused by the loss of multiple hydrolases in the lysosome, due to the transport defect. Lysosomal enzymes degrade and recycle waste material from the cell that is targeted to the lysosome via the endocytic or autophagic pathway and hence are important for the maintenance of cells and tissues (Cox and Cachon-Gonzalez 2012). As a result, one of the most characteristic histological features is the presence of enlarged lysosomes filled with undigested compounds which result in dense inclusions that have been observed in patient fibroblasts and mesenchymal cells, also called inclusion- or I-cells (Leroy and Demars 1967). High levels of acid hydrolases have been detected within the serum of patients, where they may have deleterious effects (Kornfeld and Sly 2001). Several cell types and tissues isolated from MLII patients appear to contain normal acid hydrolase levels despite complete loss of GNPTA activity (Kornfeld and Sly 2001, Martin et al. 1984).

This is not well understood, but may be the result of independent lysosomal targeting pathways or alternate routes to the lysosome, such as secretion and recapture at the plasma membrane (Fratantoni et al. 1968). These cells still contain dense inclusions and large cytoplasmic vacuoles and have been identified as lysosomal compartments. Studies have demonstrated the presence of lysosomal membrane proteins, acid hydrolases, and the storage of glycol-conjugates that have accumulated in significant quantities in these lysosomal compartments (Kornfeld and Sly 2001). Much of the MLII pathology appears to be cell and tissue specific, as evidenced by extensive vacuolisation and generation of autolysosomes in exocrine gland cells, but not in liver and muscle (Boonen et al. 2011). Despite extensive investigation into the molecular pathology of MLII, it is still not clear which characteristics of the disease are primary mechanisms of disease and which are secondary pathological phenotypes.

Without the M6P marker, the lysosomal hydrolases accumulate in the blood sera of patients and are considerably reduced in cells. Enzymatic activity present in the tissues have been reported to be 60-100% in heterozygote carriers of the MLII mutation, 0-1% in MLII patients and 1-10% in MLIIIα/β patients. Heterozygote carriers of the disease gene have no symptoms (Kudo et al. 2005, Kudo and Canfield 2006).

GNPTAB has otherwise also been found to play a role in persistent stuttering. In this case, missense mutations in highly conserved protein regions segregate with the disease. These mutations are inherited in a mostly heterozygote fashion although a few homozygote cases are reported (Kang et al. 2010). Interestingly, these stuttering mutations have a milder effect on enzymatic activity than that seen in MLII/MLIIIα/β mutations, reducing activity to ~50% in patients with persistent stuttering (Kang and Drayna 2012).

- **Clinical characteristics of mucolipidosis II**

Clinical symptoms can be observed from birth and patients show a fatal outcome in the first decade of life in MLII (Leroy and Spranger 1970) or present with a milder form of the disease in MLIII. Mucolipidoses refer to the clinically observed combination of symptoms of

mucopolysaccharidoses and sphingolipidoses (Spranger and Wiedemann 1970, Martin et al. 1975). Patients are typically characterised by dwarfism, coarse facial features, stiffness of joints, skeletal abnormalities, cardio- and hepatomegaly, difficulties in motor movements and mental retardation (Figure 1.5). Birth weight is reported to be low to normal, and post-natal growth often plateaus in the second year of life (Kornfeld and Sly 2001, Leroy et al. 2008). All children are reported to have thickening of the mitral valve leading to cardiac complications, and thickening of airway mucosa and thoracic cage leading to respiratory insufficiency. Patients affected by MLII rarely live past the first decade often as a result of frequent respiratory tract infections or congestive heart failure (Patriquin et al. 1977). Autopsies have reported cytoplasmic lysosomal inclusions in myocardium, brain, and liver.

MLII, like most LSDs, remains poorly understood, representing a barrier to therapeutic development.

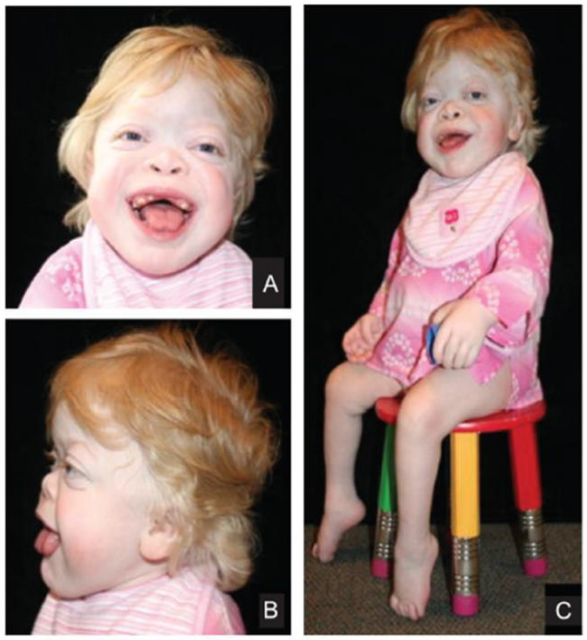

Figure 1.5. Clinical features of patients with MLII
(A) A 6 year old MLII patient presents with severe bone dysplasia, developmental delay, stiffening of the joints, coarse facial features and gingival hypertrophy. **(B)** Furthermore, shallow orbits, thick skin, and a depressed nasal bridge are detected. **(C)** In addition, short, broad hands and contractures of knee and ankle joints are common features. Taken from (Cathey et al. 2010). Copyright agreement with BMJ.

The only mouse model for MLII, a *Gnptab* knock-out mouse model, does not fully recapitulate human disease pathology and, intriguingly, does not present with CNS abnormalities. Therefore, there is a need for a novel mouse model of MLII that more fully recapitulates the human pathology.

Therefore, the aims for the *nym* homozygous mouse (*nym/nym*) were to:

- **Investigate if the *nym* homozygote mouse was a novel mouse model of MLII that recapitulates the disease pathology more fully and could be used as a tool to investigate novel drug treatments. This was conducted by analysing known pathologies such as growth retardation, skeletal abnormalities, inclusion bodies in fibroblasts and increased hydrolase activity in blood sera. Furthermore, insights from this monogenetic LSD which is less complex than common neurodegenerative diseases, offers the opportunity to help dissect novel pathways in neurodegeneration (Chapter 4).**

1.3.2. The Jabber mouse

The gene mutated in the Jabber (*jab*) mouse (*jab*/+) is *Arl1*. *ARL1/Arl1* contains 6 exons and encodes for a small 181 amino acid protein of 20kDa molecular mass. *ARL1* encodes for ADP-ribosylation factor (ARF) like 1 (ARL1) belonging to the ARF family of small GTPases. Small GTPases serve as molecular switches for a variety of cellular signalling events (Clark et al. 1993). The ARF family comprises ARF, SAR (secretion-associated and Ras-related) and ARL proteins. The ARF GTPases are crucial regulators of vesicular transport and membrane trafficking. Vesicular transport is a tightly controlled process making sure that cellular components, including proteins and lipids, are correctly localised through transport among cellular compartments such as the ER, Golgi, endosomes, lysosomes/vacuoles, and the plasma membrane. This transport is dependent on transport vesicles that are formed from one membrane compartment and fuse with another to release associated protein and lipid molecules. Vesicular transport is regulated on several levels, including vesicle production, packaging of cargo within newly formed vesicles, and attachment of the vesicle with the specified target membrane (Derby and Gleeson 2007, Spang 2008, Beck et al. 2009). The identification of genes encoding ARF GTPases in early studies has exposed related proteins which have therefore been named ARF-like (ARL) GTPases (Tamkun et al. 1991, Clark et al. 1993). The ARF family proteins are ubiquitously expressed and the amino-acid sequences are highly conserved from yeast to humans, with remarkable consistency.

ARF family GTPases share the same structural mechanism by which GDP and GTP binding is harnessed for signalling. ARL1 is one of the best conserved ARLs, which is present in protozoa, plants, yeasts and mammals and appears to play a major role in *trans*-Golgi function (Munro 2005, Stefano et al. 2006, Torres et al. 2014). ARL1 is localised to the cytosol in its GDP bound state and translocates to the membrane of the *trans*-Golgi on GTP binding (Lu et al. 2001). In more detail, when GDP bound, the N-terminal helical domain of small GTPases is wrapped within the protein and is not exposed to bind to the membrane of the *trans*-Golgi. Once GTP bound, a conformational change occurs and the N-terminal helical domain is ejected and is able to bind the membrane of the *trans*-Golgi (Figure 1.6). This anchoring method is in contrast to

the C-terminal lipid anchor used by most other members of the Ras superfamily of small G proteins (Pasqualato et al. 2002). The activation of GDP-bound G proteins is a controlled process carried out by proteins termed guanine-nucleotide exchange factors (GEFs), which interact with GDP-bound G proteins to stimulate exchange of the bound GDP for GTP. The deactivation of G proteins by GTP hydrolysis is also a controlled process, mediated by GTPase-activating proteins (GAPs). In general, G proteins have little intrinsic GTPase activity, so the actions of GAPs are critical for proper G-protein function. No specific GEFs and GAPs have been described for ARL1 but rather GAPs and GEFs that have multiple specificities, such as Gsc1, a GAP for both ARL1 and ARF1 (Benjamin et al. 2011, Liu et al. 2005).

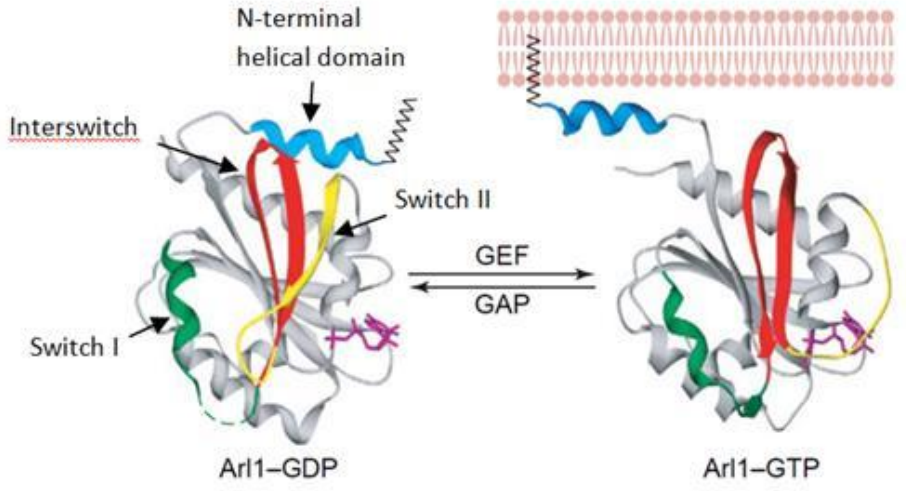

Figure 1.6. Channelling of Arl1 between its GDP bound – inactive - and GTP bound – active - state
In the GDP bound state, the N-terminal helical domain (blue) inserts into a hydrophobic groove blocking attachment to the *trans*-Golgi. The interswitch (red) region of the protein connects the switch I and switch II (green and yellow, respectively) region, which are two anti-parallel β-strands. These three structures are the main components for nucleotide binding and involved in conformational changes when GTP bound leading to exposure of the N-terminal helical domain. In the Arl1-GDP structure, switch I forms a β-strand that is typical of Arf family GTPases preventing spontaneous GTP binding. Thus Arf-family GTPases require a guanine-nucleotide-exchange factor (GEF) to allow conformational changes necessary for GTP binding. Adapted from (Wu et al. 2004).

1.3.2.1. Physiological function of Arl1

Although ARL1/Arl1 has been studied in cell culture and single-celled eukaryotes, there has been little characterisation of its role in the context of the diverse tissues of a multicellular organisms, except that the *Arl1* knock-out in *Drosophila* is embryonic lethal (Tamkun et al. 1991). Loss of ARL1 by gene deletion in yeast, or by small interfering RNA

(siRNA) in mammalian cells, resulted in abnormal trafficking between endosomes and the Golgi (Lee et al. 1997, Lu et al. 2001, Benjamin et al. 2011). ARL1 binds GRIP (**g**olgin-97, **R**anBP2alpha, **I**mh1p and **p**230/golgin-245) domains present in four human golgins (golgin-97, RanBP2alpha, Imh1p and p230/golgin-245) at the *trans*-Golgi and ARL1 specifically binds golgin-97 and golgin-245 (Panic et al. 2003, Setty et al. 2003, Lu and Hong 2003). In both yeast and mammalian cells, ARL1 has been found to bind directly to particular long coiled-coil proteins through their C-terminal GRIP domains (Van Valkenburgh et al. 2001, Setty et al. 2003, Lu and Hong 2003, Panic et al. 2003). Golgins have been hypothesised to collect incoming vesicles from endosomes and maintain the Golgi structure and function, although their precise role is unclear (Chia and Gleeson 2011, Lu et al. 2004, Yoshino et al. 2005, Munro 2011). From work conducted so far, ARL1 has been proposed to regulate retrograde trafficking within the Golgi (transport from later compartments to earlier compartments) by recruiting vesicle tetherers. However, recent tissue specific knock-downs of Arl1 in *Drosophila* have also highlighted Arl1's role in secretory granule formation, negative regulation of ER to Golgi trafficking and ER quality control (Torres et al. 2014, Lee et al. 2011).

Interestingly, recent studies have proposed linked functions between ARL1 and ARFRP1, a related GTPase. Activated, GTP-bound ARFRP1 binds to the *trans*-Golgi (Zahn et al. 2006, Zahn et al. 2008) and recruits ARL1 and its effector golgin-245 to the *trans*-Golgi (Zahn et al. 2006, Panic et al. 2003, Setty et al. 2003). Golgins exact function is unknown, but with their coiled-coil domain they can interact with many GTPases of the Rab family that are regulators of membrane trafficking (Sinka et al. 2008). Rab GTPases function in delivering vesicle loads to correct destinations and regulate vesicle budding, uncoating and mobility (Subramani and Alahari 2010). Recent work by Jaschke et al. (2012) reported that the ARFRP1-ARL1-Golgin-245-Rab2 pathway plays a role in vesicular trafficking in the intestinal epithelium (Figure 1.7). Investigations of this new pathway revealed a link between ARF GTPases and lipid metabolism (Jaschke et al. 2012), specifically in the formation of lipid droplets (LDs) and chylomicrons (Figure 1.7). Lipids are stored in the cytosol in LDs. LDs were assumed to be static organelles simply serving as lipid storage depots. Recently, with an

increasing number of studies, LDs have been described as dynamic organelles to maintain lipid homeostasis, generate energy and regulate cell signalling (Soni et al. 2009, Murphy et al. 2009, Paar et al. 2012, Murphy 2012). Dysfunction of LDs can be detrimental and lead to many metabolic diseases, such as obesity, diabetes and arteriosclerosis (Greenberg et al. 2011, Walther and Farese 2012), but also neurodegenerative diseases, although less studied (Liu et al. 2015, Ilieva et al. 2009, Turner et al. 2009). LDs store neutral lipids (triacylglyceride (TAG) and cholesteryl esters) and are surrounded by a monolayer of phospholipids and cholesterol (Wilfling et al. 2014, Hesse et al. 2013). Many coat-proteins associate with the monolayer and control the turnover of lipids, in which TAG biosynthesis and breakdown occurs at the LDs. In addition, coat-proteins are also involved in the fusion and expansion of LDs, as well as trafficking of the LDs (Kuerschner et al. 2008, Bostrom et al. 2009). A large amount of evidence has proposed that LDs originate from the ER where enzymes such as MGAT (monoacylglycerol acyltransferase) and DGAT (diacylglycerol acyltransferase) catalyse the synthesis of TAG (Wu et al., 2000). The size and number of LDs can differ significantly from cell type to cell-type and the metabolic state of a cell plays a crucial role as well. For example, surplus of fatty acids or induction of adipogenesis leads to rapid growth of LDs, whereas LDs shrink during starvation of cells (Walther and Farese 2012).

Enterocytes in the intestine synthesise and secrete chylomicrons in the postprandial state after nutrient uptake. Synthesis of these lipid storage vesicles is defective in lipoprotein deficiencies such as abetalipoproteinaemia and chylomicron retention disease (Levy 1996, Tarugi and Averna 2011). Chylomicrons are heterogeneous, lipid-rich particles and consist, like LDs, of a core of TAG and cholesteryl ester surrounded by a monolayer of lipids to which specialised proteins (apolipoproteins) bind. Due to the similarity in structure and protein components of chylomicrons and LDs the generation, of both, is likely to be very similar (Figure 1.7).

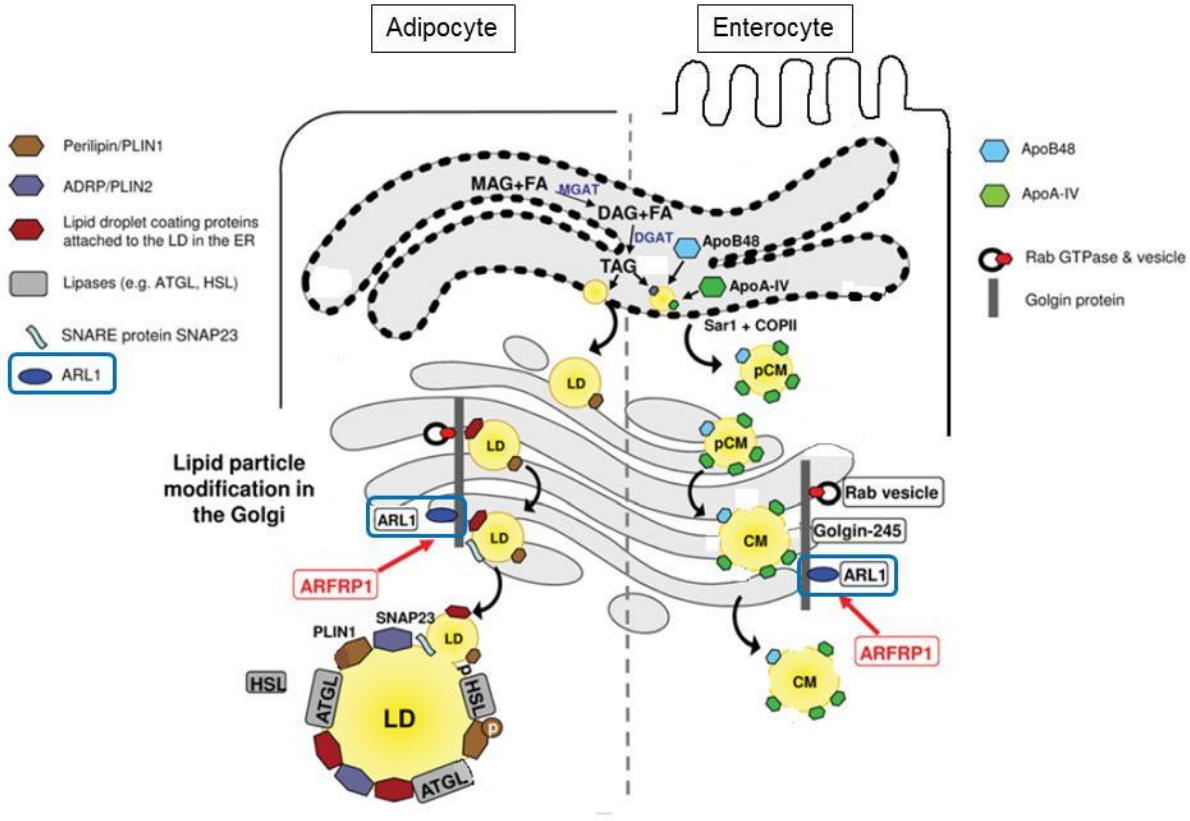

Figure 1.7. The ARFRP1–ARL1–Golgin–Rab cascade in lipid droplet formation and chylomicron maturation

ARFRP1 recruit ARL1 to the Golgi and ARL1 binds to the scaffolding protein Golgin-245, which itself interacts with Rab proteins. The **Left part** of the figure shows the stages for lipid droplet (LD) fusion and the regulation of lipases in adipocytes. Small lipid-carrying particles are transported from the ER to the Golgi where additional triacylglycerides (TAGs) are incorporated and additional proteins are attached. LDs then fuse with larger cytosolic LDs by SNARE-mediated processes. LD fusion and degradation by lipolysis is regulated by the localisation and phosphorylation of LD-coating proteins (e.g. perilipin/PLIN1, ADRP/PLIN2) and lipases (e.g. HSL, ATGL). The **Right part** of the figure shows the chylomicron formation in the ER and the Golgi in enterocytes in the intestine. Fatty acids (FA) and monoacyglyceride (MAG) from micelles or liposomes are taken up from the intestinal lumen by diffusion or transporters. In the ER resynthesised TAGs (generated by subsequent enzymatic esterification and transfer: MGAT/DGAT) are incorporated into ApoB48-containing pre-chylomicrons (pCM). Subsequently, pCMs are released to the *cis*-Golgi and transported through the Golgi, released on the *trans*-site and finally secreted into the lymph. The ARFRP1–ARL1–Golgin–Rab cascade is needed for an appropriate chylomicron assembly and its transport through the Golgi. The role of the cascade for regulating sorting of proteins to the LD required for their fusion and for inhibiting lipolysis needs to be clarified. Adapted from (Hesse et al. 2013). Copyright holder: Biosciences Report, Hesse et al. 2013

1.3.2.2. The Jabber mouse, a model of chylomicron retention disease

Drawing from the results of Chapter 3, the *jab* mutation in *Arl1* caused most of the *stv* phenotype. The *jab* mouse presented with growth retardation, progressive tremor, hind limb clasping, reduced muscle strength, demyelination, neuromuscular junction disorganisation, muscle pathology and a normal lifespan.

First described in 1961 (Anderson et al. 1961), chylomicron retention disease (CRD, also called Anderson's disease) is a rare metabolic disease presenting with symptoms such as lipid malabsorption with reduced levels of cholesterol, lethargy, chronic diarrhoea, lack of fat-soluble vitamins and neurological abnormalities (Bouma et al. 1986, Dannoura et al. 1999, Roy et al. 1987). The only mutation known to cause CRD so far is *SARA2* (protein SAR1b), located upstream of ARL1, (Figure 1.7) and with this identification, the molecular mechanisms in chylomicron transport was confirmed (Jones et al. 2003). The small intestine produces chylomicrons, which are lipoprotein particles that transport dietary lipids from the intestine to other locations in the body, after eating a meal. The incorporation of dietary fat and lipid-soluble vitamins into large lipoprotein particles is critical for transport and absorption (Figure 1.7). The study of monogenetic diseases such as CRD delivers more insights into the basic mechanisms of how lipid metabolism plays a role in neurodegeneration and provides important insights into more common diseases (Peltonen et al. 2006).

The study of Arl1 was highly interesting as it promised to elucidate a novel gene involved in lipid biosynthesis and peripheral neuropathy. In addition to previously shown growth retardation, tremor, hind limb clasping, reduced muscle strength, demyelination, neuromuscular junction disorganisation, muscle pathology and a normal lifespan (presented in Chapter 3) further analysis was conducted by Dr Emmanuelle Bitoun and Dr Janet Kenyon to characterise the *jab* mouse as a novel mouse model of CRD. The transcript and protein (Figure 1.8A+B) expression levels of *jab* Arl1 were found to be 50% reduced in *jab* mouse embryonic fibroblasts (MEFs). Localisation of Arl1 was not significantly disrupted in the *jab* MEFs and correctly localised to the *trans*-Golgi. The enzymatic function of *jab* Arl1 (L61P) showed a strong reduction in GTP binding, only retaining 55% of the wild-type activity. *Jab* Arl1 was compared to both Arl1-Q71L, which is a constitutively active form of Arl1 and binds GTP at similar levels to the wild-type, and Arl1-T31N, which is constitutively inactive and is almost completely unable to bind GTP (Figure 1.8C).

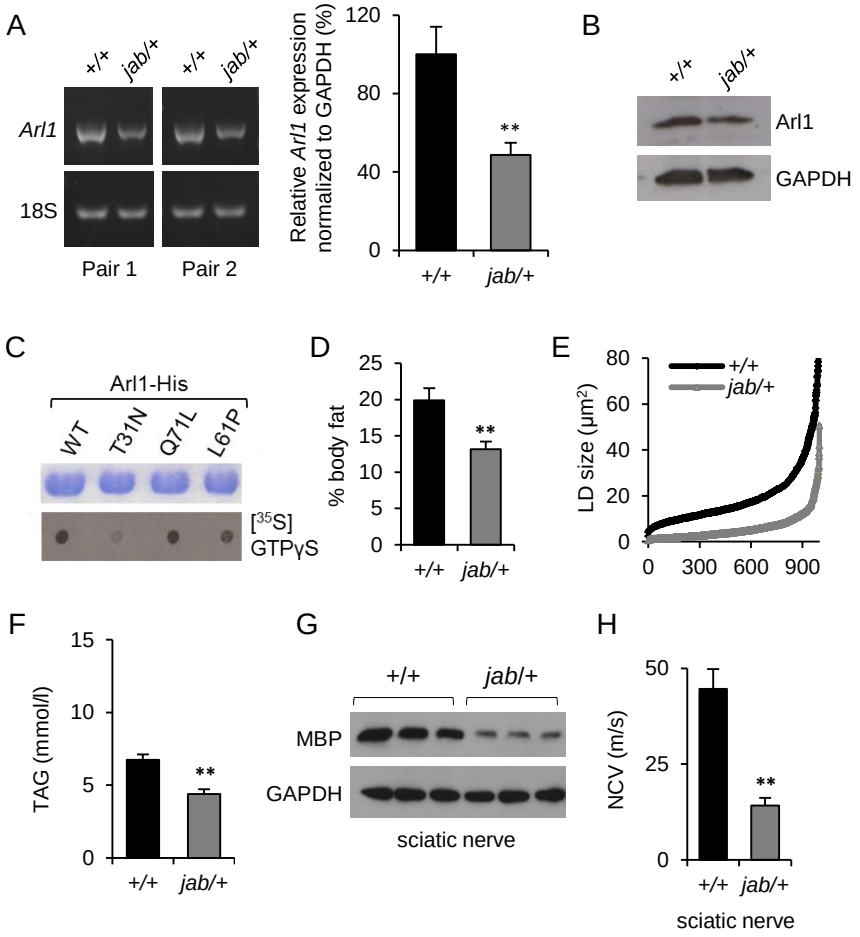

Figure 1.8. Molecular analysis of the ENU mutant Jabber (*jab*) mouse (*jab*/+)
(A) Arl1 transcript expression was analysed by quantitative RT-PCR in wild-type (+/+) and *jab* (*jab*/+) mouse embryonic fibroblasts (MEFs). **(B)** Arl1 protein expression levels were analysed by western blotting in wild-type and *jab* MEFs. **(C)** Recombinant His-tagged wild-type (WT) and mutant (T31N, Q71L, *jab* mutant (L61P)) Arl1 proteins (top panel) were tested for binding of [^{35}S] GTPγS (bottom panel). **(D)** ECHO-MRI analysis of 3 month old wild-type and *jab* mice body fat (n=6). **(E)** Quantification of lipid droplet (LD) surface area in brown adipose tissue from wild-type and *jab* mice. **(F)** Triacyglyceride (TAG) levels were measured in blood serum from wild-type and *jab* mice at 3 months of age (n=6). **(G)** Myelin basic protein (MBP) levels were analysed by western blotting in protein extracts from wild-type and *jab* sciatic nerve. GAPDH was used a as a loading control (n=3). **(H)** Nerve conductance velocity was measured in wild type (n=6) and *jab* (n=4) mice. Data are expressed as mean ± SEM. Mann-Whitney U test, **P<0.01. Data were generated by Dr Emmanuelle Bitoun, Dr Janet Kenyon and Mr Benjamin Edwards.

The *jab* mice presented with reduced weight compared to their wild-type littermates. Body fat was significantly reduced compared to controls (Figure 1.8D) and histological analysis of adipose tissue showed reduced size of LDs while the overall number was not affected (Figure 1.8E). Proper lipid storage is vital for maintaining energy homeostasis in most, if not all, eukaryotic species. The LD, long thought of as an inert organelle, is important not only for lipid storage inside cells but also metabolic regulation (Farese and Walther 2009, Wilfling et al.

2014, Martin and Parton 2006). Lipid storage in LDs is affected by seemingly unrelated cellular events, including autophagy, inflammatory processes and SNARE-dependent intracellular vesicle transport (Bostrom et al. 2007, Singh et al. 2009). In nutrient reduced conditions, lipases are recruited to LDs to initiate TAG lipolysis and release more fatty acids (Farese and Walther 2009, Wilfling et al. 2014, Zimmermann et al. 2009). However, regulation of LD dynamics under physiological and diseased conditions is still not fully understood. TAG levels, the main component of LDs, were reduced in *jab* blood serum in comparison to controls (Figure 1.8F). These data show impaired growth of LDs in the *jab* mouse and reduced lipid levels. Levels of myelin basic protein, the main component of myelin, are reduced in the *jab* mouse sciatic nerve (Figure 1.8G). Due to a defective myelin sheath, nerve conductance velocity is significantly reduced in the *jab* mouse (Figure 1.8H). These findings are classic illustrations of the neuromyotonia seen in dysmyelinated fibres (Zielasek and Toyka 1999) and this explains why the *jab* mutant develops tremors. Interestingly, histology of the *jab* intestine showed a marked increase of lipid staining. These data show impaired fat absorption in the intestine of the *jab* mouse and this is very characteristic of the metabolic disease CRD.

Lipid homeostasis linked to neurodegenerative disease has been receiving more attention, however the exact mechanisms are unclear (see 1.1.3.1) (Adibhatla and Hatcher 2008, Schmitt et al. 2014, Krahmer et al. 2013). Specifically, LDs have only been documented in a few model organisms of neurodegeneration. However, a recent study has shown LD generation caused by increased oxidative stress and highlighted the role of LDs as a pre-symptomatic pathology of neurodegenerative disease in glial cells of *Drosophila* (Liu et al. 2015, Hulshagen et al. 2008, Wang et al. 2002). Furthermore, lipid homeostatic defects are associated with ALS and growing research efforts are focusing on understanding the link between lipid metabolism defects and neurodegeneration (Ilieva et al. 2009, Turner et al. 2009). Hence, the study of genes involved in this pathology is very important, as they could potentially provide insights into molecular mechanisms also occurring in many other diseases. CRD also presents with neuropathy, but no study has focused on elucidating the mechanism of pathology. Therefore,

the *jab* mouse model offers to study lipid homeostatic defects in relation to CRD, but could potentially also be translated to more common neurodegenerative diseases.

It was, however, unknown if the pathology was caused by a specific cell type, such as the adipose tissue and/or the glial cells as these seemed to present with the most severe pathology, or if a global loss of Arl1 was necessary to cause the *jab* pathology. Consequently, *Drosophila* was chosen for further studies due to its diverse genetic tool set, allowing for tissue specific knock-outs and overexpression systems, in addition to its suppressor and enhancer screens, fast generation time and conserved function between mammals and *Drosophila*.

Therefore, the aims for the analysis of the *jab* mutation were to:

- **Generate and validate the Arl1 mutant flies, including the L61P (L60P in *Drosophila*) mutant, but also mutant forms of Arl1 that exist either preferentially in the GDP or GTP restricted bound form therefore constitutively inactive (T30N in *Drosophila*) or active (Q70L in *Drosophila*) to understand the *jab* mouse mutation in the context of GTPase constitutive inactivity and activity within a whole organism as *Drosophila* (Chapter 5).**
- **Test if Arl1 mutant flies can be used as a platform to investigate the importance of lipid metabolism and signalling leading to neurodegeneration (Chapter 5).**

2. Material and methods

2.1. Materials

2.1.1. Constructs and primers

Some constructs were already provided from the laboratory and others were made as detailed in section 2.2. Primers for construct amplification, genotyping and sequencing are listed throughout the text and qPCR primers can be found in table 2.1.

2.1.2. Antibodies

Primary antibodies are listed throughout the text. The secondary HRP antibodies anti-rabbit, anti-goat, and anti-mouse were from GE Healthcare and anti-rat was from Invitrogen and were used at a 1:2,000 dilution for western blotting. Alexa Fluor® secondary antibodies used for immunofluorescence were purchased from Invitrogen and used at a 1:400 dilution. A full list of antibodies can be found in the appendix table 3.

2.1.3. Restriction enzymes

Restriction enzymes were purchased from New England Biolabs (NEB) and used following the manufacturer's instructions.

2.1.4. Culture medium and chemicals

All culture media (L-glutamine, Dulbecco's Modified Eagle's Medium (DMEM) medium, Phosphate-buffered saline (PBS)) were supplied by Gibco® Invitrogen. Grace's insect medium was purchased from Sigma Aldrich. All chemicals used for buffers were purchased from Sigma Aldrich if not mentioned otherwise.

2.2. Cloning

2.2.1. Gnptab

2.2.1.1. Generation of tagged Gnpta expression constructs

2.2.1.1.1. Preparation of vectors and inserts

Full length cDNA sequence of mouse *Gnptab* (NM_001004164) was sub-cloned into pCR2.1-TOPO® (Invitrogen). Tagged constructs were cloned for analysis of cell localisation. Wild-type Gnpta constructs were made with a C-terminal myc-tag. Forward primers included a BamHI restriction site at the 5' end (5'-GGATCCATGCTGCTTAAGCTCCTGCAGAGA-3') and reverse primers included a myc-tag sequence and a NotI restriction site at the 3' end (5'-GCGGCCGCCTACAGATCCTCTTCTGAGATGAGTTTCTGCTCCACCCTGATTCGGTCTGGACTAGC-3'). Primers were adapted to mouse cDNA. The myc-tag was moved in front of the *nym* mutation that caused a stop codon within the sequence (*nym* Gnpta). The same forward primer sequence was used as for the wild-type Gnpta construct, but the reverse primer was as follows:5'GCGGCCGCCTACAGATCCTCTTCTGAGATGAGTTTCTGCTCATTCTGCTGCAACCGTCTGCCAGG-3').

The mouse wild-type and *nym* Gnpta cell localisation constructs were amplified via polymerase chain reaction (PCR; see Section 2.5.1.), run on an agarose gel (see Section 2.6.) and gel purified using a gel extraction kit (Qiagen). Gel purified products were A-tagged (see Section 2.5.3.) and sub-cloned into vector pCR2.1-TOPO® (Invitrogen) using the manufacturer's instructions.

2.2.1.1.2. Transformation

Wild-type Gnpta, *nym* Gnpta and pCR2.1-TOPO® ligation products were transformed into competent E.coli (TOP10®; Invitrogen). Two µl of ligation product was added to 50 µl competent cells and incubated for 30 minutes on ice. The cells were heat-shocked at 42°C for 45 seconds followed by a 2 minute recovery on ice before the addition of 1ml Luria-Bertani (LB) broth media (Invitrogen). Cells were incubated at 37°C, shaking, for 1 hour. Bacteria were spun down at 8000rpm for 5 minutes and resuspended in 200 µl of LB. 200 µl of transformed

cells were then plated on selective LB plates containing 50 µg/ml ampicillin (Sigma Aldrich), 40mg/ml X-gal in dimethylformamide (Sigma Aldrich) and 100mM Isopropyl-β-D-thiogalactopyranosid (IPTG; Sigma Aldrich) and incubated overnight at 37°C. Only bacterial colonies successfully transformed with pCR2.1-TOPO® vector containing the insert will present as white colonies.

2.2.1.1.3. Identification of recombinant plasmids

Several colonies from each transformation plate were screened for the correct insert and correct orientation using appropriate restriction site and colony PCR using the primers used for initial amplification (see Section 2.5.2.). The confirmed constructs with the correct insert were picked to inoculate ampicillin containing liquid LB media and grown at 37°C. Plasmids were extracted the next day using the Qiagen Plasmid Miniprep Kit® and clones containing wild-type Gnpta or *nym* Gnpta inserts were verified by sequencing using M13 Forward (5'-CAGTGCAGGGGAAAGAATAGTAGAC-3') and Reverse (5'-AGCGGATAACAATTTCACACAGGA-3') primers located upstream and downstream of the multiple cloning site of pCR2.1-TOPO®, and specific *Gnptab* primers dependent on construct length.

2.2.1.1.4. Restriction digest and ligation

5-10 µg plasmid DNA was digested with the appropriate enzymes and run on agarose gels. Product bands were then cut out and purified using a gel extraction kit (Qiagen) according to the manufacturer's instructions. 5' phosphate groups were removed using the calf intestinal alkaline phosphatase (CIP; NEB) to prevent the DNA plasmid from re-ligating to itself. Typically, 10 U were added to the restriction digest mixture once digestion was complete. For cloning of digested insert DNA into digested plasmids with complementary overhangs, 400 U of T4 DNA ligase (NEB) was used in a 15 µl reaction volume. Molar ratio of vector to insert was usually 1xinsert:1xvector (insert size = vector size) or 3xinsert:1xvector (insert size < vector size), and 50 ng vector was used. The complete construct in pCR2.1-TOPO® was then cut using the enzymes BamHI and NotI and ligated into PcDNA™3 (Invitrogen). At all

individual steps plasmids were transformed and plasmids extracted as described in Sections 2.2.1.1.2. and 2.2.1.1.3.. Constructs were sequenced in PcDNA^{TM}3.

2.2.2. Arl1

2.2.2.1. Generation of Arl1 expression constructs and production of transgenic *Drosophila*

Drosophila wild type, mutant T30N, mutant Q70L and mutant L60P cDNA constructs were cloned into the pOT2 vector by Dr Janet Kenyon. These constructs were used to clone the consensus sequence for a HA-tag in frame with the various Arl1 inserts at the 3'end. A SpeI site was engineered at the 5' end (Forward primer: 5'- GAGCTACTAGTATGGGTGGGGTGCT-3') and an HA-tag, stop codon and EcoRI site were added at the 3' end (Reverse primer: 5'-GTCAGGAATTCCTAAGCATAATCTGGAACATCATATGGATACTTGCGACTCTGCAG GGTG-3'). These restriction sites were necessary to move the constructs into the mENTRY® Gateway® vector (Invitrogen). Wild-type Arl1 HA-tagged constructs and non-HA-tagged constructs were generated to analyse viability with and without the C-terminal HA-tag. The forward primers for the non HA-tagged construct were identical to HA-tagged construct, however the reverse primer was as follows: 5'-GTCAGGAATTCCTACTTGCGACTCTGCAGGGG-3'. Basic cloning principles were used as described in Section 2.2.1.1. The constructs were cut out of vector pOT2® using enzymes SpeI and EcoRI and were ligated into mENTRY® Gateway® vector which had also been digested with the equivalent enzymes. The constructs in mENTRY® were transferred to the destination Gateway® vector pBID-UASC-G via the enzyme LR clonase II (Invitrogen) using manufacturer's instructions. Constructs in pBID-UASC-G Gateway® vector (Arl1-wild-type (WT), Arl1-WT::HA, Arl1-Jab::HA, Arl1-Q70L::HA and Arl1-T30N::HA) were sent for PhiC31 integrase-mediated site specific transgenesis using the VK37: (2L) 22A3 docking site. This service was conducted by GenetiVision.

2.3. DNA sequencing

The concentrations of all DNA samples were measured using the NanoDrop™ ND-1000 spectrophotometer (Thermo Scientific) at spectrophotometric absorbance at 260 nm. Sample purity was determined from the ratio of the readings at A260 nm and A280 nm. An A260/A280 ratio of 1.8 or greater for DNA and 2.0 or greater for RNA was taken to indicate an acceptable level of purity. All sequencing reactions were performed by Beckman Coulter Genomics Inc. or the University of Oxford, Department of Biochemistry Sequencing Facility.

2.4. RNA extraction and cDNA synthesis

Whole brains were dissected with Rnase-free instruments. Whole brains were stored in RNA*later*® (Qiagen) at -20°C until RNA extraction. RNA was extracted by homogenising (Bio-Gen, Pro 200 Homogeniser) half a brain in RLT lysis buffer provided in the RNeasy® Mini kit (Qiagen) including β-mercaptoethanol (β-ME) according to the manufacturer's instructions. After washing with wash-buffer provided, RNA was eluted in DEPC-treated water at a final volume of 20µl and the yield of approximately 1µg/mg tissue.

Adult *Drosophila* were stored at -80°C until RNA extraction. RNA was extracted by first disrupting adult *Drosophila* using a pestle in QIAzol® lysis reagent provided in the miRNeasy® Mini kit (Qiagen) according to the manufacturer's instructions. Then tissue was homogenising using a QIAshredder (Qiagen) spin column. Homogenate was treated with chloroform and after spinning the upper phase was collected which was subsequently mixed with 100% ethanol. Solute was applied to the miRNeasy® Mini spin column. After washing with wash-buffer provided, RNA was eluted in DEPC-treated water at a final volume of 20µl and the yield of approximately 500ng/mg tissue.

Total RNA for both mouse and *Drosophila* tissue was reverse transcribed using Expand reverse transcriptase (Roche) according to the manufacturer's instructions. Briefly, 1.0 µg of RNA, RT buffer (1x), DTT (10mM), dNTPs (1mM each), expand reverse transcriptase (50U)

and RNasin® (20U) were used per reaction and incubated for 1hour at 42°C. Oligo dts (100pmoles) were used for amplification. 1 µl product was used in subsequent PCR reactions.

2.5. Polymerase chain reaction (PCR)

2.5.1. PCR for cloning

Standard PCR reactions were conducted using the Expand High Fidelity PCR System (Roche). For a 50 µl reaction 2.6U of Expand High Fidelity enzyme mix and appropriate buffer 1x, 300nM of each primer, 200µM each dNTP (Roche) and approximately 100 ng of DNA template were added. Cycling conditions were as follow: 2 minutes denaturation at 94^{o}C, 35 cycles of 15 seconds at 94^{o}C, 30 seconds annealing and 30seconds - 4minutes extension at 72 ^{o}C (depending on size of amplification product), and then a final extension at 72^{o}C for 10 minutes, followed by 10 minutes at 4^{o}C. The annealing temperature was adapted to the primers used but started at 55^{o}C initially and was optimised to 60^{o}C for most primers. The extension time varied depending upon the size of the PCR product and was typically 1min/kb DNA. The products were mixed with DNA loading buffer and analysed using gel electrophoresis.

2.5.2. PCR for bacterial colony screening and genotyping

Colony PCR and genotyping PCR was conducted using MegaMix-Blue (Microzone Limited) which already contained all components except for primers and DNA. 300nM of each primer were added and a single bacterial colony or 1-2µl of extracted DNA.

2.5.3. PCR for A-tagging

A tagging for TA-cloning strategies was conducted using Taq DNA polymerase (Invitrogen) and following manufacturer's instructions. Only 200µM dATPs were included.

2.5.4. Semiquantative PCR

1µg of total cDNA was used per reaction with 29 cycles for *Gnptab* PCR and 16 cycles for *18S* PCR. Cycling conditions were optimised in order to remain below saturation. Primers were used at 200nM after optimisation of concentration to minimise primer-dimer formation.

Samples were run in duplicates and sample loading was normalised to the *18S* loading control. Blots were analysed using Image J and bands were quantified.

2.5.5. Quantitative RT-PCR (qPCR)

mRNA levels were analysed by qPCR using 1 µl of a 1/10 dilution of *Drosophila* cDNA in 20 µl reactions using SYBR® Green (Applied Biosystems) and a StepOnePlus™ real-time PCR machine (Applied Biosystems). Details of the primers used for qPCR can be found in appendix 2. Cycling conditions: 95˚C 10 minutes, 40 x [95˚C 15 seconds, 60˚C 1 minute], 95˚C 15 seconds. Three technical replicates per reaction were performed. Primers were used at 200 nm, after optimisation of concentration to minimise primer-dimer formation and yield low Ct values. Primer efficiencies were estimated by performing qPCR on serial dilutions of at least two independent cDNA samples. *Ribosomal protein 49 (RP49)* was used as reference genes for *Drosophila* samples. Relative gene expression was calculated using the comparative Ct (ΔΔCt) method: ΔCt = Ct *gene of interest* – Ct *RP49*, and ΔΔCt = ΔCt experimental sample – ΔCt control sample, with relative expression given using the formula 2-ΔΔCt.

Table 2.1. Primers used for qPCR

Target	Organism	Forward (5'-3')	Reverse (5'-3')
Gnptab	Mouse	GGCCTCAGAGTCAGAAAG	CAACGCAAGCATAAAACAGC
18S	Mouse	GCGGCTTGGTGACTCTAGAT	CCCTCTCCGGAATCGAAC
Arl1	*Drosophila*	CGGACGCAATCATCTATGTG	CGCCAATAAGGTCTAATACTTGTC
ILP2	*Drosophila*	CGACAGCGATCTGGACGCCC	AGGGCACTTCGCAGCGGTTC
ILP3	*Drosophila*	GGCCGCAAACTGCCCGAAAC	ACGGGGTCCAAAGTTCTCTTGGT
RP49	*Drosophila*	TACAGGCCCAAGATCGTGAA	TCTCCTTGCGCTTCTTGGA

2.6. Gel electrophoresis

DNA was mixed with a 6 X DNA loading buffer (0.25% bromphenol blue, 0.25% xylene cyanol, 15% Ficoll) and separated on agarose gels including 1 in 20,000 10 µg/ml ethidium bromide to allow visualisation of DNA under UV light (Typically, 0.8% (w/v) agarose (Sigma) was used for PCR products over one kb and 2% agarose (Sigma) for 500 bp and lower).

Agarose was dissolved in 0.5 X TBE (0.09 M Tris, 0.09 M boric acid, 2 mM EDTA) and a 100 bp or 1 kb ladder (NEB) was run alongside the DNA samples to allow size determination. Gels were run in 0.5 X TBE at 90-120 volts for 1 hour. Images were visualised and recorded on the Gel Doc™ digital imaging system (Bio-Rad).

2.7. Cell culture and transfections

Human embryonic kidney (HEK) 293 cells were maintained in a 37°C incubator humidified with 5% CO2. Cells were grown in DMEM supplemented with 10% foetal calf serum (FCS; PAA Laboratories), 2 mM glutamine and 0.1 mg/ml penicillin and streptomycin (Invitrogen). For immunofluorescence, HEK 293 cells were seeded onto poly-L-lysin-coated glass coverslips in 6-well plates at a density of approximately 0.5 x 10^5 cells per ml 24 hours prior to transfection. For protein extraction, HEK 293 cells were seeded in 6-well plates at a density of approximately 2.5 x 10^5 cells per ml 24 hours prior to transfection. Cells were transfected with 2 μg DNA and FuGENE®-6 (Roche) as a ratio of 1:3 (DNA:FuGENE®) for 24 hours; for co-transfections 1 μg of each construct was used.

12.5 day old embryos were dissected out of the uterus under sterile conditions. The heart and liver were removed and the remainder of the tissue was minced and trypsinised for 10 minutes at 37°C. DMEM containing 10% FCS (PAA Laboratories) was added to cells and cell debris was removed by centrifugation. Cells were resuspended in fresh medium and plated. The media was changed after 24 hours. Mouse embryonic fibroblasts (MEFs) were cultured in DMEM supplemented with 10% FCS and penicillin/streptomycin.

2.8. Protein extraction

Whole brain was dissected and half was homogenised using a rotor in cold lysis buffer (10mM Tris-HCL pH8, 10mM NaCl, 1mM EDTA pH8, 1%Triton™ X-100) and protease inhibitors (Roche Molecular Biochemicals).

HEK cells and MEFs were washed with phosphate buffered saline (PBS) and lysed in lysis buffer supplemented with protease inhibitors (Complete, Roche Molecular Biochemicals).

Ten adult *Drosophila* were homogenised using a pestle in 200µl cold lysis buffer or RIPA buffer (50 mM Tris-Cl, pH 8.0, 150 mM NaCl, 0.1% SDS, 1% sodium deoxycholate, 1% Triton^{TM} X-100) and protease and phosphatase inhibitors (Cell signalling).

All detergent extracts were incubated at 4°C for 1 hour and clarified by centrifugation at 14,000 rpm for 30 minutes. Protein concentration of the lysates was determined by BCA assay (Pierce Biotechnology) following manufacturer's instructions. Equal amounts of protein were loaded on polyacrylamide gels and analysed by western blot as described below.

2.9. Western blot

Protein lysates were boiled for 5 minutes at 95°C with an equal volume of 2 × SDS sample buffer (0.125 M Tris, pH 6.8/4% SDS/5% β-mercaptoethanol/60 µM bromophenol blue/20% glycerol) before separation on acrylamide gel (for 10 ml of 10% resolving gel: 4 ml H_2O, 3.3 ml 30% acrylamide mix, 2.5 ml 1.5 M Tris pH=8.8, 0.1 ml 10% SDS, 0.01 ml 10% ammonium persulphate [APS], 0.001 ml tetramethylethylenediamine [TEMED; Severn Biotech Ltd]. For 3 ml stacking gel: 2.1 ml H_2O, 0.5 ml 30% acrylamide mix, 0.38 ml 1 M Tris pH=6.8, 0.03 ml 10% SDS, 0.01 ml 10% APS, 0.01 ml TEMED). It was run at 100 V for 20 minutes and then at 120 V for ~1 hour. All samples were transferred onto PVDF membranes (Amersham) overnight at 4°C at 50V. Membranes were blocked for 1 hour at room temperature (RT) in 5% powdered milk in Tris-Buffered Saline (TBS, 50mM Tris, 150mM NaCl) containing 0.1% Tween 20 (TBST). Membranes were incubated with primary antibodies for 1 hour at RT or overnight at 4°C. Membranes were washed three times in TBST and then were incubated with a horseradish peroxidase-conjugated anti-mouse, anti-rabbit or anti-rat secondary antibody (Amersham Biosciences) at 1 in 5,000 dilution in TBST for 1 hour at RT. The membranes were washed three times for 15 minutes in TBST and the immunoreactive proteins were visualised using the ECL Western Blotting Detection Reagent kit (GE Healthcare) according to the manufacturer's instructions, using Kodak X-OMAT AR film (Kodak, Rochester, NY) or ImageQuant LAS400 (GE Healthcare). Band intensity relative to internal controls was carried out using ImageJ software. Primary antibodies used were as follow: rat anti-Lamp1 (Abcam, 1:200); rabbit

anti-Npc2 (Santa Cruz, 1:200); rabbit anti-HA (Roche, 1:1,000); mouse anti-β-tubulin (Sigma, 1:1,000); rabbit anti-kinesin (Cytoskeleton,Inc., 1:1,000); rabbit anti-Akt (Cell Signalling, 1:1,000) and rabbit anti-pAkt (Cell Signalling, 1:1,000).

2.10. Immunocytochemistry

Twenty-four hours post transfection, cells were washed with PBS solution at RT, fixed in 4% paraformaldehyde (PFA) in PBS for 15 minutes, permeabilised in 0.2% Triton X-100 in PBS for a further 15 minutes and washed in PBS. Coverslips were blocked with 1% bovine serum albumin (BSA) for 30 minutes, followed by incubation with primary antibody diluted in 1% BSA for 1 hour both at RT. The coverslips were washed in PBS and incubated with Alexa Fluor® conjugated secondary antibody diluted in PBS for 45 minutes at RT. Sections were mounted in DAPI containing fluorescent mounting media. Images were viewed on a Zeiss Axioskop 2 microscope, acquired using an AxioCam HR digital camera (Zeiss) and processed using AxioVision software (Zeiss) and Adobe Photoshop. Primary antibodies used were as follow: rabbit anti-myc (Abcam, 1:300); mouse anti-GM130 (Abcam, 1:250) and mouse anti-PDI (Abcam, 1:100).

2.11. Immunohistochemistry and more general staining methods

2.11.1. Immunofluorescence

Brains were removed from PFA perfused mice and post-fixed in 4% PFA overnight followed by cryoprotection with 10% sucrose and 30% sucrose over-night. The sucrose protected brains were embedded in optimal cutting temperature (O.C.T.) compound and sagittal sections are cut at 15 µm using a cryostat. Perfused brain sections were re-hydrated followed by antigen retrieval by boiling in 10mM sodium citrate pH 6.0 for 20 minutes. Slides were blocked for 1 hour in PBS containing 5% BSA and 0.5% Tween-20, and incubated overnight (Sigma, anti-GFAP; 1:200) or two nights (Swant, anti-D28K; 1:10,000) at 4°C with primary antibodies. After washes in PBS, anti-D28K sections were processed using the VECTASTAIN® ABC Elite (Vector Labs) kit and appropriate secondary antibodies. Slides were stained using the

ImmPACT® DAB substrate kit (Vector Labs), de-hydrated and mounted in Histomount®. Anti-GFAP sections were incubated with Alexa Fluor® conjugated secondary antibody for 1 hour, washed with PBS and mounted in fluorescent mounting media. Slides were imaged as described above. Anti-GFAP staining was conducted by Dr Emmanuel Bitoun.

Larval CNS, fat body and gut were dissected in Grace's Insect Medium, fixed for 10 minutes (20 minutes for the fat body) in 4% PFA in PBS and washed in PBS supplemented with 5% Triton X-100 and 10% horse serum (PBT). Samples were incubated sequentially in primary and secondary antibodies overnight. Hoechst 33342 (Life technologies; 1:1,000) was used to label DNA. Samples were imaged using a Zeiss LSM 510 META confocal microscope. Primary antibody used was mouse anti-repo (Developmental Studies Hybridoma Bank, 1:200). Secondary conjugated antibodies used were as follow: Alex Fluor 647 conjugated Phalloidin (Molecular Probes, 1:200) and TRITC conjugated HRP (Jackson, 1:200). After drying, clear nail polish was applied to the edges of the slides, and slides were stored at 4°C.

2.11.2. Muscle histology

For neuromuscular junction staining, fresh dissected muscles were teased apart, and placed in PBS/0.2 Triton X-100 with an appropriate dilution of Alexa Fluor® 488 conjugated α-bungarotoxin (Invitrogen) overnight at 4°C. The teased muscle samples were subsequently washed in PBS three times, before being further teased apart, placed on a slide, and covered with Histomount® (National Diagnostics) and a coverslip.

All muscle histology experiments were conducted by Dr Janet Kenyon and Benjamin Edwards.

For fibre composition analysis, fresh dissected muscles were placed in O.C.T., cut in 15µm sections on the cryostat, and stored at -80°C. Muscle sections were blocked in 5% BSA/PBS/0.3% Triton™ X-100 at RT for 1 hour. Incubation with primary antibodies diluted in 5% BSA/1X PBS/0.3% Triton™ X-100 was conducted overnight at 4°C or for 2 hours at RT. Muscle sections were then washed in PBS, followed by incubation with appropriate Alexa

Fluor® secondary antibodies at appropriate dilutions for 1-3 hours at RT. Brain sections were subsequently washed with PBS, and covered with VECTASHIELD® Mounting Medium with DAPI (Vector Lab) and a glass coverslip. After drying, clear nail polish was applied to the edges of the slides, and slides were stored at 4°C. Primary antibodies and dilutions used include: mouse anti-MYHC1 (1:200, B8-F8, German Collection of Microorganisms and Cell Cultures); mouse anti-MYHC2A (1:200; SC-71, German Collection of Microorganisms and Cell Cultures); and mouse IgM anti-MYHC2B (1:100, BF-F3, German Collection of Microorganisms and Cell Cultures). Slides were imaged as described above.

2.11.3. p-Phenylenediamine staining

p-Phylenediamine (PPD) staining was conducted by Dr Janet Kenyon. Sciatic nerves were dissected from 3 month old mice and fixed overnight in PBS with 4% PFA, cryoprotected in 30% sucrose, embedded in O.C.T. compound (VWR chemicals), sectioned, and stained with 2% PPD in 50% ethanol. Images were viewed on a Zeiss Axioskop 2 microscope, acquired using an AxioCam HR digital camera (Zeiss) and processed using AxioVision software (Zeiss) and Adobe Photoshop.

2.11.4. Haematoxylin and Eosin (H&E) staining

Peripheral tissue such as trachea and pancreas were dissected, fixed overnight in 4% PFA and cryoprotected in 30% sucrose. Tissue was then embedded in O.C.T. and sectioned at 10 µm. Slide-mounted sections were air dried, fixed in 100% ethanol for 30 seconds. The tissue sections were stained with haematoxylin for 15 minutes followed by eosin for 2 minutes for histopathological examination. Sections were then rinsed in water, dehydrated through EtOH dilutions (70%, 90% and 100%), cleared in Histo-Clear® II (National Diagnostics) and finally mounted in Histomount®. Slides were imaged as described above.

2.11.5. Luxol fast blue staining

Fresh frozen brain sections were air dried and hydrated with 95% ethyl alcohol. Sections were incubated at 56 °C overnight in 0.1% luxol fast blue solution (Solvent blue 38, Sigma). Excess stain was rinsed off with 95% ethyl alcohol followed by distilled water. Slides were differentiated in 0.05% lithium carbonate solution for 2 minutes followed by 70% ethyl alcohol for 1 minute and rinsed in distilled water. This step was repeated three times until the gray matter was clear and the white matter sharply defined. The slides were rinsed in distilled water and differentiated in 95% ethyl alcohol for 5 minutes. Slides were de-hydrated through a series of EtOH (70%, 90% and 100%), cleared in Histo-Clear® II and mounted in Histomount®. Slides were imaged as described above.

2.11.6. Periodic acid Schiff stain and filipin staining

Periodic acid-Schiff (PAS) staining was carried out using a PAS Kit (Sigma St. Louis, MO, USA) as instructed by the manufacturer. Filipin complex (Sigma, St. Louis, MO, USA) was used at a working concentration of 10 µg/ml. Brain sections were incubated for 3 hours at RT in the dark. Slides were imaged as described above.

2.11.7. Nile red staining

Wandering third instar larvae were dissected in Grace's Insect Medium, fixed for 20minutes in 4% PFA in PBS and washed in PBT. These were then stained with Nile red (0.5µg/ml, Sigma) for 30 minutes. After washing twice with PBT, the samples were imaged using a Zeiss LSM 510 META confocal microscope. The size of lipid droplets, adipocytes and the number of lipid droplets per cell were measured using Image J by measuring their boundaries by hand. The 6-10 largest lipid droplets in every fat body cell were quantified and their average size was counted as the lipid droplet size for each cell. A total of ten cells from 3 images were measured for each genotype.

2.12. Lysosomal enzyme assay

Blood sera were collected from adult wild-type (n=8), *nym* (*nym*/+) (n=8) and *nym* homozygous (*nym/nym*) mice (n=6) at 12 weeks of age by severing the jugular vein after CO_2 narcosis. Blood sera was separated by centrifugation and stored at -20°C until assayed. Brain homogenates were prepared as described in section 2.8. Activities of ß-hexosaminidase were assayed with 5mM 4-Nitrophenyl N-acetyl- ß-D-glucosaminide (Sigma), ß-galactosidase with 5mM p-Nitrophenyl-ß-D-galactopyranoside (Sigma), ß-glucuronidase with 5mM 4-Nitrophenyl ß-D-glucuronide (BioChemika), α-mannosidase with 5mM 4- Nitrophenyl α-D-mannopyranoside (Sigma), β-mannosidase with 5mM 4- Nitrophenyl β-D-mannopyranoside (Sigma), α-galactosidase with 5mM 4-Methylumbelliferyl-α-D-galactopyranoside (Sigma) and β-Glucocerebrosidase with 5mM 4-Methylumbelliferyl-β-glucoside. Blood sera and brain lysate were incubated with 5mM substrate at 37°C for 1 hour. Reactions were stopped by addition of 0.1 M glycine NaOH solution (pH 10.3) and the fluorescence was read at 399nm. Activities were expressed as nanomoles of substrate cleaved (e.g. hydrolyzed nitrophenyl) per mg of protein per hour.

2.13. Triacyglyceride assay

To determine total triacylglycerides, ten 5-day old male flies were homogenised in 200µl lysis buffer (10mM Tris-HCL pH8, 10mM NaCl, 1mM EDTA pH8, 1%Triton™ X-100), incubated at 70°C for 10 minutes and then centrifuged at 1200 rpm for 5 minutes. The supernatants were incubated with Infinity™ Triglycerides liquid stable reagent (Thermo Scientific) at 37°C for 5 minutes and absorbance was measured at 500nm wavelength. Triglyceride levels were normalised to fly/larval wet weight.

2.14. Animal husbandry

2.14.1. Mice, genotyping and treatment

Animal work was approved by the University of Oxford Ethics Panel and was carried out in accordance with UK Home Office regulations (PPL No 30/2792). Mice were weaned at 21 days and kept in same sex groups in controlled conditions (12 h light–dark cycle, at 21–22 °C with

food and water ad libitum). For the investigations in Chapter 3 and 4 only male mice were used. Females were valuable as they were used for breeding purposes and the literature had not highlighted any gender differences in Mucolipidosis II.

The Shakin Steven's (*stv*) mouse mutant was identified from a phenotype driven screen of the progeny from Balb/cAnNHsd N-ethyl-N-nitrosurea (ENU) mutagenised mice crossed to female C3H/HeNHsd produced at the MRC Harwell. The colony was maintained by back crossing against C3H/HeNHsd. The *stv* mouse mutant harboured two mutations. These two mutations were separated out through genetic crossing by Dr Janet Kenyon. Two mice named Jabber (*jab*) mouse (*jab*/+) and Nymphe (*nym*) mouse (*nym*/+) were generated. For genotyping, DNA was extracted from a mouse ear biopsy. The ear notch was incubated in 50 µl of solution A (25mM NaOH, 0.2mM EDTA) at 95°C for 30 minutes and the reaction stopped by addition of 50 µl of solution B (40mM Tris-HCl). The genotype of *nym* individual animals was confirmed by amplifying a 553 base-pair region of *Gnptab* exon 13 from genomic DNA (see Section 2.5.2) followed by digestion with MseI. Genotyping for the presence of the *nym* mutation was carried out using the following primers: *nym* Forward, 5'-GGAGACGGTGACATACAAAAATCT-3' and *nym* Reverse 5'-CACTGGATGCTCTAAGGAAGATAT-3'. The *jab* mutation was identified by PCR and direct sequencing. The heterozygotes were bred together to generate homozygotes. The *jab* homozygote mice were embryonic lethal and the *nym* homozygotes (*nym/nym*) are described in chapter 4 as a novel model of mucolipidosis II. The *jab* mouse was characterised in detail by Dr Janet Kenyon and Dr Emmanuelle Bitoun.

No obvious difference between genders was observed in the *stv, jab, nym* and *nym* homozygote mice therefore equal cohorts of male and females were used in all studies presented in this thesis.

For the 2-hydroxypropyl-β-cyclodextrin drug trial, two groups of 15 *nym* homozygote mice (C3H background) were injected weekly intraperitoneal with either PBS (10µl 1xPBS) or 2-hydroxypropyl-β-cyclodextrin diluted in PBS (4000mg/kg), starting at postnatal day 7 (P7).

After 3 months and 7 months of weekly treatment, motor coordination of the mice was assessed using a rotarod (see Section 2.15.1) (Ugo Basile, Italy) and inverted screen (see Section 2.15.2.).

2.14.2. *Drosophila* stocks, husbandry and genotyping

Stocks were maintained at 25°C under controlled conditions (12 hour light–dark cycle with food and water ad libitum) on standard medium (80g/l maize, 18g/l dried yeast, 10g/l soya flour, 80g/l malt extract, 40g/l molasses, 8g/l agar, 6.6ml acid mix). w^{1118} obtained from the Bloomington Stock Centre, was used as the control strain unless otherwise stated. The Arl1 RNAi line was obtained from the Bloomington Stock Centre (Arf72A,TRiP.JF02378 Bloomington). Tissue and behavioural analysis was conducted on Arl1 mutants and Arl1 RNAi crossed to the ubiquitious *actin*-GAL4 driver. Other stocks were *actin*-GAL4 (Bloomington), *Cg*-GAL4 and $Arl1^{1}$ (Tamkun et al., 1991). For genotyping, DNA was extracted from a whole fly which was homogenised with a pestel in 50 µl squishing buffer (10mM Tris-Cl pH8.2, 1mM EDTA, 25mM NaCl and 200ug/ml Proteinase K). This was followed by an incubation period at 37°C for 30 minutes and at 95°C for 2 minutes to inactivate the proteinase K. Transgenic mutant DNA was sequenced using primers amplifying a 540bp region of the *Drosophila Arl1* gene. Genotyping for the presence of the *Arl1* mutations was carried out using the following primers: *Arl1* Forward, 5'-ATGACTAGTATGGGTGGGGTGCTCAGCTAC-3' and *Arl1* Reverse 5'-CATGAATTCCTACTTGCGACTCTGCAGGGT-3'. DNA was PCR purified (Qiagen) and sent for sequencing.

2.15. Mouse behaviour

2.15.1. Accelerating rotarod test

A commercial rotarod device (Accelerating model, Ugo Basile, Biological Research Apparatus, Varese Italy) consisting of a grooved plastic beam 5 cm in diameter was used. Mice were placed on the beam (revolving at the default 5 rpm) facing in the opposite orientation to rotation. After 1 minute the rod speed was gradually accelerated to a maximum of 30 rpm over 4 minutes by electronic control of the motor. Mice were subjected to an acclimatisation trial one

day before the test trial. The acclimatisation trial and the test trial were in format identical. Mice ran three individual trial runs on the rotarod apparatus with 10 minutes rest in between each trial. The maximum trial length was 4 minutes. Latency to fall in each trial was recorded, and overall performance of each mouse was expressed as a mean of the 3 scores.

2.15.2. Inverted screen test

A 90cm^2 screen of wire mesh consisting of 12mm^2 of 1mm diameter wire surrounded by a 10 cm deep wooden frame was used. The mouse was placed in the centre of the wire mesh screen and the stopwatch started. Immediately the screen was rotated to the inverted position over 2 seconds, with the mouse's head declining first. The screen was maintained 27 cm above a padded surface. In between each trial the mice had a resting time of 10 minutes. Latency of how long the mice remained upside down on the screen was measured; with a maximum score of 180 seconds. Overall performance of each mouse was expressed as a mean of the 3 scores. The mice were pre-trained the day before with three trials identical to the test trials in design.

2.15.3. Spontaneous alternation Y-Maze

Maze testing was carried out as previously described (Barkus et al. 2012). Briefly, a Y-maze that had 3 arms with glass persplex walls was employed (Figure 2.1). Mice were habituated to the Y-maze for 5min but only allowed to enter two of the arms, the third one being closed off. After 5 minutes, the mice were placed back into the home cage for 5 minutes. After this period the mice were placed back into the Y-maze with all arms open. The mice were placed into the same start arm as for the habituation period and left to explore the three arms for 2 minutes and the time spent by each mouse in each arm was measured. Percentage of alternation was calculated by using the equation in figure 2.1. Entrances into the start arm were ignored. To control for any bias in arm preference, a different start, novel and familiar arm was chosen for each mouse.

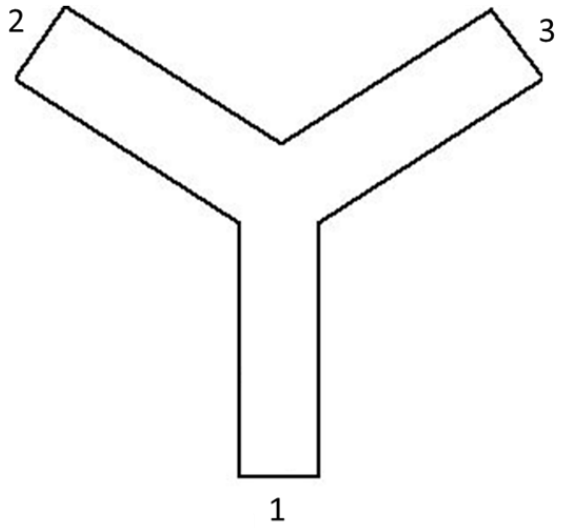

$$\% = \frac{Novel\ Arm}{Novel\ Arm + Familiar\ Arm} \times 100$$

Figure 2.1. Diagram of the Y-Maze set-up
Left side: Diagram of the Y-Maze set-up. Habitation was conducted in two of the arms and a different start arm was chosen to control for any arm preference. Right side: Equation to calculate % Alternation.

2.15.4. CatWalk^{TM} automated quantitative gait analysis

The Noldus CatWalk^{TM} System (Hamers et al. 2001) was employed to analyse the gait of the *nym* homozygous mice. A CCD camera recorded the mice from below traversing a glass floor in a dark room. The corridor walkway contains a sheet of glass encased with a fluorescent light. The optical properties of the glass result in internal reflectance of the light unless an external contact is made with the glass. When the paw is placed on the glass and applies pressure, the light changes the dynamic property of the glass and allows the light to escape internal reflectance. This illuminates the source of pressure with luminescence proportional to the intensity of pressure (Hamers et al. 2006). Wild-type littermates, *nym* and *nym* homozygous mice were placed in the corridor 10 cm wide by 90 cm long and allowed to freely move (movable wire gates prohibited the mice from exiting the walkway). As the mouse enters the field of view, a run is recorded and saved on a computer attached to the camera. If the mouse exited the field of view within 25 seconds and there was less than a 60% variation in speed, the run was compliant. Furthermore, runs were only considered if the mouse did not stop, change direction, or in any other way did not satisfactorily cross the field of view. Three compliant runs by the animals were needed for analysis and termed a trial. Between each trial, the walkway

barrier was removed and the glass was cleaned to remove any excrement or smell from the preceding trial. After each trial, the acquired data was classified. Classification is characterised by the semi-automated process of entering which limb (RH _ Right Hind, LH _ Left Hind, RF _ Right Front, LF _ Left Front) induced the recorded print and, if necessary, the print size was adjusted.

The following parameters were analysed: (i) The regularity index acts as a measure of generalised coordination (Hamers et al. 2006) by computing whether the mouse footfalls fall within regular step patterns. As the animal becomes less coordinated, there becomes an increase in missteps which results in a lower regularity index (Hamers et al. 2001). Gait regularity tests how consistently the mouse takes "normal strides" compared to "abnormal strides." Normal strides are considered to occur when either the right front paw is paired with the left hind paw or when the left front paw is paired with the right hind paw. Abnormal strides consist of any other configuration and is broken down into various "support categories" such as "one" where one paw is the only base of support, "three," "four," "lateral,", "diagonal" or "zero" with the later counting when the mouse is no longer supporting its weight through its limbs. These support subcategories were also analysed. Figure 2.2 graphically depicts step cycle, stand and swing. (ii) Stand is the duration of contact with the glass plate of the print. (iii) Single stance is the duration (in seconds) of ground contact for a single paw (Coulthard et al. 2003). (iv) The stand index is a measure for the speed at which the paw loses contact with the glass plate. (v) Swing is the duration in seconds of no contact of a paw with the glass plate.

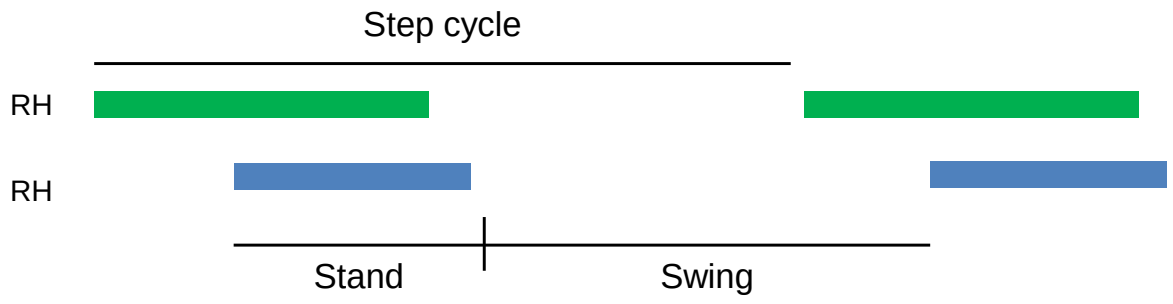

Figure 2.2. Step Cycle, Stand and Swing diagram
RH: Right hind. (Adapted from Noldus CatWalk^{TM} 9.1. Manual).

(vi) The phase dispersions parameter describes the temporal relationship between placement of two paws within a step cycle. It is used as a measure of inter-paw coordination. In wild-type animals, for the diagonal paw pairs (RF-LH, LF-RH) the target paw typically moves synchronously with the anchor so the initial contacts occur simultaneously resulting in a phase dispersions value of 0%. Girdle pairs (RF-LF, RH-LH) usually yield a phase dispersions value of 50% when walking at a moderate speed (Kloos et al. 2005). (vii) The base of support (BOS) is the average width between either the front paws or the hind paws. (viii) Stride length measures the distance from the previous position of a hind limb to the current position of the forelimb on the same side. (ix) The body speed of a step cycle of a specific paw is calculated by dividing the distance that the animal's body travelled from one initial contact of that paw to the next by the time to travel that distance. (x) Body speed variation (%) is calculated by dividing the absolute difference between the body speed and the average speed of a run by the average speed.

2.16. *Drosophila* behaviour

2.16.1. Rescue experiment null

Rescue experiments were conducted by Dr Stuart Grice. Rescues were performed to confirm the functionality of the wild-type *UAS-Arl1* and *UAS-Arl1*::HA fly stocks. Ubiquitous expression was generated using the 1032-GAL4 driver. To create the stocks the double balancer stock w^{1118}*; sp/cyo; mkrs/Tm6B* was also used. Ultimately, *1032-GAL4/1032-GAL4;+/+;* $Arl1^{1}$*/Tm6B* flies were crossed to w^{1118}*; UAS-Arl1/UAS-Arl1; Arl11/Tm6B* and w^{1118}*; UAS-Arl1::HA/UAS-Arl1:HA; Arl11/Tm6B* to test the wild-type Arl1 and Arl1::HA stocks respectively. The number of larvae that reached pupation, and eclosed, were scored for each construct and compared to w^{1118}*;* $Arl1^{1}$*/* $Arl1^{1}$ flies.

2.16.2. Developmental analysis

All stocks were cultured on standard molasses/maize meal and agar medium in plastic vials or bottles at 25˚C under a 12 hour light/dark cycle. Adult viability assays were conducted by crossing 20 female *actin*-GAL4 driver stocks (a ubiquitous driver) to 10 males harbouring *Arl1*

mutant overexpression, Arl1-RNAi or to w^{1118} for controls for 4 hours on apple juice plates with yeast to ensure similar ages. Twenty embryos per plate were then counted and lined on apple juice plates with yeast and the development of the larvae and pupae was quantified daily until hatching of flies. Number of flies hatched was quantified for each genotype.

Pupal cases were scored 4 days post-eclosion (latest 16 days after egg laying) on how many cases presented with complete hatching, incomplete hatching or an inability to hatch at all.

2.16.3. Survival assays adult flies and larvae

All stocks were cultured on standard molasses/maize meal and agar medium in plastic vials or bottles at 25˚C under a 12 hour light/dark cycle. Breedings were set up using 20 female *actin*-GAL4 virgins and 10 male *Arl1* mutant, Arl1-RNAi or w^{1118} for controls. They were left to lay eggs for 4 hours on apple juice plates with yeast to ensure similar larvae development. Once flies hatched, female and males were separated into new plastic vials and survival was analysed. Flies were flipped every 3-4 days and the number of dead flies quantified.

2.16.4. Weight and length measurements

Weight of 10 flies batched in an Eppendorf tube was weighed on an Analytical Balance AB104-S (Mettler Toledo). Six batches for each genotype and gender was quantified. Images of 30 flies per genotype and gender were captured using a standard canon camera. Measurements from head to bottom were quantified to describe the length and mid-body width described as width. Measurements were quantified using Image J.

2.16.5. Locomotor function assay

Age-matched (1-5 day old) male flies were placed individually in a 5 mm glass activity tube containing a food source (5% sucrose (Sigma) and 2% Bacto agar (BD) in distilled water) at one side and a plastic cover with an air hole at the other. The individual glass tubes were placed into the activity monitor (Trikinetics monitors DAM2, Trikinetics Inc.) and supported with rubber bands to hold them in place. Locomotor activity was recorded when the flies crossed the infrared light beam at the middle of the glass tubes. Thirty flies were used per genotype and

kept under controlled conditions (12 hour light–dark cycle at 25°C) for 4 days, day one being excluded for habituation. Data was collected by the DAM System collection software. The raw binary data is processed using DAM Filescan102X (Trikinetics, Inc.) and summed into 1 hour bins.

2.17. Statistics

Data sets were statistically analysed using either a two-tailed Student's test or a 1-way ANOVA with Dunnett's multiple comparison test. Normal distribution is assumed for these tests and was confirmed using the Shapiro-Wilk test. The two-tailed Student's test was used when comparing two data sets whereas the 1-way ANOVA was used when comparing three data sets or more. In the rare case that the data was not normally distributed as shown in the Inverted screen test comparing two samples (Figure 4.7 B), the Mann-Whitney U test was used and in the Inverted screen test comparing more than two samples (Figure 3.6), the Kuskal-Wallis 1-way ANOVA was used, which both have more statistical power for not normally distributed data. GraphPad Prism 5 software was used for all statistical analyses. Means±SEM are plotted for all graphs unless otherwise stated.

3. Analysis of the disease causing mutation in the Shakin' Stevens mouse

3.1. Introduction

The Davies group is exploiting the MRC Harwell ENU mutagenesis programme to uncover novel genes and pathways involved in neurological disease. As described in Section 1.2.2.1 of Chapter 1, ENU mutagenesis is a powerful approach to identify novel genes through the screening of mutants for movement disorders. The Davies group select mutant mice that have shown abnormal gait or behavioural phenotype in the SHIRPA assay undertaken at MRC Harwell. The mutants are then further examined for brain abnormalities or muscle pathology.

When this work began, the Shakin' Stevens mouse (Stevens (*stv*) mouse from here onwards) was identified through the SHIRPA test by its smaller size and tremor. The MRC Harwell had also shown that there were abnormalities at the neuromuscular junction (NMJ), which was confirmed by Dr Janet Kenyon and Benjamin Edwards. The *stv* mouse also presented with hind limb clasping, reduced muscle strength, demyelination, muscle pathology, a 2-3 fold increase in hydrolase activity in the blood sera and a normal lifespan. Interestingly, the *stv* mouse presented with two protein coding mutations, the chances of this being very rare (Keays et al. 2006). Haplotype analysis localised the *stv* mutations to a genetic interval of 6 Mb on mouse chromosome 10, between markers *D10Mit42* and *D10Mit178. PCR and* direct sequencing of all 28 protein-coding genes within the interval, including exonic regions and exon-intron boundaries, revealed two non-synonymous heterozygote point mutations in exon 13 of the *Gnptab* gene and exon 5 of the *Arl1* gene.

Using genetic crossing the two mutations were separated into individual mouse strains. Firstly, the Jabber (*jab*) mouse (*jab*/+), which harbours a missense mutation in the *Arl1* gene encoding for a small GTPase, as of yet not studied in a mammalian organism. Arl1 has been implicated in the regulation of vesicular transport and membrane trafficking but also recently in production of lipid droplets and chylomicrons, key players in lipid homeostasis (Hesse et al. 2013). Therefore it was of interest to elucidate the function of Arl1 in linking lipid trafficking

and neurodegeneration. Secondly, the Nymphe (*nym*) mouse (*nym*/+), which harbours a truncation mutation in the *Gnptab* gene important for correct targeting of lysosomal hydrolases to the lysosome and implicated in the autosomal recessive disorder mucolipidosis (ML) II (Kudo et al. 2005). Lysosomes are crucial components of the autophagic-lysosomal degradation pathway, which has been shown to be involved in the majority of neurodegenerative diseases (Nixon 2013). Both genes have been reviewed in Section 1.3.1 and 1.3.2 of Chapter 1 and are very interesting to study further in order to elucidate novel pathways in neurodegeneration. Based on knowledge of the genes of interest, it is anticipated that the *jab* mutation might be causing the dominant phenotype in the *stv* mouse since it has been shown to be lethal in *Drosophila* when knocked out. The *Gnptab* gene has been implicated in MLII due to homozygous or compound heterozygous nonsense or frameshift mutations, showing the necessity of both alleles to be defective. Therefore, a potential recessive phenotype is anticipated in this mutant and hypothesised not to cause the dominant phenotype in the *stv* mouse.

3.1.1. Aims of the chapter

The aim of this chapter was to determine which mutation, the *jab* or the *nym* mutation (or both), is responsible for the phenotype seen in the *stv* mouse (*jab*/+;*nym*/+). To this end, the two newly generated mouse lines were studied individually and their phenotypes compared to that of the *stv* mouse. These results may help elucidate which pathway is involved in causing the neurodegenerative phenotype observed in the *stv* mouse, and are therefore of interest in the context of neurodegenerative disease. This part of the thesis was carried out together with Dr Janet Kenyon.

The mouse phenotypes will be characterised in the following ways:

- **Analysis of the individual mutations by DNA sequencing**
- **Size and behavioural defects of the *nym* and *jab* mice** will be assessed through measurements of: weight to assess growth retardation, extension by the tail to assess hind limb clasping and inverted screen performance to assess muscle strength.
- **Myelination, NMJs and muscle pathology will be assessed in the *nym* and *jab* mice.** Hind limb clasping and tremor are parameters that indicate pathology of the nervous system, hence the peripheral nervous system (PNS) was analysed for any defects that could lead to the tremor.
- **Analysis of lysosomal hydrolase activity in blood sera in the *nym* and *jab* mice** will be assessed as the *stv* mouse presented with a 2-3 fold increase in lysosomal activity in the blood sera.

3.2. Results

3.2.1. The *stv* mouse has a truncation mutation in the *Gnptab* gene and a missense mutation in the *Arl1* gene

Genotyping of the *jab* mouse was conducted by amplifying a 347bp region of exon 5 and PCR products were sent for sequencing. The *Arl1* point mutation causes a base pair change from T to C in exon 5. This affects the open reading frame, mutating leucine 61 to a proline residue (Figure 3.1A). The *jab* mutation is located in the interswitch (white arrow, Figure 3.1B) region of the protein that connects the switch I and switch II region, which are two anti-parallel β-strands. The alignment of Arl1 peptide sequence shows that the amino acid leucine at position 61 is highly conserved (Figure 3.1C). The transcript and protein expression levels of *jab* Arl1 were found to be 50% reduced in *jab* mouse embryonic fibroblasts (MEFs) (Bitoun et al., unpublished data; Chapter 1, Figure 1.8A+B). The homozygote *jab* mouse is not viable, thus confirming a dominant mutation.

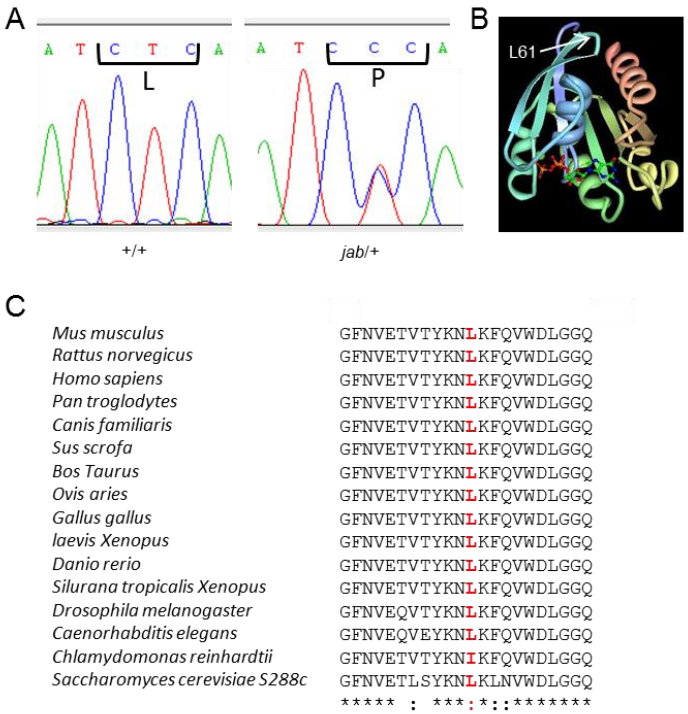

Figure 3.1. Identification of the *jab* mutation in the *Arl1* gene
(A) Sequencing traces of wild-type (+/+) and *jab* mouse (*jab/+)* of PCR amplicon in exon 5 containing the *jab* mutation 182T→C. This affects the open reading frame, mutating leucine at position 61 to proline. **(B)** X-ray structure of human Arl1 at 2.3Å resolution (Panic et al. 2003). The position of L61, affected by the mutation, is located at the end of a loop connecting two anti-parallel β strands. **(C)** Alignment of amino acid sequences for Arl1 proteins from the indicated species. The leucine substituted for a proline at position 61 in the *jab/+* mutant (L61P mutation) is highlighted in red.

The *nym* mutation was identified by amplifying a 553bp region of exon 13 and PCR products were sent for sequencing and analysed as shown in figure 3.2A. Due to the mutation being localised in a restriction site, the presence of the *nym* mutation was confirmed by amplification of the 553bp region and subsequent restriction digest using MseI. MseI only cuts when the mutation is present at the recognition site TTAA. A wild type mouse presents with a full uncut product of 553 bp, a *nym* mouse (*nym*/+) will show one band at 553bp and a cut product of one allele at 352bp and 201bp, and a homozygous *nym* mouse (*nym*/*nym*) will only present with 352bp and 201bp bands as the mutation is present in both alleles. For diagnostic purposes the 201bp band, which is very faint in detection, was not used to identify the mutants (Figure 3.2B). The *nym* mutation introduces a T to A substitution at nucleotide 2601 of the cDNA sequence (T2601→A) that changes the tyrosine into a premature stop codon at position 867 of the protein sequence (Y867X). This mutation is located within an evolutionarily conserved spacer region, 40 residues upstream of the cleavage signal between the α- and ß-subunits (Figure 3.2C). This is predicted to result in the production of a slightly truncated α-subunit (~ 95% of full-length) and the complete lack of the ß-subunit. In agreement with the loss of a functional N-acetylglucosamine-1-phosphotransferase (Gnpta) enzyme, encoded by *Gnptab*, the counterpart *nym* mutation in the human protein sequence (Y888X) has, in fact, recently been identified in a MLII patient (Cathey et al. 2010). The *nym* homozygote mouse (*nym/nym*) is viable and is further described in Chapter 4.

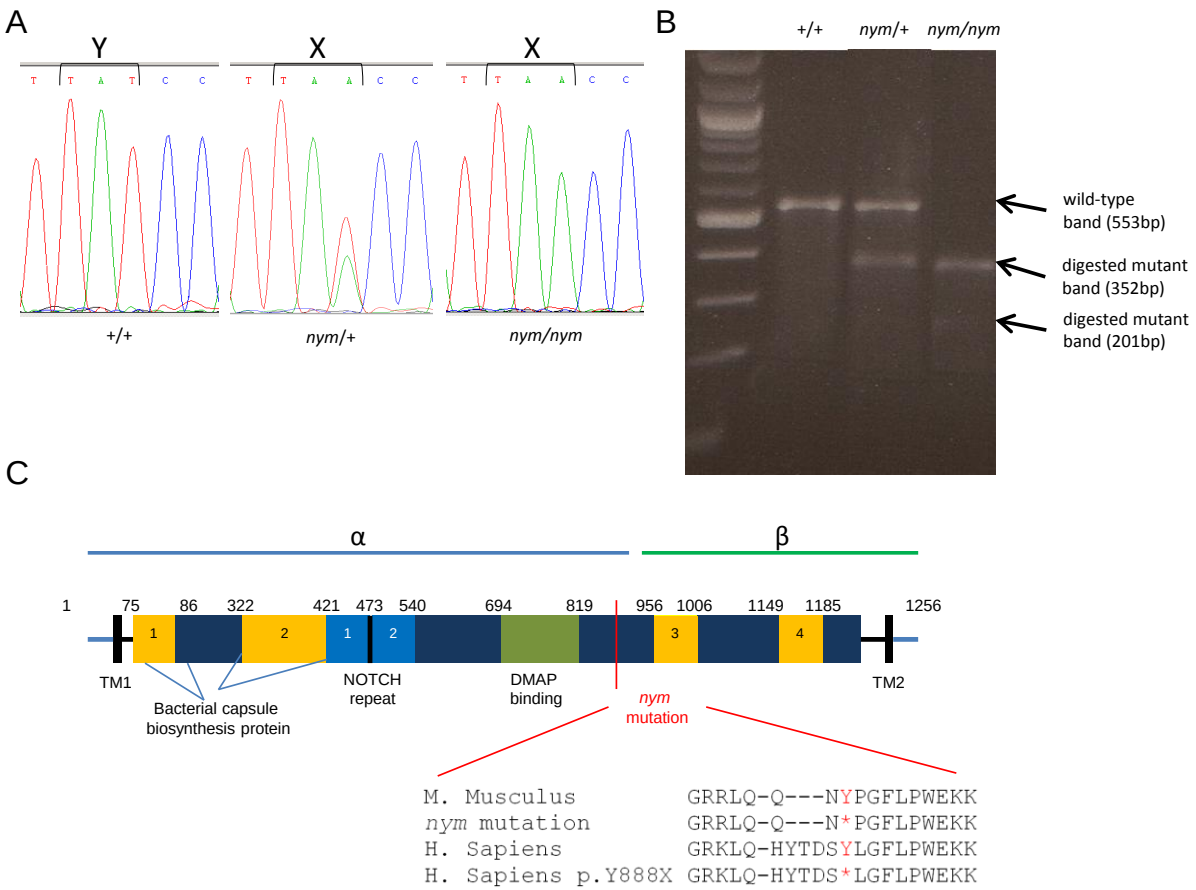

Figure 3.2. Identification of the *nym* mutation in the *Gnptab* gene
(A) Sequencing of the *Gnptab* locus identified a single-nucleotide change resulting in a coding change from a tyrosine residue (TAT) in the wild-type (+/+) to a premature stop codon (TAA) in the *nym* (*nym*/+) and *nym* homozygote (*nym/nym*) mutants. **(B)** Genotyping strategy which after MseI digest shows a 553bp band for the wild-type, a 553bp, 352bp and 201bp (very faint) band for the *nym* mouse and only a 352bp and very faint 201 bp band for the *nym* homozygous mouse. **(C)** Schematic of human GlcNAc-1-phosphotransferase (GNPTA) α/β subunits presenting the location of the *nym* mutation and its conservation from mouse to human, including the human *nym* counterpart mutation Y888X (truncation mutation indicated by an asterisk). The precursor protein is cleaved between K928 and D929 by the site-1-protease to produce two catalytically active α and β subunits. The bacterial capsule biosynthesis proteins, also called Stealth domains, are similar to bacterial genes which are important for synthesis of cell wall polysaccharides and sugar-phosphate transferases. The Stealth domains harbour the catalytic sites. The NOTCH modules found in NOTCH receptor family members have been shown to recognise lysosomal hydrolases. The DMAP interaction domain is a component of DNA methyltransferase and plays a role in lysosomal hydrolase recognition. TM: Transmembrane domain; aa: amino acid. Adapted from (Qian et al. 2015).

In the *nym* mouse, *Gnptab* mRNA levels were analysed to investigate whether the *nym* mutation, causing a truncation mutation at the end of the α-subunit, affects the nonsense mediated mRNA decay pathway leading to elimination of mRNA transcripts that contain premature stop codons (Brogna and Wen 2009). This was conducted using semiquantative RT-

PCR. *Gnptab* transcript levels were reduced by 50% in *nym* mice compared to wild-type mice (Figure 3.3).

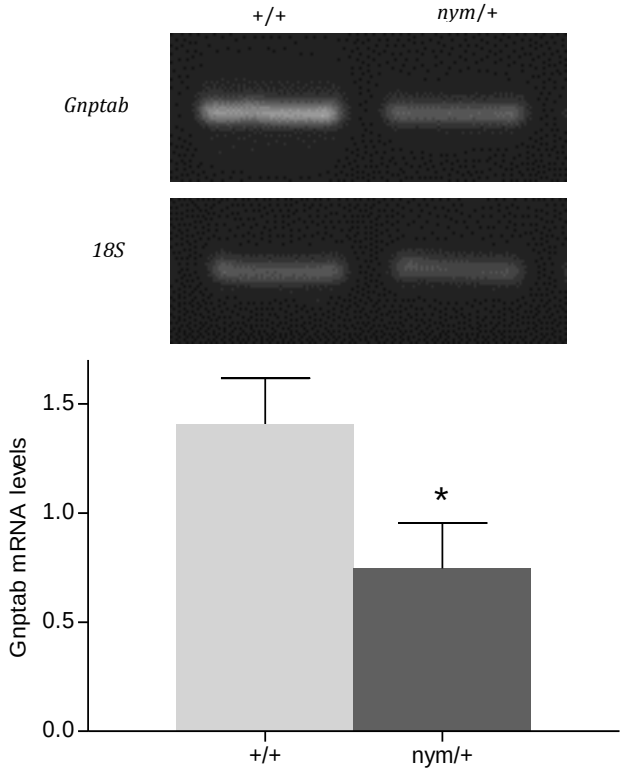

Figure 3.3. Semiquantative RT-PCR analysis of *Gnptab* mRNA reveals a reduction of 50%
(Top) Representative semi-quantative RT-PCR analysis of *Gnptab* mRNA in whole brain extracts. **(Bottom)** The amount of *Gnptab* mRNA, expressed as the ratio of densitometric measurement of the sample to the corresponding internal standard (*18S*), is shown in the lower panel. Values are expressed as mean ±SEM (n=4; two-tailed Student's t- test, *P<0.05).

3.2.2. Growth retardation, hind limb clasping and reduced muscle strength segregates with the *jab* mouse

The *stv* mouse presented with growth retardation, resulting in a 25% reduction in weight compared to wild-type controls from 3 months of age (Figure 3.4A). The *jab* and *nym* mice were therefore weighed in order to assess which mutant presented with growth retardation, similarly to the *stv* mouse. The *jab* mice presented with reduced size, as shown in the picture panel and in the weight chart (Figure 3.4B). The *jab* mice are about 25% lighter than the wild-type control from 3 months of age. In contrast, the *nym* mice have a similar size to the wild-type controls, as seen in the picture panel in figure 3.4C, and there is no significant difference observed in weight between wild-type and *nym* mice. Therefore, the weight reduction seen in the *stv* mouse is most likely to be attributed to the *jab* mutation.

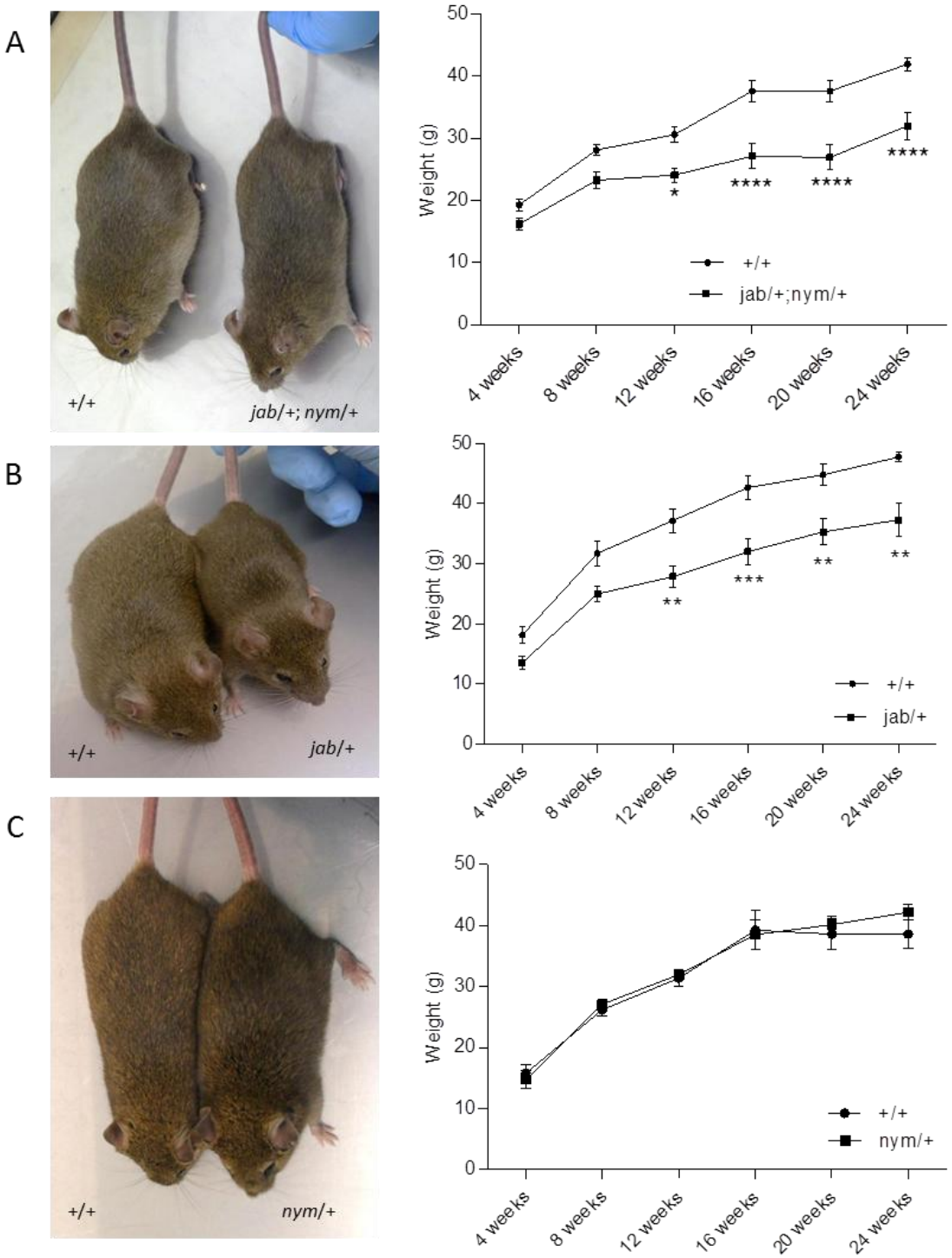

Figure 3.4. Growth retardation present in the *jab* but not in the *nym* mouse

Three-month old **(A)** *stv* (*jab*/+;*nym*/+) and **(B)** *jab* mice (*jab*/+) show significantly reduced body size and weight in comparison to their wild-type (+/+) littermates. **(C)** The *nym* mouse (*nym*/+) shows no significant body size or weight difference to the wild-type. Values are expressed as mean±SEM (n=10; two-tailed Student's t- test, *P<0.05; **P<0.01, ***P<0.001, ****P<0.0001).

Hind limb clasping is a marker of disease progression in a number of mouse models of neurodegeneration, including certain cerebellar ataxias (Chou et al., 2008). The *stv* mouse shows hind limb clasping at 3 months, therefore both *jab* and *nym* mice were assessed on this parameter. Hind limb clasping is assessed by hanging the mouse by its tail for 10 seconds. In the wild-type mice it can be observed that they balance their body by spreading their hind paws apart. This is the normal expected response and is also observed in the *nym* mice (Figure 3.5). However, both the *jab* and *stv* mice presented with hind limb clasping (Figure 3.5). Therefore, this phenotype of the *stv* mouse can also be attributed to the *jab* mutation.

Figure 3.5. The *jab* mouse presents with hind limb clasping similar to the *stv* mouse
At 3 months, male wild-type (+/+) mouse extends its hind paws to balance its body posture. In contrast the male *stv* (*jab*/+; *nym*/+) and *jab* mouse are unable to balance their body with their hind limbs and clasps them into their body and even attempts to hold on to them with their front paws. In contrast, the *nym* mouse responds similarly to the wild-type control (n=8).

As the *stv* mouse presented with reduced muscle strength (tested on the inverted screen at 3 months of age), both *jab* and *nym* mice were assessed on the inverted screen. Mice were placed on a wired mesh screen and time was measured until the mice dropped off up to a maximum time of 3 minutes. The *jab* mice showed a significantly reduced performance in comparison to the wild-type controls (Figure 3.6). These findings are almost identical to the performance of the *stv* mice. The *nym* mice presented with similar performance to the wild-type controls (Figure 3.6). Therefore, the reduced muscle strength of the *stv* mouse can be attributed to the *jab* mutation.

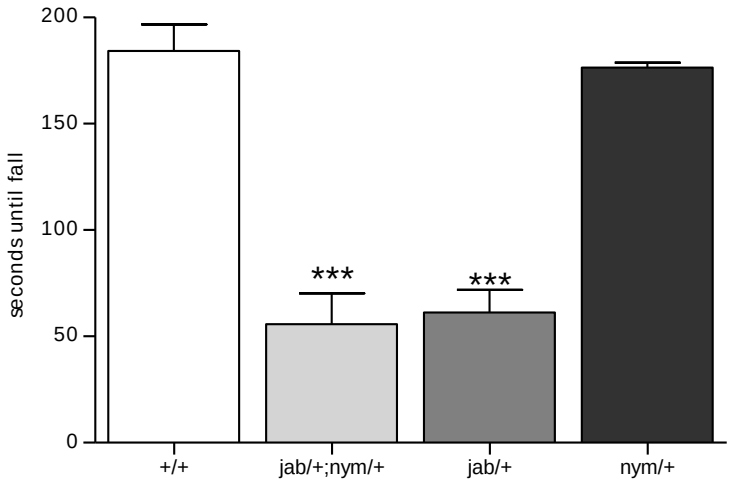

Figure 3.6. The *jab* mice showed reduced muscle strength as tested on the inverted screen almost identical to the *stv* mouse at 3 months of age
The *jab* mice present with reduced muscle strength (measured on the inverted screen) in comparison to their wild-type (+/+) littermates. The performance of the *jab* mice was very similar to the *stv* mice. Values are expressed as mean±SEM (n=10; Kruskal-Wallis 1-way ANOVA, ***P<0.001).

3.2.3. The *jab* mice present with demyelination of the sciatic nerve, neuromuscular junction disorganisation and resulting muscle pathology

The phenotypic features of the *stv* mouse, including hind limb clasping and reduced muscle strength, strongly suggest dysfunction of the nervous system. Therefore, potential defects in the peripheral nervous system, particularly peripheral nerve damage and muscle pathology, were investigated in both the *stv* mouse, as well as the separated mutants. Given the involvement of both Arl1 and Gnpta in lipid metabolism, as well as the tremor observed in the *stv* mice, myelination of the sciatic nerve was assessed. Staining of sciatic nerve sections for myelin

sheath lipids using *P*-Phenylene Diamine (PPD) was much weaker in *stv* mice compared to wild-type controls (Figure 3.7). In addition, increased white space was present in the *stv* sciatic nerve sections, indicating a potential loss of nerve fibres. Therefore, this pathology was analysed in the *jab* and *nym* mutants. The *nym* mice present with very similar strong myelin sheath lipid staining as wild-type mice. The jab mice (similarly to the *stv* mice) present with weaker staining for myelin sheath lipids and potential loss of nerve fibres (Figure 3.7).

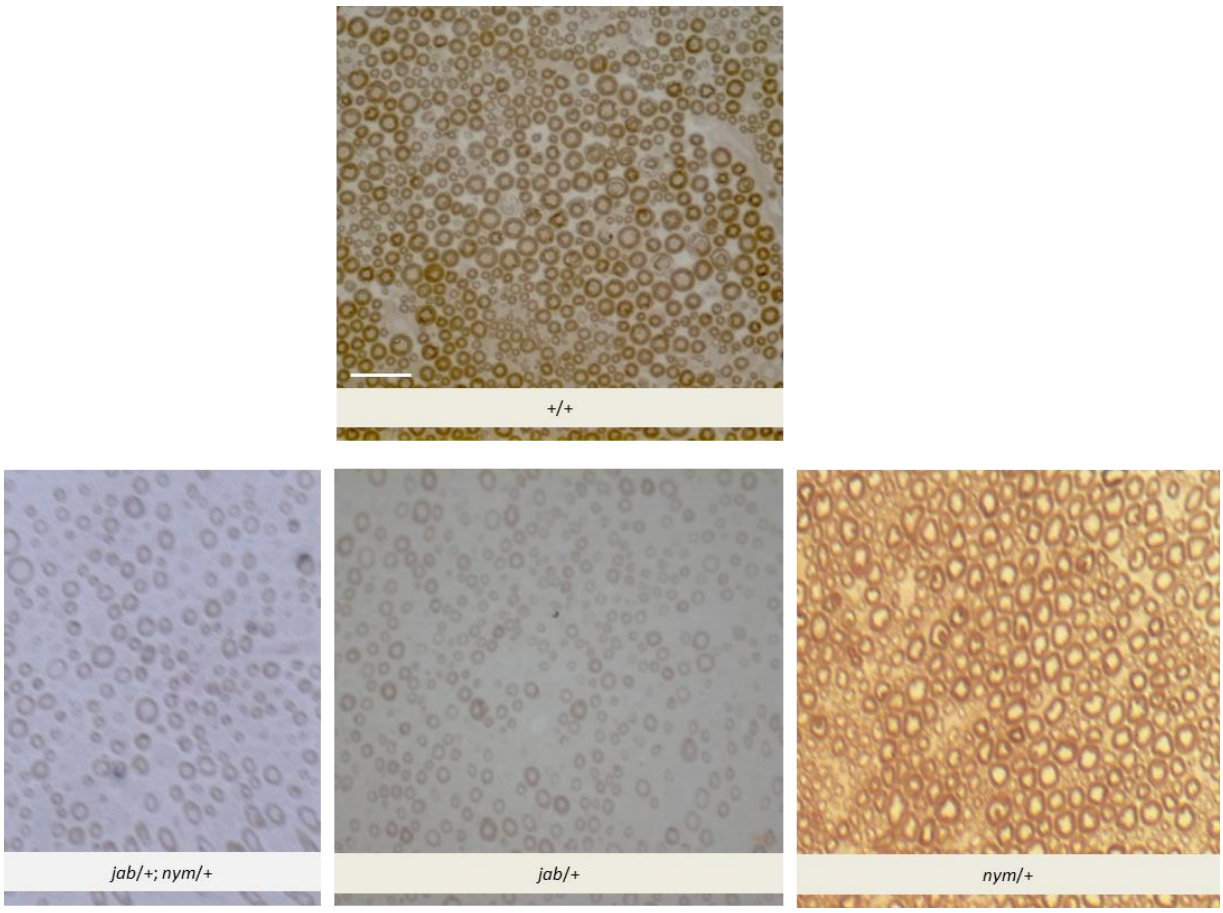

Figure 3.7. The *jab* mouse confirms the demyelination observed in the sciatic nerve in the *stv* mouse
Representative images of cross sections of sciatic nerve from wild-type (+/+), *stv* (*jab*/+; *nym*/+), *jab* and *nym* mice at 3 months of age (n=4) stained with PPD to visualize the myelin sheath. Scale bar: 20µm. (Data provided by Dr Janet Kenyon and Ben Edwards).

Morphological analysis of the NMJs from the *stv* mice revealed (by α-bungarotoxin staining) a significant change from the characteristic complex branched pretzel-like structure observed in wild-type mice. The NMJs of the *stv* mice appeared fragmented and distended, with

membrane edges less well defined (Figure 3.8). This pathology was therefore analysed in the *jab* and *nym* mutants. The *jab* mice also presented with fragmented and distended membrane edges in the NMJ morphology, whereas the *nym* mice had a defined characteristic complex branched pretzel-like structure similar to the wild-type.

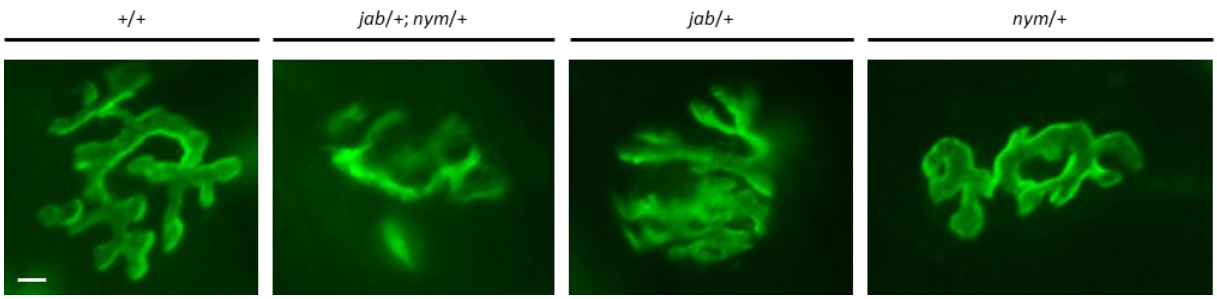

Figure 3.8. The *jab* mouse confirms the neuromuscular junction pathology seen in the *stv* mouse
Structural analysis of neuromuscular junctions in soleus muscle from wild-type (+/+), *stv* (*jab*/+; *nym*/+), *jab* and *nym* mice at 3 months of age (n=6) stained with α-bungarotoxin. Scale bar: 10μm. (Data generated together with Dr Janet Kenyon.)

From other disease models, it is know that nerve demyelination and disorganisation of the NMJs leads to muscle atrophy, which was also detected in the *stv* mice. Typically skeletal muscle is characterised by certain properties including, the number, type, and size of muscle fibres. Different muscle fibre types exist and they can be of different size and function. For example, contractile power and resistance to fatigue can vary in different muscle fibre types (Bottinelli and Reggiani 2000). A mixture of fibre types are present in human skeletal muscles and are mainly made up of a mixture of type I, IIA, and IIX muscle fibres (Schiaffino 2010). For this investigation the soleus muscle was chosen, as unlike most of the muscles in mouse, it is made up of type I and type IIA fibres (Timson et al. 1985). This composition is similar to the fibre types found in humans. In addition, a single cross-section can be taken from the soleus to provide a readout of the estimated abundance of muscle cell types, because all types of fibres pass through the belly of mouse soleus (Timson et al. 1985). Type I and type IIA fibres were differentiated through specific staining, and the number of each fibre type per cross-section was quantified. Healthy muscle presents with evenly distributes fibres as can be seen in the wild-type mouse (Figure 3.9, top panel). The *stv* mice present with a change in distribution of muscle

fibres type I and IIA, which presented as fiber type grouping and grouped atrophy, in comparison to regular grouping in the wild-types (Figure 3.9). Fiber type grouping and grouped atrophy are prominent features of long standing denervation-reinnervation-denervation. Therefore, this pathology was analysed in the *jab* and *nym* mutants. The *jab* mice also presented with abnormal grouping for type I and type IIA muscle fibres (Figure 3.9), in contrast to the regular distribution observed in wild-type and *nym* muscle. In conclusion, this pathology seems also to stem from the *jab* mutation.

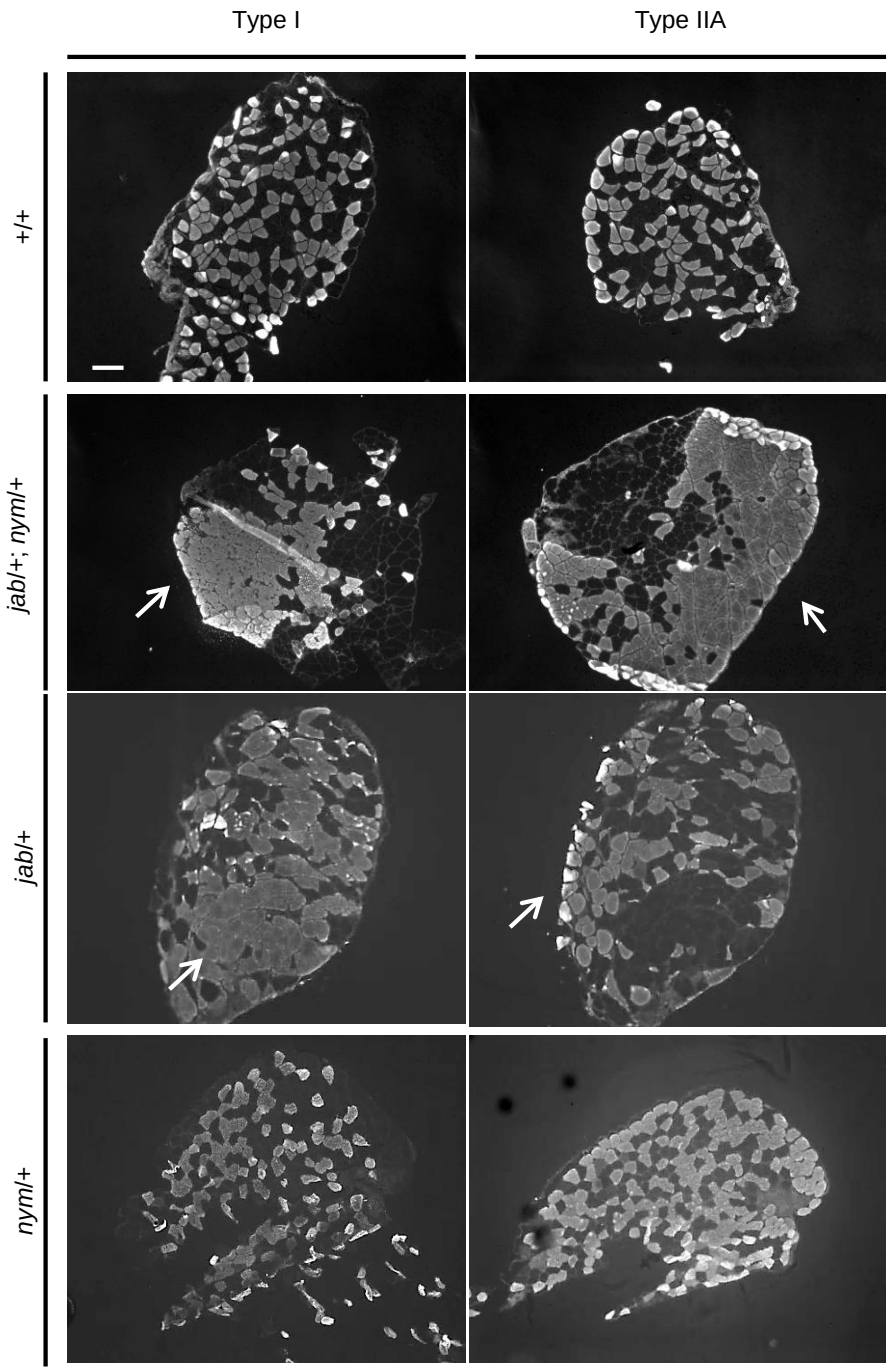

Figure 3.9. The *jab* mouse confirms the muscle pathology as seen in the *stv* mouse
Histological analysis of soleus muscle from wild-type (+/+), *stv* (*jab*/+;*nym*;+), *jab* (*jab*/+) and *nym* (*nym*/+) mouse. Type I and type IIA fibre typing was conducted and *stv* and *jab* mice present with an abnormal change of distribution of these in comparison to the wild-type mice (n = 4). Arrows (↑) are highlighting the grouped atrophy observed in the muscle sections of the *stv* and *jab* mouse. Scale bar: 100µm. (Data provided by Benjamin Edwards)

3.2.4. Increased lysosomal hydrolase activity in the blood sera segregates with the *nym* mouse

Mutations in *GNPTAB* are known to cause a defect in the synthesis of the mannose-6 phosphate (M6P) marker (Tiede et al., 2005). This marker is important in the delivery of lysosomal hydrolases to the lysosome in order to enable degradation of cellular waste material. If this marker is not present on lysosomal hydrolases, the hydrolases will not be directed to the lysosomes and therefore excreted into the blood sera. Hence, the enzymatic activity in the blood sera of the *stv* mice was analysed to gain knowledge to what extent the function of Gnpta is dysfunctional in the *stv* mice. The *stv* mice present with a 2-3 fold increase in enzymatic activities in the blood sera and therefore the enzymatic activities in the blood sera of both *nym* and *jab* mice were analysed. This was conducted using lysosomal hydrolase substrates that were linked to a fluorescent compound and once cleaved efficiently, fluorescence can be measured on the spectrometer. The *jab* blood sera presented with the same enzymatic activity found in the blood sera of wild-type animals, whereas the *nym* and *stv* mice both presented with a 2-3 fold increase in enzyme activities for β-hexosaminidase (Figure 3.10; *nym*/+: 1.7±0.1; *jab*/+;*nym*/+: 2.1±0.4) and α-mannosidase (Figure 3.10; *nym*/+: 2.4±0.2; *jab*/+;*nym*/+: 2.3±0.2). In conclusion, the 2-3 fold increase in enzymatic activities in the blood sera appears to stem from the *nym* mutation.

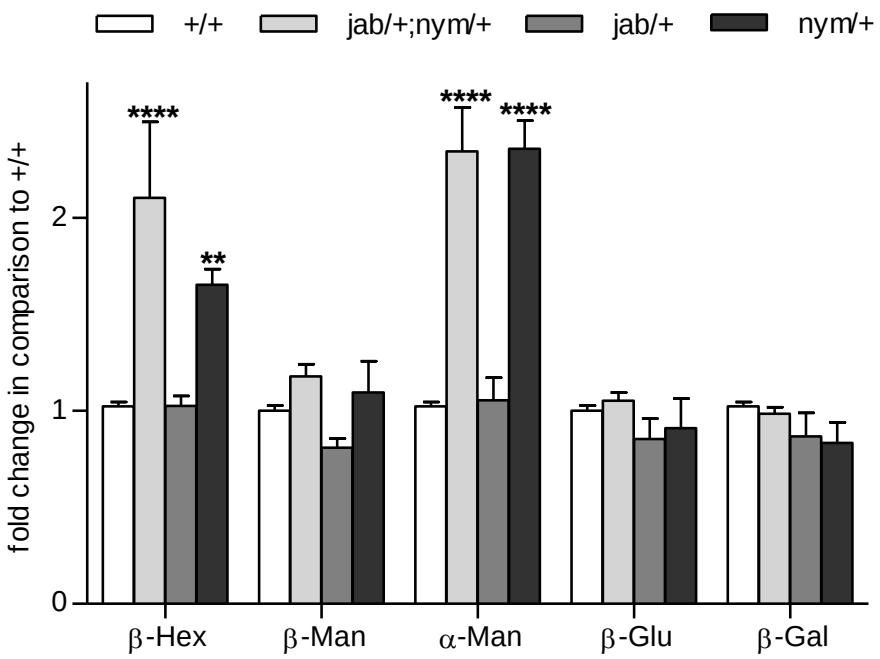

Figure 3.10. Increased enzymatic activity is present in the *nym* and *stv* mouse

The relative enzymatic activities of the lysosomal hydrolase: β-Hexosaminidase (β-Hex), β-Mannosidase (β-Man), α-Mannosidase (α-Man), β-Glucuronidase (β-Glu) and β-Galactosidase (β-Gal) were measured in blood sera of 3-month-old wild-type (+/+), *stv* (*jab*/+; *nym*/+), *jab* (*jab*/+) and *nym* (*nym*/+) mice. The specific activities of the wild-type were set to 1. Values are expressed as mean±SEM (n=8; 1-way ANOVA with Dunnett's post-hoc test, **P<0.01, ****P<0.0001).

3.3. Discussion

In summary, the *jab* mouse resembles the majority of pathological phenotypes observed in the *stv* mouse. In contrast, the *nym* mouse only presents with a 2-3 fold increase in hydrolase activity detected in the blood sera (Table 3.1). The truncation mutation in the *Gnptab* gene from the *stv* mouse corresponds to a MLII patient mutation (Cathey et al., 2010). Carriers of MLII, that are heterozygote for nonsense or frameshift mutations in *GNPTAB*, do not show any MLII pathology, despite a 2-3 fold increase in enzymatic activity. Therefore, it can be concluded that the mutation in *Arl1* appears to cause the pathology observed in the *stv* mouse and not the *Gnptab* mutation.

Table 3.1. Comparison of the double mutant *stv* to the separated out mouse mutants: *jab* and *nym*

Pathology	Stevens mouse (j*ab*/+; n*ym*/+)	Jabber mouse (*jab*/+)	Nymphe mouse (*nym*/+)
Growth retardation	✓	✓	✗
Reduced muscle strength	✓	✓	✗
Hind limb clasping	✓	✓	✗
Muscle pathology	✓	✓	✗
NMJ disorganisation	✓	✓	✗
Demyelination	✓	✓	✗
Increased hydrolase activity 2-3 fold	✓	✗	✓

3.3.1. The *nym* mouse does not show an obvious phenotype

The *nym* mouse only segregated with having a 2-3 fold increase in lysosomal hydrolases, detected in the blood sera, which is similar to what was seen in the *stv* mouse. Interestingly, the *nym* mutation has a counterpart mutation in the human protein sequence (Y888X) that has been identified in a MLII patient (Cathey et al. 2010). A 2-3 fold increase in lysosomal hydrolases in the blood sera has also been reported in carriers of MLII, but these do not present with any

pathology of MLII and appear healthy (Cathey et al. 2010), which is very similar to the *nym* mouse. Therefore, the *stv* mouse neurological dominant phenotype was caused by the *jab* mutation and not the *nym* mutation. It will be very interesting to characterise the homozygote *nym* mutant, as this mouse should present as a novel mouse model of MLII, which mimics the human mutation. Current animal models of MLII do not fully recapitulate the human disease. Hence, a mouse model of a human patient mutation that more fully models the human pathology, will be of immense value to gain a greater understanding of the disease mechanism and help when testing novel drugs for MLII.

3.3.2. The *jab* mutation causes the phenotype observed in the *stv* mouse

The mutated L→P in the *jab* mouse, presumably causes a kink in the interswitch region and alters the structural features. Further investigations are necessary to investigate the effect of the mutation on cell localisation, its ability to bind GTP and Arl1's binding partners. The homozygote *jab* mouse is not viable, which is consistent with the findings in which an *Ar11* knock-out in *Drosophila* is embryonic lethal (Tamkun et al. 1991). This suggests that Arl has a crucial role in development.

Recent work by Jaschke et al. (2012) implicated Arl1 in a pathway that leads to the formation of lipid droplets and chylomicrons reviewed in Section 1.3.2.1 of Chapter 1. The implicated defect in lipid metabolism by the recruitment of Arl1 by Arfrp1 (Hommel et al. 2010) is most possibly also implicated in the disease phenotype of the *jab* mouse. The conditional adipose tissue-specific *Arfrp1* knock-out mouse presents with growth retardation similar to the *jab* mouse. It would be of interest to follow up those observations and analyse the similarity of the phenotype in the *jab* mouse and the tissue specific knock-outs of *Arfrp1*, which were also generated in liver and intestine (Hesse et al. 2012, Jaschke et al. 2012, Hommel et al. 2010). For example, the conditional adipocyte-specific *Arfrp1* knock-out mouse showed markedly reduced amounts of brown adipose tissue, nearly absent white adipose tissue and smaller size of lipid droplets in brown adipose tissue (Hommel et al. 2010). Furthermore, the conditional enterocyte-specific *Arfrp1* knock-out mouse presented with defective lipidation of

chylomicrons and retention of these in the gut. Finally, the conditional hepatocyte-specific *Arfrp1* knock-out mouse presented with defective insulin-like growth factor (IGF) 1 secretion (a ligand for the insulin receptor) and glucose transporter (GLUT) 2 sorting, enabling glucose movement across the membrane (Hesse et al. 2012, Jaschke et al. 2012). It would be of value to analyse similar parameters in the *jab* mouse to understand to what extent these pathologies overlap and ultimately gain a better understanding of Arl1's signalling pathways.

The phenotype of the *jab* mouse seems to be driven by peripheral demyelination, leading to nerve loss, NMJ disorganisation and muscle myopathy. The type of muscle damage seen in the *jab* mouse is characteristic of denervation, and explains the muscle weakness observed in the *jab* mouse on the inverted screen test. More in depth analysis is required to fully understand this pathology, as Arl1 is expressed ubiquitously and it is surprising to cause a specifically neurological phenotype for a gene that is so widely expressed. It would also be of interest to fully confirm that the pathology arises from peripheral demyelination and not from neuronal loss in the central nervous system (CNS).

Interestingly, no report of demyelination and resulting NMJ disorganisation and muscle myopathy has been reported in the tissue specific knock-outs of *Arfrp1*, which recruits Arl1 (Hesse et al. 2013, Hesse et al. 2012, Hommel et al. 2010, Jaschke et al. 2012). Therefore, Arl1 is potentially involved in alternative pathways that lead to demyelination but are not involved with the formation of lipid droplets and chylomicrons.

3.3.3. ENU mutagenesis

Mutagenesis screens using ENU accelerate forward genetics, i.e. moving from trait to identified gene, and generate valuable alleles for uncovering the diversity of gene function. ENU can induce point mutations in DNA, leading to a variety of genetic lesions that are expressed as complete loss of function, partial loss of function, or gain of function alleles. This will reveal a more complete range of gene activity than knock-outs (Oliver et al. 2007). Haplotype analysis localised the *stv* mutations to a genetic interval of 6 Mb on mouse

chromosome 10. The chance of more than one coding mutation in a linkage to 5Mb region is very rare (Keays et al. 2006). Therefore, two mutations in a coding region, as detected in the *stv* mouse, is a very rare occurrence. However, the analysis by Keays and co-workers did mention a bias in relying on phenotypic observations and may have biased observed rates of mutation, with some genes seeming to be more prone to mutations than others. Therefore, the authors conclude that many more genes will need to be screened using genotypic methods before conclusions can be made on the uniformity of gene mutability. Furthermore, it was assumed that coding DNA is uniformly spread throughout the genome, which is unrealistic, as shown by evidence of gene clustering (Waterston et al. 2002; Wu et al. 2001).

Furthermore, introns were not sequenced for mutations in the *stv* mouse. Non-protein-coding sequences have shown to have important functions in the CNS (Belgard et al. 2011). Advances in sequencing technology and data analysis generating a genome wide database of mutants would increase the potential of ENU mutagenesis. Interestingly, ENU mutants with mutations in non-coding regions, such as the ENU-induced mutation of miR-96 linked to progressive hearing loss, have already been described (Lewis et al. 2009). In conclusion, two mutations, as detected in the *stv* mouse, is a rare occurrence in ENU mutagenesis. However, to investigate the exact probability of mutations, the full ENU mutagenesis archive would need to be sequenced fully.

3.3.4. Future work

3.3.4.1. The *nym* mouse

This chapter confirmed that the *nym* mutation has a counterpart mutation in the human protein sequence (Y888X) that has been identified in a MLII patient (Cathey et al., 2010). The heterozygote *nym* mouse was bred to homozygosity in order to investigate if the expected MLII pathology was observed in the *nym* homozygote mouse. The current animal models of MLII do not recapitulate the human pathology of MLII very well, which not only limits the research into the underlying disease mechanism but also the immense need to test novel drugs for MLII. Therefore, the homozygote *nym* mouse was characterised as a novel mouse model of MLII and used as a tool to test a novel therapy for MLII. This work is presented in Chapter 4.

3.3.4.2. The *jab* mouse

The study of the *jab* mouse has been further characterised by Dr Janet Kenyon and Dr Emmanulle Bitoun in the Davies laboratory. Based on their work in the *jab* mouse, the demyelinating phenotype in the mouse causes the disease pathology in the *jab* mouse. However, it is uncertain if a global defect of Arl1 function is causative or if a specific tissue is driving the phenotype. Consequently, *Drosophila* was chosen for further studies due to its diverse genetic tool set allowing for tissue specific knock-outs and overexpression systems, in addition to its suppressor and enhancer screens, fast generation time and conserved function between mammals and *Drosophila* (reviewed in Chapter 1, Section 1.2.1). This work is presented in Chapter 5.

4. Study of a novel mouse model of mucolipidosis II

This research was originally published in the Journal of Biological Chemistry. Leigh Paton, Emmanuelle Bitoun, Janet Kenyon, David A Priestman, Peter L Oliver, Benjamin Edwards, Frances M Platt and Kay E Davies. 2014. A Novel Mouse Model of a Patient Mucolipidosis II Mutation recapitulates Disease Pathology. J Biol Chem 289(39): 26709-21 © the American Society for Biochemistry and Molecular Biology. The text and figures in this chapter are adapted or taken from the published article. As the first author of the above publication, I took the lead on writing the sections that are included in this thesis (Appendix)

4.1. Introduction

Following up on our study of the Nymphe (*nym*) mouse (*nym*/+) in Chapter 3 which carries the previously reported patient mutation Y888X (Cathey et al. 2010), the *nym* homozygote mouse (*nym/nym*) was characterised to assess if it modelled the human disease mucolipidosis II (MLII). MLII is an autosomal, recessive and fatal lysosomal storage disease (LSD) that thus far has no cure (reviewed in Chapter 1, Section 1.3.1.), therefore making mouse models that recapitulate the human disease very valuable.

4.1.1. Existing models of mucolipidosis II

Efforts to determine the underlying pathological mechanisms behind MLII have been hindered by the lack of animal models. A few animal models have been described, but so far, only the feline model of MLII, a spontaneous mutation found in a colony of cats, recapitulates the human disease most closely showing coarse facial features, behavioural dullness, ataxia, reduced lifespan and impaired lysosomal targeting (Bosshard et al. 1996, Mazrier et al. 2003). However, the feline genome is incomplete and not well annotated. In addition, the feline's large size limits research. *Gnptab*-depleted zebrafish embryos have also been engineered using morpholinos and showed skeletal abnormalities, craniofacial defects and reduced motility. Furthermore, developmental studies were more accessible with this model and changes in the protein expression pattern of chondrogenic factors were shown (Flanagan-Steet et al. 2009, Petrey et al. 2012). A *Gnptab* gene trap mouse model (producing non-functional N-acetylglucosamine-1-phosphotransferase (Gnpta), the protein product of the *Gnptab* gene and therefore modelling a knock-out, *Gnptab* knock-out from here onwards) has also been described

and is characterised by impaired growth, retinal degeneration, lesions in secretory epithelial cells of exocrine glands and elevated levels of serum acid hydrolases (Gelfman et al. 2007, Vogel et al. 2009). This mutant presented with a relatively normal lifespan and did not develop characteristic disease features such as skeletal and facial abnormalities. The existing models of MLII are compared in table 4.1.

Table 4.1. Comparison of the existing model organisms of mucolipidosis II

MLII model	Feline	Zebrafish	Murine knock-out
Mutation	c.2655C>T leading to a truncation mutation (Mazrier et al. 2003)	Morpholino-based knock down strategy (Flanagan-Steet et al. 2009)	*Gnptab* Gene trap mouse (Gelfman et al. 2007)
Phenotype	Reduced life span	Reduced life span	**Normal** life span
	Growth retardation	Growth retardation	Growth retardation
	Skeletal abnormalities	Skeletal abnormalities	**No** skeletal abnormalities
	Craniofacial defects	Craniofacial defects	**No** Craniofacial defects
	Poor muscle tone and developed hind limb ataxia	Impaired motility	**No** report of ataxic gate
	Behaviourally dull and less playful	**No** report of behavioural dullness	**No** report of behavioural dullness
	Inclusion bodies present in fibroblasts	Impaired cartilage development	Inclusion bodies present in secretory organs (Pancreas) and connective tissue (Cartilage)
	Retinal clouding	Abnormal otolith	Retinal impairments

4.1.2. Treatments for lysosomal storage diseases and mucolipidosis II

Enzyme replacement therapy has been tested for an increasing number of LSDs (Brady 2006, Desnick and Schuchman 2012). This ability of lysosomal enzymes to cross-correct cells is facilitated by the cation-independent mannose 6-phosphate (M6P) receptor that is present, albeit in different abundances, on the surface of virtually all cells (Pohlmann et al. 1995, Achord et al. 1978). As lysosomal enzymes are invariably decorated with oligosaccharide side chains that bear M6P residues or can be modified to expose the core mannose structures, systemic delivery of recombinant enzymes has been shown to confer widespread complementation and subsequent reversal of tissue pathology in several LSDs (Desnick and Schuchman 2012, Brady 2006). However, enzyme replacement therapy fails in patients with CNS involvement due to the inability of an intravenously administered enzyme to cross the blood–brain barrier (Zirzow et al. 1999). The protein affected in MLII, GNPTA, is a membrane-bound enzyme complex localised to the Golgi apparatus and therefore enzyme replacement therapy, effective for LSDs caused by loss of soluble lysosomal hydrolases, are not likely to be successful.

Bone marrow transplantation studies (Hoogerbrugge and Valerio 1998), like enzyme replacement therapy, have shown no neurologic or intellectual improvements for LSDs. These studies highlight the limitations of bone marrow transplantation for the treatment of LSDs with CNS involvement and emphasise the need to develop novel treatments for LSDs whose primary site of pathology is the CNS. However, studies with a limited number of MLII patients have been described for bone marrow transplantation as beneficial with regard to improving neurodevelopment and cardiopulmonary complications (Grewal et al. 2003), but there is no evidence that the bone marrow transplantation improved skeletal abnormalities, which are prominent in MLII. Chondroblasts and osteoblasts in bone seem to be relatively insulated from the beneficial effects of bone marrow transplantation. The exact mechanism of bone marrow transplantation benefit remains unclear (Grewal et al. 2003, Imaizumi et al. 1994).

Experiments using retroviral transduction to deliver gene therapy have shown that gene therapy might be an interesting approach (Tiede et al. 2005). Thereby, the *GNPTAB* gene was successfully expressed in fibroblasts from an MLII patient, which led to GNPTA localising to the Golgi. Furthermore, the increased secretion of lysosomal hydrolases into the blood sera was ameliorated (Dierks et al. 2009). Interestingly, only 20-30% of remaining active enzyme was shown to lead to a reduction in disease severity and an increase in life expectancy into the third decade, therefore expression of the GNPTA enzyme would not need to be that high. But more importantly, carriers of MLII, depending on the mutation, only have a 60-80% enzymatic activity and are phenotypically normal. Hence restoring 50% of enzymatic activity would have a huge impact on patient quality of life and life-expectancy, but that is still a challenging task in the field. The amount of enzyme expression will vary with each disease, but may be less than 10% of normal levels based on observed enzyme levels in patients with attenuated forms of LSDs. Hence, the level of gene expression that is necessary for therapeutic efficacy for this group of diseases may be relatively modest.

As mentioned before there is strong evidence that lysosomal dysfunction may represent the underlying basis for many synucleinopathies (Manzoni and Lewis 2013). Therefore, there is the potential to repurpose drugs that were initially developed for LSDs for these more common neurodegenerative diseases and vice versa (Sardi et al. 2013). Moreover, studies of apparently different diseases that are presumably linked through shared metabolic pathways are likely to provide greater insights into the biology of LSDs and more common neurodegenerative diseases.

There is a need for novel therapies and to test these drugs it is especially important to have models of disease that recapitulate the human disease closely. This chapter describes the novel MLII mouse model, the *nym* homozygote mouse, which has been used to test a novel drug for MLII.

4.1.3. Aims of the chapter

- **Characterise the *nym* homozygote mouse (*nym/nym*)** by assessing any behavioural defects using behavioural tests and histological and biochemical characterisation that confirms the diagnosis of MLII.

- **Analyse the potential neurodegenerative phenotype of the *nym* homozygote mouse** that would underlie the ataxic gait in the feline model of MLII and psychomotor retardation in the MLII patients.

- **Test whether the drug 2-hydroxypropyl-β-cyclodextrin can delay progressive neurodegeneration in the *nym* homozygote mouse.**

4.2. Results

4.2.1. Reduction in *Gnptab* mRNA levels in the *nym* homozygote mouse

Gnptab mRNA levels were analysed to investigate whether the *nym* mutation, causing a truncation mutation, affects the nonsense mediated mRNA decay pathway leading to elimination of mRNA transcripts that contain premature stop codons. This was conducted using semiquantative RT-PCR. *Gnptab* transcript levels were reduced by 75% in *nym* homozygote mice compared to wild-type mice (Figure 4.1), which is consistent with nonsense mediated decay (Brogna and Wen 2009).

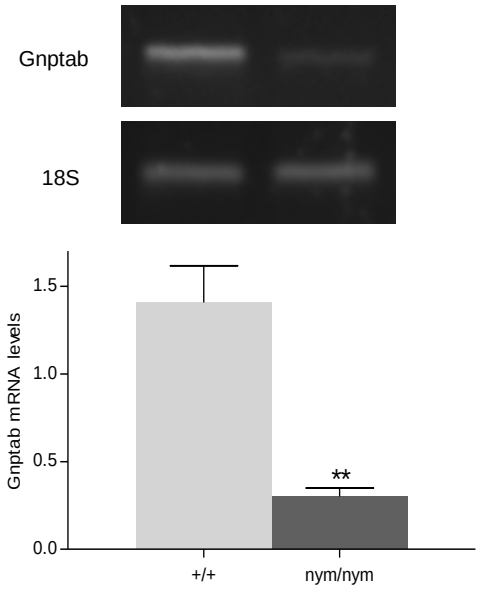

Figure 4.1. Semiquantative RT-PCR analysis of *Gnptab* mRNA reveals a reduction in brain of 75%
Semiquatative RT-PCR analysis of *Gnptab* mRNA in whole brain extracts of *nym* homozygote (*nym/nym*) and wild-type (+/+) mice. The amount of *Gnptab* mRNA, expressed as the ratio of densitometric measurement of the sample to the corresponding internal standard (*18S*), is shown in the lower panel. Values are expressed as mean SEM (n=4; two-tailed Student's t- test; **P<0.01).

4.2.2. Mislocalisation of the *nym* Gnpta protein

The endoplasmic reticulum (ER) export signal is deleted in the *nym* mutation and the remaining truncated protein would be expected to remain in the ER, thus the cellular localisation of the mutant protein was investigated. The cytoplasmic domain of the ß-subunit contains the [RK]X[RK]-type ER export signal and a C-terminal valine which are both required for cargo-receptor-mediated packaging into coat protein II (COPII) vesicles, and trafficking of the Gnpta precursor protein to the Golgi where it gets cleaved (Nufer et al. 2002, Bonifacino and Glick 2004). Sub-cellular localisation of *nym* Gnpta was monitored in transfected HEK 293

cells. As expected, the wild type Gnpta protein colocalised with the *cis*-Golgi marker GM130 (Figure 4.2, top panel) whereas the *nym* Gnpta protein did not (Figure 4.2, middle panel). The *nym* Gnpta protein remained trapped in the ER, as demonstrated by colocalisation with protein disulphide isomerase (PDI, Figure 4.2, bottom panel), an ER marker. These results confirm that the *nym* mutation leads to a dysfunctional Gnpta enzyme and implies that the *nym* homozygote mouse is a novel model of MLII. These findings support that truncation mutations present in *Gnptab* inhibit ER exit (De Pace et al. 2014).

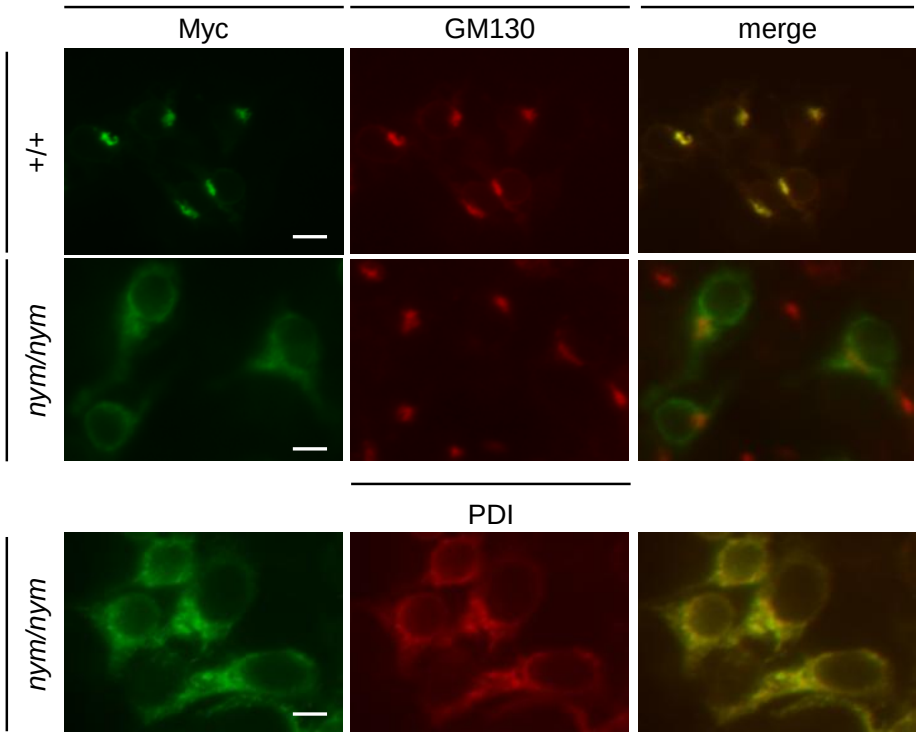

Figure 4.2. *Nym* Gnpta does not localise correctly to the Golgi
HEK 293 cells were transfected with cDNA encoding the wild-type and *nym* construct. Cells were fixed and stained with monoclonal antibodies against the myc-tag (green), the *cis*-Golgi marker protein GM130 (red) or the ER marker protein PDI (red). In merged images, yellow indicates colocalisation (n=4, scale bars: 15 μm).

4.2.3. Reduced size, facial and skeletal abnormalities are part of the pathological features of MLII in the *nym* homozygote mutant

Prominent features of MLII are growth retardation and facial and skeletal abnormalities (Cathey et al. 2010) therefore defects in these parameters were investigated in the *nym* homozygote mice. Indeed, *nym* homozygote mice remained significantly smaller than wild-type littermates (~40%) throughout life (Figure 4.3A+B). Facial and skeletal abnormalities were

evident from birth, including thickened eyelids and a flat profile with reduced nasal bridge (Figure 4.3A+C). In addition, the *nym* homozygote mice had unusually stiff and thick skin, as seen in MLII patients. *Nym* homozygote mice also displayed increased mortality compared to wild-types and survival fell below 50% by ~40 weeks of age (Figure 4.3D).

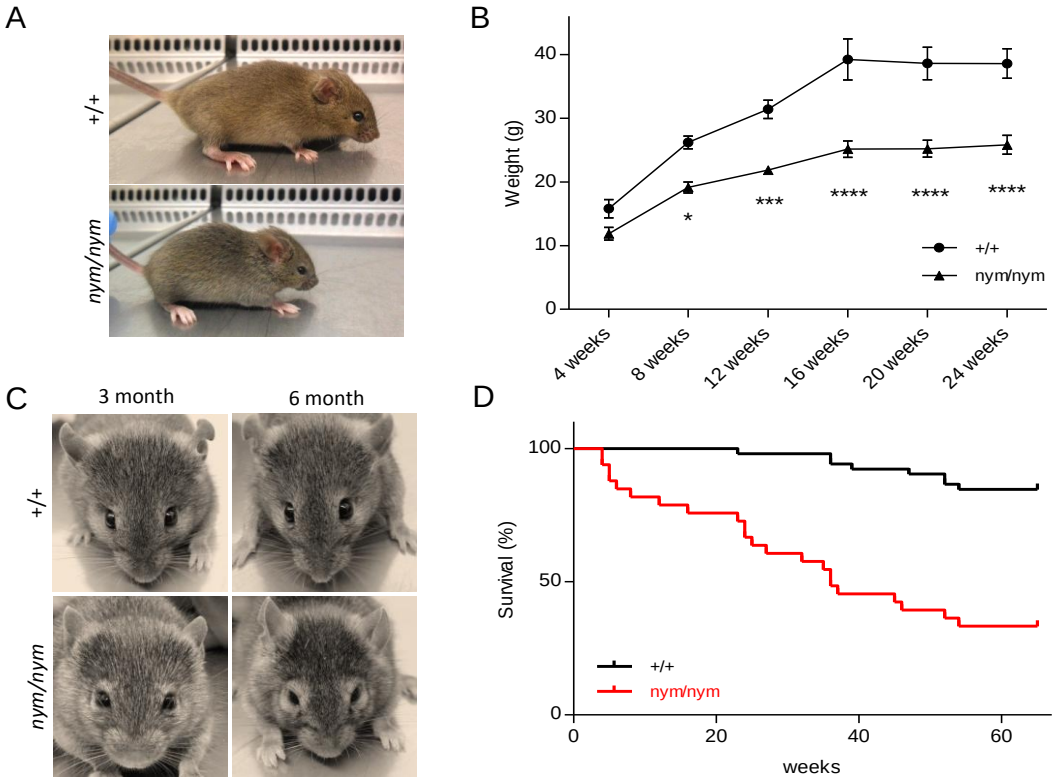

Figure 4.3. The *nym* homozygote mouse presents with growth retardation, facial dysmorphism and reduced life span

(A) One-month old *nym* homozygote mice (*nym/nym*) show reduced body size and skeletal abnormalities e.g. facial dysmorphism and curvature of the spine in male and females. **(B)** Body weight progression of *nym* homozygote mice is reduced compared to wild-type (+/+) littermates (n = 8; two-tailed Student's t-test;*P<0.05, ***P<0.001, ****P<0.0001). **(C)** Facial phenotype progresses with age. Particularly evident are the thickening of the eyelids. **(D)** Kaplan–Meier log rank test for survival showing reduced median survival of *nym* homozygote mice in comparison to wild-types (+/+: n = 52 and *nym/nym*: n = 33). Survival curves were significantly different by Mantel-Cox test, p<0.0001 (χ^2 = 30.69). Values are expressed as mean±SEM.

Similar to MLII patients, skeletal abnormalities are particularly prominent in the back of the *nym* homozygote mouse, and are pronounced in the X-ray image of the mutants with notable abnormalities seen in the spinal cord (Figure 4.4). A normal spine should appear without curves in the frontal plane whereas the *nym* homozygote mouse presents with a thoracic curve, identified as kyphosis (Figure 4.4A). Dorsal curvature of the spine is described as

kyphosis and is common in neurodegenerative disease in mouse models. This curvature is caused by a loss of muscle tone in the spinal muscles secondary to neurodegeneration (Thomas et al. 2006). Furthermore, on a lateral view the *nym* homozygote spine shows a hunched back (Figure 4.4B). Thus, these X-ray images confirm a defect in spine curvature as seen in patients.

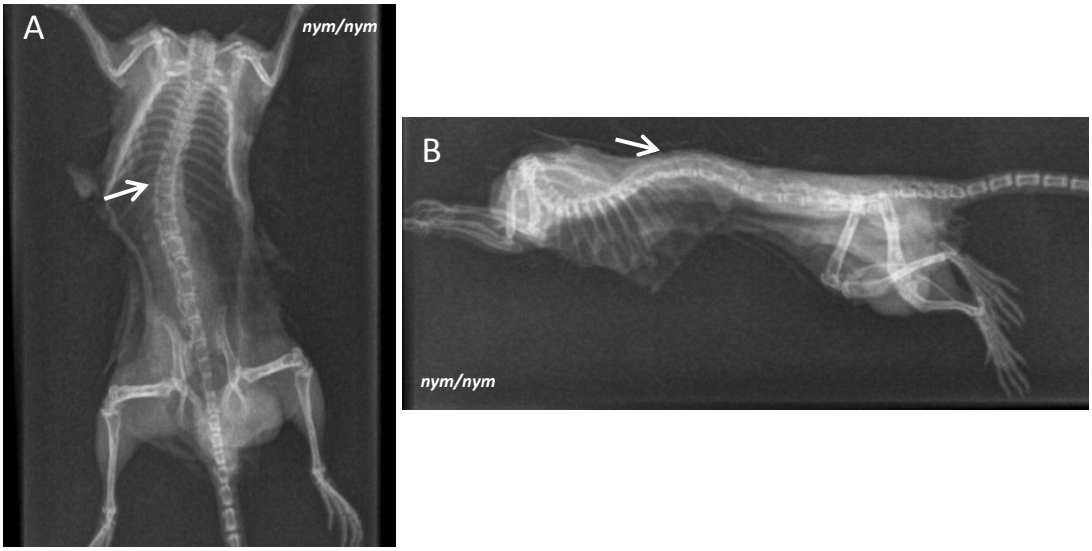

Figure 4.4. Severe skeletal abnormalities is a characteristic of the *nym* homozygote mouse
(A) Whole body exotic dorso-ventral view of the 12 month old *nym* homozygote mouse (*nym/nym*). White arrows highlight abnormal curvature. **(B)** Whole body exotic lateral view of the 12 month old *nym* homozygote mouse. White arrows highlight a hunched back.

Mating of *nym* homozygote mutants was only successful in 9% of breeding pairs (1 out of 11 *nym/nym* inter-crosses lead to offspring) indicating infertility or incapacity of females to carry pups to term. Furthermore *nym* homozygote mutants were born with a reduced frequency of 15% (*nym*/+ inter-cross offspring from a total of 498 offspring: wild-type = 122 mice, 24.5%; *nym*/+ = 303 mice, 60.8%; *nym/nym* mice = 73 mice, 14.7%) instead of the expected 25% Mendelian frequency which implies reduced survival *in utero*. An increased frequency of *nym* homozygote males also presented with penile prolapse from 3 months of age (Figure 4.6).

4.2.4. Inclusion bodies and accumulation of polysaccharides are present in fibroblasts, connective and secretory tissue of the *nym* homozygote mouse

Characteristic features of the pathology of MLII, used for the diagnosis of patients, are increased activities of lysosomal hydrolases found in the blood sera and intracellular accumulation of inclusion bodies (Kornfeld and Sly 2001). Blood serum of *nym* homozygote and wild-type mice was therefore assayed to also test the activity of lysosomal hydrolases. In the serum of *nym* homozygote mice, activities of the lysosomal hydrolases ß-hexosaminidase (*nym/nym* fold increase to wild-type: 12.1±0.8), ß-mannosidase (*nym/nym* fold increase to wild-type: 2.7±0.2), α-mannosidase (*nym/nym* fold increase to wild-type: 28.5±2.9), β-glucuronidase (*nym/nym* fold increase to wild-type: 4.1±0.9) and ß-galactosidase (*nym/nym* fold increase to wild-type: 7.8±0.9) were increased by 2.5- to 30-fold compared to wild-type controls (Figure 4.5A). These trends in fold changes are consistent with observations in the *Gnptab* knock-out mouse mice and human patients (Kollmann et al. 2012, Gelfman et al. 2007, Cathey et al. 2010). Lysosomal enzyme activities for blood sera in nmol/min/ml can be found in appendix table 1.

Fibroblasts, secretory organs, and connective tissue have all been shown to be severely affected by inclusion bodies in MLII. Cytoplasmic inclusions were therefore analysed by staining mouse embryonic fibroblasts (MEFs), pancreatic acinar cells as a sample for secretory tissue, and chondrocytes in the cartilage of the trachea as a sample for connective tissue. The characteristic inclusion bodies (indicative of lysosomal storage) were clearly present in MEFs from *nym* homozygote mice (Figure 4.5B). Chondrocytes were enlarged with the cytoplasm filled by inclusion bodies and abundant microvacuoles (Figure 4.5C, upper panels). In contrast, wild-type chondrocytes had low basic cytoplasm containing a single clear vacuole. In addition, *nym* homozygote chondrocytes were not affected by fixation-dependent shrinkage, as much as wild-type chondrocytes (Figure 4.5C, upper panels). Pancreatic sections from *nym* homozygote mice showed disorganisation of tissue structure, including enlargement of acinar cells likely caused by the presence of large vacuoles containing faint granular material (Figure 4.5C, lower

panels). Similar findings have previously been reported in the *Gnptab* knock-out mouse (Gelfman et al. 2007). Thus far, results from the *nym* homozygote mouse present very similar molecular and cellular features to the human form of MLII and therefore it was investigated next, whether the *nym* homozygote mice could also mimic the behavioural features.

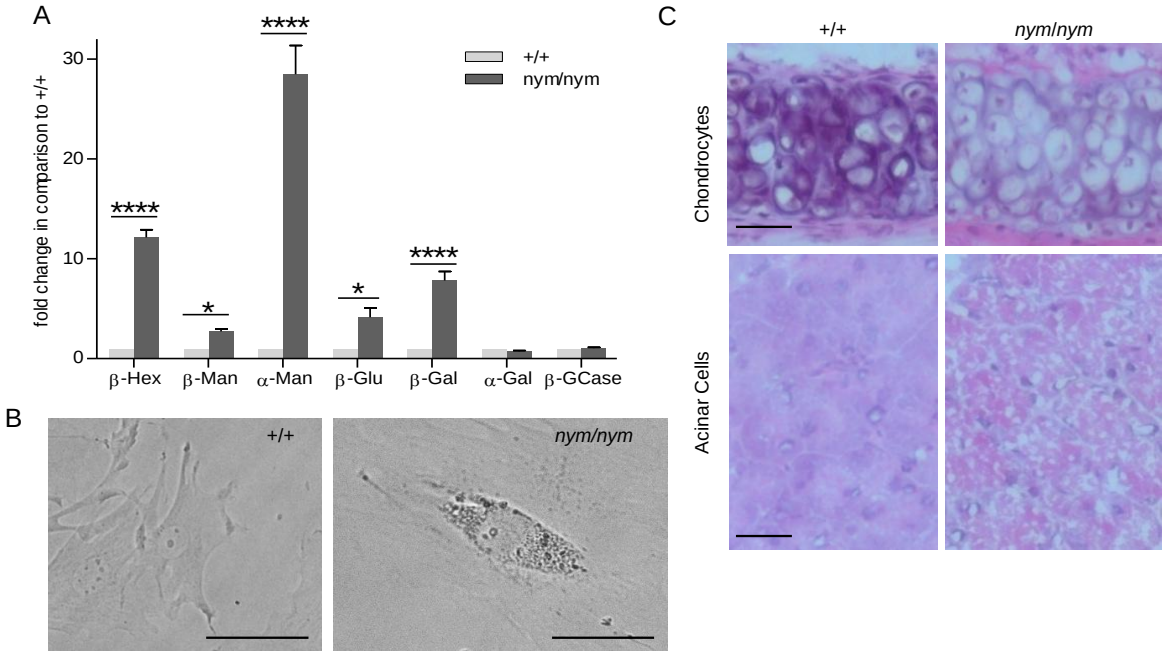

Figure 4.5. Increased lysosomal enzyme activity in blood sera and inclusion bodies present in *nym* homozygote mouse fibroblasts, secretory and connective tissue

(A) The relative enzymatic activities of the lysosomal hydrolase: β-Hexosaminidase (β-Hex), β-Mannosidase (β-Man), α-Mannosidase (α-Man), β-Glucuronidase (β-Glu), β-Galactosidase (β-Gal), α-Galactosidase (α-Gal) and β-Glucocerebrosidase (β-GCase) were measured in blood sera of 3-month-old wild-type (+/+) and *nym* homozygote *(nym/nym)* mice. The specific activities of the wild-type were set to 1. Values are expressed as mean±SEM (n=8; two-tailed Student's t-test; *P<0.05, ****P<0.0001). **(B)** Light microscopy imaging of MEFs isolated from wild-type and *nym* homozygote embryos (E12.5). Accumulation of inclusion bodies present in the *nym* homozygote MEFs can be clearly seen when compared to wild type controls (n=6, scale bar, 40µm). **(C)** Haematoxylin and Eosin (H&E) staining of chondrocytes of the trachea and acinar cells of the pancreas. **Upper panel:** The cytoplasm of hypertrophic chondrocytes is distended by microvacuoles in the *nym* homozygote mouse. These inclusions are aggregates of polysaccharides which increase in storage material with age. **Lower panel:** Marked disorganisation of the pancreas in the *nym* homozygote mouse with tightly packed cells distended by large vacuoles (n=6, scale bar, 50µm).

4.2.5. Hind limb clasping present in the *nym* homozygote mouse

Nym homozygote mice developed progressive abnormality of gait and showed limb-clasping reflexes from 5 months (Figure 4.6). Hind limb clasping is an indication of motor imbalance and has been shown to occur in various neurodegenerative disease mouse models (Guyenet et al. 2010, Fernagut et al. 2004). The *nym* homozygote mouse starts clasping its hind limbs from 5 months of age. At this age, clasping occurs after a few seconds of free hanging and they can revert for a short while into extending their hind limbs slightly. However, with progressive age the clasping behaviour of the hind limbs occurs more rapidly. In addition, from 10 months the *nym* homozygote mice clasp their hind limbs immediately once lifted up by the tail, and go so far, to use their front paws to wrap around the hind limbs to receive more support.

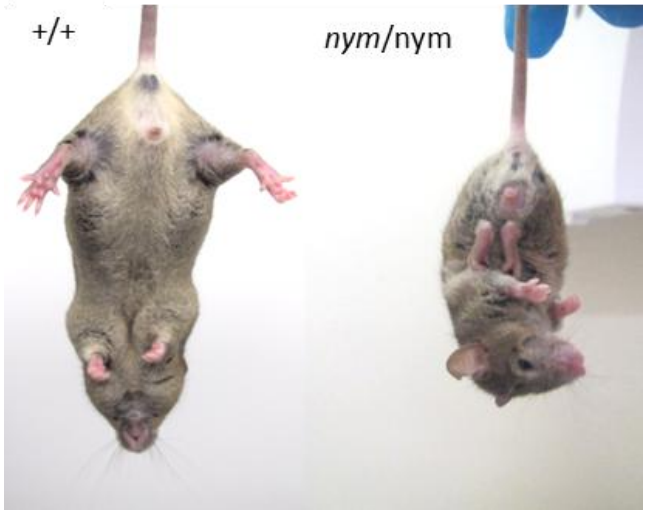

Figure 4.6. Hind limb clasping is present from 5 months in the *nym* homozygote mouse
The male wild-type (+/+) mouse extends its hind paws to balance its body posture. In contrast the male *nym* homozygote (*nym/nym)* mouse is unable to balance its body with its hind limbs and clasps them into its body and even attempts to hold on to them with its front paws. Furthermore a prolapse penis is present in the *nym* homozygote mouse (n=8).

4.2.6. Reduced motor strength and ataxia are characteristics of the *nym* homozygote mouse

Psychomotor retardation is impaired in MLII patients and a direct consequence is often slowness in mental activity and locomotion. To test these parameters, the rotarod and inverted screen tests were used to investigate specific differences in motor coordination and strength, respectively. Indeed, the *nym* homozygote mouse showed reduced muscle strength on the

inverted screen test and reduced motor balance and coordination on the rotarod at 3, 6 and 12 months (Figure 4.7A+B). The rotarod and inverted screen performances also worsened with age as seen at 6 and 12 months (Figure 4.7A+B).

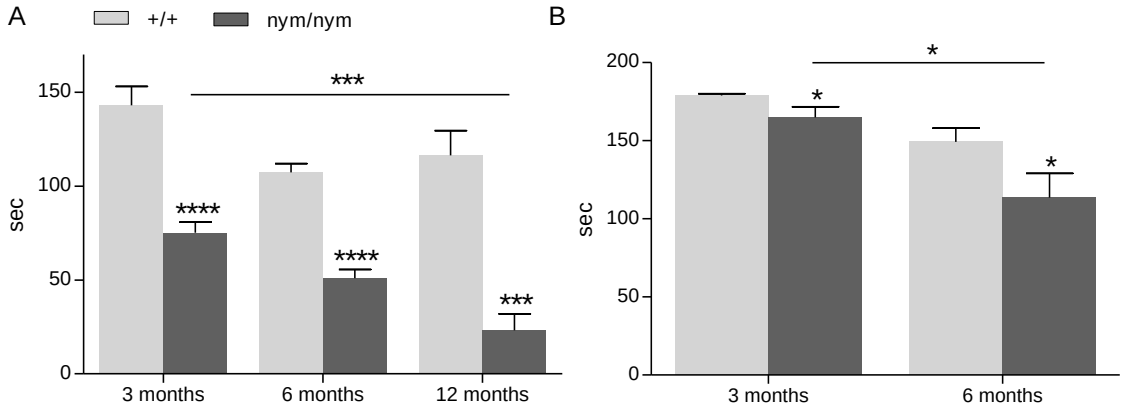

Figure 4.7. The *nym* homozygote mouse presents with impaired motor function
(A) Reduced motor co-ordination on the rotarod is present in the *nym* homozygote (*nym/nym)* mice in comparison to wild-type mice (+/+) and is significant at all ages from 3 to 12 months. The performance on the rotarod progressively worsens from 3 to 12 months. **(B)** *Nym* homozygote mice present with reduced muscle strength when measured on the inverted screen. The performance also worsens progressively with age. Values are expressed as mean±SEM (n=8; A: two-tailed Student's t-test; B: Mann Whitney U test; *P<0.05, ***P<0.001, ****P<0.0001).

As impaired motor strength and coordination was shown using the rotarod and inverted screen, locomotion was subsequently analysed in more detail by using the Noldus CatWalk™ automated gait analysis (Hamers et al. 2001), to confirm an ataxic gait. There are three main independent analytic categories of the CatWalk™ system (including subcategory used): *coordination parameters* (regularity index and phase dispersion), *static paw parameters* (stride length and single stance) and *dynamic paw parameters* (swing) (Koopmans et al. 2007). The results will be presented starting with the basic coordination defects in the *nym* homozygote mouse, then focusing specifically on the front paw movement abnormalities and finally ending with the dynamic parameters of body speed. Progression of the movement defects were analysed with age and any early indicators of movement defects found in mice, that were present at 3 months of age.

In healthy, fully coordinated animals the gait regularity value is ~100%. The wild-type mice consistently had a regularity index of around 80-100%, whereas the *nym* homozygote mice

progressively decreased in regularity index from 80% to 50-60% (Figure 4.8A). At 3 months there was no significant difference in the regularity index, hence more specific parameters were investigated to define where the reduced regularity index originates. The base of support parameter measures a larger front paw distance between the *nym* homozygote mice than between wild-type mice and this is already significant at 3 months (Figure 4.8B). This indicates an imbalance at early age and this parameter progressively worsens from 6 to 12 months implying that the *nym* homozygote mouse becomes more and more imbalanced.

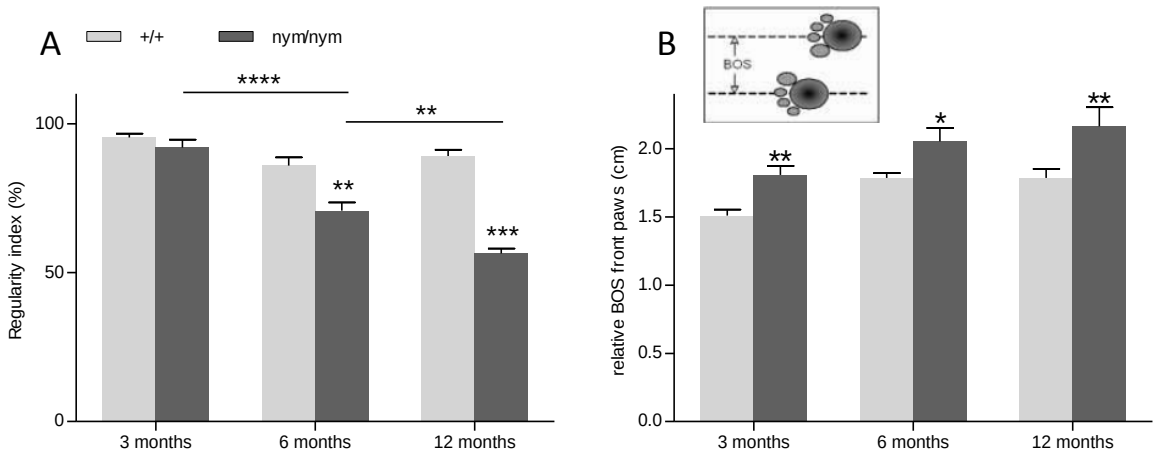

Figure 4.8. Reduced regularity index and increased front paw base of support contribute towards abnormal gait

(A) Regularity index is expressed as percentage (%) of normal step relative to the total number of paw placements of the *nym* homozygote (*nym/nym*) and wild-type (+/+) mice. **(B)** Front paw base of support (BOS) is expressed as the distance between the front paws in cm. Values are expressed as mean±SEM (n=8; two-tailed Student's t-test; *P<0.05; **P<0.01, ***P<0.001, ****P<0.0001).

To break down the regularity index and base of support in more detail, a closer look at inter limb phase dispersion was taken. In wild-type mice, in the diagonal paw pairs (left hind (LH) (anchor) - right front (RF) (target), left front (LF) (anchor) – right hind (RH) (target)) the target paw typically moves synchronously with the anchor so the initial contacts occur simultaneously resulting in a phase dispersions value of 0%. This is represented by the wild-types in this study by ~10%. However the *nym* homozygote mouse shows progressive increasing values from 3 to 12 months up to 30-40%. This means the target and anchor paw move more asynchronously with age. There is a very similar trend in both LH-RF and LF-RH movement (Figure 4.9A+B). Girdle pairs (RF-LF, RH-LH) did not show any significant difference between wild-type and *nym* homozygote mice (Figure 4.9C+D). Lateral pairs (RF-

RH, LF-LH) usually yield a phase dispersions value of 50%. This remains the same for wild-type and *nym* homozygote mice at 3 months presenting with a value of ~60%. However, there is a dramatic reduction in this value at 6 months in which the phase dispersion value is only 15-20% and progressively worsens at 12 months to 10%. An imbalance in gait is greatly noticed in the lateral pairs (Figure 4.9E+F). The *nym* homozygote mouse presents with an imbalanced gait due to abnormal performance specifically in the front paw parameters, base of support and diagonal and lateral paw pairs leading to a progressive, abnormal step cycle.

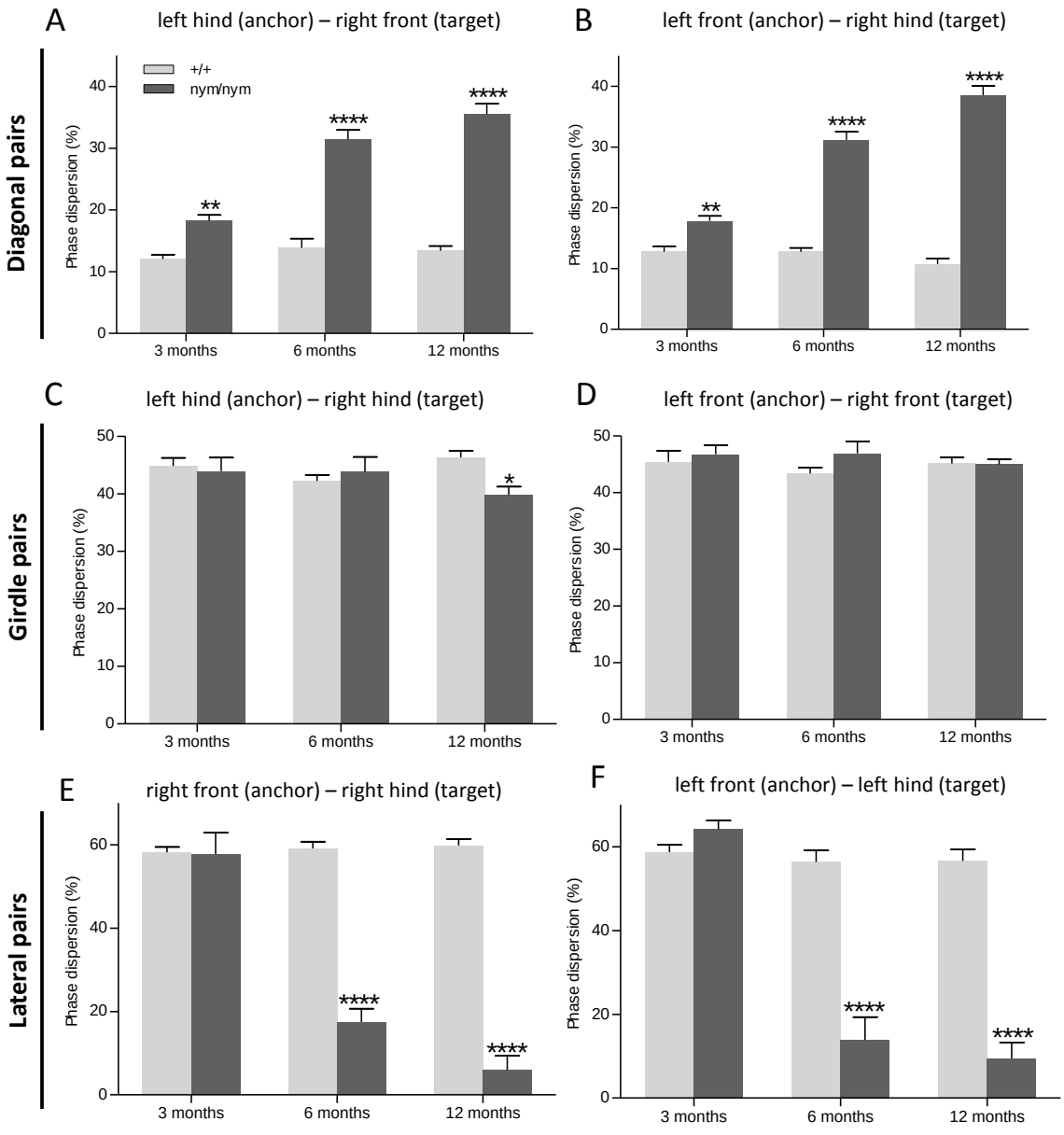

Figure 4.9. Phase dispersion, a measure of inter-paw coordination, is abnormal in diagonal and lateral paw pairs, but not in girdle paw pairs

Diagonal paw pairs: **(A)** LH-RF phase dispersion **(B)** LF-RH phase dispersion; Girdle paw pairs: **(C)** LH-RH phase dispersion **(D)** LF-RF; Lateral paw pairs: **(E)** RF-RH phase dispersion **(F)** LF-LH phase dispersion of *nym* homozygote (*nym/nym*) and wild-type (+/+) mice. Values are expressed as mean±SEM (n=8; two-tailed Student's t-test; *P<0.05; **P<0.01, ***P<0.001, ****P<0.0001).

The front paw parameters are predominantly affected in the *nym* homozygote which has already been shown by the front paw base of support. To investigate this further, the individual front paw parameters within a step cycle were analysed. The *nym* homozygote mouse showed reduced swing (increased time of the front paws spent on the glass plate) (Figure 4.10A), reduced stride length (Figure 4.10B) and reduced single stance (duration of ground contact with a single paw) (Figure 4.10C). No significant alterations were observed in the hind paw parameters.

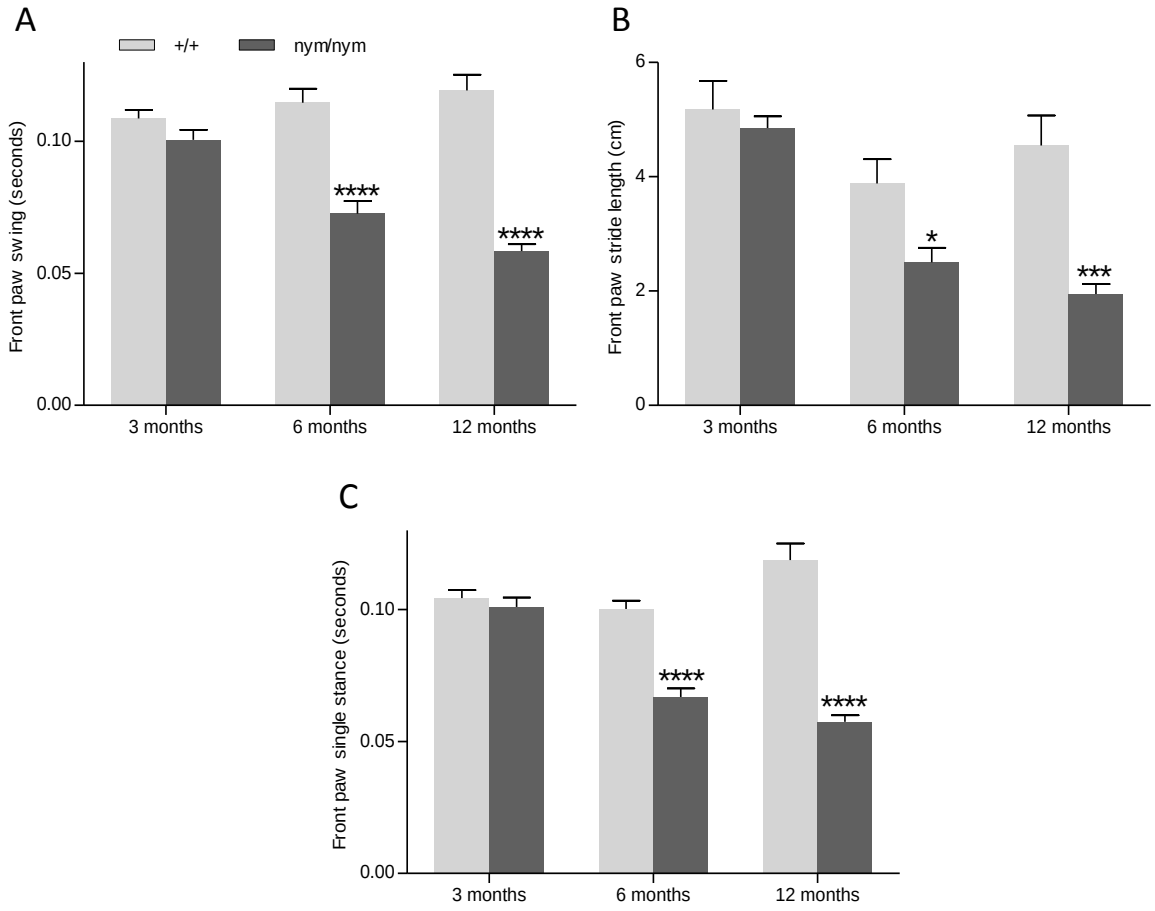

Figure 4.10. Abnormal gait specifically for the front paw parameters is present at 3, 6 and 12 months of age

(A) Swing time in seconds of wild-type (+/+) and *nym* homozygote *(nym/nym)* mice. **(B)** Stride length in cm of wild-type and *nym* homozygote mice. **(C)** Single Stance in seconds of wild-type and *nym* homozygote mice. Values are expressed as mean±SEM (n=8; two-tailed Student's t-test; *P<0.05, ***P<0.001, ****P<0.0001).

4.2.7. The *nym* homozygote mouse, like mucolipidosis II patients, present with mental retardation

As MLII patients have prominent psychomotor retardation, cognitive deficits were investigated in this mouse model using a preliminary test. The Y-Maze spontaneous alternation task was employed and it gives a measure of working or short term memory (Sanderson and Bannerman 2012). The hippocampus and the frontal cortex have been proposed to be important for these functions (Goldman-Rakic 1987). In contrast to wild-type mice, which show a high level of performance in this task, *nym* homozygote mice just about reached chance levels, which is defined as 50% alternation in choosing an arm by random (Figure 4.11). No progression of performance with age was observed. These results demonstrate, for the first time, behavioural deficits in psychomotor performance in a mouse model of MLII, which is a typical finding in MLII patients.

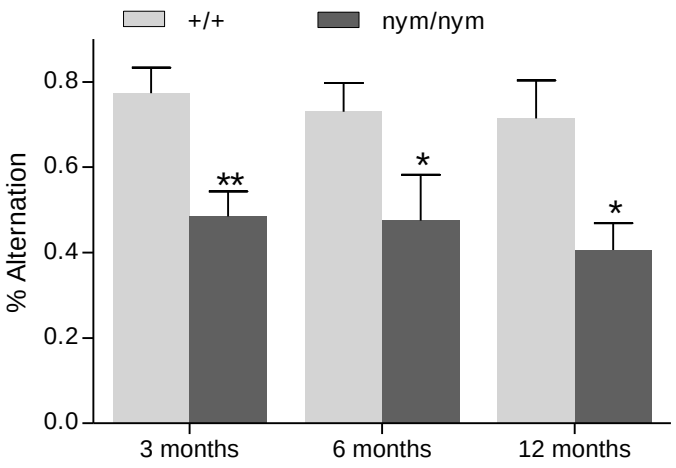

Figure 4.11. Reduced performance in the spontaneous alternation task at all ages of the *nym* homozygote mouse
Percentages (%) are shown of the spontaneous alternation in the Y-maze of *nym* homozygote (*nym/nym*) and wild-type (+/+) mice. Values are expressed as mean±SEM (n=18-25; two-tailed Student's t-test; *P<0.05; **P<0.01).

4.2.8. Progressive neurodegeneration detected in the *nym* homozygote mouse

Ataxia typically results from dysfunction of the cerebellum, that controls balance and motor coordination, hence the cerebellum and brain were analysed for any gross pathology. The *nym* homozygote brain is about 30% smaller than the wild-type brain, including the cerebellum (Figure 4.12A). The cerebellum was further investigated to see whether the mutant had any specific defects in the overall structure and total cell number. Immunohistochemical staining for

calbindin showed a substantial loss of Purkinje cells (PCs), the main cell output to the cerebellum, in 11-month-old *nym* homozygote mice with an onset from 7-months (Figure 4.12B). The PC loss and atrophy of brain tissue worsened over time from 7 months, with about 50% PC loss at 11 months (Figure 4.12B). At 3 months there was no PC loss present, however axonal spheroid formation and axonal torpedoes, typical of cell atrophy, was already observed (Figure 4.12C+D). The wild-type brain pathology did not worsen with aging and no PC loss was observed at 7 or 11 months.

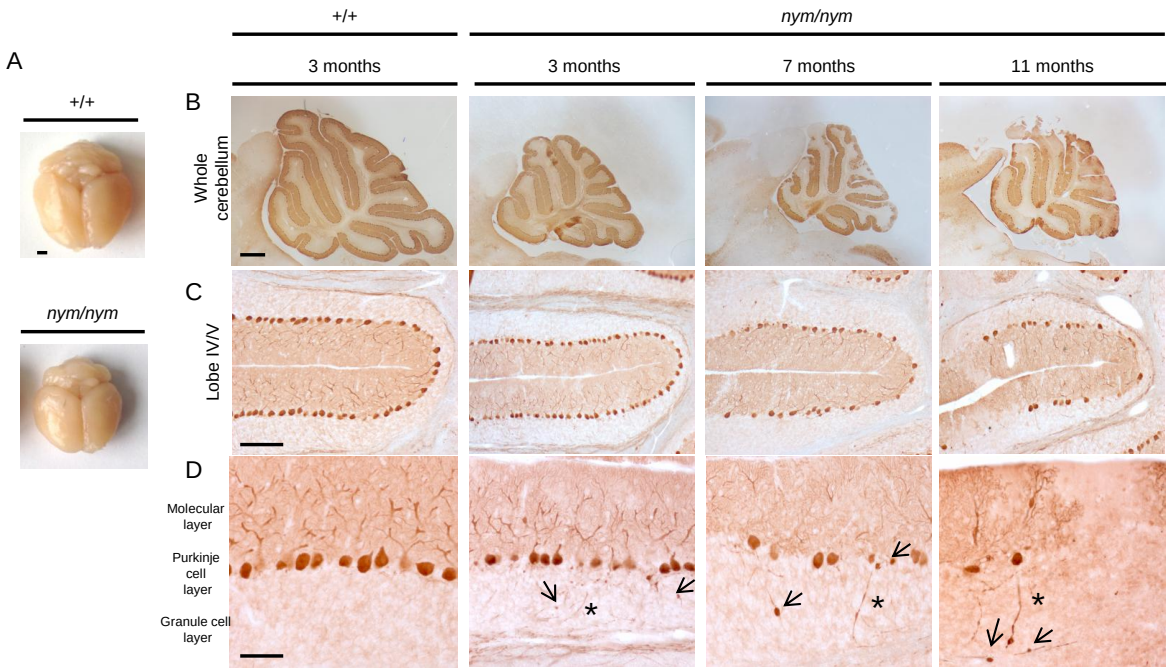

Figure 4.12. Reduced brain and cerebellum size, progressive Purkinje cell loss, axonal swelling and neuronal torpedoes is the *nym* homozygote brain
(A) The *nym* homozygote (*nym/nym*) brain is about 30% smaller than the wild-type (+/+) brain (n = 6, scale bar: 3mm). **(B)** Parasagittal brain sections were immunostained for the Purkinje cell (PC) marker calbindin. Analysis of PC degeneration in the whole cerebellum in 3, 7 and 11 month old *nym* homozygote mice showed progressive PC loss (n = 6, scale bar: 300µm). **(C)** Lobe IV/V is shown as a representative lobe of the cerebellum. The majority of PCs in lobe IV/V are still present at 3 months, but only 75% remain at 7 months and only 40-50% remain at 11 months (n = 6, PCs were counted manually in lobe IV/V, scale bar: 100µm). **(D)** Higher-magnification images of the 3 month old *nym* homozygote brain revealed axonal spheroids/torpedoes proceed PC loss. Swelling of PC axons (arrow) and neuronal torpedoes (*) in the white matter are observed already at 3 months and increase in severity with age (n = 6, scale bars: 50µm).

Cell death is often accompanied by an inflammatory response and a defect in myelination. It is unclear if these processes are secondary or primary events to cell death (Minghetti et al.

2005). Hence to further investigate the pathology observed in the cerebellum, myelination and inflammation in the *nym* homozygote brain was investigated. Brain sections were stained for myelin using luxol fast blue stain and inflammation was investigated by staining the sections for glial fibrillary acid protein (GFAP). Luxol stains the lipoproteins in the white matter tracts highlighted by the spaced lines. Demyelination of the cerebellum occurred with thinning of the white matter tracts (Figure 4.13A). A reduced width of lipoprotein staining in the white matter tracts in midst of lobe IV/V and IX, which are presented as zoomed images (Gigure 4.13A 1-4), can be clearly observed in the *nym* homozygote mouse. Preliminary data of an inflammatory response was also present, as seen by an increase in GFAP immunoreactivity in the cerebellum. Astrogliosis appears to be present in the white matter, granular and PC layer (Figure 4.13B). However, further experiments are needed to confirm exact localisation and conduct quantifications.

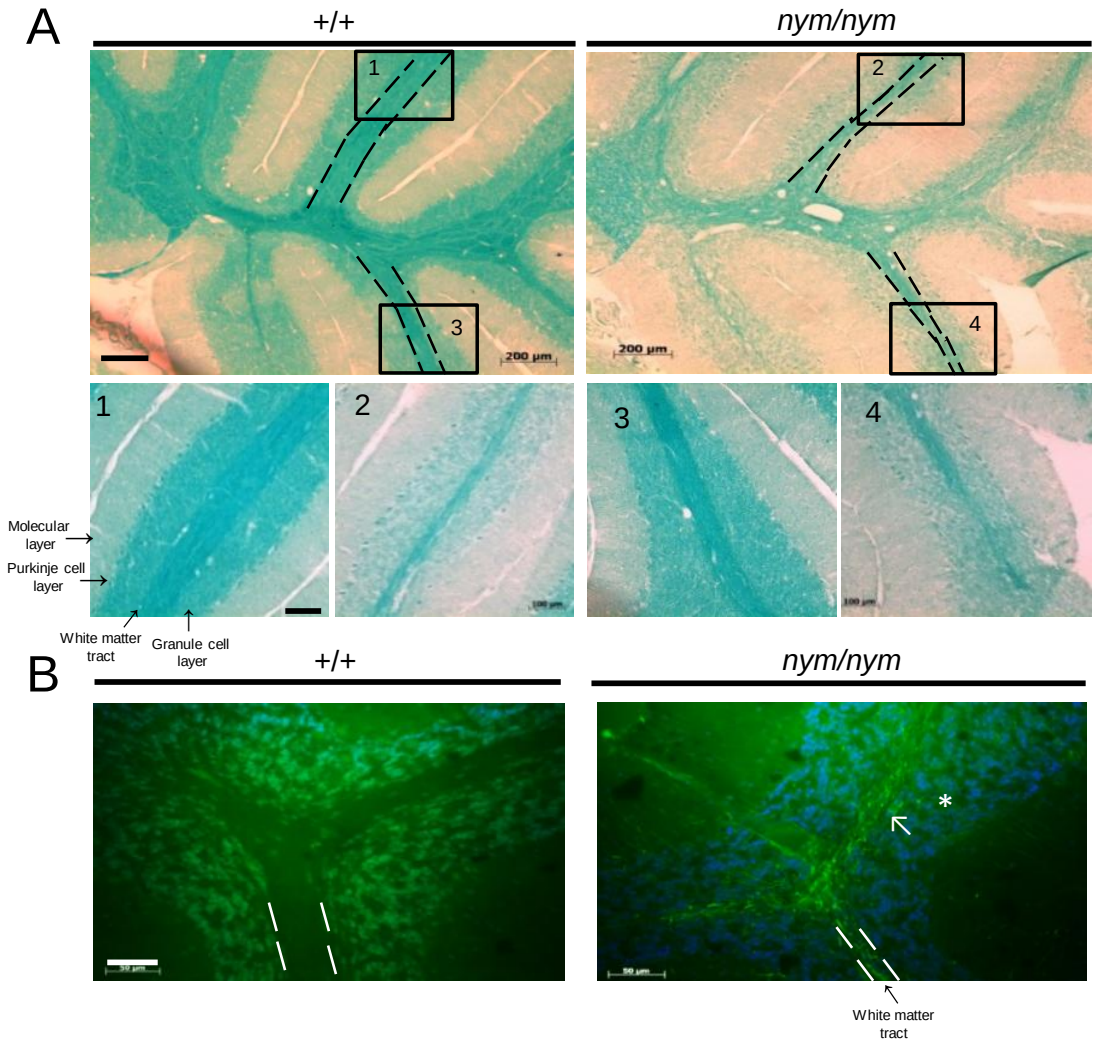

Figure 4.13. Demyelination and inflammation is present at 12 months
(A) Luxol fast blue staining of the cerebellar sections indicates decreased myelination and degeneration of the subcortical white matter in the *nym* homozygote *(nym/nym)* mouse in comparison to the wild-type (+/+) control. The lower panels are zoomed images from the numbered boxes in the top panels. Boxes 1 and 2 present a zoomed image of lobe IV/V of the +/+ and *nym/nym*, respectively. Boxes 3 and 4 present zoomed images of lobe IX of the +/+ and *nym/nym*, respectively. It can clearly be seen that the white matter tracts, which contain the myelin, are thinned in the *nym/nym* mouse. (n = 4; Top panel scale bar: 200 µm; Bottom panel scale bar: 100 µm.) **(B)** Preliminary data of strong immunoreactivity for glial fibrillary acidic protein (GFAP)(green) throughout the *nym* homozygote mouse brain and nuclei with DAPI (blue) (n = 4, scale bar: 50 µm). The DAPI stain can be discounted for in this instance as the staining has not been successful in the +/+. Spaced lines outline the white matter tracts, the arrow (↑) highlights potential granule layer inflammation and the star (*) highlights potential Purkinje cell inflammation. Further experiments are however needed to confirm exact localisation of the inflammatory response. Data produced by Dr Emmanuelle Bitoun.

The autophagy-lysosome pathway (ALP) is responsible for the degradation of waste material in the cell. The lysosomes do not have functioning hydrolases in MLII and it is expected that the process of autophagy might be deregulated as autophagosomes filled with waste material cannot fuse with lysosomes (Nixon et al. 2008). Therefore, the amount of

lysosomes present in brain homogenate was analysed as an indication of functioning of the ALP. Western blot analysis indicated a non-significant increased amount of the lysosomal-associated membrane marker 1 (Lamp1) in the *nym* homozygote brain homogenate (Figure 4.14).

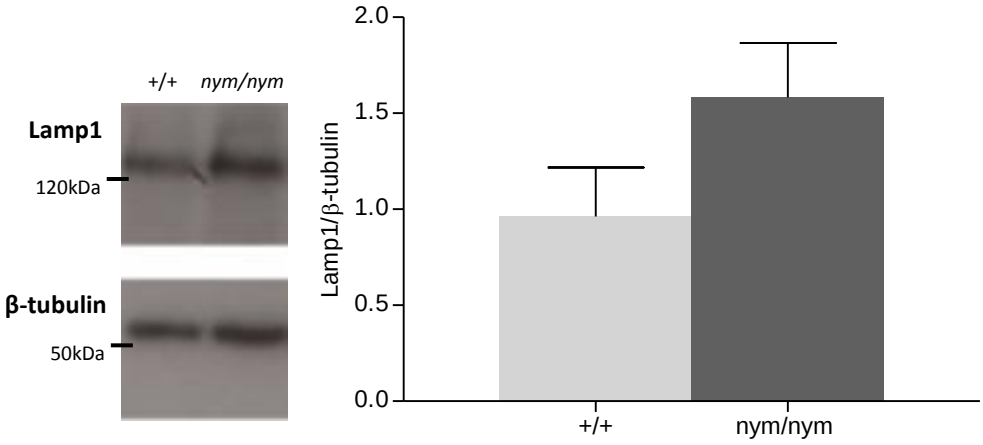

Figure 4.14. Increased Lamp1 as a marker of increased presence of lysosomes in brain homogenate at 4 months

Representative western blot showing levels of Lamp1 in wild-type (+/+) and *nym* homozygote *(nym*/*nym)* mice. β-tubulin was used as a loading control. The amount of Lamp1, expressed as the ratio of densitometric measurement of the Lamp1 to the corresponding internal standard (β-tubulin), is shown in the right panel (n = 4; two-tailed Student's t-test).

4.2.9. Deregulation of lysosomal enzymes and loss of Npc2 protein in the *nym* homozygote brain

The *nym* homozygote mouse presents with a severe brain pathology, as detailed above, leading to lysosomal activity being investigated for any deregulation in the cells of the brain. The lysosomal activity was assayed in brain homogenates of wild-type and *nym* homozygote mice. The lysosomal activity in the *nym* homozygote brain was deregulated in comparison to the wild-type. β- hexosaminidase, α-mannosidase and β-glucoronidase were increased by 1.5 fold, whereas β-galactosidase was significantly decreased by 30% (Figure 4.15A). Lysosomal enzyme activities for brain homogenate in nmol/mg/h can be seen in appendix table 2.

The cerebellar pathology in the *nym* homozygote mouse presents many similarities to another LSD called Niemann-Pick disease type C (NPC) disease. The loss of either the

membrane protein NPC1 or the soluble protein NPC2, which is trafficked by the M6P pathway to the lysosomes, can cause this disease. Hence, brain homogenate was stained for the protein Npc2 by western blotting and indeed a loss in Npc2 in the *nym* homozygote brain was observed (Figure 4.15B).

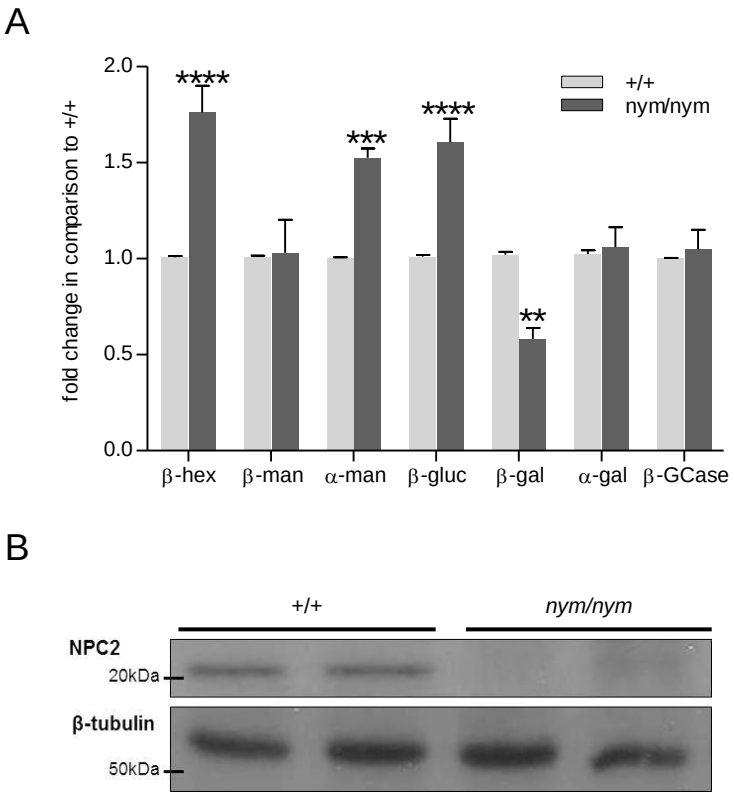

Figure 4.15. Biochemical pathological alterations in the *nym* homozygote brain
(A) The relative enzyme activities of the lysosomal hydrolases β-Hexosaminidase (β-Hex), β-Mannosidase (β-Man), α-Mannosidase (α-Man), β-Glucuronidase (β-Glu), β-Galactosidase (β-Gal), α-Galactosidase (α-Gal) and β-Glucocerebrosidase (β-GCase) were measured in whole brain homogenates of wild-type (+/+) and *nym* homozygote (*nym*/*nym)* mice (4 months of age). The specific activities of the wild-type were set to 1. Values are expressed as mean±SEM (n=8; two-tailed Student's t-test; **P<0.01, ***P<0.001, ****P<0.0001). **(B)** Representative western blot showing levels of Npc2 in two wild-type and two *nym* homozygote mice. β-tubulin was used as a loading control (n=4).

4.2.10. Increased glycolipid and cholesterol storage in the *nym* homozygote brain

Due to the deregulation of lysosomal enzymes, it was of interest to analyse which substrates accumulate in the *nym* homozygote brain. Periodic acid Schiff, a stain used to detect polysaccharides, such as glycolipids, and filipin, a highly fluorescent compound that binds to cholesterol, were used to stain brain section for accumulation. Stained brain sections revealed increased glycolipid and cholesterol storage in the cerebellum, cortex and hippocampus (Figure 4.16A+B). Specifically, the cerebellar molecular layer had increased storage of glycolipids in comparison to the granular layer (Figure 4.16B, upper panel). Large amounts of stored glycolipids were present in cortical layers 3-5 (less so in layers 1-2) (Figure 4.16B, middle panel) and in layers CA1 (cornu ammonis 1) and CA3 (cornu ammonis 3) of the hippocampus (Figure 4.16B, lower panel). These findings agree with what is observed in NPC mouse models and α-mannosidosis causing GM2 (ganglioside monosialic 2) accumulation (Gondré-Lewis et al. 2003, Goodman et al. 1991).

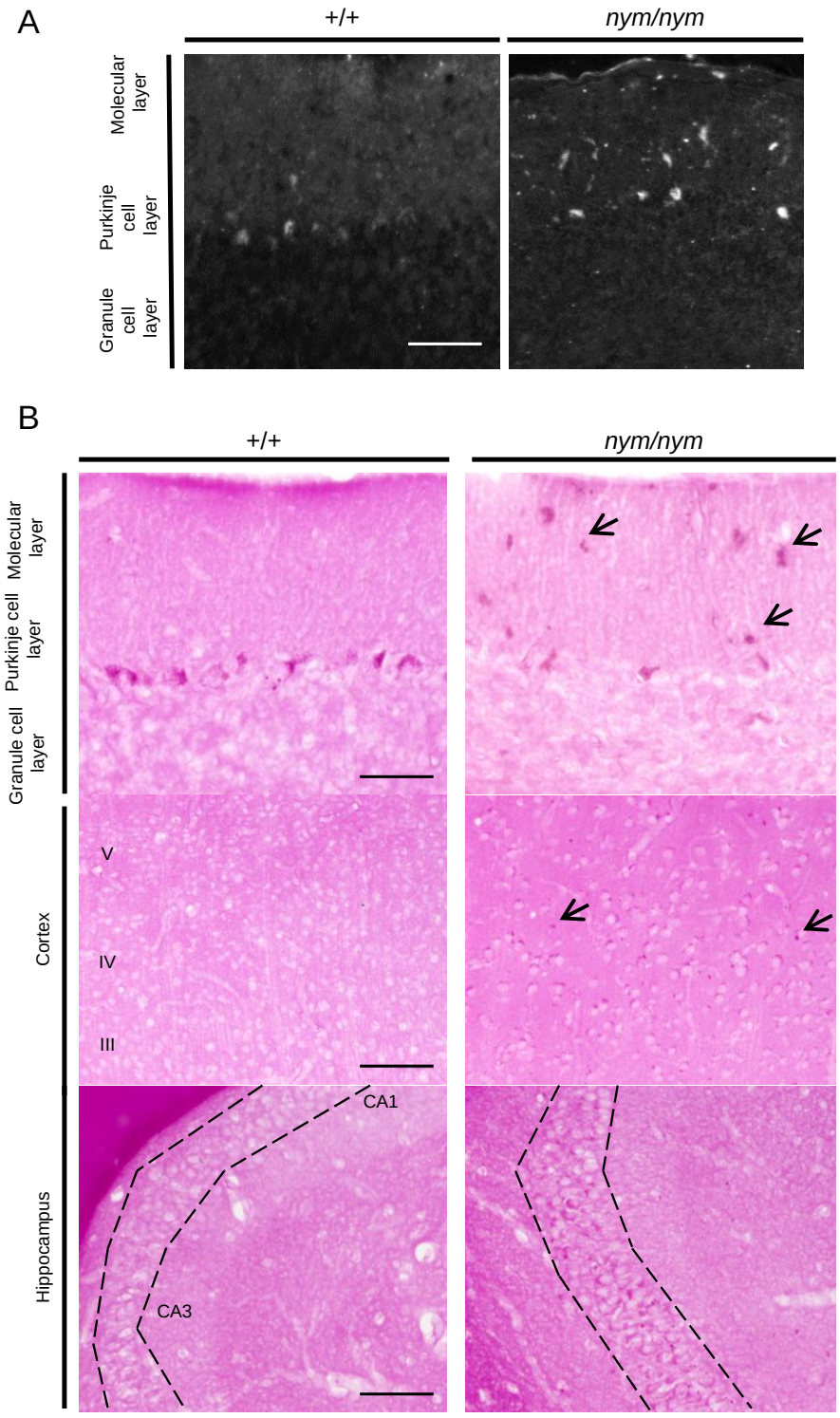

Figure 4.16. Biochemical pathological alterations in the *nym* homozygote brain

(A) *Nym* homozygote (*nym/nym*) and wild-type (+/+) brain sections were stained with filipin for detection of cholesterol. The molecular layer of the *nym* cerebellum showed increased storage in comparison to the wild-type control (n=4, scale bar: 50 µm). **(B)** *Nym* homozygote and wild-type brain sections were stained with Periodic acid-Schiff for detection of glycolipids. Increased storage was detected in the cerebellum, specifically in the molecular layer, the cortex, specifically layers 3-5 and the hippocampus, specifically layers CA1 and CA3 (n=4, scale bar: 50 µm).

4.2.11. Purkinje cell loss could not be delayed by cyclodextrin treatment

Finding a loss of Npc2 protein was intriguing as the PC degeneration in our mouse model of MLII was very similar to what is described in NPC disease. NPC disease is an autosomal-recessive LSD that leads to the accumulation of cholesterol and sphingolipids. Furthermore an increase of cholesterol in the brain of the *nym* homozygote mouse was observed which is another major hallmark of the NPC disease, suggesting that loss of Npc2 function may be a factor driving this aspect of pathogenesis. To test whether dysfunction of the Npc2 pathway is also implicated in the brain pathogenesis of the *nym* homozygote mouse, this mutant was treated with 2-hydroxypropyl-β-cyclodextrin (cyclodextrin) for 7 months when PC loss is observed. In addition, this study might help provide a potential new therapeutic strategy for MLII. Cyclodextrin has shown to delay PC death and improve the life span of NPC mouse models (Davidson et al. 2009). This drug is now in clinical trials for NPC. Hence *nym* homozygote mice were treated weekly with the drug cyclodextrin (4000mg/kg) from postnatal day 7 (P7) up to 7 months. The vehicle for this drug was PBS. This regime was chosen based on the successful trial in a NPC mouse model (Davidson et al. 2009). Mice were tested on their motor behaviour at 3 and 7 months. In addition, the brains were collected at these ages to investigate the drugs effect on cerebellar pathology. These ages were chosen as already at 3 months motor impairment and cerebellar pathology were observed and at 7 months PC loss becomes a prominent feature of the cerebellar pathology.

To investigate a delay in PC loss, the mice were assessed on their motor behaviour on the rotarod and inverted screen. However, no improvement in rotarod or inverted screen performance was observed at 3 and at 7 months (Figure 4.17 A-D).

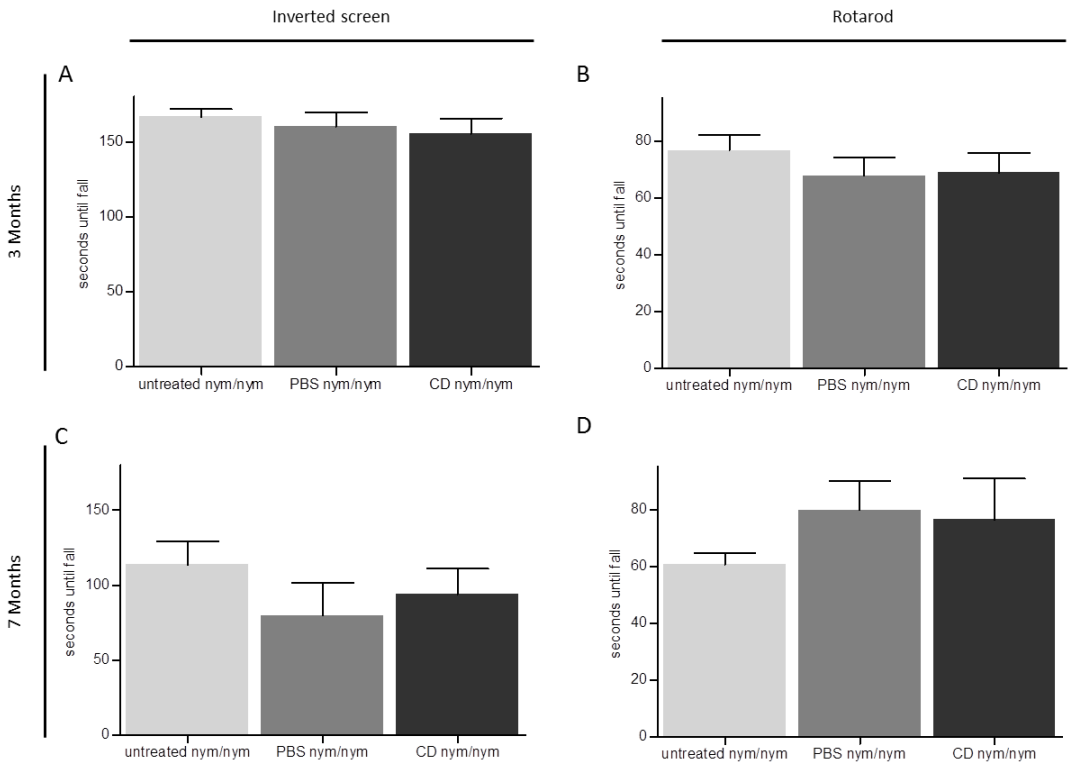

Figure 4.17. Cyclodextrin treatment does not improve motor function at 3 or 7 months of age
Three and seven month old cyclodextrin (CD) treated *nym* homozygote *(nym/nym)* mice perform the same as PBS and untreated *nym* homozygote mice on the inverted screen (3 months:**A** and 7 months:**C**) and rotarod (3 months:**B** and 7 months:**D**). Values are expressed as mean±SEM (n=8-10; 1-way ANOVA, with Dunnett's post-hoc test).

Furthermore, PC loss using calbinin was assessed. At three months the same level of swellings, axonal torpedoes and spheroids were observed in the cyclodextrin treated *nym* homozygote mice as in the vehicle treated control *nym* homozygote mice (Figure 4.18A+B).

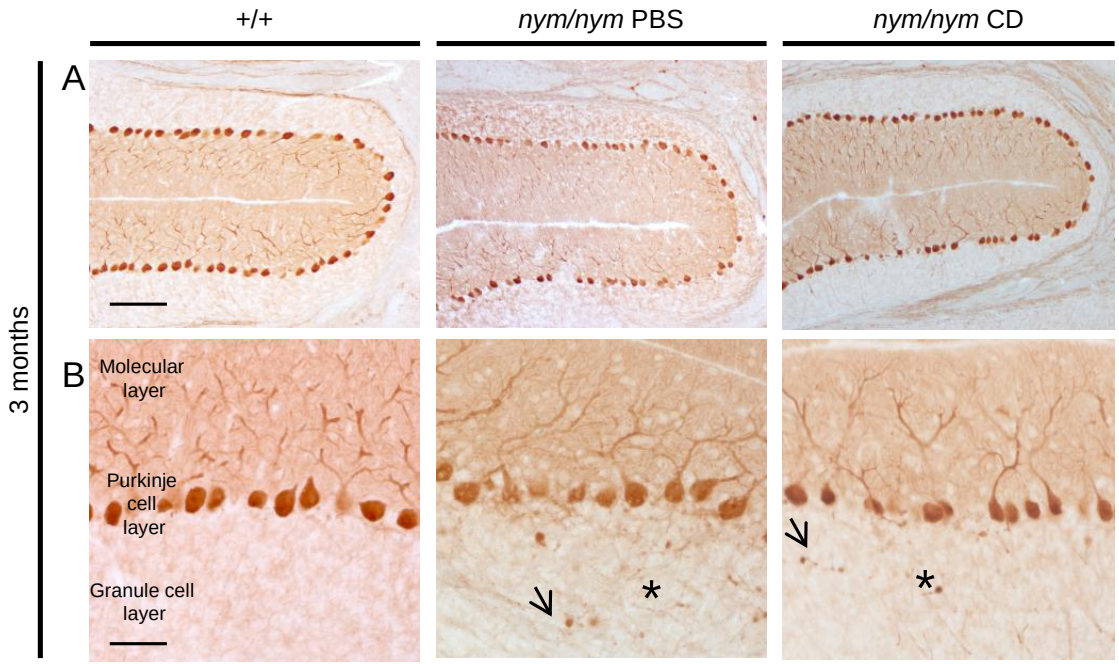

Figure 4.18. Cyclodextrin does not delay formation of axonal swellings and torpedoes at 3 months
P7 *nym* homozygote *(nym/nym)* mice were injected weekly for 7 months with cyclodextrin (CD) at 4000 mg/kg or the vehicle PBS (n=8 in each group). **(A)** No Purkinje cell (PC) loss was observed at 3 months as can be seen in lobe IV/V as a representative lobe of the cerebellum. Scale bar: 100µm **(B)** Typical signs of PC degeneration including swelling of PC dendrites (arrow) and axonal torpedoes (*) can be observed. Scale bars: 50µm.

At 7 months a similar level of PC loss was observed in the cyclodextrin treated *nym* homozygote mice as in the PBS treated control *nym* homozygote mice. Also, similar swellings, axonal torpedoes and spheroids were observed in the cyclodextrin treated *nym* homozygote mice as in the vehicle treated control *nym* homozygote mice (Figure 4.19 A+B).

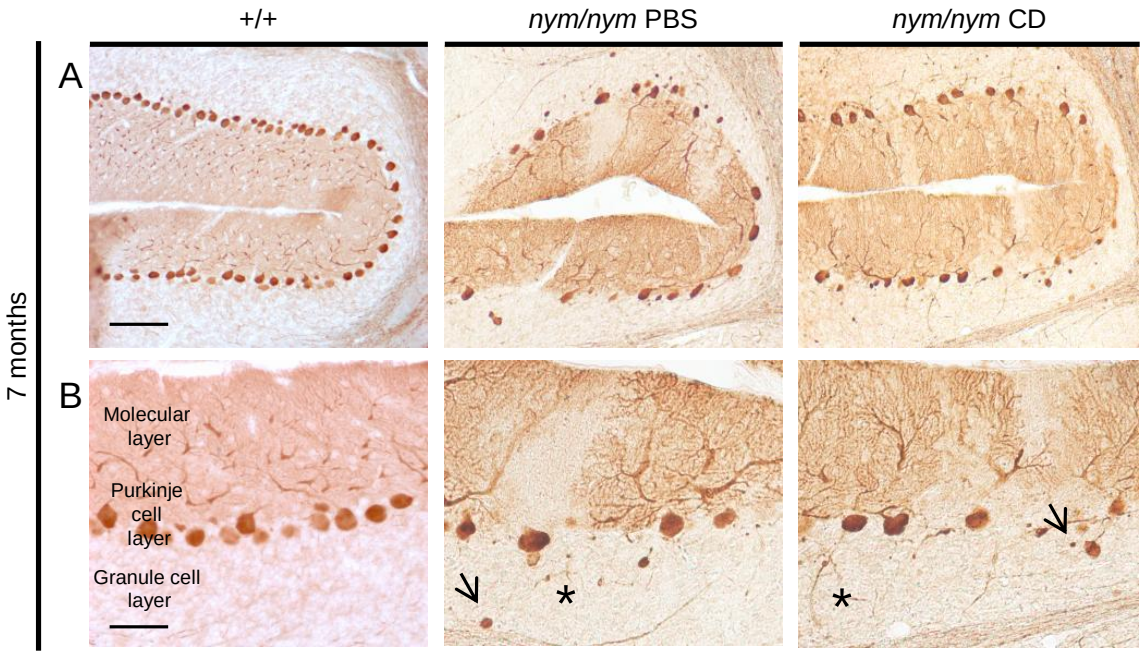

Figure 4.19. Cyclodextrin does not cause a delay of Purkinje cell loss, axonal swellings and torpedoes at 7 months

P7 *nym* homozygote *(nym/nym)* mice were injected weekly for 7 months with cyclodextrin (CD) at 4000 mg/kg or the vehicle PBS (n=8 in each group). **(A)** Purkinje cell (PC) loss was observed at 7 months in lobe IV/V as a representation of a lobe of the cerebellum in *nym* homozygote PBS and *nym* homozygote CD treated mice. Scale bar: 100µm **(B)** Typical signs of PC degeneration including swelling of PC dendrites (arrow) and axonal torpedoes (star) can be observed. Scale bars: 50µm.

4.3. Discussion

In this chapter, a novel mouse model of MLII, homozygous for a mutation in the *GNPTAB* gene that has been reported in patients with this disease, was described (Cathey et al. 2010). The novel mouse model of MLII more fully recapitulates the human pathology showing growth retardation, skeletal and facial abnormalities, increased circulating lysosomal enzymatic activities, intracellular lysosomal storage and reduced life span. Importantly, the *nym* homozygote mouse also models typical MLII behavioural deficits, including impaired motor function and psychomotor retardation, which has been investigated in this study for the first time. Histological analysis of the brain revealed progressive neurodegeneration in the cerebellum with severe PC loss as the underlying cause of the ataxic gait. In addition, based on similar features between NPC and MLII, the *nym* homozygote mice were treated with cyclodextrin, a drug previously reported to rescue PC death in a mouse model of NPC disease. No improvement in brain pathology was observed, demonstrating that cerebellar degeneration is not primarily triggered by loss of Npc2 function. This study emphasizes the value of modelling patient *GNPTAB* mutations to generate clinically relevant mouse mutants to elucidate the pathogenic molecular pathways of MLII and address their amenability to therapy.

4.3.1. The *nym* homozygote mouse presents as a novel mouse model of mucolipidosis II

The novel mouse model of MLII carries a premature stop codon mutation previously reported in a patient (Cathey et al. 2010). Importantly, unlike the existing *Gnptab* knock-out mouse model, it more completely recapitulates the characteristic pathological features observed in patients including facial and skeletal abnormalities, deregulation of lysosomal enzyme activities, abnormal intracellular storage but also psychomotor retardation, motor dysfunction and reduced life span (Table 4.2) (Kornfeld and Sly 2001). The novel *nym* homozygote mouse resembles features present in the feline model of MLII, which had so far been the animal model most closely resembling MLII patient pathology. The facial and skeletal abnormalities reported in MLII patients were very prominent in this novel mouse model, features that had not been

reported in the *Gnptab* knock-out mouse. Furthermore, reduced survival was present in the *nym* homozygote mouse, which again was not confirmed in the *Gnptab* knock-out mouse. Similarly to the *Gnptab* knock-out, inclusion bodies found in secretory organs such as the pancreas and connective tissue cartilage in the trachea were confirmed. The *nym* homozygote also presents with inclusion bodies present in the fibroblasts which is a hallmark of MLII and has also been described in the *Gnptab* knock-out mouse. In this chapter the new mouse model has been validated, resembling the majority of MLII pathology. In addition, a detailed behavioural phenotypic description was conducted, which is the first of its kind in disease models of MLII.

4.3.2. Reduced muscle strength, ataxic gait and mental retardation are present in the *nym* homozygote mouse

MLII patients present with motor impairments such as daily difficulties, as for example just standing up by themselves (Cathey et al. 2010). Ataxic gaits had been observed in the feline models of MLII, but no behavioural tests had been conducted to quantify this ataxic gait. For drug trials and general phenotypic description a detailed behavioural analysis is important. In this chapter. the mice were tested on the rotarod for motor coordination, the inverted screen for muscle strength, the CatWalk^{TM} for detailed gait analysis and the spontaneous alternation task for cognition. The *nym* homozygote mouse showed an overall reduced performance on the rotarod and inverted screen test. The inverted screen test was only able to be conducted at 3 and 6 months of age because the wild-type mice increased in weight so much that these dropped off due to their weight but not specifically their muscle strength. This limitation has also been observed by other groups, especially in mouse strains that gain weight more than others (Carlson et al. 2010). The difference in weight is a factor that can affect the performance of other behavioural assessments such as the rotarod and CatWalk^{TM}, hence it is important to perform other tests to confirm the results. Due to the weight differences in the *nym* homozygote and the wild-type mice, parameters were excluded in the CatWalk^{TM} that depended on similarity of cohort's weight.

The Noldus CatWalk^{TM} gait analysis is a very detailed method of investigating which paw set is specifically causing the defective gait and enables comparison between different disease models to draw on similarities and differences. A general defect in regular step pattern was observed in the *nym* homozygote mouse which is progressive with age. This is quite a severe observation and only occurs in severe disease models of ataxia. Furthermore, a specific deficit in gait in the front paw set was detected. More parameters were significantly different to the wild-type in the front paws than in the hind paws. This kind of pattern is typical for hind paw paralysis in which the front paws are compensating for a defect in the hind paws. This observation has already been observed in a mouse model of mutant *Opa1* (optic atrophy 1). *Opa1* encodes for a mitochondrial fusion protein and the mutant mouse presents with axonal and myelin degenerations, abnormal autophagy and mitophagy leading to ataxic gait, cardiomyopathy and deafness. These mice also showed reduced time spent on the glass plate by the front paws to compensate for hind paw paralysis (Sarzi et al. 2012). Concluding, the *nym* homozygote mouse is imbalanced, as it spends less time with one paw on the glass plate because it is compensating for hind limb paralysis with the front paws.

4.3.3. The *nym* homozygote mouse confirms the neurodegenerative phenotype observed in the *Gnptab*$^{c.3145insC}$ knock-in mouse

The *nym* homozygote mouse resembles closely a recently described *Gnptab*$^{c.3145insC}$ knock-in mouse model of another MLII human mutation, the G1028X mouse equivalent (Table 4.2) (Kollmann et al. 2012). Both mutations lead to premature stop codons: The *nym* mutation Y867X leads to the production of a slightly truncated α-subunit retaining 95% of the wild-type equivalent, and the complete lack of the β-subunit; the *Gnptab*$^{c.3145insC}$ knock-in mutation G1028X carries a complete α- and a truncated β-subunit. Both mutations lead to a loss of the C-terminus of the β-subunit that contains a transmembrane domain and an ER-exit motif [RK]X[RK]. Without the ER-exit motif the protein will reside in the ER and not locate to the Golgi (Figure 4.2). This will ultimately lead to a non-functional Gnpta protein as the assembly of α- and β-subunit will not occur as the cleavage of the precursor protein occurs at the Golgi (Marschner et al. 2011), to which the protein will not locate.

Both mutants show several biochemical and clinical features of MLII including skeletal abnormalities and facial dysmorphisms. Phenotypic comparison of the different MLII mouse models are summarised in table 4.2. The *nym* homozygote spine presents with a thoracic curve in contrast to the wild-type, but also to the *Gnptab*$^{c.3145insC}$ knock-in (Kollmann et al. 2012). This might be because the *Gnptab*$^{c.3145insC}$ knock-in was analysed at 1 month in comparison to 12 months for the *nym* homozygote mouse in which the phenotype might have progressed. Both mice present with reduced life span, however the *nym* homozygote mouse presents with a survival of ~30% at 60 weeks, whereas the *Gnptab*$^{c.3145insC}$ knock-in presents with a 2% survival chance at 60 weeks. The reason for the differences is unknown, but it might be explained by a difference in background strain, husbandry effects, or n-numbers. On this occasion only 33 *nym* homozygote mice were analysed in terms of survival in comparison to 160 animals for the *Gnptab*$^{c.3145insC}$ knock-in (Kollmann et al. 2012), therefore it is possible that testing more animals could lead to more comparative results.

The neurodegenerative phenotype is very similar between the *Gnptab*$^{c.3145insC}$ knock-in and the *nym* homozygote mice, including progressive PC loss, demyelination and inflammation. Due to the lysosomal enzymes not being localised to the lysosomes correctly, these are unable to breakdown waste material leading to excess storage of gangliosides and cholesterol in various brain regions. These findings have not been reported in the *Gnptab* knock-out. Furthermore, the *Gnptab* knock-out mice did not display all the clinical features and symptoms of MLII patients which are modelled in the feline MLII model, *Gnptab*$^{c.3145insC}$ knock-in and *nym* homozygote mice (Gelfman et al. 2007, Vogel et al. 2009). However, recent studies reanalysed the brains of the *Gnptab* knock-out mice and revealed progressive neurodegeneration, PC loss, reactive microgliosis and hind limb-clasping at 4 to 6-months of age (Kollmann et al. 2012, Idol et al. 2014). Hence, the *Gnptab* knock-out brain does present with neurodegeneration as observed in the *nym* homozygote and *Gnptab*$^{c.3145insC}$ knock-in mice, but did not mention any facial or skeletal abnormalities or a reduced life span. Therefore these

results still highlight the potential toxic role of the remaining truncated Gnpta protein product present in the *nym* homozygote and *Gnptab*$^{c.3145insC}$ knock-in mice.

Lysosomal enzyme activities in serum show very similar trends in the *nym* homozygote and *Gnptab*$^{c.3145insC}$ knock-in mice, but also in the *Gnptab* knock-out mice despite the difference in phenotype. Therefore missorting of lysosomal enzymes is unlikely to be causing the differences in phenotype between the mice and perhaps differences can be attributed to the residual Gnpta protein in the *Gnptab*$^{c.3145insC}$ knock-in and *nym* homozygote mice exerting a potential toxic gain of function. These results highlight the value of clinically relevant point mutants compared to null models, as the null does not present with patient relevant pathology of reduced life span, skeletal and facial abnormalities (Table 4.2).

Psychomotor retardation is a common pathology in MLII patients, however neurodegeneration has so far not been reported in human MLII patients, except for minimal signs of neuronal and glial involvement (Martin et al. 1975). Patients die in their first decade of life in which PC death and early markers of neurodegeneration, e.g. inflammation, neuronal torpedoes and swelling of PC axons with formation of spheroids in the granular layer, would not be expected to be present. No investigations have been conducted so far in MLII patients, but the early markers might be cause for psychomotor retardation and should be investigated further.

A well-established link between cerebellar pathology and motor dysfunction has already been made (Ito 2000) and is supported by many cerebellar mutant mice that have ataxic phenotypes namely *Lurcher*, *hot-foot* and *staggerer* (Lalonde and Strazielle 2001). In the past decade, the cerebellum has also emerged as an important brain region for the control of higher cognitive functions (Schmahmann 1991). Connections run from the prefrontal cortex to the cerebellum that confirm involvement to cognitive networks (Schmahmann and Pandya 1997). Indeed, reports of cerebellar ataxia and psychomotor retardation segregate in many studies as Cayman cerebellar ataxia (Nystuen et al. 1996), isolated cerebellar hypoplasia (Ventura et al.

2006) and LSDs such as Niemann-Pick type C disease (Turpin et al. 1991). The spontaneous alternation task, which was conducted in the *nym* homozygote mice, is a measure of working or short term memory (Sanderson and Bannerman 2012) and the hippocampus and the frontal cortex have been argued to be important for these functions (Goldman-Rakic 1987). Microglia activation was observed in the *Gnptab*$^{c.3145insC}$ knock-in mouse in all brain regions. The strongest intensity was observed in the cerebellum, cerebral cortex, hippocampus and thalamus (Kollmann et al. 2012). This could explain why the *nym* homozygote mutant underperformed in the spontaneous alternation task. This is the first behavioural observation that these mice not only have motor slowness assessed by rotarod, CatWalk^{TM} and inverted screen, but also cognitive slowness challenged in the alternation task. Behavioural dullness is a hallmark of the human pathology and has been observed in the feline model of MLII, but so far in no other mouse model, which supports the *nym* homozygote being a human disease relevant model (Cathey et al. 2010, Mazrier et al. 2003). Interestingly, a recent report of parkinsonism in a MLIII patient has been characterised, broadening the link to more common neurodegenerative diseases (Hara et al. 2013). Further research will be necessary to confirm the exact brain region of dysfunction via measuring electrical activity in different brain regions to observe abnormalities in long-term potentiation which is known to be involved in memory formation (Matynia et al. 2002).

Table 4.2. Comparison of the *nym* homozygote mouse to *Gnptab*$^{c.3145insC}$ knock-in and *Gnptab* knock-out mice

MLII model	*Nym* homozygote mouse	*Gnptab* knock-out mouse	*Gnptab*$^{c.3145insC}$ knock-in mouse
Mutation	Patient mutation (c.2664C>G) in mouse: c.2601T>A leading to a truncation mutation	*Gnptab* gene trap mouse (Gelfman et al. 2007, Idol et al. 2014)	Patient mutation (c.3145insC) leading to a protein truncation G1028X (Kollmann et al. 2012)
Phenotype	Reduced life span	**Normal** life span	Reduced life span
	Growth retardation	Growth retardation	Growth retardation
	Skeletal abnormalities	**No** skeletal abnormalities	Skeletal abnormalities
	Craniofacial defects	**No** Craniofacial defects	Craniofacial defects
	Ataxic gait and reduced muscle strength and motor coordination analysed by CatWalk™, rotarod and inverted screen	Ataxic gate and reduced muscle strength and motor coordination	Presented with ataxic gait
	Mental retardation shown by the spontaneous alternation task	**No** report of behavioural dullness	**No** report of behavioural dullness
	Progressive neurodegeneration	Progressive neurodegeneration	Progressive neurodegeneration
	Inclusion bodies present in fibroblasts	Includion bodies present in secretory organs (Pancreas) and connective tissue (Cartilage)	Inclusion bodies present in fibroblasts
	Not analysed	Retinal impairments	Retinal impairments

Targeting efficiency of lysosomal enzymes to the lysosome is cell-type- and tissue-specific in human, and disease models of MLII (Owada and Neufeld 1982, Waheed et al. 1982, Boonen et al. 2011). Storage of glycolipids was observed in certain cell types of the *nym* homozygote brain. The M6P pathway is important in targeting the majority of lysosomal hydrolases to the lysosome, so high levels of storage would be anticipated. However, the storage of glycolipids and the pathology in general is not as severe as in single enzyme deficiency models such as Sandhoff disease in which greater glycolipid storage is observed and the mice have a greatly attenuated lifespan (Jeyakumar et al. 1999, Jeyakumar et al. 2003). This highlights the importance of alternative pathways that can deliver lysosomal hydrolases to the lysosomes and need to be further studied which is in agreement with Braulke and coworkers observations (Braulke and Bonifacino 2009, Kollmann et al. 2012).

4.3.4. Cyclodextrin does not delay Purkinje cell loss in the *nym* homozygote mouse

In this chapter it has been shown that loss of M6P residues in *nym* homozygote mice led to a loss of the Npc2 protein, that is involved in the lysosomal export of cholesterol and sphingolipids in the *nym* homozygote brain. Owing to the missorting of Npc2, a drug trial over 7 months was conducted, the age when PC death is observed, with cyclodextrin. This drug has shown to increase the life span and delay PC loss in an NPC disease model (Davidson et al. 2009). However, this treatment did not delay PC loss or motor impairment, suggesting that, the reduced levels of lysosomal Npc2 in MLII is not the primary mechanism that triggers PC degeneration. The pathology in the NPC mouse model, in which cyclodextrin was able to delay PC loss, has a more severe disease progression, with death around 3 months (Davidson et al. 2009). Mice were treated in this study from P7 and an earlier time point for the slower progressing disease in the *nym* homozygote mouse could have potentially improved the drug regime. However, dose and frequency of drug injections should have been adequate, although it is possible that a higher dose may show different affects. It is not entirely known how the drug functions as it has been shown that the drug does not reach the brain compartment (Pontikis et al. 2013). However, it is known that cyclodextrin can sequester cholesterol and stimulates

cholesterol trafficking for removal from the lysosomal compartments in cell culture (Vance and Karten 2014, Yancey et al. 1996). Further investigations would be necessary to exactly determine if cyclodextrin reduced cholesterol in the brain of the *nym* homozygous mouse. In the *nym* homozygote mouse no measurements were made to analyse peripheral organs or CNS cholesterol levels to assess cyclodextrin efficacy of cholesterol reduction. Furthermore, in other cyclodextrin treatment studies in NPC disease, rescue of myelination and amelioration of impaired autophagic flux was observed (Liao et al. 2009, Tamura and Yui 2015, Song et al. 2014). Demyelination of the cerebellum and impaired autophagy are present in the *nym* homozygote and *Gnptab*$^{c.3145insC}$ knock-in mouse. Therefore, future studies should focus on the analysis of which effect the cyclodextrin treatment had in the *nym* homozygote mouse to help understand the mechanism of action of cyclodextrin.

In MLII the majority of lysosomal enzymes are not delivered to the lysosomes and more heterogeneous substrates accumulate in the cells than in single enzyme deficient LSDs. Hence, analysis of cholesterol reduction in the brain needs to be investigated. If this was the case, it can be concluded that for the MLII CNS pathology reducing cholesterol is not sufficient to delay PC loss. If cholesterol was not removed in the CNS, then potentially, due to an increased load of accumulated substrates, the drug is unable to sequester cholesterol as it did in other mouse models of NPC disease. Further studies are necessary to draw conclusions why a delay in PC death was not observed in the *nym* homozygote mouse.

Taken together, the findings of this novel mouse model of MLII, suggest it will be a useful system to better understand pathogenic mechanisms and evaluate modifying therapies of disease. Furthermore, it will provide a new platform for screening novel drugs against LSDs.

5. Generation of Arl1 mutants in *Drosophila* to investigate tissue-specific pathology

5.1. Introduction

The Davies laboratory has characterised the novel ENU mutant, Jabber (*jab*) mouse, derived from the Stevens mouse (see Chapter 3), as a potential novel mouse model of chylomicron retention disease (CRD) as it presented with the typical symptoms including fat malabsorption, lethargy, and neurological deficits (Chapter 1, Section 1.3.2. and Chapter 3). In addition the only known gene mutated in this disease, *SARA2* (protein Sar1b), is situated upstream of *Arl1* involved in the process of chylomicron formation (reviewed in Chapter 1, Section 1.3.2.; Bitoun et al., unpublished; (Georges et al. 2011, Jones et al. 2003, Peretti et al. 2010). The physiological function of the gene mutated in the *jab* mouse, *Arl1*, a small GTPase involved in vesicle membrane trafficking at the *trans*-Golgi, has so far not been very well understood (Munro 2005), reviewed in Chapter 1, Section 1.3.2.). For the first time *Arl1* has been investigated in a mammalian organism derived from ENU mutagenesis and established the critical role for Arl1 in lipid transport, storage and axon myelination essential for the maintenance of lipid homeostasis and nervous system function. Arl1 is expressed ubiquitously in the mouse and *Drosophila*. It was however unknown if the pathology was affected by (i) a specific cell type, such as the adipose tissue, presenting with reduced LD size, or (ii) the glial cells, leading to demyelination in the *jab* mouse, or (iii) a systemic loss of Arl1 was responsible for the *jab* phenotype. Furthermore, the molecular pathways involved in lipid homeostasis are varied and a model that would enable the study of pathways involved in lipid homeostasis, potentially implicated in the *jab* pathology, would provide invaluable information to the functioning of Arl1 in health and disease.

Consequently, *Drosophila* was chosen for further studies due to its diverse genetic tool set. This allowed for tissue specific knock-outs and overexpression systems, in addition to its suppressor and enhancer screens, fast generation time and conserved function between mammals and *Drosophila* (reviewed in Chapter 1, Section 1.2.1). The *jab* mouse mutation,

L61P (L60P in *Drosophila*), was generated but also mutant forms of Arl1 in the GDP (constitutively inactive (CI) (T30N in *Drosophila*)) or GTP (constitutively active (CA) (Q70L in *Drosophila*) restricted bound form (Table 5.1, Chapter 1). These additional mutants are well characterised in the family of small GTPases and within Arl1 studies in cell culture (Lu et al. 2001) and enable further understanding of the *jab* mouse mutation in the context of CI and CA GTPase within a whole organism like *Drosophila*.

Table 5.1. Mutant Arl1 constructs studied in *Drosophila*

Constructs	Physiological Models	GTP binding activity	Function	References
Arl1-Jab::HA (*jab* mutation;L60P)	**Mouse model (unpublished)**	**Intermediate (Figure 1.8C)**	**Impaired GTP binding**	**unpublished**
Arl1-Q70L::HA	**Cells and yeast**	**Strong (Figure 1.8C)**	**CA GTP bound GTPase**	**Lu et al., 2001**
Arl1-T30N::HA	**Cells and yeast**	**Non existent (Figure 1.8C)**	**CI GDP bound GTPase**	**Lu et al., 2001**

Constitutively active = CA; Constitutively inactive = CI

5.1.1. Studying lipid metabolism and metabolic dysfunction in *Drosophila*

In addition to *Drosophila's* large genetic tool set, *Drosophila* has already been used as a tool to provide key insights into conserved metabolic processes (Rajan and Perrimon 2013, Baker and Thummel 2007). The metabolism of *Drosophila* is carried out by a well-balanced network of organs, many of which are analogous to those of their mammalian counterparts: the gut absorbs nutrients (Figure 5.1A, Midgut: orange) and the fat body, equivalent in function to white adipose tissue and liver in mammals, stores nutrients and is a primary regulator of energy metabolism (Figure 5.1A, Fat body: yellow; (Colombani et al. 2003). Lipid droplets (LDs), in which triacyglycerides (TAG) and sterol esters are stored, are the main form of stored fat in the fat body but can also be found throughout the fly. However, the fat body is not simply a storage depot of fuel reserves. Instead, it remotely coordinates systemic larval growth with nutrient availability by integrating insulin and target of rapamycin (TOR) signalling (Baker and Thummel 2007).

The insulin pathway is conserved and essential for cell growth in response to nutrient changes (Hietakangas and Cohen 2009, Geminard et al. 2009, Edgar 2006, Sousa-Nunes et al.

2011, Teleman 2009). The insulin signalling pathway is initiated by insulin receptor substrates, such as insulin or *Drosophila* insulin like peptides (Dilps) - counterparts to the mammalian insulin and insulin-like growth factors (IGFs) - binding the insulin receptor (InR). This then leads to a cascade of events starting with phosphatidylinositol 3-kinase (PI3K) catalysing the conversion of phosphatidylinositol 4,5-bisphosphate (PIP2) into phosphatidylinositol 3,4,5-triphosphate (PIP3). PIP3 phosphorylates and activates protein kinase B (Akt). The phosphorylation of Akt leads to the activation of mammalian target of rapamycin (mTOR). mTOR has various downstream effectors, including ribosomal protein S6 kinase beta-1 (S6K) and eukaryotic initiation factor 4E (eIF-4E) binding protein-1 (4E-BP), contributing to increased cell growth and differentiation. Phosphatase and tensin homolog deleted on chromosome 10 (PTEN), a phosphoprotein phosphatase, acts as a negative regulator of this pathway converting PIP3 to PIP2 (active and negative regulators of the insulin pathway respectively, see figure 5.1B; (Britton et al. 2002, Goberdhan and Wilson 2003, Goberdhan et al. 1999).

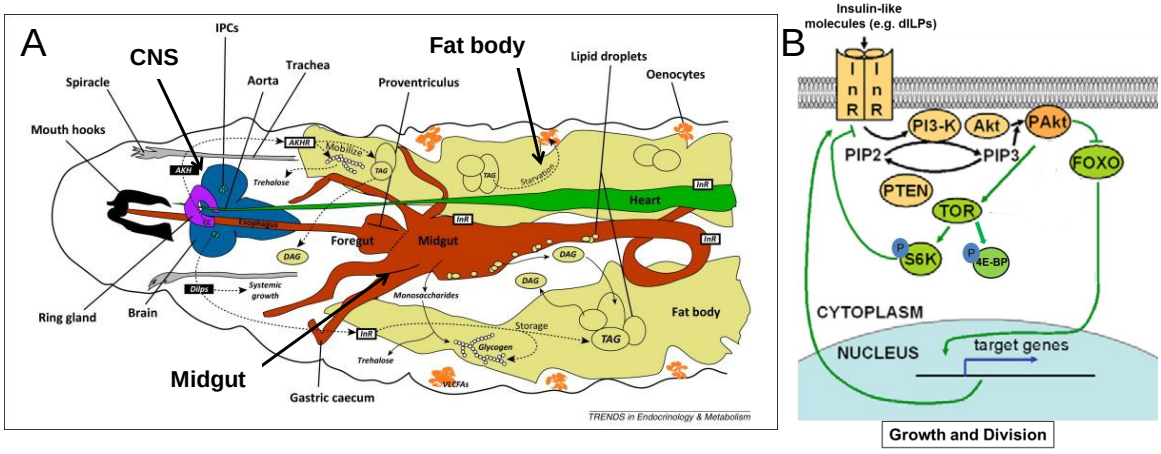

Figure 5.1. Schematic of the *Drosophila* metabolic network and the insulin receptor-TOR signalling pathway

(A) Shown is a dorsolateral view of an anterior third-instar larva packed with fat. The fly insulin receptor (InR) mediates functions similar to those of insulin and IGF receptors. Absorbed dietary lipids are trafficked from the gut by lipophorins in the hemolymph as diacylglycerides (DAGs) and are stored in lipid droplets as triacylglycerides (TAGs). Adapated from (Padmanabha and Baker 2014). **(B)** Schematic illustrating the InR/PI3K/Akt signalling cascade in *Drosophila*. Details described in text except for forkhead box O (FOXO), a transcription factor. In its unphosphrylated state, FOXO, leads to transcription of genes e.g. glucose production, but also prevents transcription of peroxisome proliferator-activated receptor gamma (PPARγ) and therefore blocks adipogenesis. Adapted from (Vereshchagina and Wilson 2006).

Studies in *Drosophila* have shown the close link between lipid homeostasis deregulation and neurodegeneration. Apolipoportein D (ApoD, a carrier protein of lipids), known as *Glial Lazarillo* (*GLaz*) in *Drosophila*, is conserved between human and *Drosophila*. *Drosophila* mutants of *GLaz* present with reduced resistance to oxidative stress and starvation, as well as impaired fat storage and shortened life spans (Sanchez et al. 2006). On the contrary, overexpressing *GLaz* as well as human ApoD, led to an extended life span and increased resistance to oxidative stress and starvation (Hull-Thompson et al. 2009, Muffat et al. 2008). Therefore, a protein facilitating the transport of lipids and ultimately lipids, are crucial to protect the organism from stress (Sanchez et al. 2006, Walker et al. 2006). Another example is Friedreich's ataxia (FRDA), an autosomal recessive neurodegenerative disease, which causes degeneration in the central and peripheral nervous systems. FRDA has recently been modelled in *Drosophila* and has shown a connection between lipid metabolism defects and neurodegeneration (Navarro et al. 2010). The *Drosophila* model provided novel insights that frataxin is necessary for glial cells and the removal of frataxin from glial cells led to increased LD accumulation, increased sensitivity to oxidative insults, neurodegeneration and locomotor activity defects. Interestingly, *GLaz* overexpression rescued the pathology of frataxin removal and present with the opportunity that controlling lipid metabolism by apolipoproteins might offer a new strategy for the treatment of FRDA patients (Navarro et al. 2010). These studies highlight the importance of a strict balance between fat storage and breakdown to maintain the energy homeostasis.

5.1.2. Aims of the chapter

Based on the evidence that *Drosophila* has been successfully used to dissect the link between lipid metabolic deregulation and neurodegeneration, the strategy of studying Arl1 in *Drosophila* was very promising for the dissection of tissue specific function and the elucidation of the molecular pathway in the *jab* mouse.

The aims of this chapter were to:

- **Create and validate physiological function of Arl1 constructs** expressed in *Drosophila* by overexpressing wild-type Arl1 and wild-type Arl1::HA tagged versions in the *Arl1* null background.

- **Characterise Arl1-Jab::HA, Arl1-Q70L::HA, Arl1-T30N::HA and Arl1-RNAi mutants overexpressed in a wild-type background** by analysing the same parameters such as growth retardation, motor activity, LD morphology, TAG concentrations, lipid retention in the gut and glial cell morphology, studied in the *jab* mouse.

- **Characterise Arl1-Jab::HA, Arl1-Q70L::HA, Arl1-T30N::HA and Arl1-RNAi mutants overexpressed in the fat body and glial tissue specifically** to understand if the pathology is driven by a global defect or a cell specific defect.

- **Analyse the insulin signalling pathway** in relation to deregulation of the major lipid metabolism pathway, specifically *Drosophila* insulin-like peptides (Dilps) by qPCR and phosphorylation of Akt.

5.2. Results

5.2.1. Arl1-WT and Arl1-WT::HA constructs rescue the *Arl1* null mutant

To understand the functional defect of the *jab Arl1* mutation, *Arl1* mutant transgenics were generated in *Drosophila.* The gene has been referred to as *Arl1* or *Arflike at 72A (Arf72A*, CG6025) in *Drosophila* (Tamkun et al. 1991, Lee et al. 2011, Torres et al. 2014). In this study the gene will be referred to as *Arl1* for simplicity. Arl1 is highly conserved between species, presenting with more than 85% amino acid sequence similarity to mouse and human protein. Therefore, the use of *Drosophila* as a model organism was highly relevant and a similar phenotype to the *jab* mouse was anticipated (Figure 5.2).

The mutant forms were constructed according to other reported mutants of small GTPases, such as Rabs and Arfs (Dascher and Balch 1994, Chavrier and Goud 1999). The two conserved GTPase motifs GXXXXGK(S/T) and DXXGQ, which are important for guanine nucleotide binding and hydrolysis, are located accordingly as shown in figure 5.2. The UAS-Gal4 system was used for the expression of the different mutant constructs (Southall et al. 2008). Arl1-T30N::HA was created by replacing the Thr residue at position 30 in GXXXXGKT motif with Asn. This mutant was expected to have much higher affinity towards GDP than GTP and to function as a dominant-negative mutant, CI, of Arl1, which is shown by an inability to bind GTP (reviewed in Chapter 1, Section 1.3.2.; Figure 1.8C). Arl1-Q70L::HA was created by replacing the Gln at position 70 in DXXGQ motif with Leu and this mutant is expected to be restricted mainly to the GTP-bound, CA form due to its impaired GTP hydrolysis activity (Lu et al. 2001). Wild-type constructs were also cloned and all constructs were HA tagged at the C-terminus because the N-terminus is myristoylated and is essential for correct membrane localisation. A wild-type construct was also cloned without a HA tag to ensure that the tag was not interfering with the function of Arl1.

To ensure equivalent expression levels between the mutant constructs, *Drosophila* ϕC31 transgenesis compatible vectors were used to allow specific and uniform transgene expression as they integrate into the same genomic location, specifically using the pBID-

UASC-G plasmid (Figure 5.2; (Ji-Wu Wang et al. 2012)). Expression levels are validated in section 5.2.2.

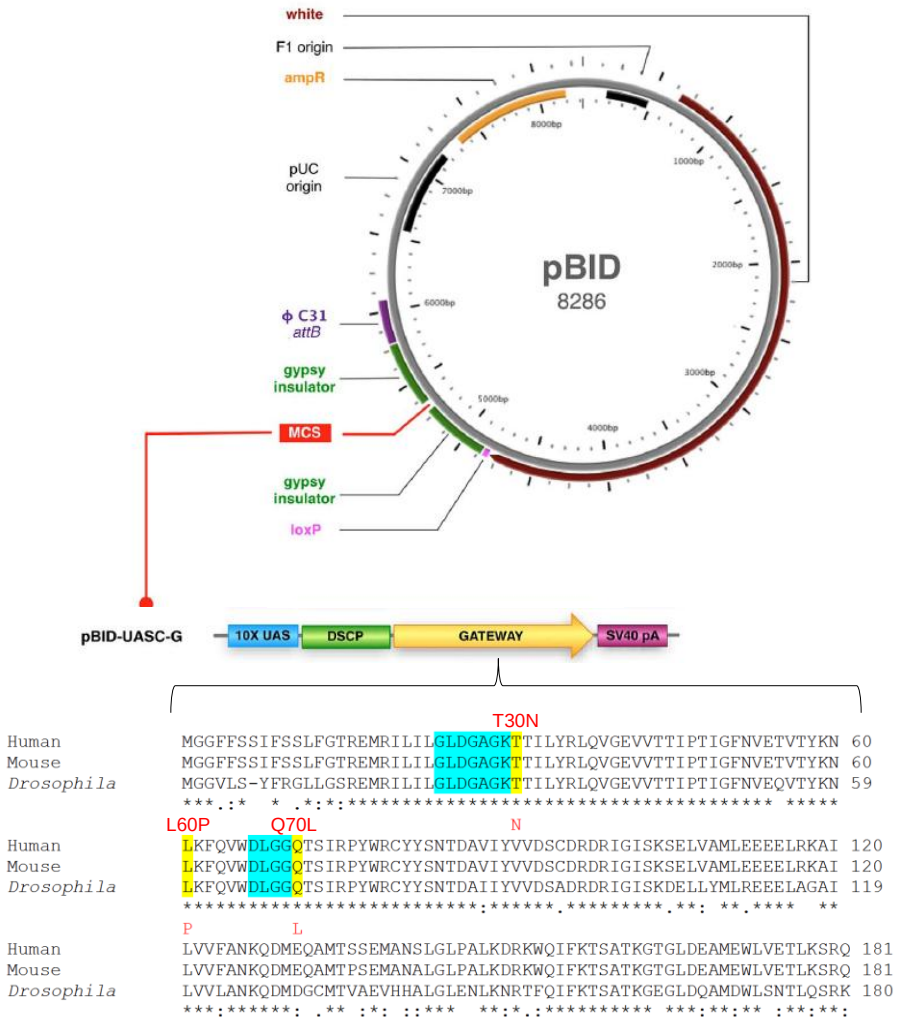

Figure 5.2. Cloning of Arl1 mutants into pBID-UASC-G showing high conservation of Arl1 between human, mouse and *Drosophila*
Above: pBID vector map. pBID includes a mini-white gene , a ϕC31 integrase compatible *attB* sequence (ϕC31 attB), a *loxP* site and an ampicillin resistance (ampR) gene. The multiple cloning site (MCS) is surrounded by gypsy insulator sequences to protect against genomic position effects. pBID-UASC-G has a Gateway cloning cassette. **Below:** Three transgenics were generated based on the T30N (CI), L60P (*jab* mouse mutation, denoted as Jab) and Q70L (CA) within the pBID-UASC-G vector (mutations highlighted in yellow). Boxes in blue show the conserved GTPase motifs that are necessary for GTP and GDP binding (adapted from(Ji-Wu Wang et al. 2012)).

To understand if the HA tagged constructs functioned similarly to endogenous Arl1, the Arl1-WT and Arl1-WT::HA constructs were overexpressed in the *Arl1*^{1} homozygote larval lethal mutant. The *Arl1*^{1} mutant contains a point mutation causing a change from the amino acid glycine at position 2 to aspartate (Torres et al. 2014). Arl1 is N-terminally myristoylated, a post-translational protein lipidation modification, which is important for membrane targeting, and

this modification requires a glycine at position 2 following the initiator methionine, with the latter being cleaved off prior to the addition of myristate (Lee et al. 1997, Farazi et al. 2001). Myristolation of Arl1 and other Arfs have been shown to be essential for membrane targeting and function, explaining the severity of the $Arl1^{1}$ point mutation (Lu et al. 2001, Torres et al. 2014). To confirm $Arl1^{1}$ mutant larval lethality in this study, $Arl1^{1}$ heterozygote mutants were crossed and homozygous offspring were counted daily until death. $Arl1^{1}$ homozygote mutants presented with an elongated 2nd instar phase, and death occurred (at the latest) after 6-8 days, which is consistent with previous studies (Figure 5.3A; (Tamkun et al. 1991)). Next, the rescue of ubiquitous expression of Arl1-WT and Arl1-WT*::HA* protein was analysed, to see if these behave as endogenous Arl1. Arl1 is expressed ubiquitously, therefore ubiquitous drivers are used in this study. Low ubiquitous expression of Arl1-WT and Arl1-WT*::HA* transgenic expression, driven by the ubiquitous driver *1032*-GAL4 in the $Arl1^{1}$ homozygote background rescued their lethality (Figure 5.3B). The cloned constructs were able to rescue the larval lethal $Arl1^{1}$ homozygote (called *Arl1* null from here onwards), suggesting that the Arl1-WT and Arl1-WT*::HA* constructs behave as the endogenous protein. Therefore, for future studies w^{1118}, which is the background control stock in which the pBID-UASC-G plasmid was expressed, Arl1-WT and Arl1-WT*::HA* are used as controls.

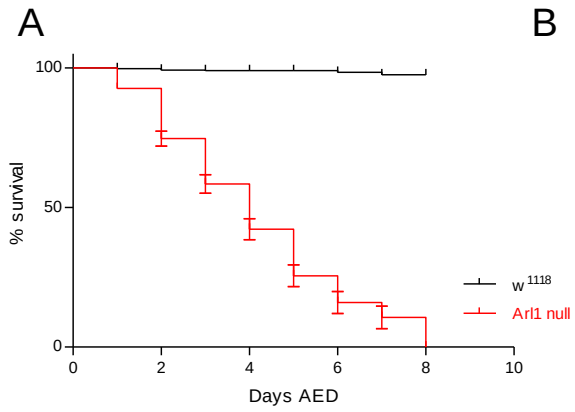

Table 1. Arl1 null is rescued by transgenic Arl1 and Arl1::HA generated with pBID.

Genotype	Eclosion (% of pupae)
Control (w^{1118})	96 ± 1.5
$Arl1^1$/Y	0
$Arl1^1$/Y;;genomic Arl1	90 ± 1.8
$Arl1^1$/Y;;genomic Arl1::HA	92 ± 2.4

A genomic fragment including the Arl1 and Arl1::HA coding region and promoter cloned into pBID and integrated into the attP2 landing site on chromosome III can restore normal adult eclosion frequency when introduced into $Arl1^1$ mutant.

Figure 5.3. *Arl1*^{1} homozygote mutant is larval lethal and is rescued by expression of Arl1-WT and Arl1-WT::HA
(A) Kaplan–Meier log rank test for survival showing reduced median survival of *Arl1* null in comparison to w^{1118} control (w^{1118}: n = 120 and *Arl1* null: n = 120). Survival curves were significantly different by Mantel-Cox test, $p<0.0001$ (χ^2 = 325.1). Survival of *Arl1*^{1} homozygote larvae was analysed from 4 individual crosses choosing 30 larvae each (n=120). Survival was quantified daily. **(B)** Arl1-WT and Arl1-WT::HA rescued the *Arl1* null.

5.2.2. Developmental delay and reduced survival observed in Arl1-T30N::HA and Arl1 Q70L::HA Arl1 mutant flies

To understand the function of Arl1, wild-type, mutants (Arl1-Jab::HA, Q70L::HA and Arl1-T30N::HA) and Arl1-RNAi were overexpressed using *actin*-Gal4 driver, a ubiquitous driver (Angelichio et al. 1991, Wilder 2000). Arl1 wild-type and mutants were detected in whole fly extracts (Figure 5.4A+B) whereas the Arl1-Jab::HA expresses at lower levels compared to Arl1-WT::HA, Arl1-T30N::HA and Arl1-Q70L::HA constructs. Similar findings were shown by previous work in the *jab* mouse embryonic fibroblasts in which Arl1 protein levels were reduced by 50% (Figure 1.8A, Bitoun et al., unpublished). No antibody was available for the endogenous Arl1 protein therefore the levels of endogenous Arl1 in the controls and RNAi line were not able to be measured. However the measurement of transcript levels of the *Arl1* constructs, overexpressed by *actin*-Gal4, were analysed and a 2-3 fold higher expression than endogenous *Arl1* mRNA levels was detected (Figure 5.4C). The Arl1-RNAi was found to only knock down 30% of the gene (72.4±9.2% remaining *Arl1* mRNA) and there is no major larval lethality observed in the Arl1-RNAi mutant flies (Figure 5.4C). To

investigate the importance of Arl1 dose, the RNAi mutant was studied in parallel to the other mutants.

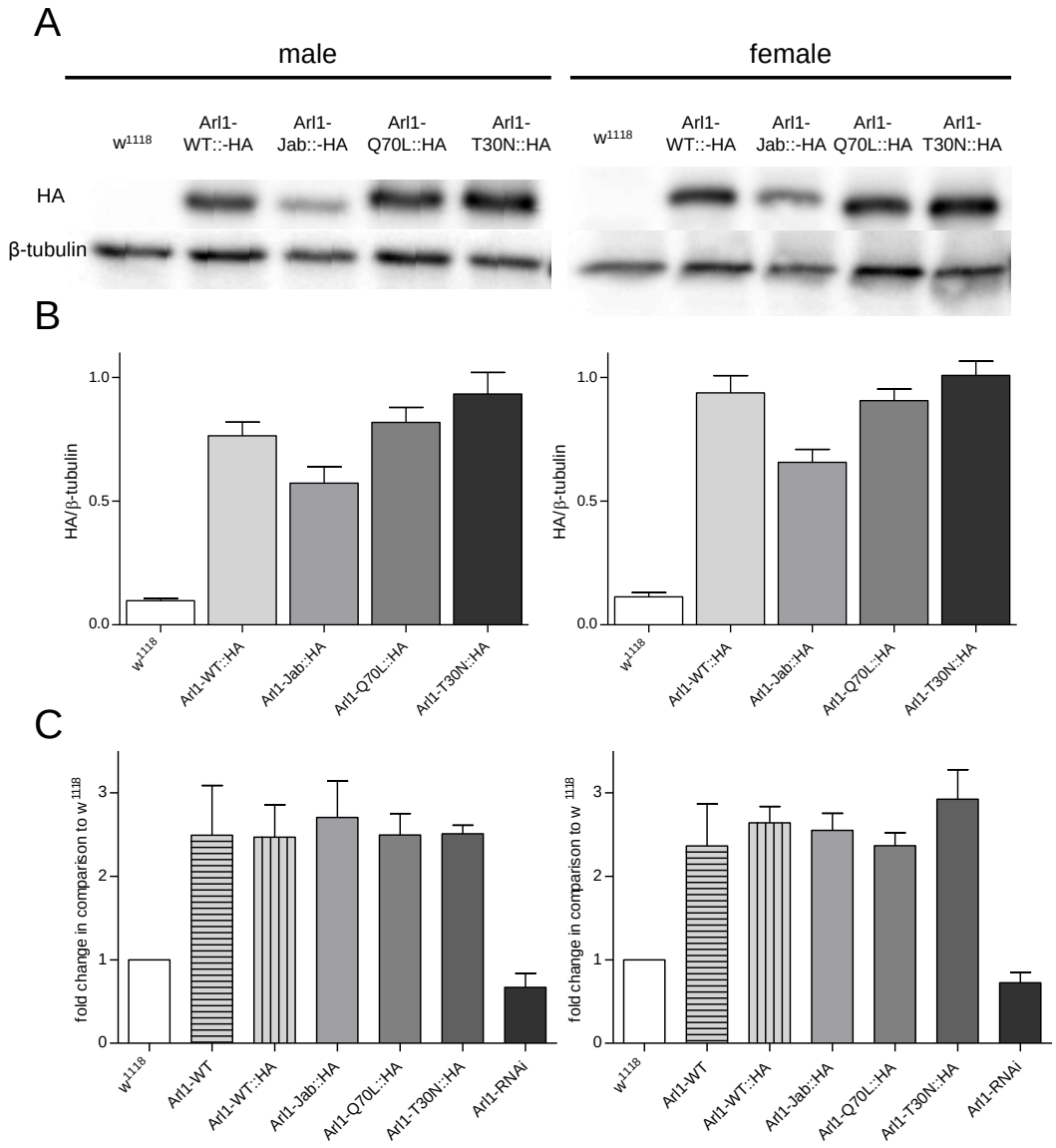

Figure 5.4. Expression of pBID transgene is similar at mRNA level but shows reduced protein levels for Arl1-Jab::HA
(A) Expression of wild-type Arl1 (Arl1-WT::HA) and mutant Arl1 (Arl1-Jab::HA, Arl1-Q70L::HA and Arl1-T30N::HA) in whole fly from pBID-UASC-G inserts driven by *actin* –GAL4. The loading control was β-tubulin. **(B)** Quantification of protein expression levels using Image J (n=3) **(C)** mRNA expression of wild-type *Arl1*, mutant *Arl1* and *Arl1* knocked down by RNAi in whole fly from pBID-UASC-G inserts driven by *actin* –GAL4 detected by qRT-PCR. The amount of *Arl1* mRNA is expressed as the fold increase to w^{1118}, representing the endogenous *Arl1* level. *Rp49* was used as the internal control (n=3). Values are expressed as mean±SEM.

Arl1 has been shown to be important in development as the *jab* homozygote and the *Arl1* null mutant are larval lethal (Tamkun et al. 1991). Furthermore, lipid regulation in *Drosophila* development is crucial to advance to pupal stage and to reach a critical weight for

metamorphosis. Critical weight involves passing a size threshold that controls the regulation of metamorphic processes (Mirth and Riddiford 2007, Kühnlein 2012, Church and Robertson 1966). Therefore, *Drosophila* developmental stages were analysed by scoring them daily. *Drosophila* development follows different stages: embryo, 1st instar larval stage, 2nd instar larval stage (L2), 3rd instar larval stage (L3), prepupa, pupa and eclosion (Figure 1.3).

Critical weight is reached during L3 stage and enables *Drosophila* to molt into pupa. If this weight is not sufficient, intermediate pupae are formed or smaller adult *Drosophila* are produced (Kühnlein 2012, Xie et al. 2010). Therefore time until L3 stage and pupariation was investigated to understand at which stage Arl1 is crucial for *Drosophila* development. At 4 days after egg deposition (AED) about 80% of all genotypes except for Arl1-Q70L::HA and Arl1-T30N::HA mutant larvae reached L3 stage. Arl1-Q70L::HA mutant larvae only reached 57.2±10.5% and Arl1-T30N::HA mutant larvae only 42.6±6.7% L3 stage at 4 days AED. In addition 100% L3 stage was only completed by day 7 AED for Arl1-Q70L::HA and Arl1-T30N::HA mutant larvae in comparison to 6 days AED for the remainder of the genotypes (Figure 5.5A). Pupariation was completed by the wild-type control by day 7 AED; however the Arl1-Q70L::HA mutant larvae only reached 52.14±10.2% and Arl1-T30N::HA mutant larvae only reached 5.3±7.0% pupariation at day 7 AED. At day 9, 80% of pupariation (Arl1-Q70L::HA: 85.2±7.6%; Arl1-T30N::HA: 86.7±2.5%) has been reached and by day 10 - three days delayed - complete pupariation can be observed for both Arl1-Q70L::HA and Arl1-T30N::HA mutant larvae (Figure 5.5B). The controls w^{1118}, Arl1-WT and Arl1-WT::HA, but also Arl1-Jab::HA mutant and Arl1-RNAi did not show a delay in development to L3 or pupal stage. Arl1-Q70L::HA and Arl1-T30N::HA mutant larvae presented with a one day delay to reach L3 stage and needed two additional days to reach pupa, but ultimately reached L3 and pupal stages (Figure 5.5B).

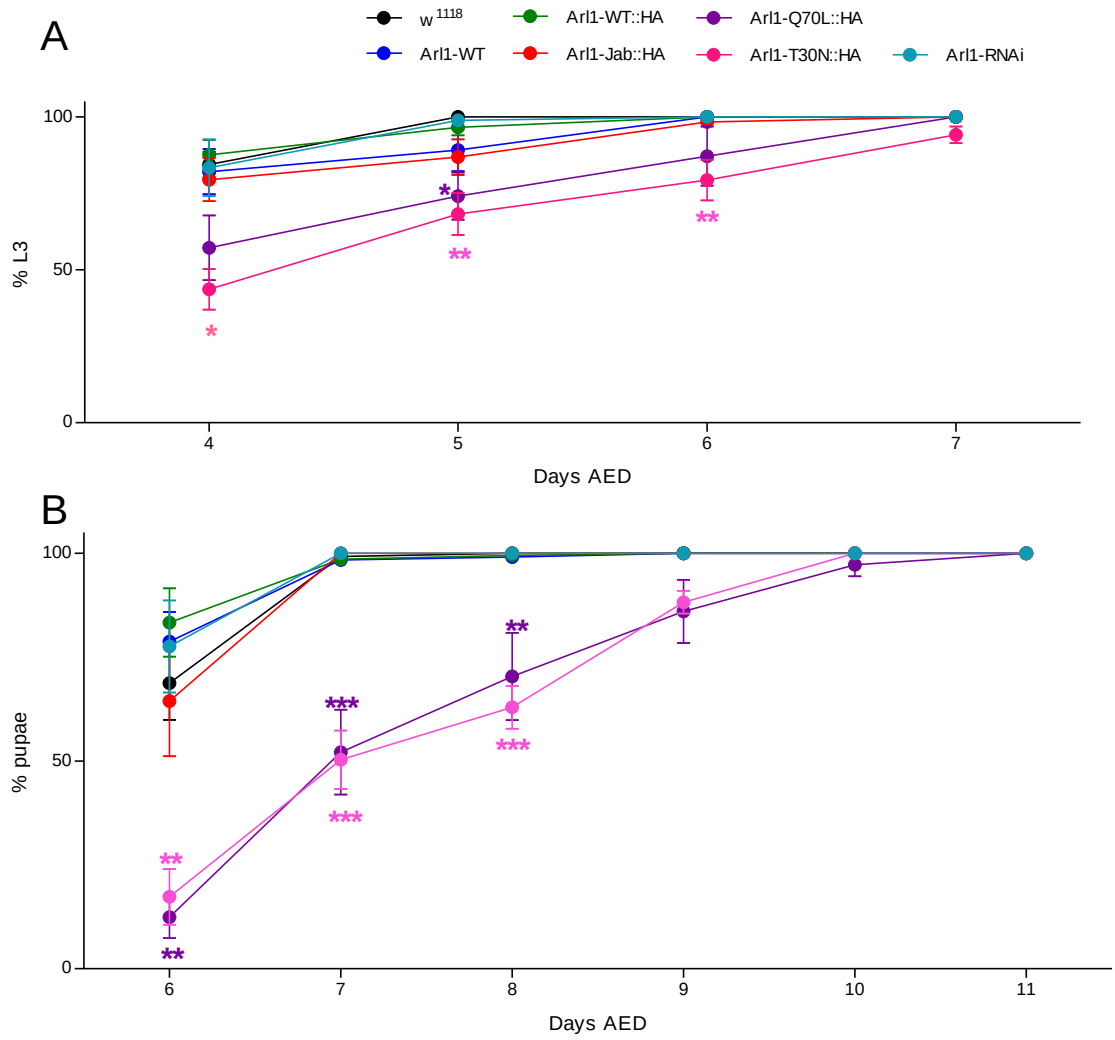

Figure 5.5. Delay in development present in Arl1-T30N::HA and Arl1-Q70L::HA mutants being overexpressed using *actin*-Gal4
Drosophila development from egg to eclosion was followed. **(A)** The time until third instar larval stage (L3) completed was measured. **(B)** The time until full pupariation was investigated in which L3 larvae have formed to pupae. Values are expressed as mean±SEM (n = 80-150; 1-way ANOVA with Dunnett's post-hoc test *P<0.05; **P<0.01; ***P<0.001).

Efficiency of metamorphosis and ability to eclose was also investigated. The time point when flies eclosed from the pupal case was monitored daily and the number of offspring were counted. A delay in eclosion and severe reduction in offspring was observed for the Arl1-Q70L::HA and Arl1-T30N::HA mutants (Figure 5.6). Full eclosion is usually completed by day 11 in wild-types. In contrast, the Arl1-Q70L::HA mutant flies had only reached 63±12.0% and the Arl1-T30N::HA mutant flies only 44±2.2% eclosion by 11 days. The maximum eclosion reached for both genotypes was 85% at day 14, three days delayed compared to control *Drosophila* development (Figure 5.6A). However, when accounting for prior delays in

development, metamorphosis does not seem to be occurring at a slower rate. The number of total *Drosophila* offspring in the F1 generation was quantified. The Arl1-Q70L::HA and Arl1-T30N::HA mutants presented with 50% reduced offspring for male flies. The female flies showed 50% reduced offspring for the Arl1-T30N::HA mutant, but the Arl1-Q70L::HA mutant only presented with 25% reduced offspring (Figure 5.6B). In both genders the Arl1-RNAi mutant presented with about 25% reduced offspring. This however was not significant (Figure 5.6B).

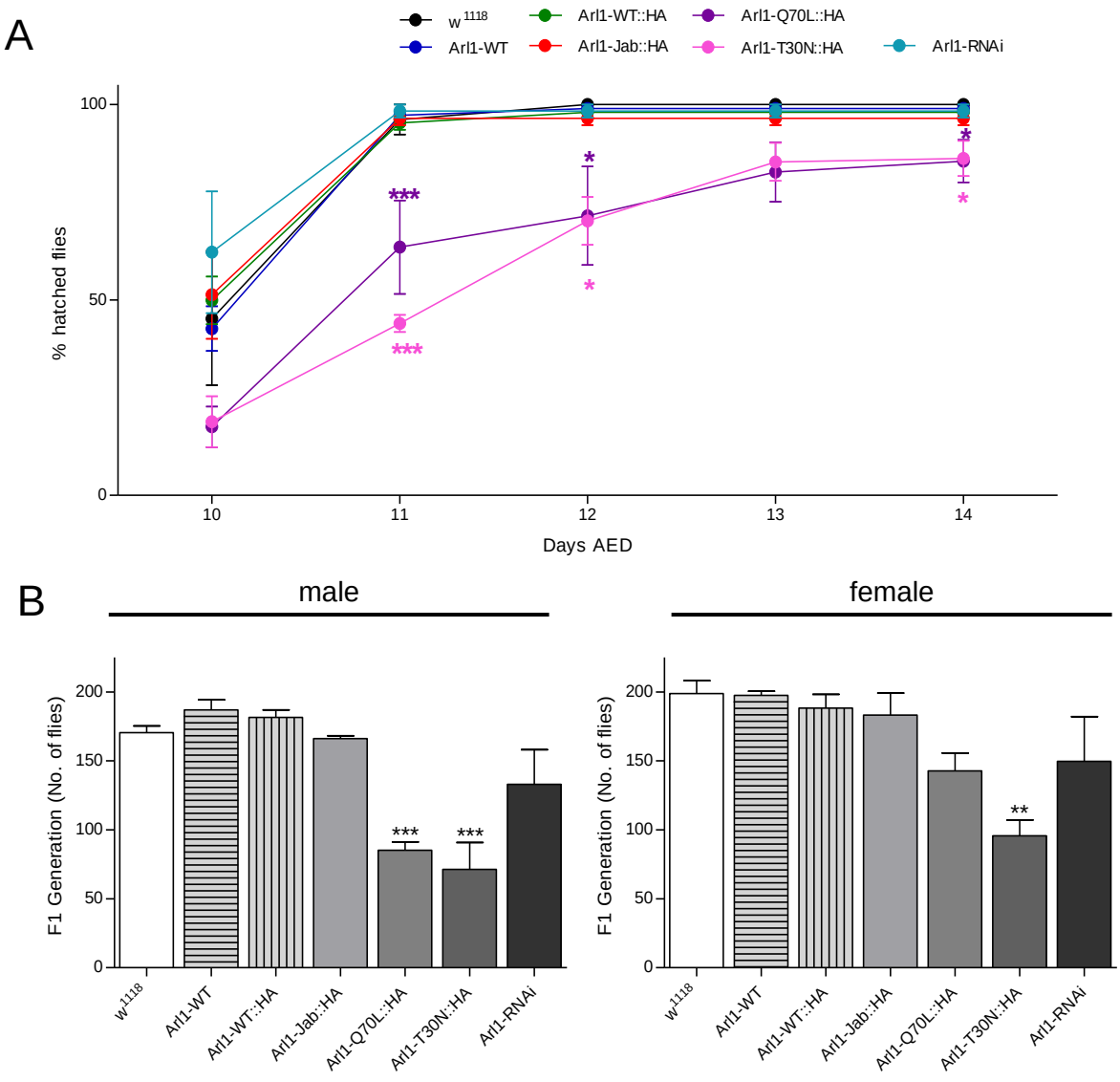

Figure 5.6. Delay in development and reduced offspring in the Arl1-T30N::HA and Arl1-Q70L::HA mutants, being overexpressed using *actin*-Gal4
(A) Time until eclosion was measured and Arl1-T30N::HA and Arl1-Q70L::HA mutants did not fully eclose. **(B)** Total number of *Drosophila* eclosed from seven different egg layings (n = 60-200) Values are expressed as mean±SEM (n = 80-150; 1-way ANOVA with Dunnett's post-hoc test *P<0.05; **P<0.01, ***P<0.001).

Incomplete eclosion and a reduction in offspring was observed for the Arl1-T30N::HA and Arl1-Q70L::HA mutants (Figure 5.6B). Therefore eclosion defects were analysed by visualising the pupal cases after eclosion was completed. Analysis was conducted at day 16 days AED and pupal case appearance was quantified. Pupal cases were separated into three phenotypes: full eclosion (Figure 5.7A, left panel), partial eclosion (Figure 5.7A, middle panel) and incomplete eclosion (Figure 5.7A, right panel). About 17.0±2.2% of pupae for both Arl1-T30N::HA and Arl1-Q70L::HA were unable to separate from the puparial case, leading to

partial eclosion (Figure 5.7A, middle panel and B). In addition, 4.5±1.0% of mutants pupae did not eclose at all, leading to incomplete eclosion (Figure 5.7A, right panel and C). About 2% of Arl1-Jab::HA mutant and Arl1-RNAi pupae were unable to separate from the puparial case during eclosion which in this analysis is not significant (Figure 5.7B). The T30N::HA and Arl1-Q70L::HA mutants have shown very similar phenotypes so far, which suggests that a balanced activity of Arl1 is important. Both the Arl1-Jab::HA and the Arl1-RNAi do not show a delay in development however they do show a minimal defect in eclosion.

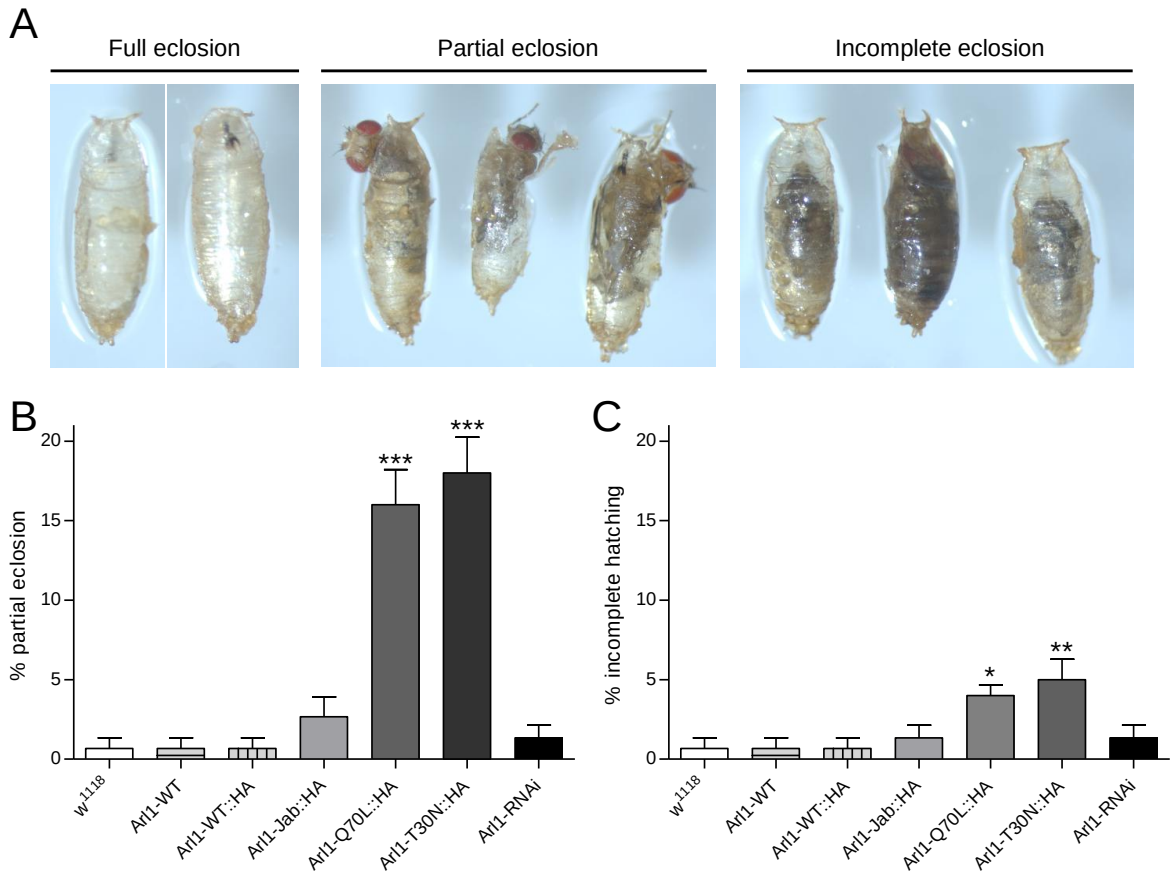

Figure 5.7. Incomplete eclosion is present in all Arl1 mutants
(A) (left panel) Normal eclosion can be seen for w^{1118}, Arl1-WT and Arl1-WT::HA constructs. Partial eclosion (middle panel) and incomplete eclosion (right panel) can be observed Arl1-Jab, Arl1-Q70L, Arl1-T30N mutants and Arl1-RNAi flies. **(B)** Quantification of the partial eclosion phenotype in all genotypes. **(C)** Quantification of the incomplete eclosion phenotype in all genotypes (n=80-150; Values are expressed as mean±SEM. 1-way ANOVA with Dunnett's post-hoc test *P<0.05; **P<0.01, ***P<0.001).

Incomplete eclosion of the Arl1-T30N::HA and Arl1-Q70L::HA mutants present part of the cause for the reduction in offspring, but it was also of interest how much larval lethality plays a role during development. Hatched larvae were therefore quantified daily as part of the earlier analysis. The Arl1-T30N::HA mutant showed the most severe larval attrition with only 57.25±7.5% survival (Figure 5.8A). The Arl1-Q70L::HA mutant showed only 66.16±8.1% larval survival and the Arl1-RNAi only 70.1±13.3% survival (Figure 5.8A). It therefore seems that the Arl1-T30N::HA and Arl1-Q70L::HA mutants and the Arl1-RNAi specifically affect larval survival. The reduction in *Drosophila* offspring for Arl1-T30N::HA and Arl1-Q70L::HA is caused by both reduced larval survival and an inability to complete eclosion. Consistent with findings in the *jab* mouse, the Arl1-Jab::HA mutant flies do not present with any obvious developmental delay.

A delay in development has been identified for the Arl1-T30N::HA and Arl1-Q70L::HA mutants specifically at crucial stages in which lipid levels regulate further development. Lipid homeostasis is crucial for development in the adults and therefore the effects on survival were analysed. Flies were separated by gender and dead flies were counted every 3-4 days. Male flies survive for an average of 75 days whereas the females survive up to 100 days. This data is similar to reports in the literature (Xie et al. 2010, Watson et al. 2008). Both Arl1-Q70L::HA and Arl1-T30N::HA mutants show 50% reduced survival in both male and female adults. The Arl1-RNAi fly line interestingly shows a reduced survival of about 30-40% (Figure 5.8B). Consistent with findings from the *jab* mouse, the Arl1-Jab::HA mutants have a normal life span (Figure 5.8B). In conclusion Arl1 is crucial for development and survival in *Drosophila*.

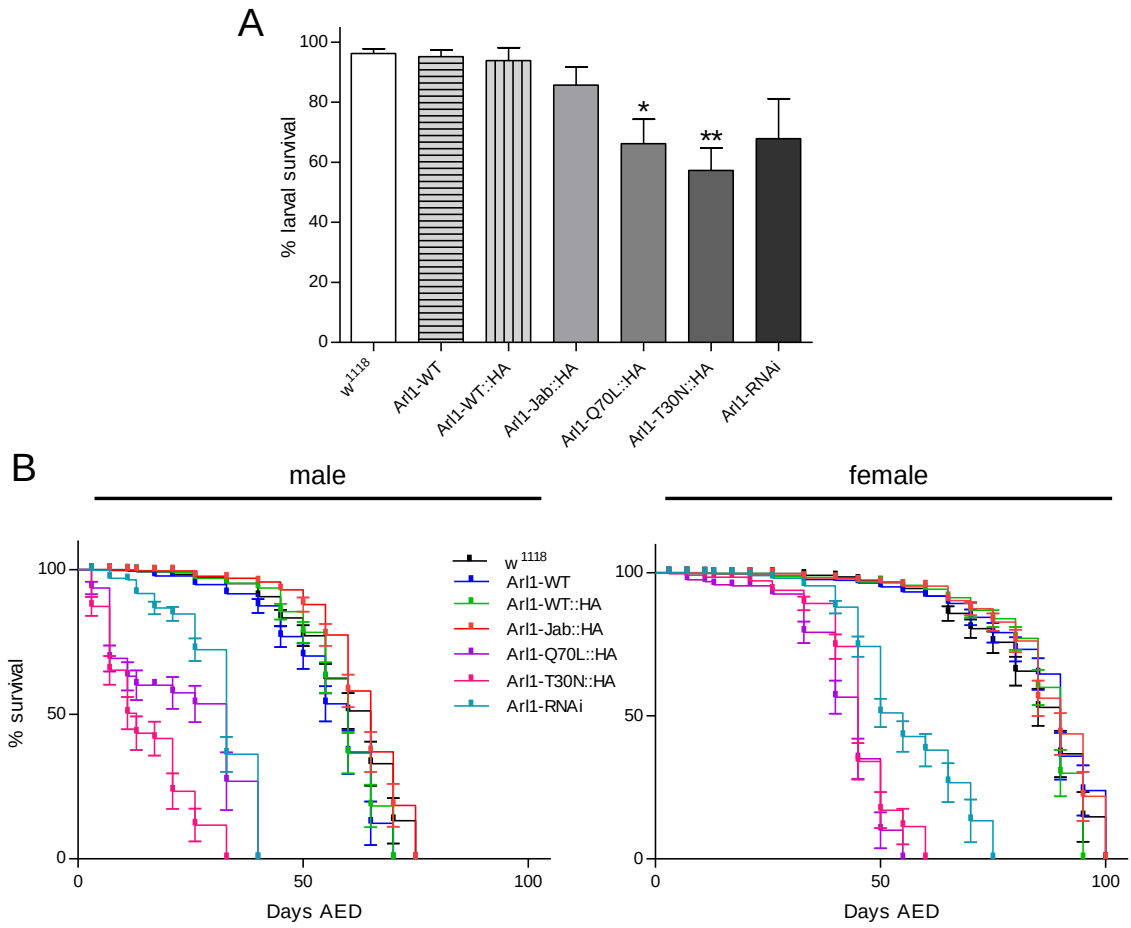

Figure 5.8. Reduced larval attrition, F1 generation offspring and survival is present in the Arl1-Q70l::HA, Arl1-T30N::HA and Arl1-RNAi overexpressing mutants using *actin*-Gal4
(A) Percentage of larvae that completed all stages to pupariation were assessed (n = 180). **(B)** Kaplan–Meier log rank test for survival showing reduced median survival of Arl1-Q70L::HA, Arl1-T30N::HA and Arl1-RNAi for both male and females in comparison to w^{1118}, Arl1-WT, Arl1-WT::HA and Arl1-Jab::HA (each genotype n=80-150). Survival curves were significantly different by Mantel-Cox test, $p<0.0001$ for both male (Arl1-Q70L::HA $\chi^2 = 143.4$; Arl1-T30N::HA $\chi^2 = 216.5$; Arl1-RNAi $\chi^2 = 102.0$) and females (Arl1-Q70L::HA $\chi^2 = 133.4$; Arl1-T30N::HA $\chi^2 = 125.0$; Arl1-RNAi $\chi^2 = 81.2$). Age matched flies were separated by gender and every 3-4 days transferred to new tubes. Survival was analysed every 3-4 days (Values are expressed as mean±SEM; 1-way ANOVA with Dunnett's post-hoc test *P<0.05; **P<0.01).

5.2.3. Growth retardation and reduced locomotor activity

To investigate whether the Arl1-Jab::HA *Drosophila* model was a model of the *jab* mouse, various phenotypes were assessed including growth retardation, motor activity, LD morphology, TAG levels, retention of lipids in the gut and glial cell morphology. First of all, growth retardation was investigated in the *Drosophila* Arl1 mutants by weighing groups of 10 flies and measuring their length for all genotypes. The Arl1 mutants are significantly smaller (Figure 5.9A), with the Arl1-Q70L::HA and Arl1-T30N::HA mutants approximately 25-30% reduced in weight, whereas the Arl1-Jab::HA mutant and Arl1-RNAi flies were only 10% lighter in weight (Figure 5.9B). The same trend was observed for fly length (Figure 5.9C). There are some mild gender differences in which the Arl1-RNAi male mutants were not significantly smaller in length or lighter in weight. The Arl1-Jab::HA male mutants were significantly smaller in length but not lighter in weight. These results might highlight the lipid metabolic differences between males and females that have been observed in previous studies (Scheitz et al. 2013, Parisi et al. 2011, Hoffman et al. 2014).

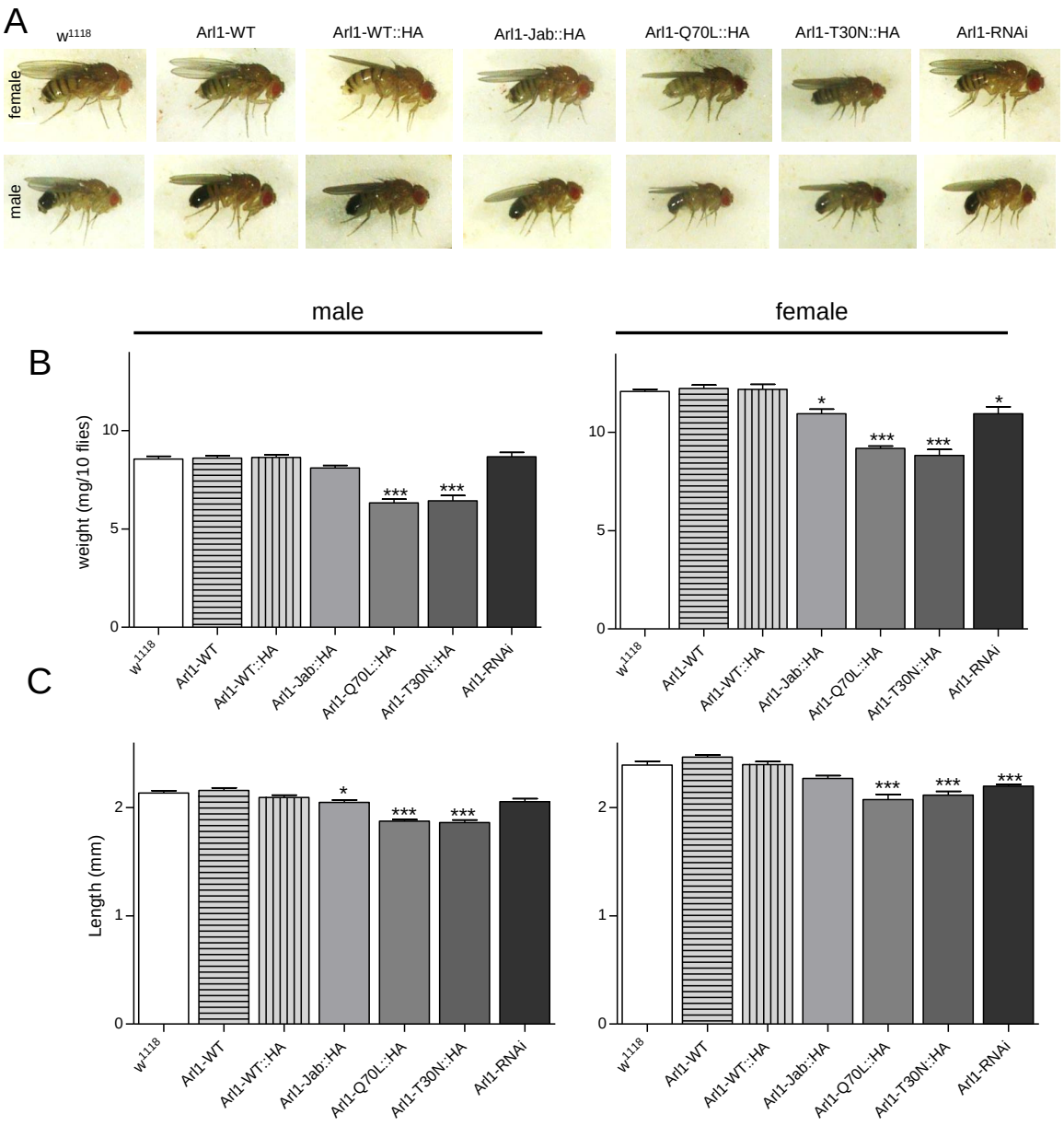

Figure 5.9. Arl1 mutants present with reduced size and weight
(A) Five-day old flies were imaged and representative images are presented. Scale bar: 0.5mm. **(B)** Ten flies were batched together from each genotype and weighed (n=60). **(C)** Images were taken of a total of 30 flies for which length measurements were taken. Values are expressed as mean±SEM (1-way ANOVA with Dunnett's post-hoc test *P<0.05, ***P<0.001).

The locomotor activity was measured next as the *jab* mouse presents with tremor and reduced motor coordination. Locomotor activity was measured at 7, 14 and 21 days. Locomotion was assessed by a commercially available locomotor activity monitoring system (Trikinetics Inc.) which measures movement of *Drosophila*. Similar to what was observed in the *jab* mouse, there is reduced motor activity in Arl1 mutant adult flies at all ages. Motor

activity was reduced significantly between 25-30%. Indeed, a motor phenotype was observed not only for the Arl1-Q70L::HA and Arl1-T30N::HA that had shown more defects in this study, but also for the Arl1-Jab::HA and Arl1-RNAi (Figure 5.10). No progression in motor activity was observed. The data suggests that Arl1 is also involved in locomotor activity in *Drosophila*, as in the mouse.

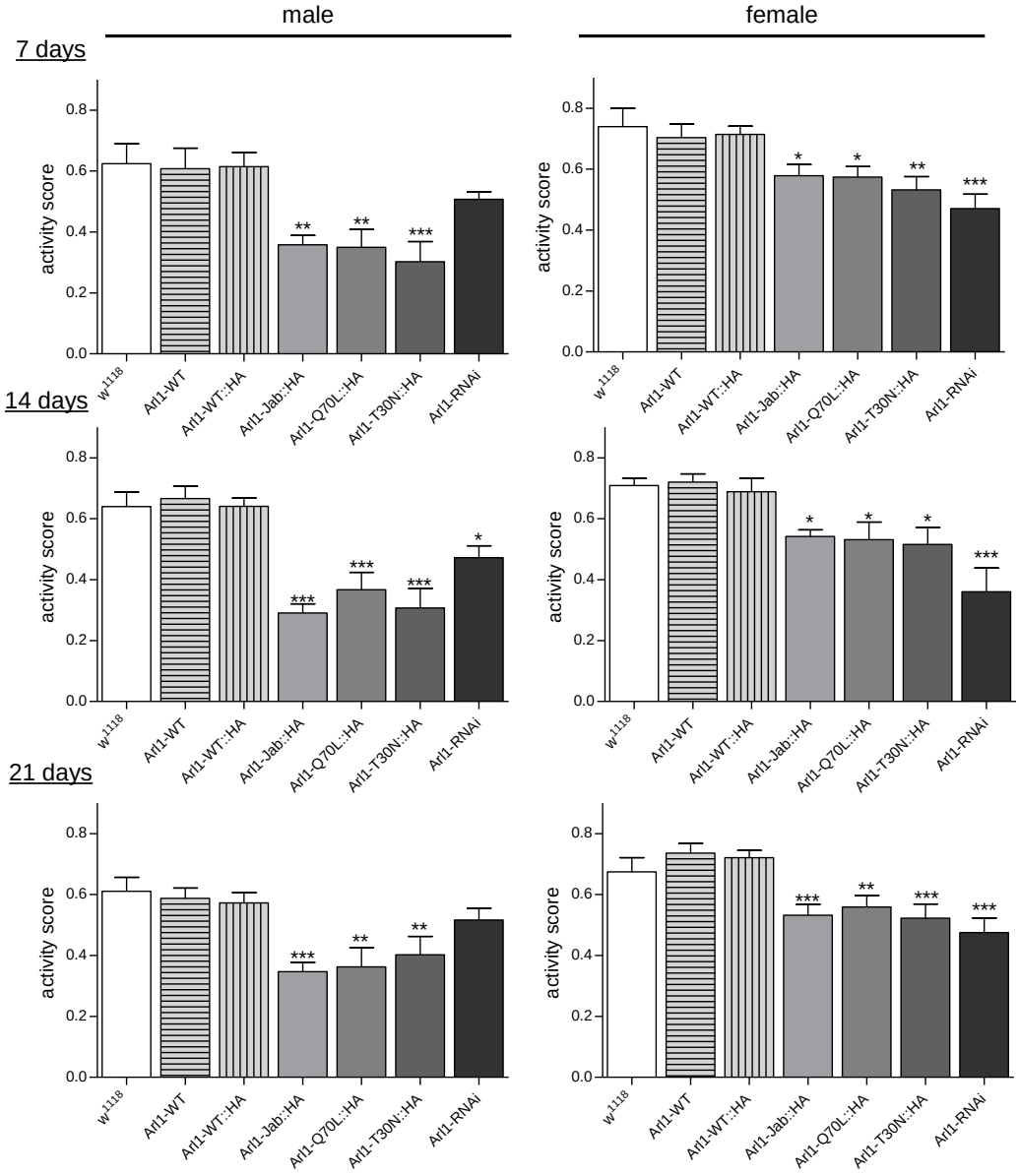

Figure 5.10. Significant motor defects could be observed by the mutants being overexpressed using *actin*-Gal4

Activity of flies was measured using the locomotor activity monitoring system (Trikinetics Inc.). Male and female flies (30 flies per genotype and sex) were kept at 25°C and entrained for 1 day in 12:12 LD (light:dark) cycles. The last 3 days were used for data analysis. For each fly line, the locomotor activity levels of individual flies (n=18-30) were measured in 60 min bins and then averaged to obtain a group profile representative for that line. Values are expressed as mean±SEM (1-way ANOVA with Dunnett's post-hoc test *P<0.05; **P<0.01, ***P<0.001).

5.2.4. Changes in lipid droplet size in the *Drosophila* fat body

As seen before the Arl1 adult fly mutants are significantly shorter and lighter. This hints towards a defect in differentiation and growth (Tennessen and Thummel 2011). LDs were present at reduced size in the *jab* mouse and therefore LDs were also analysed in the Arl1 mutants. Lipid storage is an elementary feature of cell metabolism and must be tightly controlled (Beller et al. 2010). The fat body from male L3 larvae were dissected from age matched genotypes at 4 days AED as the fat body is easily accessible in the *Drosophila* larval system. Male larvae were analysed from this point to exclude any hormonal changes that occur in the female organism. The fat bodies were stained with the lipophilic stain Nile Red and imaged for LD morphology. Three parameters were assessed: (i) LD size to analyse defects in formation or fusion of LDs, (ii) number of LDs within a single adipocyte – the cells of the fat body - which gives insights on fusion ability and (iii) size of the adipocytes to highlight any growth defects. LD size of 100µm^2 in the wild-type was consistent with previous studies (Bi et al. 2012). LD size was significantly reduced by about 20% in the Arl1-Jab::HA and by about 40% in the Arl1-RNAi larvae (w^{1118} and Arl1-WT::HA: 110.5±9.8µm^2; Arl1-Jab::HA: 79.1±4.4µm^2;. Arl1-RNAi: 60.3±5.2µm^2). The LD size of the Arl1-RNAi larvae almost compared in size to the *Arl1* null which presented with greater than 50% reduction in size compared to the wild-type controls (*Arl1* null: 40.5±5.2µm^2). In contrast, the LDs of the Arl1-T30N::HA larvae were double in size compared to the wild-type controls. No difference in LD size was observed in the Arl1-Q70L::HA larvae (Figure 5.11 A+B). The number of LDs per adipocyte were significantly reduced by 30% in the Arl1-Q70L::HA larvae and by 60% or more in the Arl1-T30N::HA and *Arl1* null larvae respectively, in comparison to the wild-type control (w^{1118} and Arl1-WT::HA: 14.0±1.2 LDs/adipocyte; Arl1-Q70L::HA: 8.4±0.8 LDs/adipocyte; Arl1-T30N::HA: 5.8±0.6 LDs/adipocyte; *Arl1* null: 4.0±0.3 LDs/adipocyte). No difference in the number of LDs per adipocyte was observed in the Arl1-Jab::HA and Arl1-RNAi larvae in comparison to the wild-type controls (Figure 5.11 A+C). Adipocyte cell size was significantly reduced by 25% in the Arl1-Jab::HA, by 50% in the Arl1-Q70L::HA and the Arl1-T30N::HA larvae, and by 90% in the *Arl1* null larvae in comparison to the wild-type controls (w^{1118} and

Arl1-WT::HA: 3950.2±220.5µm^2; Arl1-Jab::HA: 2981.5±251.7µm2; Arl1-Q70L::HA: 1749.6±104.9µm^2; Arl1-T30N::HA: 1473.3±128.0µm^2; *Arl1* null: 242.9±16.8µm^2;). Adipocyte cell size did not differ in the Arl1-RNAi larvae compared to the wild-type controls (Figure 5.11 A+D). Consistent with findings in the *jab* mouse, LDs were also of reduced size in the Arl1-Jab::HA mutants. In conclusion, Arl1 plays an important role in LD biogenesis and growth of adipocytes in the male larval fat body.

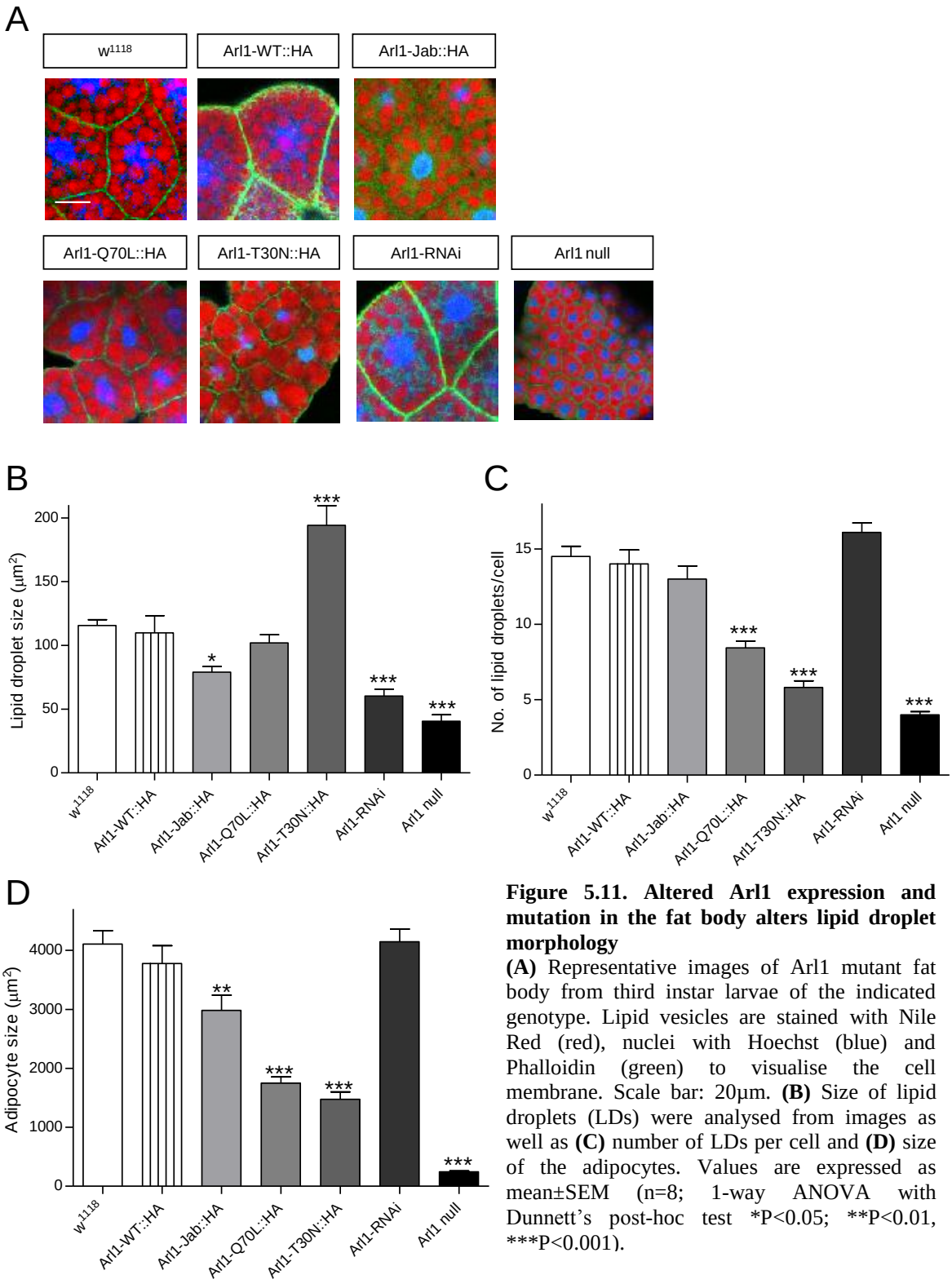

Figure 5.11. Altered Arl1 expression and mutation in the fat body alters lipid droplet morphology
(A) Representative images of Arl1 mutant fat body from third instar larvae of the indicated genotype. Lipid vesicles are stained with Nile Red (red), nuclei with Hoechst (blue) and Phalloidin (green) to visualise the cell membrane. Scale bar: 20µm. **(B)** Size of lipid droplets (LDs) were analysed from images as well as **(C)** number of LDs per cell and **(D)** size of the adipocytes. Values are expressed as mean±SEM (n=8; 1-way ANOVA with Dunnett's post-hoc test *P<0.05; **P<0.01, ***P<0.001).

LDs mainly contain TAG and in past reports it has been shown that Arl1 might play an important role in LD fusion and lipolysis (Hommel et al. 2010). Due to TAG levels being abnormal in the *jab* mouse, TAG levels were also investigated in the Arl1 mutants. TAG levels

were measured in whole male adult *Drosophila* homogenate. Larvae were used for the analysis of *Arl1* null TAG levels as they do not reach adulthood. Interestingly, the Arl1-Jab::HA mutants also presented with reduced, but not significant, levels of TAGs as the *jab* mouse. Reductions in TAG levels were also observed in Arl1-Q70L::HA, although not significant, and in Arl1-T30N::HA mutants and Arl1-RNAi flies, which were significant (Figure 5.12A). The *Arl1* null larvae presented with significant reduction in TAG levels (Figure 5.12B). Therefore Arl1 seems to monitor the homeostasis of TAG levels in *Drosophila*.

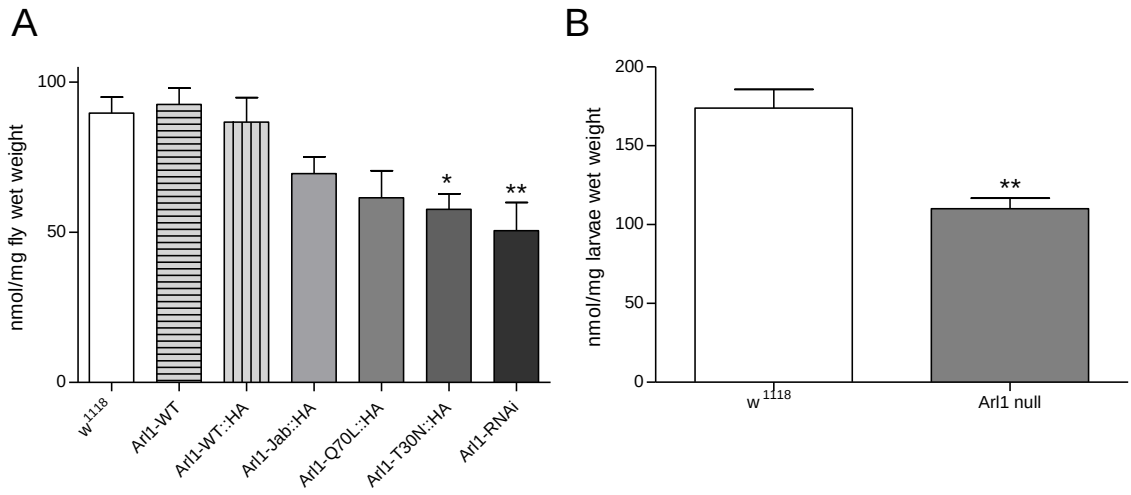

Figure 5.12. Altered Arl1 in expression and mutation in the fat body alters TAG content
(A) TAG content of whole fly homogenate. **(B)** TAG content in whole larvae. TAG content was normalised to the amount of fly/larvae wet weight. Values are expressed as mean±SEM (n= 30 flies; 1-way ANOVA with Dunnett's post-hoc test or two-tailed Student's t-test *P<0.05; **P<0.01).

5.2.5. Lipid retention in the gut

The *jab* mouse models CRD. A hallmark of CRD is retention of lipids in the gut, as seen in the *jab* mouse (Chapter 1, Section 1.3.2.). As *Drosophila* was being validated to study CRD, lipid retention in the Arl1 *Drosophila* mutants was analysed. Due to ease of accessibility, the larval gut was dissected from L3 larvae of age matched genotypes and stained with Nile Red, a lipophilic stain. The Nile Red stain quantification showed a 2-fold increase in lipid retention in the Arl1-Jab::HA mutant and the Arl1-Q70L::HA mutant, and a 3-4 fold increase for the Arl1-T30N::HA and Arl1-RNAi mutants (Figure 5.13A+B) in comparison to the wild-type control. These results suggest the conserved function of Arl1 in *Drosophila* and mouse in the assembly of chylomicrons for lipid absorption (Jaschke et al. 2012).

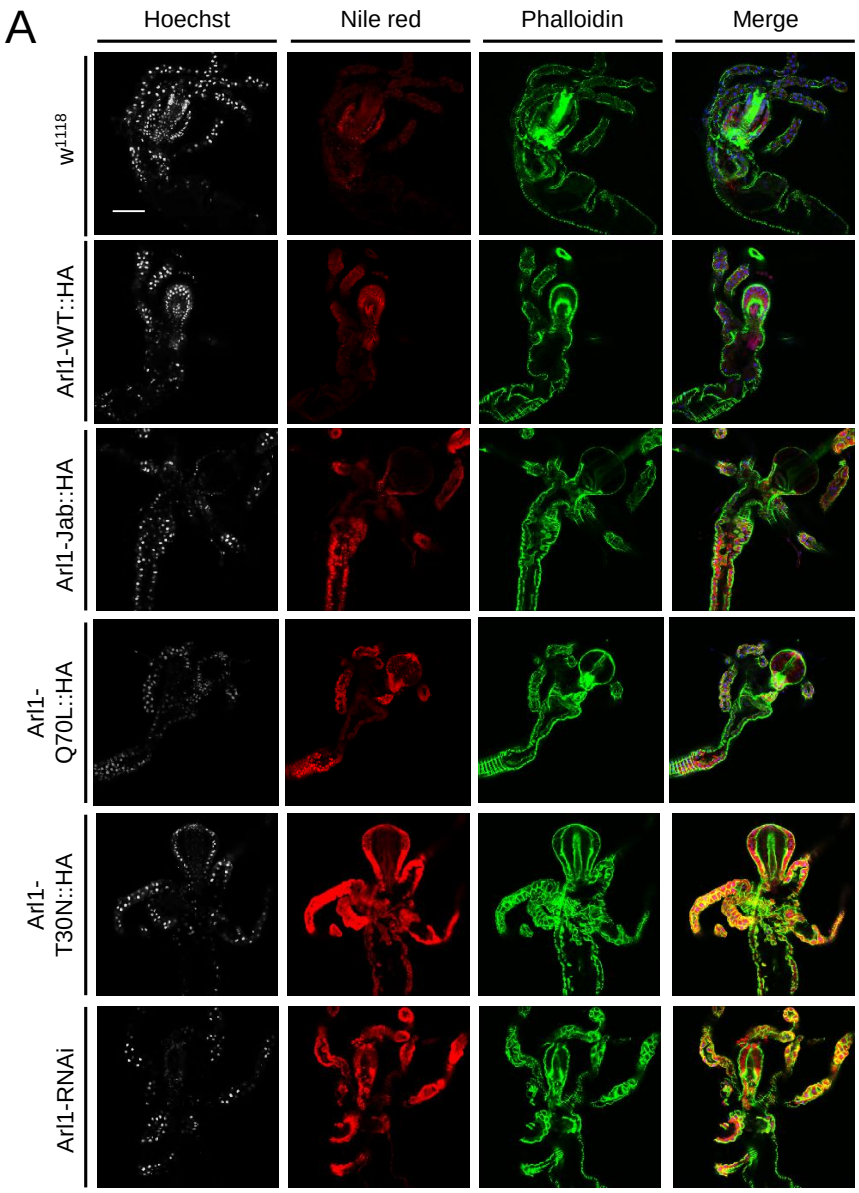
A
Hoechst
Nile red
Phalloidin
Merge
w1118
Arl1-WT::HA
Arl1-Jab::HA
Arl1-Q70L::HA
Arl1-T30N::HA
Arl1-RNAi

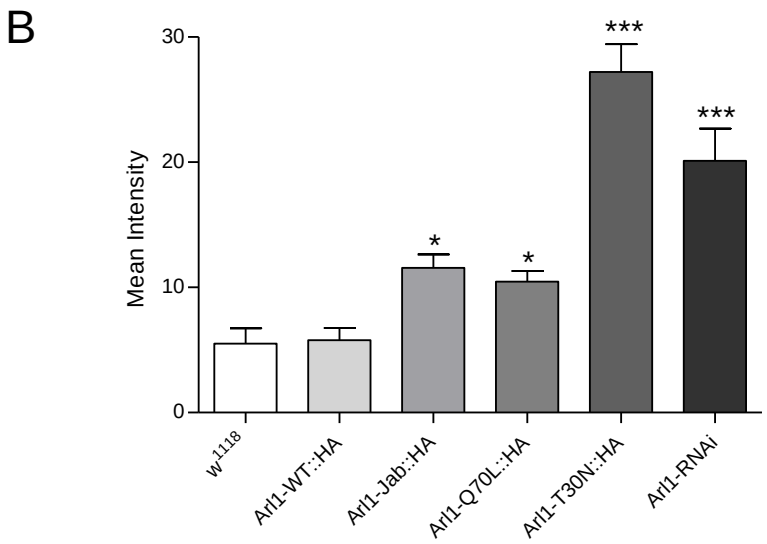
B
Mean Intensity
30
20
10
0
***
***
*
*
w1118
Arl1-WT::HA
Arl1-Jab::HA
Arl1-Q70L::HA
Arl1-T30N::HA
Arl1-RNAi

Figure 5.13. Lipid retention increases in the gut by two-fold in the Arl1-Jab::HA and Arl1-Q70L::HA mutants and 3-4 fold increase in the Arl1-T30N::HA and Arl1-RNAi mutants
(A) Representative images of Arl1 *Drosophila* gut stained with Hoechst (white/blue in merge), Nile red (red) and Phalloidin (green). Scale bar: 100µm. **(B)** Nile red staining intensity was measured using Image J. Values are expressed as mean±SEM (n=3 L3; 1-way ANOVA with Dunnett's post-hoc test *P<0.05, ***P<0.001).

5.2.6. No significant abnormalities were observed in glial cell morphology

The *jab* mouse presented with demyelination in the PNS and CNS. Although myelin is not present in *Drosophila,* glial cells in *Drosophila* are similar to mammalian glial cells. Peripherai wrapping glial cells in *Drosophila* function similarly to mammalian non-myelinating Schwann cells in the PNS (Freeman and Doherty 2006). Due to ease of access the CNS from L3 male larvae were dissected. Neurons exiting the CNS and ensheathed by glial cells were analysed by counting the number of glial nuclei and measuring the width of the phalloidin membrane stain, staining the glial membrane sheath. The number of glia nuclei was not significantly different between the wild-type and Arl1 mutant flies (Figure 5.14A+B). The width of the glial membrane stain was measured and a slight, but not significant, reduction in width was found between the wild-type and all Arl1 mutants (Figure 5.14A+C). In conclusion, no obvious defects in the glial morphology were observed in *Drosophila* harbouring Arl1 defects.

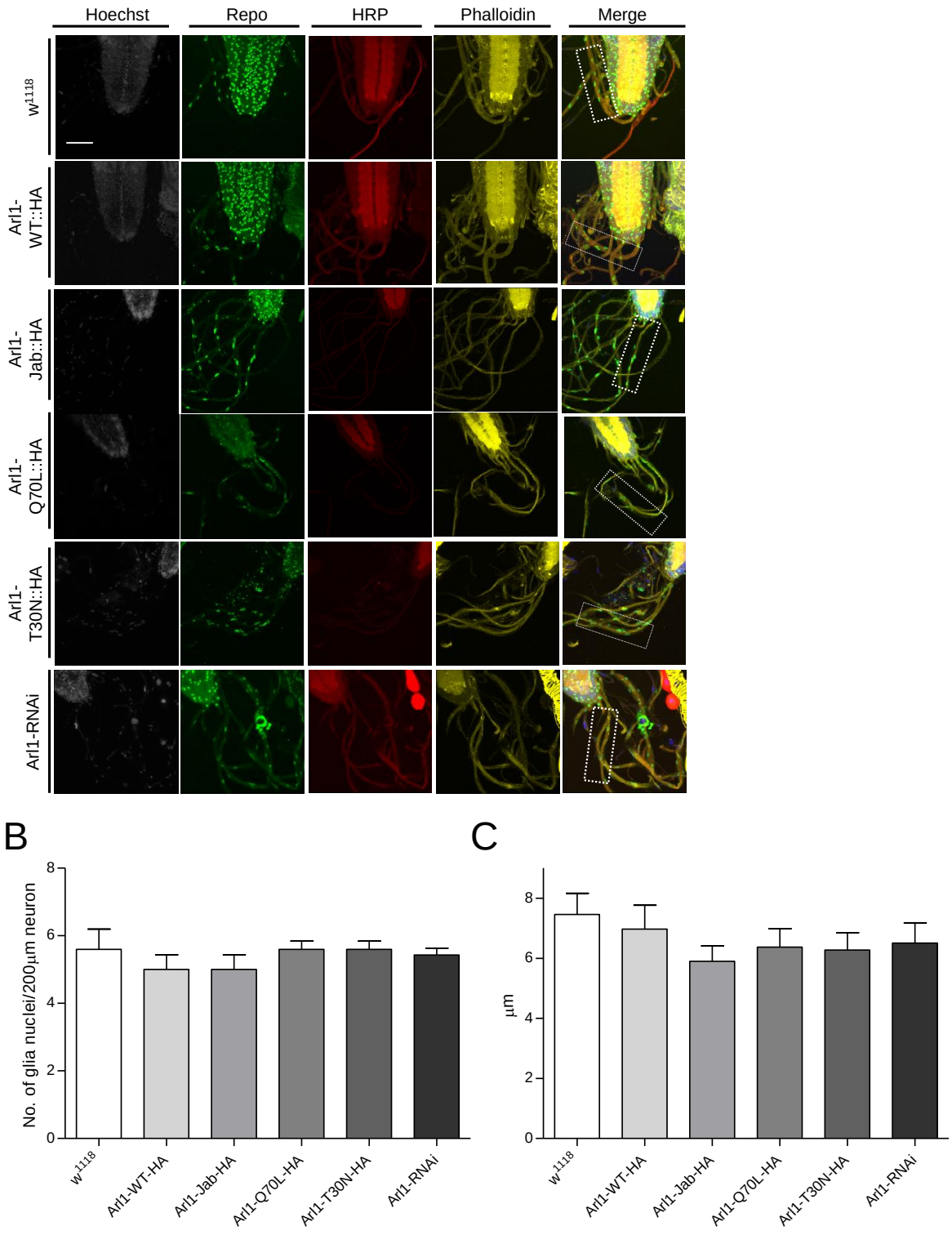

Figure 5.14. Altered Arl1 in expression and mutation in glial cells does not significantly alter morphology

(A) Representative images of Arl1 mutant CNS stained with Hoechst (white/blue in merge), Repo (green), HRP (red) and Phalloidin (yellow).Scale bar: 100µm. **(B)** Number of glial cells on a 200µm stretch were counted and no significant difference was found between the genotypes. Dotted white boxes illustrate an example of a neuron analysed. **(C)** Glia-neuron width was measured using Image J and a slight reduction can be observed, but is not significant, in the mutants versus wild-types. Values are expressed as mean±SEM (n= 3 L3; 1-way ANOVA with Dunnett's post-hoc test).

5.2.7. Reduction in weight is not only governed by defective Arl1 in the fat body

The most prominent pathology in the *jab* mouse is LD size reduction in adipose tissue and demyelination of the PNS, which suggests an important function of Arl1 in these tissues. As present in the *jab* mouse, a reduction in LD size was also observed in the fat body of Arl1 mutant flies. Furthermore the fat body has been implicated in growth by sensing nutrients and responding to these and initiating growth in the organism (Mirth and Riddiford 2007). Therefore, in order to test the importance of Arl1 in this tissue, Arl1 mutants and Arl1 RNAi were overexpressed specifically in the fat body using the fat body Gal4 driver *Cg (collagen type IV)*-GAL4 (Asha et al. 2003, Sousa-Nunes et al. 2011). This driver also expresses in some glial cells. Weight of the mutant flies was used as a measure of lipid metabolic defect. However, no significant difference was observed in weight (Figure 5.15).

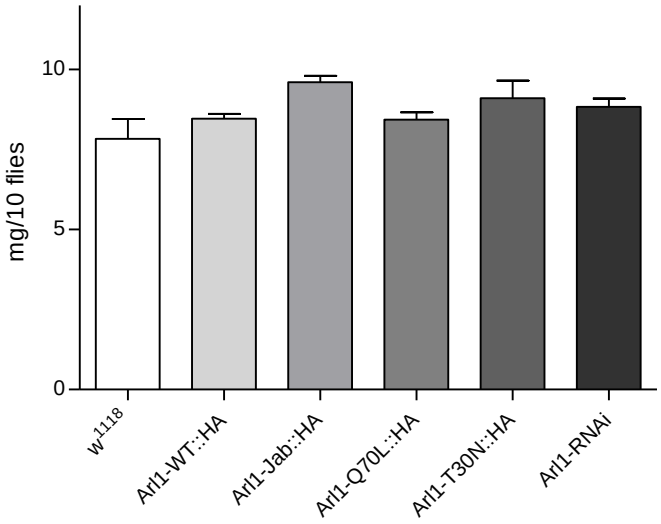

Figure 5.15. Overexpression of Arl1 mutant constructs in the fat body does not lead to a weight loss as seen in ubiquitous expression
Arl1 mutant constructs were crossed to fatbody-Gal4 driver and 10 flies were weighed per sample. Weight between the different genotypes was not altered significantly. Values are expressed as mean±SEM (n= 60; 1-way ANOVA with Dunnett's post-hoc test).

5.2.8. Impaired insulin signalling pathway

In the Arl1 mutants and Arl1-RNAi lipids are retained in the gut, potentially leading to nutrient deprivation. The smaller size of flies suggests involvement of a growth pathway defect in which insulin plays a crucial role. Specifically, Dilps and the insulin receptor signalling pathway have been implicated in regulating nutrition-dependent growth rates (Oldham and Hafen 2003, Sousa-Nunes et al. 2011, Mirth and Riddiford 2007). The insulin Akt/PI3K

pathway is well characterised and therefore Arl1 was investigated if it could be part of the insulin pathway. Specifically, *Dilp2* (Figure 5.16A) and *Dilp3* (Figure 5.16B) have been shown to be reduced in the *Drosophila* mutants using qPCR. The dILPs activate the insulin Akt/PI3K pathway and lead to phosphorylation of Akt which then activates downstream signalling partners. The level of phosphorylation of Akt was measured by western blot and showed a slight reduction in phosphorylated Akt for the *Drosophila* mutants (Figure 5.16C). These data suggest that Arl1 defects lead to insulin pathway impairments.

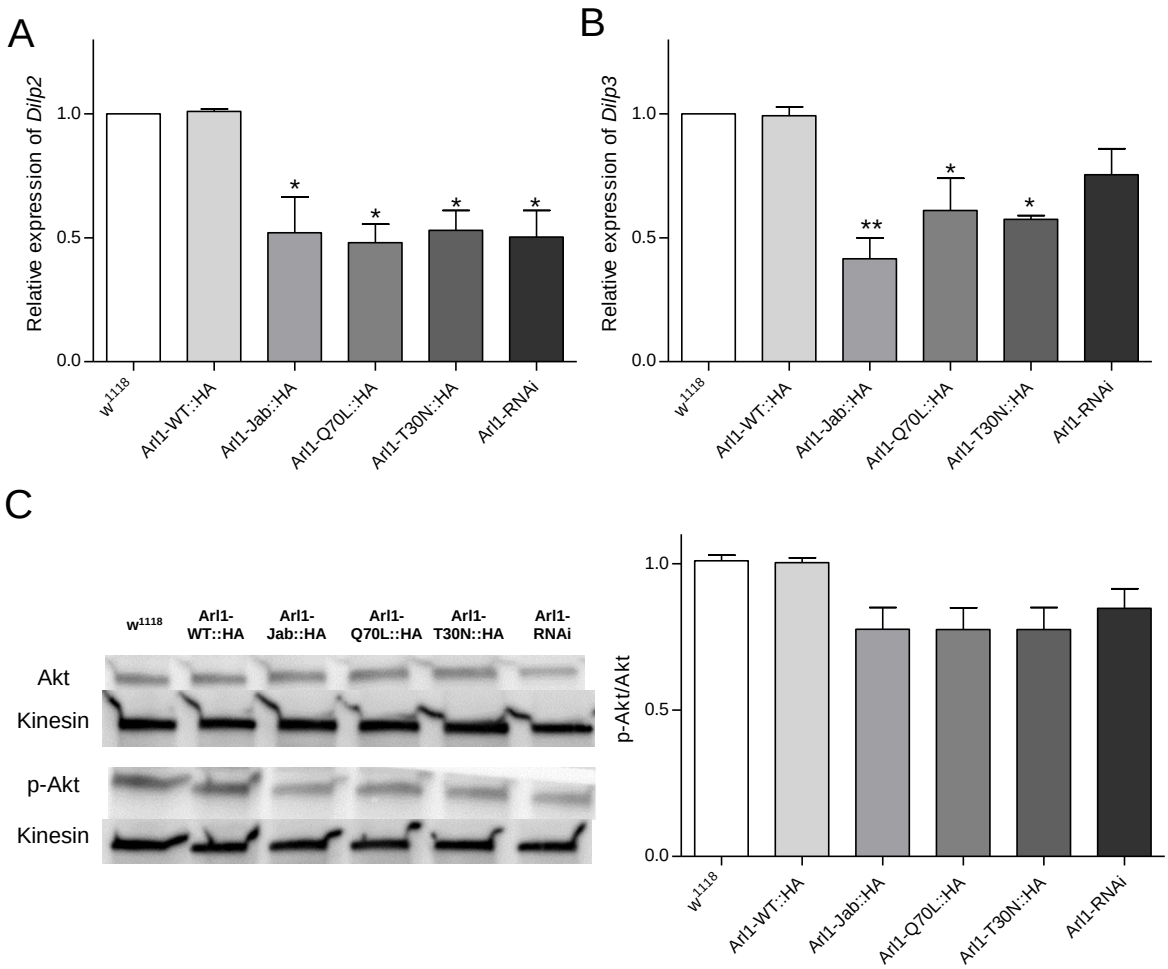

Figure 5.16. Reduced levels of *Drosophila* insulin-like peptides (Dilps) and insulin signalling in the Arl1 mutant *Drosophila*
(A) mRNA expression of *Dilp2* and **(B)** *Dilp3* was detected by qRT-PCR (n = 3). **(C)** Western blot analysis of Akt and p-Akt in whole fly lysate from w^{1118}, wild-type and mutant Arl1 overexpression by *actin*-Gal4 in *Drosophila* (n = 2). Values are expressed as mean±SEM (1-way ANOVA with Dunnett's post-hoc test *P<0.05; **P<0.01).

5.3. Discussion

In this chapter, novel *Drosophila* Arl1 mutants are described that are well suited for further studies of Arl1, dissecting molecular mechanisms linking lipid homeostatic defects to neurologic disease. The *jab* mouse model, a potential novel model of the lipid metabolism disease CRD, is the first report of Arl1's involvement in lipid deregulation leading to neurodegeneration. It is not clear how changes in lipid homeostasis cause neurodegeneration therefore it is important to generate models that enable further investigation of the underlying molecular mechanisms. To investigate the role of Arl1 tissue specifically, *Drosophila* Arl1 mutants were generated and validated. The *Arl1* gene shows strong conservation between fly and mouse as the *jab Drosophila* mutant recapitulates the key phenotype observed in the *jab* mouse. The *jab Drosophila* mutant presents with normal life span (Figure 5.8), growth retardation (Figure 5.9), motor defects (Figure 5.10), reduced lipid droplet size (Figure 5.11), reduced TAG levels (Figure 5.12) and retention of lipids in the gut (Figure 5.13). This highlights the value and the validity of using *Drosophila* as a model organism to further investigate Arl1 function. *Arl1* is one of the most conserved genes of this family, reflecting its fundamental role in eukaryotic cells (Pasqualato et al. 2002).

Until now, only knock-out studies have been conducted to investigate Arl1 *in vivo* function (Tamkun et al. 1991, Torres et al. 2014, Lee et al. 2011). Previous studies of Arl1 in *Drosophila* have been conducted using the *Arl1* null, which is a limited *in vivo* model organism as it only survives until larval stage. Studies using the *Arl1* RNAi highlight Arl1's role in secretory granule biogenesis (Torres et al. 2014), negative regulator of ER-Golgi traffic and acting in part in ER quality control (Lee et al. 2011) which supports Arl1's importance in vesicle membrane trafficking at the *trans*-Golgi network (*trans*-Golgi) (Lowe et al. 1996, Behnia et al. 2004, Nishimoto-Morita et al. 2009, Chia and Gleeson 2011). In this chapter, the Arl1 RNAi line from the Bloomington Stock Centre was used and led to an *Arl1* knock-down of only 30% (Figure 5.4C). Interestingly, knock-down of 30% *Arl1* mRNA already led to

pathology in this chapter but it would be necessary to confirm this pathology with additional Arl1 RNAi lines to exclude off target effects of the specific RNAi used.

5.3.1. Similarities in phenotype observed between the following pairs: *Jab* and RNAi as well as Q70L and T30N

A lesson emerging from systemic knock-out studies has shown that by only employing loss of function mutations the understanding of gene functions will be limited (Prelich 2012). Constitutively active, inactive and *jab* Arl1 mutations were generated (Table 5.1) as well as the Arl1 RNAi and used to understand Arl1's function. Point mutations or deletion mutations, that inactivate one function of a protein but still enable interaction with other proteins, have been commonly used. This approach has also been employed in the study of Arl1 and other small GTPases, and overexpression increases the likelihood of these mutants to cause a mutant phenotype (Lu et al. 2001, Zahn et al. 2006, Chen et al. 2010). In this chapter, the translation of this approach to a whole organism, as *Drosophila*, is presented and has already proven to be valuable for other small GTPases (Klemm et al. 2013). Phenotypes of Arl1 mutants compared to the Arl1-WT::HA control are presented in table 5.2 and discussed below.

Overexpressing Arl1-WT::HA did not lead to any obvious pathology. These results confirm the observations made in a prior study in mammalian cells in which surplus Arl1 localises to the cytoplasm, suggesting that *trans*-Golgi localisation and activation of Arl1 is saturable (Lu et al. 2001). Interestingly, the *jab* mutant flies are similar in phenotype to the Arl1-RNAi mutant flies showing no severe developmental delay, but slightly reduced size, reduced motor activity, reduced LD size and normal number of LDs within the fat body's adipocytes. In contrast to the *jab* mutant flies, the Arl1-RNAi mutant flies also presented with reduced life span of 20-30% and retention of lipids by a 3-fold increase in the *Drosophila* gut versus a 2-fold increase in the *jab* mutant flies. Stainings were conducted using Nile Red, a common stain for lipophilic compounds. However, Oil Red O has also been used and argued to be a more specific staining method and could be used in future studies to confirm Nile Red staining in this study (O'Rourke et al. 2009, Mehlem et al. 2013, Gutierrez et al. 2007). A higher amount of lipid retention in the gut was also observed in the Arl1-T30N::HA mutants presenting with premature death;

however, the Arl1-Q70L::HA mutants only present with a 2-fold increase in lipid retention in the gut and also presents with premature death, whereas the *jab* mutants do not. Therefore, lipid retention levels might not be the leading cause of premature death in the mutants. Further studies are needed to confirm the cause of premature death. No studies have been conducted on cell death, which might be an effect secondary to lipid defects, and help to elucidate cause of premature death in the Arl1 mutants. Neurons are essential for signalling processes for critical organs. They are particularly sensitive to insults in homeostasis and rely on high energy levels. Therefore, deregulation in lipid metabolism might make them less stress resistant and lead to death. Due to the similarity between the RNAi and *jab* fly lines, one might hypothesise that the *jab* mutation sequesters wild-type protein and causes loss of wild-type function, or another toxic gain of function causing dysfunction of the wild-type protein. However, potentially something more complex is happening, as a more severe phenotype would be expected in the *jab* mouse which only contains 50% of endogenous Arl1 wild-type protein. Further analysis will be necessary to confirm these findings.

5.3.1.1. The function of Arl1 in *Drosophila* development

The T30N mutation, the CI form of Arl1, has shown to fragment the Golgi apparatus (Golgi) since Golgi proteins were not able to localise to the Golgi. The Q70L mutation, the constitutively active form of Arl1, has been shown to expand the Golgi in which Golgi proteins could still localise to the Golgi, but vesicle trafficking was dysfunctional (Lu et al. 2001). These experiments in cells already highlight similar signalling defects caused by oppositely functioning proteins. Indeed, Arl1-T30N::HA and Arl1-Q70L::HA mutants led to a similar phenotype in *Drosophila*. This highlights the importance of maintaining a strict level of Arl1 activation. Too much activity or too little is both detrimental to the system. Arl1-T30N::HA and Arl1-Q70L::HA mutants present with severe developmental delay. *Drosophila* development is characterised by crucial changing levels of TAG synthesis and mobilisation, which cause a large increase of body fat content during larval development followed by a 3-fold reduction during metamorphosis (Church and Robertson 1966). The fat body in particular has an

important role in linking nutrient availability to growth. The *Arl1* null mutant is lethal at a late L2 stage and suggests crucial involvement of Arl1 at this stage. Interestingly, an important factor for pupariation and metamorphosis is the critical weight that needs to be reached, which occurs during the transition from L2 to L3 stage. If nutrient deprivation occurs prior to reaching critical weight, then the larvae do not grow, are unable to initiate metamorphosis and die (Mirth and Riddiford 2007, Beadle et al. 1938). Therefore, the complete loss of Arl1function (as in the *Arl1* null) most likely leads to inability to reach critical weight and early death at larval stage, due to Arl1's involvement in lipid homeostasis. Interestingly, the Arl1-T30N::HA and Arl1-Q70L::HA mutants both present with delays in development, specifically in reaching L3 and pupal stage. High larval lethality is observed for both the genotypes (30-40%), therefore suggesting nutrient deprivation prior to reaching critical weight. The remainder of larvae reached metamorphosis but 10-20% were unable to hatch or were not able to complete metamorphosis. The flies that hatched were severely growth retarded. Interestingly, studies have shown that when larvae were starved after reaching critical weight, larvae presented with reduced growth but metamorphosed into tiny adults (Mirth and Riddiford 2007, Beadle et al. 1938). These results highlight Arl1's involvement in lipid accumulation prior to L3 stage to advance to L3 and pupal stage. TAG levels were shown to be reduced in whole adult fly homogenate and it is highly likely that TAG levels are also reduced in larvae in comparison to wild-type controls (following previous results discussed) and lead to developmental delay. Future studies should confirm TAG levels during larval stages. Furthermore, it would be essential to ensure feeding ability and analysis of the gut content of larvae. Interestingly, lipid retention in the gut was observed and highlights the potential of impaired nutrient absorption as observed in the conditional enterocyte-specific *Arfrp1* knock out mouse (Jaschke et al. 2012). Arfrp1 recruits Arl1 and suggests an overlap in pathology (See Chapter 1, Figure 1.7). This study has highlighted the role of Arl1 in growth, development and nutrient accumulation.

5.3.1.2. Arl1's function in lipid droplet biogenesis

A difference observed between Arl1-T30N::HA and Arl1-Q70L::HA mutants is the LD phenotype, in which the Arl1-T30N::HA mutant increases LD size to double the size of the wild-type control and has 60% reduced amount of LDs, and the Arl1-Q70L::HA mutant maintains the LD size but has only 30% reduced amount of LDs in comparison to the wild-type control. Both present with 50% reduced adipocyte size in comparison to the wild-type control, suggesting an involvement in differentiation and growth of adipocytes. Interestingly, the *jab Drosophila* mutant is similar to the *jab* mouse in that it also presents with a slightly reduced adipocyte cell size. Work on the *jab* mouse has confirmed a reduction in the adipose differentiation factors PPAR-γ and CCAAT/enhancer-binding protein alpha (C/EBP-α) (Bitoun et al., unpublished).

Interestingly, the *Arl1* null has a similar trend in phenotype to the Arl1-T30N::HA mutant with larger and fewer LDs, both ultimately harboring dysfunctional Arl1. It needs to be taken into consideration, that the *Arl1* null is more severely developmentally delayed and hence smaller in size. LDs are formed at the ER and further processed at the Golgi, where Arl1 is located at the *trans*-Golgi. Interestingly, larger LDs have been associated with an inefficiency of lipolysis and an aggregation of lipid in the LDs (Guo et al. 2008). Proton-assisted amino acid transporters (PAT) family proteins *p*erilipin, adipocyte differentiation-related protein (ADRP), and tail-interacting protein of 47 kDa (TIP47) attach to LDs and restrict the access of lipases or facilitate their enzymatic activity under appropriate metabolic conditions (Bickel et al. 2009). Arl1 recruits the Arf-GEF BIG1 and BIG2 and activates Arf1 (McDonold and Fromme 2014, Torres et al. 2014, Christis and Munro 2012). The Arf1-coat protein (COPI) machinery is required for the localisation of the major TAG lipase adipose triglyceride lipase (ATGL) (Beller et al. 2008, Soni et al. 2009, Ellong et al. 2011). Therefore further studies on localisation of PATs and associated lipases such as ATGL on LD surfaces would be crucial in the understanding of a lipolysis defect in the Arl1 mutants (Jambunathan et al. 2011, Cartwright et al. 2014, Guo et al. 2008, Hommel et al. 2010).

Arl1-Jab::HA mutant and Arl1-RNAi have much smaller LD and more LDs per cell. The mechanism behind this phenotype might be due to impaired fusion and growth (Klemm et al. 2013, Chao Wang et al. 2012). Boström and co-workers demonstrated that the soluble *N*-ethylmaleimide-sensitive factor adaptor protein receptor (SNAP23) is necessary for fusion of LDs (Bostrom et al. 2007). Conditional adipocyte-specific *Arfrp1* knock out mice presented with reduced amount of SNAP23 localised to LDs (Hommel et al. 2010). As Arfrp1 recruits Arl1, investigating SNAP23 localisation in the fat body of the Arl1 *Drosophila* mutants would be necessary to confirm this defect. Proteins localised at the LD are crucial for intracellular locomotion, efficient lipolysis when energy is needed and signalling mechanisms. From the results presented in this chapter, Arl1 might play an important role in further processing of LD at the *trans*-Golgi.

Furthermore, levels of Arl1 defect seem to be crucial due to the differences seen between the low level of defect in Arl1-Jab::HA mutant and Arl1-RNAi (leading to smaller LDs) in contrast to the more severe defect in Arl1-Q70L::HA, Arl1-T30N::HA and *Arl1* null (leading to fewer and larger LDs). Despite the exact mechanism for this being unknown, adipose cell sizes are also irregularly formed in the mutants and it could be concluded that Arl1 plays an important role in LD formation, as suggested in studies by Hommel et al., 2010. Despite their implication in energy metabolism and disease, LDs have been grossly understudied. Lipid metabolism defects might cause defects in the most sensitive cells of the organism, for example neurons and glia which have been less studied. The *jab* mouse presents with neuropathy and it is crucial to understand Arl1's role in this new pathogenic mechanism that can elucidate insights into lipid metabolism deregulation and neuropathy. Interestingly, a recent study has highlighted LD accumulation in glial cells as a promoter of neurodegenerative disease (Liu et al. 2015) and highlights the importance of understanding altered lipid metabolism leading to neurodegeneration.

The *jab* mouse presents with pronounced peripheral demyelination which is cause for the neuromuscular junction (NMJ), muscle and locomotor defects (Bitoun et al., unpublished). Both the Arl1-Jab::HA and the Arl1-RNAi do not show a delay in development, however they

do show a defect in eclosion as well as the Arl1-T30N::HA and Arl1-Q70L::HA mutants. This phenotype is reminiscent of those observed in *nip* and *Sod1* mutant flies, which are models of neuromuscular disease (Xie et al. 2010, Kirby et al. 2002). Incomplete eclosion, in which the fly is unable to separate from the puparial case during eclosion, has been associated with motor phenotypes such as ALS *Drosophila* models and implies a motor defect in the Arl1 mutants (Wang et al. 2011, Kirby et al. 2002). Ensheathing glia also play a crucial role in *Drosophila* and therefore mechanisms maintaining glial health that are important for myelination can be studied using *Drosophila* (Ghosh et al. 2013, Xie and Auld 2011, Navarro et al. 2010). Unfortunately, in order to visualize the glial membrane most studies expressed a membrane tagged GFP (UAS-mCD8-GFP) (Lee and Luo 1999, Ghosh et al. 2013) using the glial cell driver, *repo*-Gal4. A slight reduction in width of the glial membranes was detected, which might suggest there are defects occurring that potentially could lead to the locomotor phenotype observed in the flies. In particular, glial ensheathment at the NMJs should be analysed as well as the NMJs themselves as they were shown to be disorganised in the *jab* mouse (Chapter 3). The findings in this study are preliminary and further analysis is needed.

Table 5.2. Comparison of phenotypes of the different Arl1 mutations to Arl1-WT::HA control

	Development	Survival	Size	Motor Activity	Fat pathology	Signalling	Retention of lipids in the Gut
Jab	Normal	Normal	Slightly reduced	Reduced	LD size↓ No. of LD≈	Dilps↓ pAkt↓	2-fold↑
Q70L	Delayed	50% reduced	Reduced	Reduced	LD size≈ No. of LD↓	Dilps↓ pAkt↓	2-fold↑
T30N	delayed	50% reduced	Reduced	Reduced	LD size↑ No. of LD↓	Dilps↓ pAkt↓	4-fold↑
RNAi	Normal	30-40% reduced	Slightly reduced	reduced	LD size↓ No. of LD≈	Dilps↓ pAkt↓	3-fold↑

LD=Lipid droplets; "≈" = about equal to wild-type; Dilps = *Drosophila* insulin-like peptides; pAkt = phosphorylated Akt

A limitation to the study using CI and CA mutants of GTPases, is the potential aberrant localisation not characteristic of endogenous Arl1. Therefore it is crucial to confirm localisation of mutant Arl1 and investigate known Arl1 binding partners in order to assess the functionality of the overexpression. However, in support of the mutants exerting Arl1 specific pathology are the findings made in the Arl1-RNAi which affect the same tissue and mechanisms. Unfortunately, this chapter lacked an antibody for the endogenous Arl1 protein in *Drosophila*. Future efforts should focus on the production of such an antibody in order to compare overexpressed constructs with endogenous Arl1. For the first time, *in vivo* function of the CI and CA form of Arl1 has been characterised and elucidated that Arl1 is highly sensitive to a balanced level of activity, as both mutations lead to very similar pathology in *Drosophila*.

Previous expression profiling studies indicate that Arl1 is likely to act in most tissues, but given the different membrane trafficking requirements of different cell types, the function of Arl1 varies. Higher expression is present in the salivary glands, accessory glands, malpighion tubules, fat body and gut, which all have important roles in secretion (Chintapalli et al. 2007). Due to strong defects observed in the fat body and higher expression levels of Arl1, it was questioned if this tissue might drive the pathology. Weight was analysed to provide as initial parameter, due to significant growth retardation in the mutants (Figure 5.9B). Preliminary results present no changes in weight, which highlights that Arl1 does not seem to play a role in fat body to increase weight. The need for additional tissues to be defective and a potential systemic defect in Arl1 is stressed. However expression levels and fat body pathology, as well as the use of additional fat body drivers, should be investigated in further studies to draw any conclusion. Interestingly, another gene, dSir2 (implicated in lipid metabolism), presented only a life span defect when diet, specifically yeast, was restricted (Banerjee et al. 2012). Therefore, it would be of interest to alter diet to potentially exert an effect when Arl1 is altered in the fat body.

5.3.2. Defects in the insulin signalling pathway are observed in the Arl1 mutants

Growth defect, development delay and LD abnormalities present as an insulin defective phenotype. Indeed, the insulin signalling pathway is crucial for cell growth in response to nutrient conditions (Edgar 2006, Sousa-Nunes et al. 2011, Geminard et al. 2009, Hietakangas and Cohen 2009, Teleman 2009, Goberdhan and Wilson 2003). The Arl1 mutant flies presented with growth retardation and retention of lipids in the gut, consistent with findings in the *jab* mouse and most probably leading to nutrient deprivation in the organism. To confirm this, levels of amino and fatty acids will need to be measured in the haemolymph. Interestingly, it has been shown that nutritional stimuli, known to be excreted by the fat body (Britton and Edgar 1998), induce the expression of Dilps in a subset of glia. This pathway involving the insulin Receptor/PI3K pathway is required by neuroblasts to exit quiescence and differentiate (Sousa-Nunes et al. 2011). This is an interesting link especially as the *jab* mouse presents with lipid homeostatic defects and demyelination of the PNS, and suggests Arl1's involvement in defective neuroblast proliferation potentially leading to immature glial cells. Indeed, on a whole organism level, reduction in Dilps were measured by qPCR which might be caused by reduction in nutrients sensed by the fat body. Furthermore, downstream Akt phosphorylation was impaired in all mutants and suggests involvement of Arl1 and the insulin signalling pathway. To support dysfunction of the insulin signalling pathway further, downstream proteins of Akt should be measured especially the activation of mTOR which subsequently phosphorylates S6K and 4E-BP, important for cell growth and differentiation. The findings from the study of the conditional hepatocyte-specific *Arfrp1* knock-out mice supported Arl1's involvement in the insulin signalling pathway, as it showed ineffective targeting of IGF1, a substrate of the insulin signalling pathway, for secretion. IGF1 has been associated with neuronal survival and promoting Schwann cell myelination (Wine et al. 2009, Liang et al. 2007, Ye et al. 2002, Fernandez and Torres-Aleman 2012, Carro et al. 2002). Interestingly, the insulin signalling pathway has also been implicated in *Drosophila* glia proliferation important for ensheathing neurons and providing protection from neurodegeneration (Callan et al. 2012, Chell and Brand 2010, Sousa-Nunes et al. 2011, Avet-Rochex et al. 2012). In addition, dysfunctional Akt

signalling has also been implicated in HD presenting with locomotor defects, which were ameliorated by Akt in a *Drosophila* HD model (Lievens et al. 2008). Finally links have also been made between the insulin signalling pathway and LD biogenesis (Bostrom et al. 2009, Olofsson et al. 2011, Liu et al. 2014, Grahn et al. 2014). These results warrant further investigation of Arl1's role in the insulin signalling pathway and how it leads to the pathology observed in the *jab* mouse.

In summary, this chapter has confirmed the highly conserved function of Arl1 between mouse and *Drosophila*, thus validating the use of *Drosophila* for future studies to help elucidate the molecular mechanisms linking lipid homeostatic defects and neuropathy in the *jab* mouse. Furthermore, tissue specific studies can be conducted to understand which tissue is most dependent on the function of Arl1 and might be driving the *jab* pathology. Arl1, present at the *trans*-Golgi, functioning as a signalling hub, might act as a common regulator and is an exciting novel player linking lipid deregulation and neuropathy. It is still unknown exactly how lipid homeostatic defects lead to neurodegeneration and therefore tractable, model organisms, such as *Drosophila*, are crucial to elucidate novel pathways. The tractable model organism *Drosophila*, allows the use of diverse genetic tool sets in a short time frame, which is not possible in mouse.

6. Discussion

The aim of this project was to understand the molecular mechanisms underlying movement disorders and to identify new genes involved in neurodegeneration. The Stevens mouse was identified from the Harwell N-ethyl-N-nitrosourea (ENU) mutagenesis screen by its smaller size and tremor. It harbours two mutations, a truncation mutation in the *Gnptab* gene and a missense mutation in the *Arl1* gene. Genetic crossing into individual mouse strains, separated the two mutations. The Nymphe (*nym*/+) mouse harboured the mutation in the *Gnptab* gene and the Jabber (*jab*/+) mouse harboured the mutation in the *Arl1* gene. In this thesis, both have provided important new insights into two pathways characteristic of neurodegeneration (Figure 6.1): the autophagy-lysosome pathway, a protein degradation pathway in the *nym* homozygote mouse (Chapter 4; reviewed in Chapter 1 Section 1.1), and lipid metabolism defects in the *jab* mouse (Chapter 5; reviewed in Chapter 1 Section 1.1). This work has highlighted the value of a phenotype-driven approach to investigate novel neurodegenerative pathways.

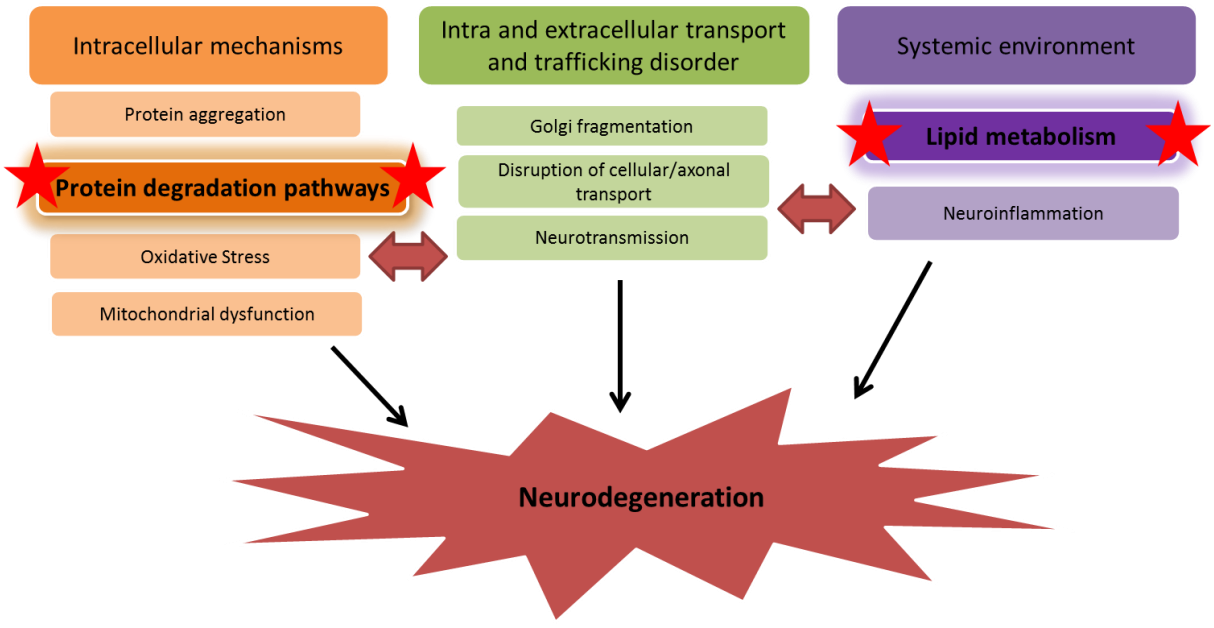

Figure 6.1. Molecular pathways leading to neurodegeneration
Pathways of focus in this thesis are highlighted by red stars. Displayed are pathways influencing the balance of neuronal survival and degeneration within broader functional groups based on their major site or mode of action: intracellular mechanisms, intra- and extracellular transport and trafficking disorder, and systemic environment. (Adapted from Ramanan and Saykin 2013).

6.1. The Nymphe mouse: link between lysosomal storage dysfunction and neurodegeneration

The work in this thesis characterised a novel mouse model of the lysosomal storage disease mucolipidosis (MLII) homozygous for a patient mutation in the *GNPTAB* gene. This mouse model more fully recapitulates the human pathology showing growth retardation, skeletal and facial abnormalities, increased circulating lysosomal enzymatic activities, increased intracellular lysosomal storage and reduced life span. Importantly, MLII behavioural deficits were characterised for the first time, including impaired motor function and psychomotor retardation. Histological analysis of the brain revealed progressive neurodegeneration in the cerebellum with severe Purkinje cell loss as the underlying cause of the ataxic gait. In addition, based on the loss of Niemann Pick type C (Npc) 2 protein expression in the brain, the mice were treated with 2-hydroxypropyl-β-cyclodextrin, a drug previously reported to rescue Purkinje cell death in a mouse model of NPC disease. No improvement in brain pathology was observed and indicates that cerebellar degeneration is not primarily triggered by loss of *Npc2* function.

This study has characterised a more disease relevant mouse model than the previously available *Gnptab* knock-out mouse model which lacks some of the characteristic features of MLII. This result emphasises the value of modelling MLII patient mutations to generate clinically relevant mouse mutants to elucidate the pathogenic molecular pathways of MLII and address their amenability to therapy. Furthermore, progressive neurodegeneration was characterised for one of the first times in MLII, confirming the initial findings made in the knock-in (Kollmann et al., 2012). MLII patients present with psychomotor retardation suggesting nervous system involvement. This study suggests that early markers of neurodegeneration might be cause for psychomotor retardation and should be investigated further in MLII patients.

6.2. The Jabber mouse: Linking lipid metabolism defects and neurodegeneration

The Jabber (*jab)* mouse, the first Arl1 mutant described in a mammalian organism, presents with growth retardation, lipodystrophy, lipid retention in the gut, tremor, hind limb clasping, reduced muscle strength, demyelination, neuromuscular junction disorganisation and muscle pathology (Bitoun et al., unpublished data). Arl1 is involved in the production of lipid droplets and chylomicrons, key players in lipid homeostasis (Hesse et al. 2013). The *jab* mouse model is a potential novel model of the lipid metabolism disease chylomicron retention disease (CRD) and is the first report of Arl1's involvement in lipid deregulation leading to neurodegeneration (Bitoun et al., unpublished data). It was not clear how changes in lipid homeostasis cause neurodegeneration, therefore it was important to generate models that enable further investigation of the underlying molecular mechanisms. *Drosophila* is a tractable model to elucidate these specific molecular mechanisms and in support of this strategy, the *Arl1* gene shows strong sequence conservation (over 80%) between *Drosophila* and mouse. A limiting factor in the use of *Drosophila*, modelling the demyelinating pathology in the *jab* mouse, is that *Drosophila* does not contain myelin as in mammals. However, *Drosophila* and mouse glial cells, which form the myelin sheath in mammals, show strong similarities. Peripheral wrapping glial cells in *Drosophila* and mammalian non-myelinating Schwann cells (SCs) both extend their membrane and ensheath axons crucial for insulation and function of neurons (Freeman et al., 2010). *Drosophila* Arl1 mutants were therefore generated to investigate the role of Arl1. Strong phenotypic conservation was observed as the *jab Arl1 Drosophila* mutant recapitulates the key phenotypes observed in the *jab* mouse. The *jab Drosophila* mutant presents with normal life span, growth retardation, motor defects, reduced lipid droplet size, reduced triacyglyceride levels and retention of lipids in the gut. In addition, the study of constitutively active and inactive mutants of Arl1 has highlighted the need for strict regulation of Arl1 activity. Finally, the insulin signalling pathway, an important metabolic signalling pathway, was shown to play a role in the *jab* pathology.

The phenotypic conservation between an Arl1 mutant, the *jab* mutation, in mouse and *Drosophila* was confirmed which is crucial for future studies of Arl1 in *Drosophila*. The generation of novel Arl1 *Drosophila* mutants now enable further analysis of the function of Arl1 in a tissue-specific manner and elucidation of the pathway involved between lipid metabolism defects and neurodegeneration in the *jab* mouse, which may also be relevant to CRD.

This work raises many questions. The main pathology in the *jab* mouse is demyelination of the peripheral nervous system (PNS), causative of tremor, neuromuscular junction disorganisation and muscle myopathy. Therefore, future studies would focus on investigating how a defect in Arl1 leads to this demyelination. As highlighted before, the extension of glial membrane, an essential step of myelination in mammals, is also essential for the peripheral wrapping glial membrane in *Drosophila*, which conduct very similar functions to non-myelinating SCs. Importantly, the molecular mechanism within these tissues is highly conserved and therefore glial defects in the *jab* mouse leading to demyelination are likely to be conserved in *Drosophila* (Freeman and Doherty 2006, Barres 2008, Kretzschmar et al. 1997).

6.2.1. Future work

Therefore, future studies should focus on characterising the peripheral wrapping glial cells in *Drosophila*. In the *jab* mouse only myelin basic protein and conduction velocity was analysed but as *Drosophila* does not express myelin. Further analysis of the demyelination defect of the PNS in the *jab* mouse would advance the understanding of how the *jab* mutation leads to demyelination. Analysis of the PNS would require the analysis of: (i) myelin protein synthesis to understand if the myelin loss is due to defects in the protein synthesis; (ii) lipid composition as the myelin sheath is made up mainly of lipids; (iii) the number of SCs, percentage of proliferating SCs and apoptosis to highlight if a loss of SCs or dedifferentiated SCs were the cause of demyelination; (iv) axonal apoptosis that might have been caused due to glial cell apoptosis, (v) mitochondrial metabolism and cytoskeletal deficits within the SCs

which have been shown to be implicated in myelination. The same analysis as in the *jab* mouse, detailed above, should be conducted in *Drosophila*.

By using the diverse tool set of *Drosophila*, the molecular mechanisms involved in the demyelination defect of the *jab* mouse could be dissected in *Drosophila*. Arl1 is located at the *trans*-Golgi network which acts as a clustering site of proteins involved in multiple signalling pathways. Therefore Golgi dysfunction due to structure and loss of signalling partners can have significant effects on various signalling pathways. The following pathways might be further investigated in regards to causing a glial cell defect in the *jab* mouse and in the *Drosophila* models.

Firstly, it would be of interest to test whether Arl1 leads to demyelination because of dysfunctional extension of glial membrane which is crucial for insulation of neurons (White and Kramer-Albers 2014). Arl1 plays an important role in vesicle formation/trafficking as highlighted by its importance in secretory granule formation in the salivary gland (Torres et al. 2014). Interestingly, myelin biogenesis requires intricate membrane sorting and trafficking machinery in the glial cells for plasma membrane extension and similar processes are required for wrapping glia in *Drosophila* (Aggarwal et al. 2011a). Sorting the myelin component has been suggested to occur at the Golgi (Simons et al. 2000), by endocytic recycling (Winterstein et al. 2008), and at the level of the plasma membrane (Aggarwal et al. 2011b). Arl1 is a Golgi protein and suggests a potential role for Arl1 in membrane sorting and trafficking machinery of the glial cells to form membranes crucial for myelination. Interestingly, Arl1 has recently been implicated in membrane organisation, controlling the transfer of phospholipid molecules, such as phosphatidylserine, at membrane bilayers by a phospholipid flippase (Graham 2013). Phosphatidylserine is a major lipid in the plasma membrane and its concentration determines recruitment of peripheral membrane proteins and influences integral membrane protein function (Leventis and Grinstein 2010). In addition mutations in the phospholipid flippases have been associated with neurodegenerative phenotypes including axonal neurodegeneration (Onat et al. 2013, Zhu et al. 2012).

Secondly, the question remains, whether Arl1 is important for glial cell differentiation, a crucial step for proper myelination. Preliminary data has been generated by the Davies lab in the *jab* mouse of defective SC differentiation. Arl1 has been shown in normal conditions to activate phospholipase D1 (PLD1), which in turn generates the bioactive signalling lipid phosphatidic acid (PA). PA has been shown to activate Akt/mTOR and ERK1/2 signalling pathways (Fang et al. 2001, Winter et al. 2010) which are important in SC differentiation in the PNS (Sherman et al. 2012, Newbern et al. 2011). Interestingly, reduced levels of PA were shown in the *jab* sciatic nerve. Furthermore reduced levels of phospho-ERK2 and expression of UDP galactosyltransferase 8A (Ugt8a), a key marker of SC terminal differentiation, to levels matching those of the Arl1 transcript, have been shown (Bitoun et al., unpublished data). Interestingly, reduced levels of phosphorylated Akt have been detected in the Arl1 *Drosophila* mutants and highlights converging signalling pathways between PA and the insulin signalling pathway, discussed in the next section.

Finally, glial cells are sensitive to metabolic defects and therefore it was tested whether Arl1 might regulate any metabolic pathways. Nutrient decline potentially occurring due to lipids being retained in the gut in the *jab Drosophila* mutant might lead to signalling defects between the fat body and glial cells which leads to reduced *Drosophila* insulin-like peptides (Dilps) excretion (Sousa-Nunes et al. 2011). The insulin signalling pathway is highly implicated in metabolic sensing of nutrients and preliminary experiments have shown reduced levels of Dilps and phosphorylated Akt involved in the insulin signalling pathway of mutant Arl1 *Drosophila*. Further experiments investigating dietary supply and altering diet in the *Drosophila* models should provide insights into how much this pathway is driving the *jab* pathology. Support of Arl1's involvement in the insulin signalling pathway, stems from findings that Arfrp1, recruiting Arl1 to the Golgi, controls secretion of IGF1 in hepatocytes. The conditional hepatocyte-specific *Arfrp1* knock-out mouse shows reduced levels of IGF1, a ligand of the insulin receptor, due to ineffective targeting of IGF1 to the membrane for secretion. Therefore, Arl1 defects could also lead to ineffective targeting of IGF1. IGF1 has been associated with

neuronal survival and promoting SC myelination (Wine et al. 2009, Liang et al. 2007, Ye et al. 2002, Fernandez and Torres-Aleman 2012).

To understand the complexity of human disease a combination of model organisms is essential to understand disease pathology. Cross-species conservation has shown that the genetically tractable *Drosophila* system can complement studies in the mouse to conduct tissue-specific genetic manipulations and decipher molecular mechanisms in disease.

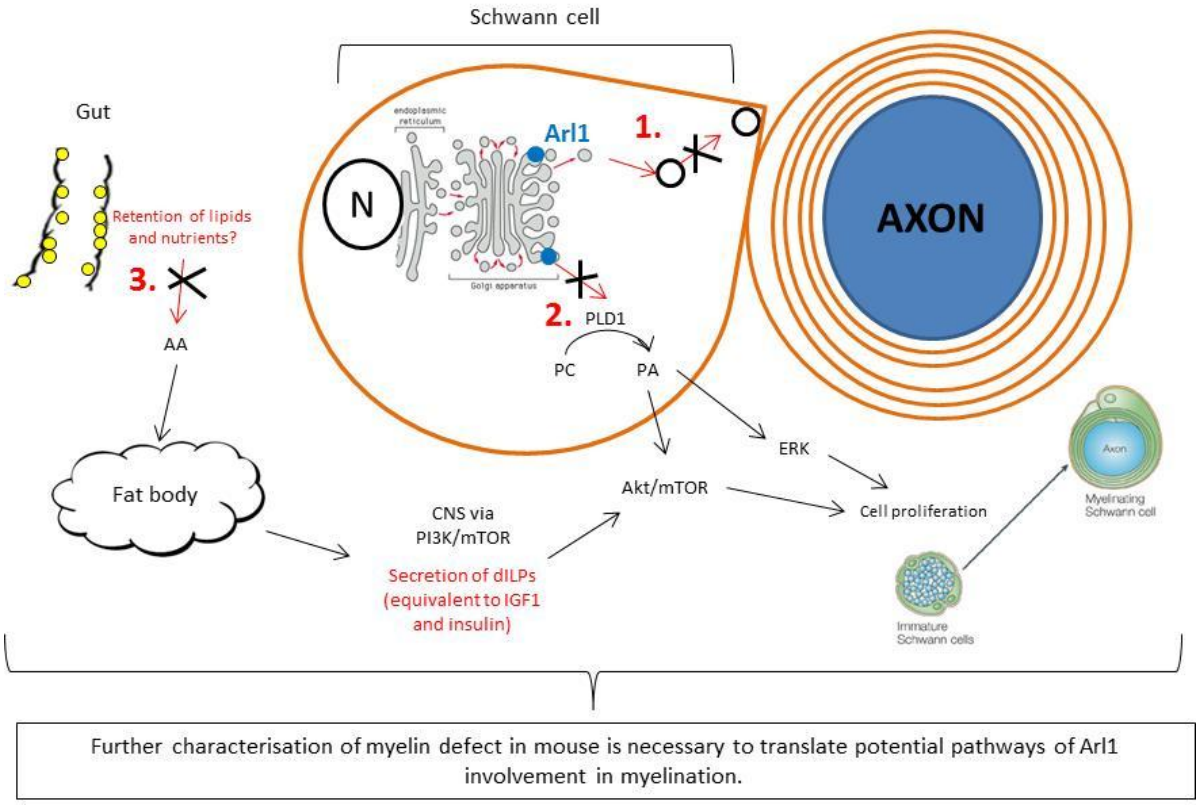

Figure 6.2 Illustration of future pathways to work on for Arl1 with a focus on myelination
More details and explanations can be found in the text. **1.** The first pathway would look to investigate if Arl1 plays a role in membrane sorting and trafficking which is important for membrane extension to form the myelin sheath. Similar processes are required for wrapping glia in *Drosophila*. **2.** The second pathway to investigate is whether Arl1 plays a role in the differentiation process of glial cells. This is of interest as Arl1 has been shown to activate pholpholipase D1 (PLD1) which in turn generates bioactive signalling lipid phosphatidic acid (PA) from phosphatidic choline (PC). PA has been shown to activate Akt/mTOR and ERK signalling which are important in Schwann cell differentiation in the PNS. **3.** Lastly, the third pathway the involvement of Arl1 in metabolic pathways such as the insulin signalling pathway should be investigated. In *Drosophila* it has been shown that amino acids (AA) are sensed by the fat body which in turn generates a fat body specific signal and signals to the CNS via a PI3K/mTOR pathway to release *Drosophila* insulin-like peptides (dILPs; equivalent to mammalian insulin and IGF1). These dILPs are ligands for the insulin receptor and activate the Akt/mTOR pathway which is important in glial cell differentiation. Further characterisation of the myelin defect in the jab mouse is necessary to translate potential pathways of Arl1 involved in myelination. Partly adapted from Jessen and Mirsky 2005.

6.3. Concluding statement

In conclusion, the work in this thesis has highlighted the value of a phenotype-driven approach to investigate novel neurodegenerative pathways and demonstrates how mouse and *Drosophila* mutants can successfully be used to understand the function of new molecules and pathways involved in neurodegeneration and to test potential therapies for neurodegenerative diseases. In this thesis, a rare lysosomal storage disease and a novel gene involved in lipid homeostasis modelling CRD were studied to gain insights into the importance of maintaining cellular homeostasis through the maintenance of degradation pathways and lipid metabolism, respectively. In the future, it will remain crucial to use a range of cellular and animal models, each with their own experimental advantages, in order to one day make neurodegenerative diseases potentially preventable and curable.

References

Acevedo-Arozena, A., Wells, S., Potter, P., Kelly, M., Cox, R. D. and Brown, S. D. (2008) 'ENU mutagenesis, a way forward to understand gene function', *Annu Rev Genomics Hum Genet,* 9, 49-69.

Achord, D. T., Brot, F. E., Bell, C. E. and Sly, W. S. (1978) 'Human beta-glucuronidase: in vivo clearance and in vitro uptake by a glycoprotein recognition system on reticuloendothelial cells', *Cell,* 15(1), 269-78.

Adams, M., Celniker, S., Holt, R., Evans, C., Gocayne, J., Amanatides, P., Scherer, S., Li, P., Hoskins, R. and Galle, R. (2000) 'The genome sequence of Drosophila melanogaster', *Science,* 287, 2185 - 2195.

Adibhatla, R. M. and Hatcher, J. F. (2008) 'Altered Lipid Metabolism in Brain Injury and Disorders', *Sub-cellular biochemistry,* 49, 241-268.

Aggarwal, S., Yurlova, L. and Simons, M. (2011a) 'Central nervous system myelin: structure, synthesis and assembly', *Trends Cell Biol,* 21(10), 585-93.

Aggarwal, S., Yurlova, L., Snaidero, N., Reetz, C., Frey, S., Zimmermann, J., Pahler, G., Janshoff, A., Friedrichs, J., Muller, D. J., Goebel, C. and Simons, M. (2011b) 'A size barrier limits protein diffusion at the cell surface to generate lipid-rich myelin-membrane sheets', *Dev Cell,* 21(3), 445-56.

Aharon-Peretz, J., Rosenbaum, H. and Gershoni-Baruch, R. (2004) 'Mutations in the glucocerebrosidase gene and Parkinson's disease in Ashkenazi Jews', *N Engl J Med,* 351(19), 1972-7.

Allan, B. B. and Balch, W. E. (1999) 'Protein sorting by directed maturation of Golgi compartments', *Science,* 285(5424), 63-6.

Anchisi, L., Dessi, S., Pani, A. and Mandas, A. (2013) 'Cholesterol homeostasis: a key to prevent or slow down neurodegeneration', *Front Physiol,* 3(486).

Anderson, C. M., Townley, R. R., Freemanm and Johansen, P. (1961) 'Unusual causes of steatorrhoea in infancy and childhood', *Med J Aust,* 48(2), 617-22.

Andlin-Sobocki, P., Jonsson, B., Wittchen, H. U. and Olesen, J. (2005) 'Cost of disorders of the brain in Europe', *Eur J Neurol,* 1, 1-27.

Angelichio, M. L., Beck, J. A., Johansen, H. and Ivey-Hoyle, M. (1991) 'Comparison of several promoters and polyadenylation signals for use in heterologous gene expression in cultured Drosophila cells', *Nucleic Acids Research,* 19(18), 5037-5043.

Antonini, A. and Albin, R. L. (2013) 'Dopaminergic treatment and nonmotor features of Parkinson disease: the horse lives'.

Asha, H., Nagy, I., Kovacs, G., Stetson, D., Ando, I. and Dearolf, C. R. (2003) 'Analysis of Ras-induced overproliferation in Drosophila hemocytes', *Genetics,* 163(1), 203-15.

Aubry, L., Bugi, A., Lefort, N., Rousseau, F., Peschanski, M. and Perrier, A. L. (2008) 'Striatal progenitors derived from human ES cells mature into DARPP32 neurons in vitro and in quinolinic acid-lesioned rats', *Proc Natl Acad Sci U S A,* 105(43), 16707-12.

Avet-Rochex, A., Kaul, A. K., Gatt, A. P., McNeill, H. and Bateman, J. M. (2012) 'Concerted control of gliogenesis by InR/TOR and FGF signalling in the Drosophila post-embryonic brain', *Development,* 139(15), 2763-72.

Awada, R., Parimisetty, A. and d'Hellencourt, C. L. (2013) *Influence of Obesity on Neurodegenerative Diseases, Neurodegenerative Diseases*.

Badger, J. L., Cordero-Llana, O., Hartfield, E. M. and Wade-Martins, R. (2014) 'Parkinson's disease in a dish - Using stem cells as a molecular tool', *Neuropharmacology,* 76, 88-96.

Baker, K. D. and Thummel, C. S. (2007) 'Diabetic larvae and obese flies-emerging studies of metabolism in Drosophila', *Cell Metab,* 6(4), 257-66.

Ballabio, A. and Gieselmann, V. (2009) 'Lysosomal disorders: from storage to cellular damage', *Biochim Biophys Acta,* 1793(4), 684-96.

Ballatori, N., Krance, S. M., Marchan, R. and Hammond, C. L. (2009) 'Plasma membrane glutathione transporters and their roles in cell physiology and pathophysiology', *Mol Aspects Med,* 30(1-2), 13-28.

Banerjee, K. K., Ayyub, C., Ali, S. Z., Mandot, V., Prasad, N. G. and Kolthur-Seetharam, U. (2012) 'dSir2 in the adult fat body, but not in muscles, regulates life span in a diet-dependent manner', *Cell Rep,* 2(6), 1485-91.

Barkus, C., Dawson, L. A., Sharp, T. and Bannerman, D. M. (2012) 'GluN1 hypomorph mice exhibit wide-ranging behavioral alterations', *Genes Brain Behav,* 11(3), 342-51.

Barres, B. A. (2008) 'The mystery and magic of glia: a perspective on their roles in health and disease', *Neuron,* 60(3), 430-40.

Baschieri, F. and Farhan, H. (2012) 'Crosstalk of small GTPases at the Golgi apparatus', *Small GTPases,* 3(2), 80-90.

Bauer, P. O. and Nukina, N. (2009) 'The pathogenic mechanisms of polyglutamine diseases and current therapeutic strategies', *J Neurochem,* 110(6), 1737-65.

Baumeister, W., Walz, J., Zuhl, F. and Seemuller, E. (1998) 'The proteasome: paradigm of a self-compartmentalizing protease', *Cell,* 92(3), 367-80.

Beadle, G. W., Tatum, E. L. and Clancy, C. W. (1938) 'Food Level in Relation to Rate of Development and Eye Pigmentation in Drosophila Melanogaster', *Biological Bulletin,* 75(3), 447-462.

Beck, R., Ravet, M., Wieland, F. T. and Cassel, D. (2009) 'The COPI system: Molecular mechanisms and function', *FEBS Letters,* 583(17), 2701-2709.

Becker, E. B., Oliver, P. L., Glitsch, M. D., Banks, G. T., Achilli, F., Hardy, A., Nolan, P. M., Fisher, E. M. and Davies, K. E. (2009) 'A point mutation in TRPC3 causes abnormal Purkinje cell development and cerebellar ataxia in moonwalker mice', *Proc Natl Acad Sci U S A,* 106(16), 6706-11.

Beckers, J., Wurst, W. and de Angelis, M. H. (2009) 'Towards better mouse models: enhanced genotypes, systemic phenotyping and envirotype modelling', *Nat Rev Genet,* 10(6), 371-80.

Behnia, R., Panic, B., Whyte, J. R. and Munro, S. (2004) 'Targeting of the Arf-like GTPase Arl3p to the Golgi requires N-terminal acetylation and the membrane protein Sys1p', *Nat Cell Biol,* 6(5), 405-13.

Belgard, T. G., Marques, A. C., Oliver, P. L., Abaan, H. O., Sirey, T. M., Hoerder-Suabedissen, A., Garcia-Moreno, F., Molnar, Z., Margulies, E. H. and Ponting, C. P. (2011) 'A transcriptomic atlas of mouse neocortical layers', *Neuron,* 71(4), 605-16.

Bellen, H. J., Tong, C. and Tsuda, H. (2010) '100 years of Drosophila research and its impact on vertebrate neuroscience: a history lesson for the future', *Nat Rev Neurosci,* 11(7), 514-22.

Beller, M., Bulankina, A. V., Hsiao, H.-H., Urlaub, H., Jäckle, H. and Kühnlein, R. P. (2010) 'PERILIPIN-Dependent Control of Lipid Droplet Structure and Fat Storage in Drosophila', *Cell metabolism,* 12(5), 521-532.

Beller, M., Sztalryd, C., Southall, N., Bell, M., Jäckle, H., Auld, D. S. and Oliver, B. (2008) 'COPI Complex Is a Regulator of Lipid Homeostasis', *PLoS Biol,* 6(11), e292.

Benjamin, J. J., Poon, P. P., Drysdale, J. D., Wang, X., Singer, R. A. and Johnston, G. C. (2011) 'Dysregulated Arl1, a regulator of post-Golgi vesicle tethering, can inhibit endosomal transport and cell proliferation in yeast', *Mol Biol Cell,* 22(13), 2337-47.

Bi, J., Xiang, Y., Chen, H., Liu, Z., Grönke, S., Kühnlein, R. P. and Huang, X. (2012) 'Opposite and redundant roles of the two Drosophila perilipins in lipid mobilization', *Journal of Cell Science,* 125(15), 3568-3577.

Bickel, P. E., Tansey, J. T. and Welte, M. A. (2009) 'PAT proteins, an ancient family of lipid droplet proteins that regulate cellular lipid stores', *Biochim Biophys Acta,* 6, 419-40.

Bilen, J. and Bonini, N. M. (2007) 'Genome-Wide Screen for Modifiers of Ataxin-3 Neurodegeneration in Drosophila', *PLoS Genetics,* 3(10), e177.

Bitoun, E., Finelli, M. J., Oliver, P. L., Lee, S. and Davies, K. E. (2009) 'AF4 is a critical regulator of the IGF-1 signaling pathway during Purkinje cell development', *J Neurosci,* 29(49), 15366-74.

Bitoun, E., Oliver, P. L. and Davies, K. E. (2007) 'The mixed-lineage leukemia fusion partner AF4 stimulates RNA polymerase II transcriptional elongation and mediates coordinated chromatin remodeling', *Hum Mol Genet,* 16(1), 92-106.

Boles, M. K., Wilkinson, B. M., Wilming, L. G., Liu, B., Probst, F. J., Harrow, J., Grafham, D., Hentges, K. E., Woodward, L. P., Maxwell, A., Mitchell, K., Risley, M. D., Johnson, R., Hirschi, K., Lupski, J. R., Funato, Y., Miki, H., Marin-Garcia, P., Matthews, L., Coffey, A. J., Parker, A., Hubbard, T. J., Rogers, J., Bradley, A., Adams, D. J. and Justice, M. J. (2009) 'Discovery of candidate disease genes in ENU-induced mouse mutants by large-scale sequencing, including a splice-site mutation in nucleoredoxin', *PLoS Genet,* 5(12), 11.

Bonifacino, J. S. and Glick, B. S. (2004) 'The mechanisms of vesicle budding and fusion', *Cell,* 116(2), 153-66.

Boonen, M., van Meel, E., Oorschot, V., Klumperman, J. and Kornfeld, S. (2011) 'Vacuolization of mucolipidosis type II mouse exocrine gland cells represents accumulation of autolysosomes', *Mol Biol Cell,* 22(8), 1135-47.

Bosshard, N. U., Hubler, M., Arnold, S., Briner, J., Spycher, M. A., Sommerlade, H. J., von Figura, K. and Gitzelmann, R. (1996) 'Spontaneous mucolipidosis in a cat: an animal model of human I-cell disease', *Vet Pathol,* 33(1), 1-13.

Bostrom, P., Andersson, L., Li, L., Perkins, R., Hojlund, K., Boren, J. and Olofsson, S. O. (2009) 'The assembly of lipid droplets and its relation to cellular insulin sensitivity', *Biochem Soc Trans,* 37(Pt 5), 981-5.

Bostrom, P., Andersson, L., Rutberg, M., Perman, J., Lidberg, U., Johansson, B. R., Fernandez-Rodriguez, J., Ericson, J., Nilsson, T., Boren, J. and Olofsson, S. O. (2007) 'SNARE proteins mediate fusion between cytosolic lipid droplets and are implicated in insulin sensitivity', *Nat Cell Biol,* 9(11), 1286-93.

Botella, L. M., Moya, A., González, M. C. and Ménsua, J. L. (1985) 'Larval stop, delayed development and survival in overcrowded cultures of Drosophila melanogaster: Effect of urea and uric acid', *Journal of Insect Physiology,* 31(3), 179-185.

Bottinelli, R. and Reggiani, C. (2000) 'Human skeletal muscle fibres: molecular and functional diversity', *Prog Biophys Mol Biol,* 73(2-4), 195-262.

Bouma, M. E., Beucler, I., Aggerbeck, L. P., Infante, R. and Schmitz, J. (1986) 'Hypobetalipoproteinemia with accumulation of an apoprotein B-like protein in intestinal cells. Immunoenzymatic and biochemical characterization of seven cases of Anderson's disease', *J Clin Invest,* 78(2), 398-410.

Bowerman, M., Vincent, T., Scamps, F., Perrin, F. E., Camu, W. and Raoul, C. (2013) 'Neuroimmunity dynamics and the development of therapeutic strategies for amyotrophic lateral sclerosis', *Frontiers in Cellular Neuroscience,* 7, 214.

Brady, R. O. (2006) 'Enzyme replacement for lysosomal diseases', *Annu Rev Med,* 57, 283-96.

Brand, A. and Perrimon, N. (1993) 'Targeted gene expression as a means of altering cell fates and generating dominant phenotypes', *Development,* 118, 401 - 415.

Braulke, T. and Bonifacino, J. S. (2009) 'Sorting of lysosomal proteins', *Biochim Biophys Acta,* 4, 605-14.

Braun, M. M., Osecheck, M. and Joyce, N. C. (2012) 'Nutrition assessment and management in amyotrophic lateral sclerosis', *Phys Med Rehabil Clin N Am,* 23(4), 751-71.

Britton, J. S. and Edgar, B. A. (1998) 'Environmental control of the cell cycle in Drosophila: nutrition activates mitotic and endoreplicative cells by distinct mechanisms', *Development,* 125(11), 2149-58.

Britton, J. S., Lockwood, W. K., Li, L., Cohen, S. M. and Edgar, B. A. (2002) 'Drosophila's Insulin/PI3-Kinase Pathway Coordinates Cellular Metabolism with Nutritional Conditions', *Developmental Cell,* 2(2), 239-249.

Brogna, S. and Wen, J. (2009) 'Nonsense-mediated mRNA decay (NMD) mechanisms', *Nat Struct Mol Biol,* 16(2), 107-13.

Brown, S. D. and Balling, R. (2001) 'Systematic approaches to mouse mutagenesis', *Curr Opin Genet Dev,* 11(3), 268-73.

Bruce-Keller, A. J., Keller, J. N. and Morrison, C. D. (2009) 'Obesity and Vulnerability of the CNS', *Biochimica et biophysica acta,* 1792(5), 395-400.

Burd, C. G., Strochlic, T. I. and Gangi Setty, S. R. (2004) 'Arf-like GTPases: not so Arf-like after all', *Trends Cell Biol,* 14(12), 687-94.

Cai, D. (2013) 'Neuroinflammation and neurodegeneration in overnutrition-induced diseases', *Trends Endocrinol Metab,* 24(1), 40-7.

Callan, M. A., Clements, N., Ahrendt, N. and Zarnescu, D. C. (2012) 'Fragile X Protein is required for inhibition of insulin signaling and regulates glial-dependent neuroblast reactivation in the developing brain', *Brain Res,* 26, 151-61.

Carlson, C. G., Rutter, J., Bledsoe, C., Singh, R., Hoff, H., Bruemmer, K., Sesti, J., Gatti, F., Berge, J. and McCarthy, L. (2010) 'A simple protocol for assessing inter-trial and inter-examiner reliability for two noninvasive measures of limb muscle strength', *J Neurosci Methods,* 186(2), 226-30.

Carro, E., Trejo, J., Gomez-Isla, T., LeRoith, D. and Torres-Aleman, I. (2002) 'Serum insulin-like growth factor I regulates brain amyloid-beta levels', *Nat Med,* 8, 1390 - 1397.

Cartwright, B. R., Binns, D. D., Hilton, C. L., Han, S., Gao, Q. and Goodman, J. M. (2014) 'Seipin performs dissectible functions in promoting lipid droplet biogenesis and regulating droplet morphology', *Mol Biol Cell,* 24, 08-1303.

Cathey, S. S., Leroy, J. G., Wood, T., Eaves, K., Simensen, R. J., Kudo, M., Stevenson, R. E. and Friez, M. J. (2010) 'Phenotype and genotype in mucolipidoses II and III alpha/beta: a study of 61 probands', *J Med Genet,* 47(1), 38-48.

Chang, H. C.-H., Dimlich, D. N., Yokokura, T., Mukherjee, A., Kankel, M. W., Sen, A., Sridhar, V., Fulga, T. A., Hart, A. C., Van Vactor, D. and Artavanis-Tsakonas, S. (2008) 'Modeling Spinal Muscular Atrophy in Drosophila', *PLoS One,* 3(9), e3209.

Chavrier, P. and Goud, B. (1999) 'The role of ARF and Rab GTPases in membrane transport', *Curr Opin Cell Biol,* 11(4), 466-75.

Chell, J. M. and Brand, A. H. (2010) 'Nutrition-responsive glia control exit of neural stem cells from quiescence', *Cell,* 143(7), 1161-73.

Chen, H. and Chan, D. C. (2009) 'Mitochondrial dynamics–fusion, fission, movement, and mitophagy–in neurodegenerative diseases', *Human Molecular Genetics,* 18(R2), R169-R176.

Chen, K. Y., Tsai, P. C., Hsu, J. W., Hsu, H. C., Fang, C. Y., Chang, L. C., Tsai, Y. T., Yu, C. J. and Lee, F. J. (2010) 'Syt1p promotes activation of Arl1p at the late Golgi to recruit Imh1p', *J Cell Sci,* 123(Pt 20), 3478-89.

Cheng, H., Kari, G., Dicker, A. P., Rodeck, U., Koch, W. J. and Force, T. (2011) 'A novel preclinical strategy for identifying cardiotoxic kinase inhibitors and mechanisms of cardiotoxicity', *Circ Res,* 109(12), 1401-9.

Chia, P. Z. and Gleeson, P. A. (2011) 'The regulation of endosome-to-Golgi retrograde transport by tethers and scaffolds', *Traffic,* 12(8), 939-47.

Chintapalli, V. R., Wang, J. and Dow, J. A. T. (2007) 'Using FlyAtlas to identify better Drosophila melanogaster models of human disease', *Nat Genet,* 39(6), 715-720.

Chowdhury, S. K. R., Smith, D. R. and Fernyhough, P. (2013) 'The role of aberrant mitochondrial bioenergetics in diabetic neuropathy', *Neurobiology of Disease,* 51(0), 56-65.

Christis, C. and Munro, S. (2012) 'The small G protein Arl1 directs the trans-Golgi-specific targeting of the Arf1 exchange factors BIG1 and BIG2', *J Cell Biol,* 196(3), 327-35.

Church, R. B. and Robertson, F. W. (1966) 'Biochemical analysis of genetic differences in the growth of Drosophila', *Genet Res,* 7(3), 383-407.

Clark, J., Moore, L., Krasinskas, A., Way, J., Battey, J., Tamkun, J. and Kahn, R. A. (1993) 'Selective amplification of additional members of the ADP-ribosylation factor (ARF) family: cloning of additional human and Drosophila ARF-like genes', *Proc Natl Acad Sci U S A,* 90(19), 8952-6.

Colombani, J., Raisin, S., Pantalacci, S., Radimerski, T., Montagne, J. and Leopold, P. (2003) 'A nutrient sensor mechanism controls Drosophila growth', *Cell,* 114(6), 739-49.

Cooper, O., Hargus, G., Deleidi, M., Blak, A., Osborn, T., Marlow, E., Lee, K., Levy, A., Perez-Torres, E., Yow, A. and Isacson, O. (2010) 'Differentiation of human ES and Parkinson's disease iPS cells into ventral midbrain dopaminergic neurons requires a high activity form of SHH, FGF8a and specific regionalization by retinoic acid', *Molecular and Cellular Neuroscience,* 45(3), 258-266.

Corbett, A., Pickett, J., Burns, A., Corcoran, J., Dunnett, S. B., Edison, P., Hagan, J. J., Holmes, C., Jones, E., Katona, C., Kearns, I., Kehoe, P., Mudher, A., Passmore, A., Shepherd, N., Walsh, F. and Ballard, C. (2012) 'Drug repositioning for Alzheimer's disease', *Nat Rev Drug Discov,* 11(11), 833-846.

Coulthard, P., Simjee, S. U. and Pleuvry, B. J. (2003) 'Gait analysis as a correlate of pain induced by carrageenan intraplantar injection', *J Neurosci Methods,* 128(1-2), 95-102.

Coutinho, M. F., Matos, L. and Alves, S. (2015) 'From bedside to cell biology: a century of history on lysosomal dysfunction', *Gene,* 555(1), 50-8.

Coutinho, M. F., Prata, M. J. and Alves, S. (2012) 'Mannose-6-phosphate pathway: a review on its role in lysosomal function and dysfunction', *Mol Genet Metab,* 105(4), 542-50.

Cox, T. M. and Cachon-Gonzalez, M. B. (2012) 'The cellular pathology of lysosomal diseases', *J Pathol,* 226(2), 241-54.

Croci, L., Barili, V., Chia, D., Massimino, L., van Vugt, R., Masserdotti, G., Longhi, R., Rotwein, P. and Consalez, G. G. (2011) 'Local insulin-like growth factor I expression is essential for Purkinje neuron survival at birth', *Cell Death Differ,* 18(1), 48-59.

Dannoura, A. H., Berriot-Varoqueaux, N., Amati, P., Abadie, V., Verthier, N., Schmitz, J., Wetterau, J. R., Samson-Bouma, M. E. and Aggerbeck, L. P. (1999) 'Anderson's disease: exclusion of apolipoprotein and intracellular lipid transport genes', *Arterioscler Thromb Vasc Biol,* 19(10), 2494-508.

Dascher, C. and Balch, W. E. (1994) 'Dominant inhibitory mutants of ARF1 block endoplasmic reticulum to Golgi transport and trigger disassembly of the Golgi apparatus', *J Biol Chem,* 269(2), 1437-48.

Davidson, C. D., Ali, N. F., Micsenyi, M. C., Stephney, G., Renault, S., Dobrenis, K., Ory, D. S., Vanier, M. T. and Walkley, S. U. (2009) 'Chronic cyclodextrin treatment of murine Niemann-Pick C disease ameliorates neuronal cholesterol and glycosphingolipid storage and disease progression', *PLoS One,* 4(9), e6951.

Davies, P. and Maloney, A. J. (1976) *Selective loss of central cholinergic neurons in Alzheimer's disease,* Lancet. 1976 Dec 25;2(8000):1403.

Davies, S. E. (2012) *Analysis of SMN function in development and Nedd4, a putative modifier of Parkinson's disease, in Drosophila melanogaster,* unpublished thesis University of Oxford.

Dawson, T. M., Ko, H. S. and Dawson, V. L. (2010) 'Genetic animal models of Parkinson's disease', *Neuron,* 66(5), 646-61.

de la Monte, S. M. (2012) 'Brain Insulin Resistance and Deficiency as Therapeutic Targets in Alzheimer's Disease', *Current Alzheimer Research,* 9(1), 35-66.

De Moed, G. H., Kruitwagen, C. L. J. J., De Jong, G. and Scharloo, W. (1999) 'Critical weight for the induction of pupariation in Drosophila melanogaster: genetic and environmental variation', *Journal of Evolutionary Biology,* 12(5), 852-858.

De Pace, R., Coutinho, M. F., Koch-Nolte, F., Haag, F., Prata, M. J., Alves, S., Braulke, T. and Pohl, S. (2014) 'Mucolipidosis II-Related Mutations Inhibit the Exit from the Endoplasmic Reticulum and Proteolytic Cleavage of GlcNAc-1-Phosphotransferase Precursor Protein (GNPTAB)', *Hum Mutat,* 35(3), 368-76.

De Strooper, B. and Scorrano, L. (2012) 'Close encounter: mitochondria, endoplasmic reticulum and Alzheimer's disease', *The EMBO Journal,* 31(21), 4095-4097.

De Vos, K. J., Grierson, A. J., Ackerley, S. and Miller, C. C. (2008) 'Role of axonal transport in neurodegenerative diseases', *Annu Rev Neurosci,* 31, 151-73.

del Valle Rodriguez, A., Didiano, D. and Desplan, C. (2011) 'Power tools for gene expression and clonal analysis in Drosophila', *Nat Methods,* 9(1), 47-55.

Denny, P., Bate, R. and Mallon, A.-M. (2001) 'What use is the human genome for understanding the mouse?', *Genome Biology,* 2(11), comment2009.1-comment2009.5.

Derby, M. C. and Gleeson, P. A. (2007) 'New insights into membrane trafficking and protein sorting', *Int Rev Cytol,* 261, 47-116.

Desnick, R. J. and Schuchman, E. H. (2012) 'Enzyme replacement therapy for lysosomal diseases: lessons from 20 years of experience and remaining challenges', *Annu Rev Genomics Hum Genet,* 13, 307-35.

Desport, J. C., Preux, P. M., Magy, L., Boirie, Y., Vallat, J. M., Beaufrere, B. and Couratier, P. (2001) 'Factors correlated with hypermetabolism in patients with amyotrophic lateral sclerosis', *Am J Clin Nutr,* 74(3), 328-34.

Devine, M. J., Ryten, M., Vodicka, P., Thomson, A. J., Burdon, T., Houlden, H., Cavaleri, F., Nagano, M., Drummond, N. J., Taanman, J.-W., Schapira, A. H., Gwinn, K., Hardy, J., Lewis, P. A. and Kunath, T. (2011) 'Parkinson's disease induced pluripotent stem cells with triplication of the α-synuclein locus', *Nat Commun,* 2, 440.

Dierks, T., Schlotawa, L., Frese, M. A., Radhakrishnan, K., von Figura, K. and Schmidt, B. (2009) 'Molecular basis of multiple sulfatase deficiency, mucolipidosis II/III and Niemann-Pick C1 disease - Lysosomal storage disorders caused by defects of non-lysosomal proteins', *Biochim Biophys Acta,* 4, 710-25.

Dupuis, L., Oudart, H., Rene, F., Gonzalez de Aguilar, J. L. and Loeffler, J. P. (2004) 'Evidence for defective energy homeostasis in amyotrophic lateral sclerosis: benefit of a high-energy diet in a transgenic mouse model', *Proc Natl Acad Sci U S A,* 101(30), 11159-64.

Dupuis, L., Pradat, P. F., Ludolph, A. C. and Loeffler, J. P. (2011) 'Energy metabolism in amyotrophic lateral sclerosis', *Lancet Neurol,* 10(1), 75-82.

Edgar, B. A. (2006) 'How flies get their size: genetics meets physiology', *Nat Rev Genet,* 7(12), 907-16.

Ellong, E. N., Soni, K. G., Bui, Q. T., Sougrat, R., Golinelli-Cohen, M. P. and Jackson, C. L. (2011) 'Interaction between the triglyceride lipase ATGL and the Arf1 activator GBF1', *PLoS One,* 6(7), 18.

Elsea, S. H. and Lucas, R. E. (2002) 'The mousetrap: what we can learn when the mouse model does not mimic the human disease', *Ilar J,* 43(2), 66-79.

Fan, J., Hu, Z., Zeng, L., Lu, W., Tang, X., Zhang, J. and Li, T. (2008) 'Golgi apparatus and neurodegenerative diseases', *Int J Dev Neurosci,* 26(6), 523-34.

Fang, Y., Vilella-Bach, M., Bachmann, R., Flanigan, A. and Chen, J. (2001) 'Phosphatidic acid-mediated mitogenic activation of mTOR signaling', *Science,* 294(5548), 1942-5.

Fanous, A. H., Zhao, Z., van den Oord, E. J., Maher, B. S., Thiselton, D. L., Bergen, S. E., Wormley, B., Bigdeli, T., Amdur, R. L., O'Neill, F. A., Walsh, D., Kendler, K. S. and Riley, B. P. (2010) 'Association study of SNAP25 and schizophrenia in Irish family and case-control samples', *Am J Med Genet B Neuropsychiatr Genet,* 5(2), 663-74.

Farazi, T. A., Waksman, G. and Gordon, J. I. (2001) 'The Biology and Enzymology of ProteinN-Myristoylation', *Journal of Biological Chemistry,* 276(43), 39501-39504.

Farese, R. V., Jr. and Walther, T. C. (2009) 'Lipid droplets finally get a little R-E-S-P-E-C-T', *Cell,* 139(5), 855-60.

Farquhar, M. G. and Palade, G. E. (1998) 'The Golgi apparatus: 100 years of progress and controversy', *Trends Cell Biol,* 8(1), 2-10.

Fergani, A., Oudart, H., Gonzalez De Aguilar, J. L., Fricker, B., Rene, F., Hocquette, J. F., Meininger, V., Dupuis, L. and Loeffler, J. P. (2007) 'Increased peripheral lipid clearance in an animal model of amyotrophic lateral sclerosis', *J Lipid Res,* 48(7), 1571-80.

Fernagut, P. O., Diguet, E., Bioulac, B. and Tison, F. (2004) 'MPTP potentiates 3-nitropropionic acid-induced striatal damage in mice: reference to striatonigral degeneration', *Exp Neurol,* 185(1), 47-62.

Fernandez-Funez, P., Nino-Rosales, M. L., de Gouyon, B., She, W. C., Luchak, J. M., Martinez, P., Turiegano, E., Benito, J., Capovilla, M., Skinner, P. J., McCall, A., Canal, I., Orr, H.

T., Zoghbi, H. Y. and Botas, J. (2000) 'Identification of genes that modify ataxin-1-induced neurodegeneration', *Nature,* 408(6808), 101-6.

Fernandez, A. and Torres-Aleman, I. (2012) 'The many faces of insulin-like peptide signalling in the brain', *Nat Rev Neurosci,* 13, 225 - 239.

Ferraiuolo, L., Kirby, J., Grierson, A. J., Sendtner, M. and Shaw, P. J. (2011) 'Molecular pathways of motor neuron injury in amyotrophic lateral sclerosis', *Nat Rev Neurol,* 7(11), 616-630.

Flanagan-Steet, H., Sias, C. and Steet, R. (2009) 'Altered chondrocyte differentiation and extracellular matrix homeostasis in a zebrafish model for mucolipidosis II', *Am J Pathol,* 175(5), 2063-75.

Forman, M. S., Lee, V. M. and Trojanowski, J. Q. (2005) 'Nosology of Parkinson's disease: looking for the way out of a quagmire', *Neuron,* 47(4), 479-82.

Fratantoni, J. C., Hall, C. W. and Neufeld, E. F. (1968) 'Hurler and Hunter syndromes: mutual correction of the defect in cultured fibroblasts', *Science,* 162(3853), 570-2.

Freeman, M. R. and Doherty, J. (2006) 'Glial cell biology in Drosophila and vertebrates', *Trends Neurosci,* 29(2), 82-90.

Frydman, J. (2001) 'Folding of newly translated proteins in vivo: the role of molecular chaperones', *Annu Rev Biochem,* 70, 603-47.

Fujita, Y., Ohama, E., Takatama, M., Al-Sarraj, S. and Okamoto, K. (2006) 'Fragmentation of Golgi apparatus of nigral neurons with alpha-synuclein-positive inclusions in patients with Parkinson's disease', *Acta Neuropathol,* 112(3), 261-5.

Gama Sosa, M. A., De Gasperi, R. and Elder, G. A. (2012) 'Modeling human neurodegenerative diseases in transgenic systems', *Hum Genet,* 131(4), 535-63.

Gao, C., Holscher, C., Liu, Y. and Li, L. (2011) 'GSK3: a key target for the development of novel treatments for type 2 diabetes mellitus and Alzheimer disease', *Rev Neurosci,* 23(1), 1-11.

Gao, X., Simon, K. C., Schwarzschild, M. A. and Ascherio, A. (2012) 'Prospective study of statin use and risk of Parkinson disease', *Arch Neurol,* 69(3), 380-4.

Gasser, T. (2009) 'Mendelian forms of Parkinson's disease', *Biochimica et Biophysica Acta (BBA) - Molecular Basis of Disease,* 1792(7), 587-596.

Gebhardt, M. D. and Stearns, S. C. (1993) 'Phenotypic plasticity for life history traits in Drosophila melanogaster. I. Effect on phenotypic and environmental correlations', *Journal of Evolutionary Biology,* 6(1), 1-16.

Gelfman, C. M., Vogel, P., Issa, T. M., Turner, C. A., Lee, W. S., Kornfeld, S. and Rice, D. S. (2007) 'Mice lacking alpha/beta subunits of GlcNAc-1-phosphotransferase exhibit growth retardation, retinal degeneration, and secretory cell lesions', *Invest Ophthalmol Vis Sci,* 48(11), 5221-8.

Geminard, C., Rulifson, E. J. and Leopold, P. (2009) 'Remote control of insulin secretion by fat cells in Drosophila', *Cell Metab,* 10(3), 199-207.

Georges, A., Bonneau, J., Bonnefont-Rousselot, D., Champigneulle, J., Rabes, J. P., Abifadel, M., Aparicio, T., Guenedet, J. C., Bruckert, E., Boileau, C., Morali, A., Varret, M., Aggerbeck, L. P. and Samson-Bouma, M. E. (2011) 'Molecular analysis and intestinal expression of SAR1 genes and proteins in Anderson's disease (Chylomicron retention disease)', *Orphanet J Rare Dis,* 6(1), 1750-1172.

Ghosh, A., Kling, T., Snaidero, N., Sampaio, J. L., Shevchenko, A., Gras, H., Geurten, B., Gopfert, M. C., Schulz, J. B., Voigt, A. and Simons, M. (2013) 'A global in vivo

Drosophila RNAi screen identifies a key role of ceramide phosphoethanolamine for glial ensheathment of axons', *PLoS Genet*, 9(12), 12.

Glick, B. S. and Nakano, A. (2009) 'Membrane traffic within the Golgi apparatus', *Annu Rev Cell Dev Biol*, 25, 113-32.

Glickman, M. H. and Ciechanover, A. (2002) 'The ubiquitin-proteasome proteolytic pathway: destruction for the sake of construction', *Physiol Rev*, 82(2), 373-428.

Goberdhan, D. C., Paricio, N., Goodman, E. C., Mlodzik, M. and Wilson, C. (1999) 'Drosophila tumor suppressor PTEN controls cell size and number by antagonizing the Chico/PI3-kinase signaling pathway', *Genes Dev*, 13(24), 3244-58.

Goberdhan, D. C. and Wilson, C. (2003) 'The functions of insulin signaling: size isn't everything, even in Drosophila', *Differentiation*, 71(7), 375-97.

Goker-Alpan, O., Schiffmann, R., LaMarca, M. E., Nussbaum, R. L., McInerney-Leo, A. and Sidransky, E. (2004) 'Parkinsonism among Gaucher disease carriers', *J Med Genet*, 41(12), 937-40.

Goldman-Rakic, P. S. (1987) 'Circuitry of the frontal association cortex and its relevance to dementia', *Arch Gerontol Geriatr*, 6(3), 299-309.

Gondré-Lewis, M. C., McGlynn, R. and Walkley, S. U. 'Cholesterol Accumulation in NPC1-Deficient Neurons Is Ganglioside Dependent', *Current Biology*, 13(15), 1324-1329.

Goodman, L. A., Livingston, P. O. and Walkley, S. U. (1991) 'Ectopic dendrites occur only on cortical pyramidal cells containing elevated GM2 ganglioside in alpha-mannosidosis', *Proc Natl Acad Sci U S A*, 88(24), 11330-4.

Gorman, A. M. (2008) 'Neuronal cell death in neurodegenerative diseases: recurring themes around protein handling', *J Cell Mol Med*, 12(6A), 2263-80.

Gotz, J., Ittner, L. M. and Kins, S. (2006) 'Do axonal defects in tau and amyloid precursor protein transgenic animals model axonopathy in Alzheimer's disease?', *J Neurochem*, 98(4), 993-1006.

Goud, B. and Gleeson, P. A. (2010) 'TGN golgins, Rabs and cytoskeleton: regulating the Golgi trafficking highways', *Trends Cell Biol*, 20(6), 329-36.

Graham, T. R. (2013) 'Arl1 gets into the membrane remodeling business with a flippase and ArfGEF', *Proc Natl Acad Sci U S A*, 110(8), 2691-2.

Grahn, T. H., Kaur, R., Yin, J., Schweiger, M., Sharma, V. M., Lee, M. J., Ido, Y., Smas, C. M., Zechner, R., Lass, A. and Puri, V. (2014) 'Fat-specific protein 27 (FSP27) interacts with adipose triglyceride lipase (ATGL) to regulate lipolysis and insulin sensitivity in human adipocytes', *J Biol Chem*, 289(17), 12029-39.

Greenberg, A. S., Coleman, R. A., Kraemer, F. B., McManaman, J. L., Obin, M. S., Puri, V., Yan, Q. W., Miyoshi, H. and Mashek, D. G. (2011) 'The role of lipid droplets in metabolic disease in rodents and humans', *J Clin Invest*, 121(6), 2102-10.

Grewal, S., Shapiro, E., Braunlin, E., Charnas, L., Krivit, W., Orchard, P. and Peters, C. (2003) 'Continued neurocognitive development and prevention of cardiopulmonary complications after successful BMT for I-cell disease: a long-term follow-up report', *Bone Marrow Transplant*, 32(9), 957-60.

Guo, Y., Walther, T. C., Rao, M., Stuurman, N., Goshima, G., Terayama, K., Wong, J. S., Vale, R. D., Walter, P. and Farese, R. V. (2008) 'Functional genomic screen reveals genes involved in lipid-droplet formation and utilization', *Nature*, 453(7195), 657-661.

Gurney, M. E., Pu, H., Chiu, A. Y., Dal Canto, M. C., Polchow, C. Y., Alexander, D. D., Caliendo, J., Hentati, A., Kwon, Y. W., Deng, H. X. and et al. (1994) 'Motor neuron

degeneration in mice that express a human Cu,Zn superoxide dismutase mutation', *Science*, 264(5166), 1772-5.

Gustavsson, A., Svensson, M., Jacobi, F., Allgulander, C., Alonso, J., Beghi, E., Dodel, R., Ekman, M., Faravelli, C., Fratiglioni, L., Gannon, B., Jones, D. H., Jennum, P., Jordanova, A., Jonsson, L., Karampampa, K., Knapp, M., Kobelt, G., Kurth, T., Lieb, R., Linde, M., Ljungcrantz, C., Maercker, A., Melin, B., Moscarelli, M., Musayev, A., Norwood, F., Preisig, M., Pugliatti, M., Rehm, J., Salvador-Carulla, L., Schlehofer, B., Simon, R., Steinhausen, H. C., Stovner, L. J., Vallat, J. M., Van den Bergh, P., van Os, J., Vos, P., Xu, W., Wittchen, H. U., Jonsson, B. and Olesen, J. (2011) 'Cost of disorders of the brain in Europe 2010', *Eur Neuropsychopharmacol*, 21(10), 718-79.

Gutierrez, E., Wiggins, D., Fielding, B. and Gould, A. P. (2007) 'Specialized hepatocyte-like cells regulate Drosophila lipid metabolism', *Nature*, 445(7125), 275-280.

Guyenet, S. J., Furrer, S. A., Damian, V. M., Baughan, T. D., La Spada, A. R. and Garden, G. A. (2010) 'A simple composite phenotype scoring system for evaluating mouse models of cerebellar ataxia', *J Vis Exp*, 21(39).

Halliwell, B. (2006) 'Oxidative stress and neurodegeneration: where are we now?', *J Neurochem*, 97(6), 1634-58.

Hamamichi, S., Rivas, R. N., Knight, A. L., Cao, S., Caldwell, K. A. and Caldwell, G. A. (2008) 'Hypothesis-based RNAi screening identifies neuroprotective genes in a Parkinson's disease model', *Proc Natl Acad Sci U S A*, 105(2), 728-33.

Hamers, F. P., Koopmans, G. C. and Joosten, E. A. (2006) 'CatWalk-assisted gait analysis in the assessment of spinal cord injury', *J Neurotrauma*, 23(3-4), 537-48.

Hamers, F. P., Lankhorst, A. J., van Laar, T. J., Veldhuis, W. B. and Gispen, W. H. (2001) 'Automated quantitative gait analysis during overground locomotion in the rat: its application to spinal cord contusion and transection injuries', *J Neurotrauma*, 18(2), 187-201.

Hara, M., Inokuchi, T., Taniwaki, T., Otomo, T., Sakai, N., Matsuishi, T. and Yoshino, M. (2013) 'An adult patient with mucolipidosis III alpha/beta presenting with parkinsonism', *Brain Dev*, 35(5), 462-5.

Hara, T., Nakamura, K., Matsui, M., Yamamoto, A., Nakahara, Y., Suzuki-Migishima, R., Yokoyama, M., Mishima, K., Saito, I., Okano, H. and Mizushima, N. (2006) 'Suppression of basal autophagy in neural cells causes neurodegenerative disease in mice', *Nature*, 441(7095), 885-9.

Hardy, J. and Higgins, G. (1992) 'Alzheimer's disease: the amyloid cascade hypothesis', *Science*, 256, 184 - 185.

Hargus, G., Ehrlich, M., Hallmann, A. L. and Kuhlmann, T. (2014) 'Human stem cell models of neurodegeneration: a novel approach to study mechanisms of disease development', *Acta Neuropathol*, 127(2), 151-73.

Heintz, N. and Zoghbi, H. Y. (2000) 'Insights from mouse models into the molecular basis of neurodegeneration', *Annu Rev Physiol*, 62, 779-802.

Henchcliffe, C. and Beal, M. F. (2008) 'Mitochondrial biology and oxidative stress in Parkinson disease pathogenesis', *Nat Clin Pract Neurol*, 4(11), 600-9.

Hesse, D., Jaschke, A., Chung, B. and Schurmann, A. (2013) 'Trans-Golgi proteins participate in the control of lipid droplet and chylomicron formation', *Biosci Rep*, 33(1), 1-9.

Hesse, D., Jaschke, A., Kanzleiter, T., Witte, N., Augustin, R., Hommel, A., Puschel, G. P., Petzke, K. J., Joost, H. G., Schupp, M. and Schurmann, A. (2012) 'GTPase ARFRP1 is essential for normal hepatic glycogen storage and insulin-like growth factor 1 secretion', *Mol Cell Biol*, 32(21), 4363-74.

Hietakangas, V. and Cohen, S. M. (2009) 'Regulation of tissue growth through nutrient sensing', *Annu Rev Genet,* 43, 389-410.

Hoehn, M. M. and Yahr, M. D. (1967) 'Parkinsonism: onset, progression and mortality', *Neurology,* 17(5), 427-42.

Hoffman, J. M., Soltow, Q. A., Li, S., Sidik, A., Jones, D. P. and Promislow, D. E. (2014) 'Effects of age, sex, and genotype on high-sensitivity metabolomic profiles in the fruit fly, Drosophila melanogaster', *Aging Cell,* 13(4), 596-604.

Hommel, A., Hesse, D., Volker, W., Jaschke, A., Moser, M., Engel, T., Bluher, M., Zahn, C., Chadt, A., Ruschke, K., Vogel, H., Kluge, R., Robenek, H., Joost, H. G. and Schurmann, A. (2010) 'The ARF-like GTPase ARFRP1 is essential for lipid droplet growth and is involved in the regulation of lipolysis', *Mol Cell Biol,* 30(5), 1231-42.

Hoogerbrugge, P. M. and Valerio, D. (1998) 'Bone marrow transplantation and gene therapy for lysosomal storage diseases', *Bone Marrow Transplant,* 21(2), S34-6.

Hull-Thompson, J., Muffat, J., Sanchez, D., Walker, D. W., Benzer, S., Ganfornina, M. D. and Jasper, H. (2009) 'Control of Metabolic Homeostasis by Stress Signaling Is Mediated by the Lipocalin NLaz', *PLoS Genetics,* 5(4), e1000460.

Hulshagen, L., Krysko, O., Bottelbergs, A., Huyghe, S., Klein, R., Van Veldhoven, P. P., De Deyn, P. P., D'Hooge, R., Hartmann, D. and Baes, M. (2008) 'Absence of functional peroxisomes from mouse CNS causes dysmyelination and axon degeneration', *J Neurosci,* 28(15), 4015-27.

Idol, R. A., Wozniak, D. F., Fujiwara, H., Yuede, C. M., Ory, D. S., Kornfeld, S. and Vogel, P. (2014) 'Neurologic abnormalities in mouse models of the lysosomal storage disorders mucolipidosis II and mucolipidosis III gamma', *PLoS One,* 9(10).

Ilieva, H., Polymenidou, M. and Cleveland, D. W. (2009) 'Non–cell autonomous toxicity in neurodegenerative disorders: ALS and beyond', *The Journal of Cell Biology,* 187(6), 761-772.

Imaizumi, M., Gushi, K., Kurobane, I., Inoue, S., Suzuki, J., Koizumi, Y., Suzuki, H., Sato, A., Gotoh, Y., Haginoya, K. and et al. (1994) 'Long-term effects of bone marrow transplantation for inborn errors of metabolism: a study of four patients with lysosomal storage diseases', *Acta Paediatr Jpn,* 36(1), 30-6.

Irrcher, I., Aleyasin, H., Seifert, E. L., Hewitt, S. J., Chhabra, S., Phillips, M., Lutz, A. K., Rousseaux, M. W., Bevilacqua, L., Jahani-Asl, A., Callaghan, S., MacLaurin, J. G., Winklhofer, K. F., Rizzu, P., Rippstein, P., Kim, R. H., Chen, C. X., Fon, E. A., Slack, R. S., Harper, M. E., McBride, H. M., Mak, T. W. and Park, D. S. (2010) 'Loss of the Parkinson's disease-linked gene DJ-1 perturbs mitochondrial dynamics', *Hum Mol Genet,* 19(19), 3734-46.

Isaacs, A. M., Davies, K. E., Hunter, A. J., Nolan, P. M., Vizor, L., Peters, J., Gale, D. G., Kelsell, D. P., Latham, I. D., Chase, J. M., Fisher, E. M. C., Bouzyk, M. M., Potter, A., Masih, M., Walsh, F. S., Sims, M. A., Doncaster, K. E., Parsons, C. A., Martin, J., Brown, S. D. M., Rastan, S., Spurr, N. K. and Gray, I. C. (2000) 'Identification of two new Pmp22 mouse mutants using large-scale mutagenesis and a novel rapid mapping strategy', *Human Molecular Genetics,* 9(12), 1865-1871.

Isaacs, A. M., Jeans, A., Oliver, P. L., Vizor, L., Brown, S. D., Hunter, A. J. and Davies, K. E. (2002) 'Identification of a new Pmp22 mouse mutant and trafficking analysis of a Pmp22 allelic series suggesting that protein aggregates may be protective in Pmp22-associated peripheral neuropathy', *Mol Cell Neurosci,* 21(1), 114-25.

Ito, M. (2000) 'Mechanisms of motor learning in the cerebellum', *Brain Res,* 886(1-2), 237-245.

Jaiswal, M., Sandoval, H., Zhang, K., Bayat, V. and Bellen, H. J. (2012) 'Probing mechanisms that underlie human neurodegenerative diseases in Drosophila', *Annu Rev Genet,* 46, 371-96.

Jambunathan, S., Yin, J., Khan, W., Tamori, Y. and Puri, V. (2011) 'FSP27 promotes lipid droplet clustering and then fusion to regulate triglyceride accumulation', *PLoS One,* 6(12), 14.

Jaschke, A., Chung, B., Hesse, D., Kluge, R., Zahn, C., Moser, M., Petzke, K. J., Brigelius-Flohe, R., Puchkov, D., Koepsell, H., Heeren, J., Joost, H. G. and Schurmann, A. (2012) 'The GTPase ARFRP1 controls the lipidation of chylomicrons in the Golgi of the intestinal epithelium', *Hum Mol Genet,* 21(14), 3128-42.

Jeans, A. F., Oliver, P. L., Johnson, R., Capogna, M., Vikman, J., Molnar, Z., Babbs, A., Partridge, C. J., Salehi, A., Bengtsson, M., Eliasson, L., Rorsman, P. and Davies, K. E. (2007) 'A dominant mutation in Snap25 causes impaired vesicle trafficking, sensorimotor gating, and ataxia in the blind-drunk mouse', *Proc Natl Acad Sci U S A,* 104(7), 2431-6.

Jeibmann, A. and Paulus, W. (2009) 'Drosophila melanogaster as a model organism of brain diseases', *Int J Mol Sci,* 10(2), 407-40.

Jellinger, K. A. (2010) 'Basic mechanisms of neurodegeneration: a critical update', *Journal of Cellular and Molecular Medicine,* 14(3), 457-487.

Jeyakumar, M., Butters, T. D., Cortina-Borja, M., Hunnam, V., Proia, R. L., Perry, V. H., Dwek, R. A. and Platt, F. M. (1999) 'Delayed symptom onset and increased life expectancy in Sandhoff disease mice treated with N-butyldeoxynojirimycin', *Proceedings of the National Academy of Sciences,* 96(11), 6388-6393.

Jeyakumar, M., Thomas, R., Elliot-Smith, E., Smith, D. A., van der Spoel, A. C., d'Azzo, A., Perry, V. H., Butters, T. D., Dwek, R. A. and Platt, F. M. (2003) 'Central nervous system inflammation is a hallmark of pathogenesis in mouse models of GM1 and GM2 gangliosidosis', *Brain,* 126(Pt 4), 974-87.

Johnson, D. K., Rinchik, E. M., Moustaid-Moussa, N., Miller, D. R., Williams, R. W., Michaud, E. J., Jablonski, M. M., Elberger, A., Hamre, K., Smeyne, R., Chesler, E. and Goldowitz, D. (2005) 'Phenotype screening for genetically determined age-onset disorders and increased longevity in ENU-mutagenized mice', *Age,* 27(1), 75-90.

Johnson, R. D., Oliver, P. L. and Davies, K. E. (2008) 'SNARE proteins and schizophrenia: linking synaptic and neurodevelopmental hypotheses', *Acta Biochim Pol,* 55(4), 619-28.

Jones, B., Jones, E. L., Bonney, S. A., Patel, H. N., Mensenkamp, A. R., Eichenbaum-Voline, S., Rudling, M., Myrdal, U., Annesi, G., Naik, S., Meadows, N., Quattrone, A., Islam, S. A., Naoumova, R. P., Angelin, B., Infante, R., Levy, E., Roy, C. C., Freemont, P. S., Scott, J. and Shoulders, C. C. (2003) 'Mutations in a Sar1 GTPase of COPII vesicles are associated with lipid absorption disorders', *Nat Genet,* 34(1), 29-31.

Kang, C. and Drayna, D. (2012) 'A role for inherited metabolic deficits in persistent developmental stuttering', *Mol Genet Metab,* 107(3), 276-80.

Kang, C., Riazuddin, S., Mundorff, J., Krasnewich, D., Friedman, P., Mullikin, J. C. and Drayna, D. (2010) 'Mutations in the lysosomal enzyme-targeting pathway and persistent stuttering', *N Engl J Med,* 362(8), 677-85.

Karasinska, J. M. and Hayden, M. R. (2011) 'Cholesterol metabolism in Huntington disease', *Nat Rev Neurol,* 7(10), 561-72.

Karran, E., Mercken, M. and Strooper, B. D. (2011) 'The amyloid cascade hypothesis for Alzheimer's disease: an appraisal for the development of therapeutics', *Nat Rev Drug Discov,* 10(9), 698-712.

Keays, D. A., Clark, T. G. and Flint, J. (2006) 'Estimating the number of coding mutations in genotypic- and phenotypic-driven N-ethyl-N-nitrosourea (ENU) screens', *Mamm Genome*, 17(3), 230-8.

Keller, J. N., Schmitt, F. A., Scheff, S. W., Ding, Q., Chen, Q., Butterfield, D. A. and Markesbery, W. R. (2005) 'Evidence of increased oxidative damage in subjects with mild cognitive impairment', *Neurology*, 64(7), 1152-6.

Khandelwal, P. J., Herman, A. M., Hoe, H. S., Rebeck, G. W. and Moussa, C. E. (2011) 'Parkin mediates beclin-dependent autophagic clearance of defective mitochondria and ubiquitinated Abeta in AD models', *Hum Mol Genet*, 20(11), 2091-102.

Kim, R. H., Smith, P. D., Aleyasin, H., Hayley, S., Mount, M. P., Pownall, S., Wakeham, A., You-Ten, A. J., Kalia, S. K., Horne, P., Westaway, D., Lozano, A. M., Anisman, H., Park, D. S. and Mak, T. W. (2005) 'Hypersensitivity of DJ-1-deficient mice to 1-methyl-4-phenyl-1,2,3,6-tetrahydropyrindine (MPTP) and oxidative stress', *Proc Natl Acad Sci U S A*, 102(14), 5215-20.

Kirby, K., Hu, J., Hilliker, A. J. and Phillips, J. P. (2002) 'RNA interference-mediated silencing of Sod2 in Drosophila leads to early adult-onset mortality and elevated endogenous oxidative stress', *Proc Natl Acad Sci U S A*, 99(25), 16162-7.

Klemm, R. W., Norton, J. P., Cole, R. A., Li, C. S., Park, S. H., Crane, M. M., Li, L., Jin, D., Boye-Doe, A., Liu, T. Y., Shibata, Y., Lu, H., Rapoport, T. A., Farese, R. V., Jr., Blackstone, C., Guo, Y. and Mak, H. Y. (2013) 'A conserved role for atlastin GTPases in regulating lipid droplet size', *Cell Rep*, 3(5), 1465-75.

Kloos, A. D., Fisher, L. C., Detloff, M. R., Hassenzahl, D. L. and Basso, D. M. (2005) 'Stepwise motor and all-or-none sensory recovery is associated with nonlinear sparing after incremental spinal cord injury in rats', *Exp Neurol*, 191(2), 251-65.

Kokjohn, T. A. and Roher, A. E. (2009) 'Amyloid precursor protein transgenic mouse models and Alzheimer's disease: understanding the paradigms, limitations, and contributions', *Alzheimers Dement*, 5(4), 340-7.

Kollmann, K., Damme, M., Markmann, S., Morelle, W., Schweizer, M., Hermans-Borgmeyer, I., Rochert, A. K., Pohl, S., Lubke, T., Michalski, J. C., Kakela, R., Walkley, S. U. and Braulke, T. (2012) 'Lysosomal dysfunction causes neurodegeneration in mucolipidosis II 'knock-in' mice', *Brain*, 135(Pt 9), 2661-75.

Komatsu, M., Waguri, S., Chiba, T., Murata, S., Iwata, J., Tanida, I., Ueno, T., Koike, M., Uchiyama, Y., Kominami, E. and Tanaka, K. (2006) 'Loss of autophagy in the central nervous system causes neurodegeneration in mice', *Nature*, 441(7095), 880-4.

Komatsu, M., Waguri, S., Koike, M., Sou, Y. S., Ueno, T., Hara, T., Mizushima, N., Iwata, J., Ezaki, J., Murata, S., Hamazaki, J., Nishito, Y., Iemura, S., Natsume, T., Yanagawa, T., Uwayama, J., Warabi, E., Yoshida, H., Ishii, T., Kobayashi, A., Yamamoto, M., Yue, Z., Uchiyama, Y., Kominami, E. and Tanaka, K. (2007) 'Homeostatic levels of p62 control cytoplasmic inclusion body formation in autophagy-deficient mice', *Cell*, 131(6), 1149-63.

Koopmans, G. C., Deumens, R., Brook, G., Gerver, J., Honig, W. M., Hamers, F. P. and Joosten, E. A. (2007) 'Strain and locomotor speed affect over-ground locomotion in intact rats', *Physiol Behav*, 92(5), 993-1001.

Kornfeld, S. (1987) 'Trafficking of lysosomal enzymes', *Faseb J*, 1(6), 462-8.

Kornfeld, S. and Sly, W. S. (2001) *I-cell disease and pseudo-Hurler polydystrophy: disorders of lysosomal enzyme phosphorylation and localization., The metabolic and molecular bases of inherited disease.*, New York: McGraw-Hill Inc.

Kraft, C., Peter, M. and Hofmann, K. (2010) 'Selective autophagy: ubiquitin-mediated recognition and beyond', *Nat Cell Biol,* 12(9), 836-841.

Krahmer, N., Farese, R. V., Jr. and Walther, T. C. (2013) 'Balancing the fat: lipid droplets and human disease', *EMBO Mol Med,* 5(7), 905-15.

Krainc, D. (2010) 'Clearance of mutant proteins as a therapeutic target in neurodegenerative diseases', *Arch Neurol,* 67(4), 388-92.

Kretzschmar, D., Hasan, G., Sharma, S., Heisenberg, M. and Benzer, S. (1997) 'The swiss cheese mutant causes glial hyperwrapping and brain degeneration in Drosophila', *J Neurosci,* 17(19), 7425-32.

Kroner, Z. (2009) 'The relationship between Alzheimer's disease and diabetes: Type 3 diabetes?', *Altern Med Rev,* 14(4), 373-9.

Kudo, M., Bao, M., D'Souza, A., Ying, F., Pan, H., Roe, B. A. and Canfield, W. M. (2005) 'The alpha- and beta-subunits of the human UDP-N-acetylglucosamine:lysosomal enzyme N-acetylglucosamine-1-phosphotransferase [corrected] are encoded by a single cDNA', *J Biol Chem,* 280(43), 36141-9.

Kudo, M. and Canfield, W. M. (2006) 'Structural Requirements for Efficient Processing and Activation of Recombinant Human UDP-N-acetylglucosamine:Lysosomal-enzyme-N-acetylglucosamine-1-phosphotransferase', *Journal of Biological Chemistry,* 281(17), 11761-11768.

Kuerschner, L., Moessinger, C. and Thiele, C. (2008) 'Imaging of lipid biosynthesis: how a neutral lipid enters lipid droplets', *Traffic,* 9(3), 338-52.

Kühnlein, R. P. (2012) 'Lipid droplet-based storage fat metabolism in Drosophila: Thematic Review Series: Lipid Droplet Synthesis and Metabolism: from Yeast to Man', *Journal of Lipid Research,* 53(8), 1430-1436.

Lalonde, R. and Strazielle, C. (2001) 'Motor performance and regional brain metabolism of spontaneous murine mutations with cerebellar atrophy', *Behav Brain Res,* 125(1-2), 103-8.

Langston, J. W., Ballard, P., Tetrud, J. W. and Irwin, I. (1983) 'Chronic Parkinsonism in humans due to a product of meperidine-analog synthesis', *Science,* 219(4587), 979-80.

Lee, E. J., Woo, M. S., Moon, P. G., Baek, M. C., Choi, I. Y., Kim, W. K., Junn, E. and Kim, H. S. (2010) 'Alpha-synuclein activates microglia by inducing the expressions of matrix metalloproteinases and the subsequent activation of protease-activated receptor-1', *J Immunol,* 185(1), 615-23.

Lee, F. J., Huang, C. F., Yu, W. L., Buu, L. M., Lin, C. Y., Huang, M. C., Moss, J. and Vaughan, M. (1997) 'Characterization of an ADP-ribosylation factor-like 1 protein in Saccharomyces cerevisiae', *J Biol Chem,* 272(49), 30998-1005.

Lee, J., Lee, J. and Ju, B. G. (2011) 'Drosophila arf72A acts as an essential regulator of endoplasmic reticulum quality control and suppresses autosomal-dominant retinopathy', *The International Journal of Biochemistry & Cell Biology,* 43(9), 1392-1401.

Lee, T. and Luo, L. (1999) 'Mosaic analysis with a repressible cell marker for studies of gene function in neuronal morphogenesis', *Neuron,* 22(3), 451-61.

Leroy, J. G., Cathey, S. and Friez, M. J. (2008) 'Mucolipidosis II', *GeneReviews®* [online], available: http://www.ncbi.nlm.nih.gov/books/NBK1828/ [accessed 2012 May 10].

Leroy, J. G. and Demars, R. I. (1967) 'Mutant enzymatic and cytological phenotypes in cultured human fibroblasts', *Science,* 157(3790), 804-6.

Leroy, J. G. and Spranger, J. W. (1970) 'I-cell disease', *N Engl J Med,* 283(11), 598-9.

Lesage, S. and Brice, A. (2009) 'Parkinson's disease: from monogenic forms to genetic susceptibility factors', *Hum Mol Genet*, 18(R1).

Leventis, P. A. and Grinstein, S. (2010) 'The distribution and function of phosphatidylserine in cellular membranes', *Annu Rev Biophys*, 39, 407-27.

Levy, E. (1996) 'The genetic basis of primary disorders of intestinal fat transport', *Clin Invest Med*, 19(5), 317-24.

Lewis, M. A., Quint, E., Glazier, A. M., Fuchs, H., De Angelis, M. H., Langford, C., van Dongen, S., Abreu-Goodger, C., Piipari, M., Redshaw, N., Dalmay, T., Moreno-Pelayo, M. A., Enright, A. J. and Steel, K. P. (2009) 'An ENU-induced mutation of miR-96 associated with progressive hearing loss in mice', *Nat Genet*, 41(5), 614-8.

Lewis, S. (2012) 'Neurological disorders: SHANK2 misbehaves in autism', *Nat Rev Neurosci*, 13(8), 517-517.

Liang, G., Cline, G. W. and Macica, C. M. (2007) 'IGF-1 stimulates de novo fatty acid biosynthesis by Schwann cells during myelination', *Glia*, 55(6), 632-41.

Liao, G., Cheung, S., Galeano, J., Ji, A. X., Qin, Q. and Bi, X. (2009) 'Allopregnanolone treatment delays cholesterol accumulation and reduces autophagic/lysosomal dysfunction and inflammation in Npc1-/- mouse brain', *Brain research*, 1270, 140-151.

Lieschke, G. J. and Currie, P. D. (2007) 'Animal models of human disease: zebrafish swim into view', *Nat Rev Genet*, 8(5), 353-67.

Lievens, J. C., Iche, M., Laval, M., Faivre-Sarrailh, C. and Birman, S. (2008) 'AKT-sensitive or insensitive pathways of toxicity in glial cells and neurons in Drosophila models of Huntington's disease', *Hum Mol Genet*, 17(6), 882-94.

Lin, M. T. and Beal, M. F. (2006) 'Mitochondrial dysfunction and oxidative stress in neurodegenerative diseases', *Nature*, 443(7113), 787-795.

Link, C. D. (2001) 'Transgenic invertebrate models of age-associated neurodegenerative diseases', *Mech Ageing Dev*, 122(14), 1639-49.

Liu, L., Jiang, Q., Wang, X., Zhang, Y., Lin, R. C., Lam, S. M., Shui, G., Zhou, L., Li, P., Wang, Y., Cui, X., Gao, M., Zhang, L., Lv, Y., Xu, G., Liu, G., Zhao, D. and Yang, H. (2014) 'Adipose-specific knockout of SEIPIN/BSCL2 results in progressive lipodystrophy', *Diabetes*, 63(7), 2320-31.

Liu, L., Zhang, K., Sandoval, H., Yamamoto, S., Jaiswal, M., Sanz, E., Li, Z., Hui, J., Graham, B. H., Quintana, A. and Bellen, H. J. (2015) 'Glial Lipid Droplets and ROS Induced by Mitochondrial Defects Promote Neurodegeneration', *Cell*, 160(1-2), 177-90.

Liu, Y., Liu, F., Grundke-Iqbal, I., Iqbal, K. and Gong, C. X. (2011) 'Deficient brain insulin signalling pathway in Alzheimer's disease and diabetes', *J Pathol*, 225(1), 54-62.

Liu, Y. W., Huang, C. F., Huang, K. B. and Lee, F. J. (2005) 'Role for Gcs1p in regulation of Arl1p at trans-Golgi compartments', *Mol Biol Cell*, 16(9), 4024-33.

Lowe, S. L., Wong, S. H. and Hong, W. (1996) 'The mammalian ARF-like protein 1 (Arl1) is associated with the Golgi complex', *J Cell Sci*, 109(Pt 1), 209-20.

Lozano, R., Naghavi, M., Foreman, K., Lim, S., Shibuya, K., Aboyans, V., Abraham, J., Adair, T., Aggarwal, R., Ahn, S. Y., AlMazroa, M. A., Alvarado, M., Anderson, H. R., Anderson, L. M., Andrews, K. G., Atkinson, C., Baddour, L. M., Barker-Collo, S., Bartels, D. H., Bell, M. L., Benjamin, E. J., Bennett, D., Bhalla, K., Bikbov, B., Abdulhak, A. B., Birbeck, G., Blyth, F., Bolliger, I., Boufous, S., Bucello, C., Burch, M., Burney, P., Carapetis, J., Chen, H., Chou, D., Chugh, S. S., Coffeng, L. E., Colan, S. D., Colquhoun, S., Colson, K. E., Condon, J., Connor, M. D., Cooper, L. T., Corriere, M., Cortinovis, M., de Vaccaro, K. C., Couser, W., Cowie, B. C., Criqui, M.

H., Cross, M., Dabhadkar, K. C., Dahodwala, N., De Leo, D., Degenhardt, L., Delossantos, A., Denenberg, J., Des Jarlais, D. C., Dharmaratne, S. D., Dorsey, E. R., Driscoll, T., Duber, H., Ebel, B., Erwin, P. J., Espindola, P., Ezzati, M., Feigin, V., Flaxman, A. D., Forouzanfar, M. H., Fowkes, F. G. R., Franklin, R., Fransen, M., Freeman, M. K., Gabriel, S. E., Gakidou, E., Gaspari, F., Gillum, R. F., Gonzalez-Medina, D., Halasa, Y. A., Haring, D., Harrison, J. E., Havmoeller, R., Hay, R. J., Hoen, B., Hotez, P. J., Hoy, D., Jacobsen, K. H., James, S. L., Jasrasaria, R., Jayaraman, S., Johns, N., Karthikeyan, G., Kassebaum, N., Keren, A., Khoo, J.-P., Knowlton, L. M., Kobusingye, O., Koranteng, A., Krishnamurthi, R., Lipnick, M., Lipshultz, S. E., et al. (2011) 'Global and regional mortality from 235 causes of death for 20 age groups in 1990 and 2010: a systematic analysis for the Global Burden of Disease Study 2010', *The Lancet*, 380(9859), 2095-2128.

Lu, B. and Vogel, H. (2009) 'Drosophila models of neurodegenerative diseases', *Annu Rev Pathol*, 4, 315-42.

Lu, L. and Hong, W. (2003) 'Interaction of Arl1-GTP with GRIP domains recruits autoantigens Golgin-97 and Golgin-245/p230 onto the Golgi', *Mol Biol Cell*, 14(9), 3767-81.

Lu, L., Horstmann, H., Ng, C. and Hong, W. (2001) 'Regulation of Golgi structure and function by ARF-like protein 1 (Arl1)', *J Cell Sci*, 114(Pt 24), 4543-55.

Lu, L., Tai, G. and Hong, W. (2004) 'Autoantigen Golgin-97, an effector of Arl1 GTPase, participates in traffic from the endosome to the trans-golgi network', *Mol Biol Cell*, 15(10), 4426-43.

Lucin, K. M. and Wyss-Coray, T. (2009) 'Immune activation in brain aging and neurodegeneration: too much or too little?', *Neuron*, 64(1), 110-22.

Mallik, M. and Lakhotia, S. C. (2010) 'Modifiers and mechanisms of multi-system polyglutamine neurodegenerative disorders: lessons from fly models', *J Genet*, 89(4), 497-526.

Mancuso, M., Orsucci, D., Siciliano, G. and Murri, L. (2008) 'Mitochondria, mitochondrial DNA and Alzheimer's disease. What comes first?', *Curr Alzheimer Res*, 5(5), 457-68.

Manzoni, C. and Lewis, P. A. (2013) 'Dysfunction of the autophagy/lysosomal degradation pathway is a shared feature of the genetic synucleinopathies', *Faseb J*, 27(9), 3424-9.

Marschner, K., Kollmann, K., Schweizer, M., Braulke, T. and Pohl, S. (2011) 'A Key Enzyme in the Biogenesis of Lysosomes Is a Protease That Regulates Cholesterol Metabolism', *Science*, 333(6038), 87-90.

Martin, J. J., Leroy, J. G., Farriaux, J. P., Fontaine, G., Desnick, R. J. and Cabello, A. (1975) 'I-cell disease (mucolipidosis II):a report on its pathology', *Acta Neuropathol*, 33(4), 285-305.

Martin, J. J., Leroy, J. G., van Eygen, M. and Ceuterick, C. (1984) 'I-cell disease. A further report on its pathology', *Acta Neuropathol*, 64(3), 234-42.

Martin, S. and Parton, R. G. (2006) 'Lipid droplets: a unified view of a dynamic organelle', *Nat Rev Mol Cell Biol*, 7(5), 373-378.

Martins, I. J., Hone, E., Foster, J. K., Sunram-Lea, S. I., Gnjec, A., Fuller, S. J., Nolan, D., Gandy, S. E. and Martins, R. N. (2006) 'Apolipoprotein E, cholesterol metabolism, diabetes, and the convergence of risk factors for Alzheimer's disease and cardiovascular disease', *Mol Psychiatry*, 11(8), 721-36.

Matynia, A., Kushner, S. A. and Silva, A. J. (2002) 'Genetic approaches to molecular and cellular cognition: a focus on LTP and learning and memory', *Annu Rev Genet*, 36, 687-720.

Mazrier, H., Van Hoeven, M., Wang, P., Knox, V. W., Aguirre, G. D., Holt, E., Wiemelt, S. P., Sleeper, M. M., Hubler, M., Haskins, M. E. and Giger, U. (2003) 'Inheritance, biochemical abnormalities, and clinical features of feline mucolipidosis II: the first animal model of human I-cell disease', *J Hered,* 94(5), 363-73.

McDonold, C. M. and Fromme, J. C. (2014) 'Four GTPases differentially regulate the Sec7 Arf-GEF to direct traffic at the trans-golgi network', *Dev Cell,* 30(6), 759-67.

McMurray, C. T. (2001) 'Huntington's disease: new hope for therapeutics', *Trends Neurosci,* 24(11 Suppl), S32-8.

Mehlem, A., Hagberg, C. E., Muhl, L., Eriksson, U. and Falkevall, A. (2013) 'Imaging of neutral lipids by oil red O for analyzing the metabolic status in health and disease', *Nat. Protocols,* 8(6), 1149-1154.

Meikle, P. J., Hopwood, J. J., Clague, A. E. and Carey, W. F. (1999) 'Prevalence of lysosomal storage disorders', *Jama,* 281(3), 249-54.

Minghetti, L., Ajmone-Cat, M. A., De Berardinis, M. A. and De Simone, R. (2005) 'Microglial activation in chronic neurodegenerative diseases: roles of apoptotic neurons and chronic stimulation', *Brain Res Brain Res Rev,* 48(2), 251-6.

Mirth, C. K. and Riddiford, L. M. (2007) 'Size assessment and growth control: how adult size is determined in insects', *Bioessays,* 29(4), 344-55.

Morfini, G. A., Burns, M., Binder, L. I., Kanaan, N. M., LaPointe, N., Bosco, D. A., Brown, R. H., Jr., Brown, H., Tiwari, A., Hayward, L., Edgar, J., Nave, K. A., Garberrn, J., Atagi, Y., Song, Y., Pigino, G. and Brady, S. T. (2009) 'Axonal transport defects in neurodegenerative diseases', *J Neurosci,* 29(41), 12776-86.

Morgan, T. H. (1915) *The Mechanisms of Medelian Heredity,* New York: H. Holt and company.

Muffat, J., Walker, D. W. and Benzer, S. (2008) 'Human ApoD, an apolipoprotein up-regulated in neurodegenerative diseases, extends lifespan and increases stress resistance in Drosophila', *Proc Natl Acad Sci U S A,* 105(19), 7088-93.

Muller, B. and Grossniklaus, U. (2010) 'Model organisms--A historical perspective', *J Proteomics,* 73(11), 2054-63.

Munro, S. (2005) 'The Arf-like GTPase Arl1 and its role in membrane traffic', *Biochem Soc Trans,* 33(Pt 4), 601-5.

Munro, S. (2011) 'The golgin coiled-coil proteins of the Golgi apparatus', *Cold Spring Harb Perspect Biol,* 3(6).

Murphy, D. J. (2012) 'The dynamic roles of intracellular lipid droplets: from archaea to mammals', *Protoplasma,* 249(3), 541-85.

Murphy, S., Martin, S. and Parton, R. G. (2009) 'Lipid droplet-organelle interactions; sharing the fats', *Biochim Biophys Acta,* 6, 441-7.

Navarro, J. A., Ohmann, E., Sanchez, D., Botella, J. A., Liebisch, G., Molto, M. D., Ganfornina, M. D., Schmitz, G. and Schneuwly, S. (2010) 'Altered lipid metabolism in a Drosophila model of Friedreich's ataxia', *Hum Mol Genet,* 19(14), 2828-40.

Nelis, E., Haites, N. and Van Broeckhoven, C. (1999) 'Mutations in the peripheral myelin genes and associated genes in inherited peripheral neuropathies', *Hum Mutat,* 13(1), 11-28.

Neufeld, E. F. (1991) 'Lysosomal storage diseases', *Annu Rev Biochem,* 60, 257-80.

Newbern, J. M., Li, X., Shoemaker, S. E., Zhou, J., Zhong, J., Wu, Y., Bonder, D., Hollenback, S., Coppola, G., Geschwind, D. H., Landreth, G. E. and Snider, W. D. (2011) 'Specific functions for ERK/MAPK signaling during PNS development', *Neuron,* 69(1), 91-105.

Nishimoto-Morita, K., Shin, H. W., Mitsuhashi, H., Kitamura, M., Zhang, Q., Johannes, L. and Nakayama, K. (2009) 'Differential effects of depletion of ARL1 and ARFRP1 on membrane trafficking between the trans-Golgi network and endosomes', *J Biol Chem,* 284(16), 10583-92.

Nistico, R., Mehdawy, B., Piccirilli, S. and Mercuri, N. (2011) 'Paraquat- and Rotenone-induced Models of Parkinson's disease', *International Journal of Immunopathology and Pharmacology,* 24(2), 313-322.

Nixon, R. A. (2013) 'The role of autophagy in neurodegenerative disease', *Nat Med,* 19(8), 983-997.

Nixon, R. A. and Yang, D. S. (2011) 'Autophagy failure in Alzheimer's disease--locating the primary defect', *Neurobiol Dis,* 43(1), 38-45.

Nixon, R. A., Yang, D. S. and Lee, J. H. (2008) 'Neurodegenerative lysosomal disorders: a continuum from development to late age', *Autophagy,* 4(5), 590-9.

Nolan, P. M., Peters, J., Strivens, M., Rogers, D., Hagan, J., Spurr, N., Gray, I. C., Vizor, L., Brooker, D., Whitehill, E., Washbourne, R., Hough, T., Greenaway, S., Hewitt, M., Liu, X., McCormack, S., Pickford, K., Selley, R., Wells, C., Tymowska-Lalanne, Z., Roby, P., Glenister, P., Thornton, C., Thaung, C., Stevenson, J. A., Arkell, R., Mburu, P., Hardisty, R., Kiernan, A., Erven, A., Steel, K. P., Voegeling, S., Guenet, J. L., Nickols, C., Sadri, R., Nasse, M., Isaacs, A., Davies, K., Browne, M., Fisher, E. M., Martin, J., Rastan, S., Brown, S. D. and Hunter, J. (2000) 'A systematic, genome-wide, phenotype-driven mutagenesis programme for gene function studies in the mouse', *Nat Genet,* 25(4), 440-3.

Nufer, O., Guldbrandsen, S., Degen, M., Kappeler, F., Paccaud, J. P., Tani, K. and Hauri, H. P. (2002) 'Role of cytoplasmic C-terminal amino acids of membrane proteins in ER export', *J Cell Sci,* 115(Pt 3), 619-28.

Nystuen, A., Benke, P. J., Merren, J., Stone, E. M. and Sheffield, V. C. (1996) 'A cerebellar ataxia locus identified by DNA pooling to search for linkage disequilibrium in an isolated population from the Cayman Islands', *Hum Mol Genet,* 5(4), 525-31.

O'Rourke, E. J., Soukas, A. A., Carr, C. E. and Ruvkun, G. (2009) 'C. elegans Major Fats Are Stored in Vesicles Distinct from Lysosome-Related Organelles', *Cell metabolism,* 10(5), 430-435.

Oldham, S. and Hafen, E. (2003) 'Insulin/IGF and target of rapamycin signaling: a TOR de force in growth control', *Trends Cell Biol,* 13(2), 79-85.

Oliver, P. L., Bitoun, E., Clark, J., Jones, E. L. and Davies, K. E. (2004) 'Mediation of Af4 protein function in the cerebellum by Siah proteins', *Proc Natl Acad Sci U S A,* 101(41), 14901-6.

Oliver, P. L., Bitoun, E. and Davies, K. E. (2007) 'Comparative genetic analysis: the utility of mouse genetic systems for studying human monogenic disease', *Mamm Genome,* 18(6-7), 412-24.

Oliver, P. L. and Davies, K. E. (2005) 'Analysis of human neurological disorders using mutagenesis in the mouse', *Clin Sci,* 108(5), 385-97.

Oliver, P. L. and Davies, K. E. (2012) 'New insights into behaviour using mouse ENU mutagenesis', *Human Molecular Genetics*.

Oliver, P. L., Finelli, M. J., Edwards, B., Bitoun, E., Butts, D. L., Becker, E. B., Cheeseman, M. T., Davies, B. and Davies, K. E. (2011) 'Oxr1 is essential for protection against oxidative stress-induced neurodegeneration', *PLoS Genet,* 7(10), 20.

Oliver, P. L., Sobczyk, M. V., Maywood, E. S., Edwards, B., Lee, S., Livieratos, A., Oster, H., Butler, R., Godinho, S. I., Wulff, K., Peirson, S. N., Fisher, S. P., Chesham, J. E.,

Smith, J. W., Hastings, M. H., Davies, K. E. and Foster, R. G. (2012) 'Disrupted circadian rhythms in a mouse model of schizophrenia', *Curr Biol,* 22(4), 314-9.

Olofsson, S. O., Andersson, L., Haversen, L., Olsson, C., Myhre, S., Rutberg, M., Mobini, R., Li, L., Lu, E., Boren, J. and Bostrom, P. (2011) 'The formation of lipid droplets: possible role in the development of insulin resistance/type 2 diabetes', *Prostaglandins Leukot Essent Fatty Acids,* 85(5), 215-8.

Onat, O. E., Gulsuner, S., Bilguvar, K., Nazli Basak, A., Topaloglu, H., Tan, M., Tan, U., Gunel, M. and Ozcelik, T. (2013) 'Missense mutation in the ATPase, aminophospholipid transporter protein ATP8A2 is associated with cerebellar atrophy and quadrupedal locomotion', *Eur J Hum Genet,* 21(3), 281-5.

Owada, M. and Neufeld, E. F. (1982) 'Is there a mechanism for introducing acid hydrolases into liver lysosomes that is independent of mannose 6-phosphate recognition? evidence from I-cell disease', *Biochemical and Biophysical Research Communications,* 105(3), 814-820.

Paar, M., Jüngst, C., Steiner, N. A., Magnes, C., Sinner, F., Kolb, D., Lass, A., Zimmermann, R., Zumbusch, A., Kohlwein, S. D. and Wolinski, H. (2012) 'Remodeling of Lipid Droplets during Lipolysis and Growth in Adipocytes', *Journal of Biological Chemistry,* 287(14), 11164-11173.

Padmanabha, D. and Baker, K. D. (2014) 'Drosophila gains traction as a repurposed tool to investigate metabolism', *Trends in Endocrinology & Metabolism,* 25(10), 518-527.

Panic, B., Whyte, J. R. and Munro, S. (2003) 'The ARF-like GTPases Arl1p and Arl3p act in a pathway that interacts with vesicle-tethering factors at the Golgi apparatus', *Curr Biol,* 13(5), 405-10.

Papadeas, S. T., Kraig, S. E., O'Banion, C., Lepore, A. C. and Maragakis, N. J. (2011) 'Astrocytes carrying the superoxide dismutase 1 (SOD1G93A) mutation induce wild-type motor neuron degeneration in vivo', *Proc Natl Acad Sci U S A,* 108(43), 17803-8.

Parisi, M., Li, R. and Oliver, B. (2011) 'Lipid profiles of female and male Drosophila', *BMC Research Notes,* 4(1), 198.

Pasqualato, S., Renault, L. and Cherfils, J. (2002) 'Arf, Arl, Arp and Sar proteins: a family of GTP-binding proteins with a structural device for 'front–back' communication', *EMBO Reports,* 3(11), 1035-1041.

Patriquin, H. B., Kaplan, P., Kind, H. P. and Giedion, A. (1977) 'Neonatal mucolipidosis II (I-cell disease): clinical and radiologic features in three cases', *AJR Am J Roentgenol,* 129(1), 37-43.

Peltonen, L., Perola, M., Naukkarinen, J. and Palotie, A. (2006) 'Lessons from studying monogenic disease for common disease', *Human Molecular Genetics,* 15(suppl 1), R67-R74.

Peretti, N., Sassolas, A., Roy, C. C., Deslandres, C., Charcosset, M., Castagnetti, J., Pugnet-Chardon, L., Moulin, P., Labarge, S., Bouthillier, L., Lachaux, A. and Levy, E. (2010) 'Guidelines for the diagnosis and management of chylomicron retention disease based on a review of the literature and the experience of two centers', *Orphanet J Rare Dis,* 5(24), 1750-1172.

Petrey, A. C., Flanagan-Steet, H., Johnson, S., Fan, X., De la Rosa, M., Haskins, M. E., Nairn, A. V., Moremen, K. W. and Steet, R. (2012) 'Excessive activity of cathepsin K is associated with cartilage defects in a zebrafish model of mucolipidosis II', *Dis Model Mech,* 5(2), 177-90.

Pickart, C. M. and Fushman, D. (2004) 'Polyubiquitin chains: polymeric protein signals', *Curr Opin Chem Biol,* 8(6), 610-6.

Platt, F. M., Boland, B. and van der Spoel, A. C. (2012) 'The cell biology of disease: lysosomal storage disorders: the cellular impact of lysosomal dysfunction', *J Cell Biol,* 199(5), 723-34.

Pohlmann, R., Boeker, M. W. and von Figura, K. (1995) 'The two mannose 6-phosphate receptors transport distinct complements of lysosomal proteins', *J Biol Chem,* 270(45), 27311-8.

Pontikis, C. C., Davidson, C. D., Walkley, S. U., Platt, F. M. and Begley, D. J. (2013) 'Cyclodextrin alleviates neuronal storage of cholesterol in Niemann-Pick C disease without evidence of detectable blood-brain barrier permeability', *J Inherit Metab Dis,* 36(3), 491-8.

Poorthuis, B. J., Wevers, R. A., Kleijer, W. J., Groener, J. E., de Jong, J. G., van Weely, S., Niezen-Koning, K. E. and van Diggelen, O. P. (1999) 'The frequency of lysosomal storage diseases in The Netherlands', *Hum Genet,* 105(1-2), 151-6.

Poupětová, H., Ledvinová, J., Berná, L., Dvořáková, L., Kožich, V. and Elleder, M. (2010) 'The birth prevalence of lysosomal storage disorders in the Czech Republic: comparison with data in different populations', *Journal of Inherited Metabolic Disease,* 33(4), 387-396.

Prelich, G. (2012) 'Gene Overexpression: Uses, Mechanisms, and Interpretation', *Genetics,* 190(3), 841-854.

Prinz, M., Priller, J., Sisodia, S. S. and Ransohoff, R. M. (2011) 'Heterogeneity of CNS myeloid cells and their roles in neurodegeneration', *Nat Neurosci,* 14(10), 1227-1235.

Pritchett, D., Wulff, K., Oliver, P. L., Bannerman, D. M., Davies, K. E., Harrison, P. J., Peirson, S. N. and Foster, R. G. (2012) 'Evaluating the links between schizophrenia and sleep and circadian rhythm disruption', *J Neural Transm,* 119(10), 1061-75.

Proitsi, P., Kim, M., Whiley, L., Pritchard, M., Leung, R., Soininen, H., Kloszewska, I., Mecocci, P., Tsolaki, M., Vellas, B., Sham, P., Lovestone, S., Powell, J. F., Dobson, R. J. B. and Legido-Quigley, C. (2015) 'Plasma lipidomics analysis finds long chain cholesteryl esters to be associated with Alzheimer/'s disease', *Transl Psychiatry,* 5, e494.

Pun, S., Santos, A. F., Saxena, S., Xu, L. and Caroni, P. (2006) 'Selective vulnerability and pruning of phasic motoneuron axons in motoneuron disease alleviated by CNTF', *Nat Neurosci,* 9(3), 408-19.

Qian, Y., Flanagan-Steet, H., van Meel, E., Steet, R. and Kornfeld, S. A. (2013) 'The DMAP interaction domain of UDP-GlcNAc:lysosomal enzyme N-acetylglucosamine-1-phosphotransferase is a substrate recognition module', *Proc Natl Acad Sci U S A,* 110(25), 10246-51.

Raas-Rothschild, A., Cormier-Daire, V., Bao, M., Genin, E., Salomon, R., Brewer, K., Zeigler, M., Mandel, H., Toth, S., Roe, B., Munnich, A. and Canfield, W. M. (2000) 'Molecular basis of variant pseudo-hurler polydystrophy (mucolipidosis IIIC)', *J Clin Invest,* 105(5), 673-81.

Rademakers, R., Neumann, M. and Mackenzie, I. R. (2012) 'Advances in understanding the molecular basis of frontotemporal dementia', *Nat Rev Neurol,* 8(8), 423-434.

Rajan, A. and Perrimon, N. (2013) 'Of flies and men: insights on organismal metabolism from fruit flies', *BMC Biol,* 11(38), 1741-7007.

Ramanan, V. K. and Saykin, A. J. (2013) 'Pathways to neurodegeneration: mechanistic insights from GWAS in Alzheimer's disease, Parkinson's disease, and related disorders', *Am J Neurodegener Dis,* 2(3), 145-75.

Rana, A., Rera, M. and Walker, D. W. (2013) 'Parkin overexpression during aging reduces proteotoxicity, alters mitochondrial dynamics, and extends lifespan', *Proc Natl Acad Sci U S A,* 110(21), 8638-43.

Reed, T. T. (2011) 'Lipid peroxidation and neurodegenerative disease', *Free Radic Biol Med,* 51(7), 1302-19.

Reinhardt, P., Glatza, M., Hemmer, K., Tsytsyura, Y., Thiel, C. S., Höing, S., Moritz, S., Parga, J. A., Wagner, L., Bruder, J. M., Wu, G., Schmid, B., Röpke, A., Klingauf, J., Schwamborn, J. C., Gasser, T., Schöler, H. R. and Sterneckert, J. (2013) 'Derivation and Expansion Using Only Small Molecules of Human Neural Progenitors for Neurodegenerative Disease Modeling', *PLoS One,* 8(3), e59252.

Reiter, L. T., Potocki, L., Chien, S., Gribskov, M. and Bier, E. (2001) 'A systematic analysis of human disease-associated gene sequences in Drosophila melanogaster', *Genome Res,* 11(6), 1114-25.

Reitman, M. L., Varki, A. and Kornfeld, S. (1981) 'Fibroblasts from patients with I-cell disease and pseudo-Hurler polydystrophy are deficient in uridine 5'-diphosphate-N-acetylglucosamine: glycoprotein N-acetylglucosaminylphosphotransferase activity', *J Clin Invest,* 67(5), 1574-9.

Ribe, E. M., Serrano-Saiz, E., Akpan, N. and Troy, C. M. (2008) 'Mechanisms of neuronal death in disease: defining the models and the players', *Biochem J,* 415(2), 165-82.

Rogers, D. C., Fisher, E. M., Brown, S. D., Peters, J., Hunter, A. J. and Martin, J. E. (1997) 'Behavioral and functional analysis of mouse phenotype: SHIRPA, a proposed protocol for comprehensive phenotype assessment', *Mamm Genome,* 8(10), 711-3.

Rogers, D. C., Peters, J., Martin, J. E., Ball, S., Nicholson, S. J., Witherden, A. S., Hafezparast, M., Latcham, J., Robinson, T. L., Quilter, C. A. and Fisher, E. M. (2001) 'SHIRPA, a protocol for behavioral assessment: validation for longitudinal study of neurological dysfunction in mice', *Neurosci Lett,* 306(1-2), 89-92.

Roote, J. and Prokop, A. (2013) 'How to design a genetic mating scheme: a basic training package for Drosophila genetics', *G3,* 3(2), 353-8.

Rosenthal, N. and Brown, S. (2007) 'The mouse ascending: perspectives for human-disease models', *Nat Cell Biol,* 9(9), 993-9.

Ross, C. A. and Poirier, M. A. (2005) 'Opinion: What is the role of protein aggregation in neurodegeneration?', *Nat Rev Mol Cell Biol,* 6(11), 891-8.

Roy, C. C., Levy, E., Green, P. H., Sniderman, A., Letarte, J., Buts, J. P., Orquin, J., Brochu, P., Weber, A. M., Morin, C. L., Marcel, Y., Deckelbaum, R. J. and et al. (1987) 'Malabsorption, hypocholesterolemia, and fat-filled enterocytes with increased intestinal apoprotein B. Chylomicron retention disease', *Gastroenterology,* 92(2), 390-9.

Rubinsztein, D. C., Codogno, P. and Levine, B. (2012) 'Autophagy modulation as a potential therapeutic target for diverse diseases', *Nat Rev Drug Discov,* 11(9), 709-30.

Rubinsztein, D. C., Gestwicki, J. E., Murphy, L. O. and Klionsky, D. J. (2007) 'Potential therapeutic applications of autophagy', *Nat Rev Drug Discov,* 6(4), 304-12.

Ryan, N. S. and Rossor, M. N. (2010) 'Correlating familial Alzheimer's disease gene mutations with clinical phenotype', *Biomark Med,* 4(1), 99-112.

Said, G. (2007) 'Diabetic neuropathy[mdash]a review', *Nat Clin Pract Neuro,* 3(6), 331-340.

Sanchez, D., Lopez-Arias, B., Torroja, L., Canal, I., Wang, X., Bastiani, M. J. and Ganfornina, M. D. (2006) 'Loss of glial lazarillo, a homolog of apolipoprotein D, reduces lifespan and stress resistance in Drosophila', *Curr Biol,* 16(7), 680-6.

Sanderson, D. J. and Bannerman, D. M. (2012) 'The role of habituation in hippocampus-dependent spatial working memory tasks: evidence from GluA1 AMPA receptor subunit knockout mice', *Hippocampus*, 22(5), 981-94.

Sardi, S. P., Clarke, J., Viel, C., Chan, M., Tamsett, T. J., Treleaven, C. M., Bu, J., Sweet, L., Passini, M. A., Dodge, J. C., Yu, W. H., Sidman, R. L., Cheng, S. H. and Shihabuddin, L. S. (2013) 'Augmenting CNS glucocerebrosidase activity as a therapeutic strategy for parkinsonism and other Gaucher-related synucleinopathies', *Proc Natl Acad Sci U S A*, 110(9), 3537-42.

Sarzi, E., Angebault, C., Seveno, M., Gueguen, N., Chaix, B., Bielicki, G., Boddaert, N., Mausset-Bonnefont, A. L., Cazevieille, C., Rigau, V., Renou, J. P., Wang, J., Delettre, C., Brabet, P., Puel, J. L., Hamel, C. P., Reynier, P. and Lenaers, G. (2012) 'The human OPA1delTTAG mutation induces premature age-related systemic neurodegeneration in mouse', *Brain*, 135(Pt 12), 3599-613.

Scheitz, C. J. F., Guo, Y., Early, A. M., Harshman, L. G. and Clark, A. G. (2013) 'Heritability and Inter-Population Differences in Lipid Profiles of Drosophila melanogaster', *PLoS One*, 8(8), e72726.

Scheper, W. and Hoozemans, J. J. (2009) 'Endoplasmic reticulum protein quality control in neurodegenerative disease: the good, the bad and the therapy', *Curr Med Chem*, 16(5), 615-26.

Schiaffino, S. (2010) 'Fibre types in skeletal muscle: a personal account', *Acta Physiologica*, 199(4), 451-463.

Schmahmann, J. D. (1991) 'An emerging concept. The cerebellar contribution to higher function', *Arch Neurol*, 48(11), 1178-87.

Schmahmann, J. D. and Pandya, D. N. (1997) 'Anatomic organization of the basilar pontine projections from prefrontal cortices in rhesus monkey', *J Neurosci*, 17(1), 438-58.

Schmitt, F., Hussain, G., Dupuis, L., Loeffler, J.-P. and Henriques, A. (2014) 'A plural role for lipids in motor neuron diseases: energy, signaling and structure', *Frontiers in Cellular Neuroscience*, 8.

Setty, S. R., Shin, M. E., Yoshino, A., Marks, M. S. and Burd, C. G. (2003) 'Golgi recruitment of GRIP domain proteins by Arf-like GTPase 1 is regulated by Arf-like GTPase 3', *Curr Biol*, 13(5), 401-4.

Sheridan, R., Lampe, K., Shanmukhappa, S. K., Putnam, P., Keddache, M., Divanovic, S., Bezerra, J. and Hoebe, K. (2011) 'Lampe1: An ENU-Germline Mutation Causing Spontaneous Hepatosteatosis Identified through Targeted Exon-Enrichment and Next-Generation Sequencing', *PLoS One*, 6(7), e21979.

Sherman, D. L., Krols, M., Wu, L.-M., Grove, M., Nave, K.-A., Gangloff, Y.-G. and Brophy, P. J. (2012) 'Arrest of Myelination and Reduced Axon Growth when Schwann Cells Lack mTOR', *The Journal of neuroscience : the official journal of the Society for Neuroscience*, 32(5), 1817-1825.

Shibuya, T. and Morimoto, K. (1993) 'A review of the genotoxicity of 1-ethyl-1-nitrosourea', *Mutat Res*, 297(1), 3-38.

Sidransky, E., Nalls, M. A., Aasly, J. O., Aharon-Peretz, J., Annesi, G., Barbosa, E. R., Bar-Shira, A., Berg, D., Bras, J., Brice, A., Chen, C. M., Clark, L. N., Condroyer, C., De Marco, E. V., Durr, A., Eblan, M. J., Fahn, S., Farrer, M. J., Fung, H. C., Gan-Or, Z., Gasser, T., Gershoni-Baruch, R., Giladi, N., Griffith, A., Gurevich, T., Januario, C., Kropp, P., Lang, A. E., Lee-Chen, G. J., Lesage, S., Marder, K., Mata, I. F., Mirelman, A., Mitsui, J., Mizuta, I., Nicoletti, G., Oliveira, C., Ottman, R., Orr-Urtreger, A., Pereira, L. V., Quattrone, A., Rogaeva, E., Rolfs, A., Rosenbaum, H., Rozenberg, R.,

Samii, A., Samaddar, T., Schulte, C., Sharma, M., Singleton, A., Spitz, M., Tan, E. K., Tayebi, N., Toda, T., Troiano, A. R., Tsuji, S., Wittstock, M., Wolfsberg, T. G., Wu, Y. R., Zabetian, C. P., Zhao, Y. and Ziegler, S. G. (2009) 'Multicenter analysis of glucocerebrosidase mutations in Parkinson's disease', *N Engl J Med,* 361(17), 1651-61.

Simons, M., Kramer, E. M., Thiele, C., Stoffel, W. and Trotter, J. (2000) 'Assembly of myelin by association of proteolipid protein with cholesterol- and galactosylceramide-rich membrane domains', *J Cell Biol,* 151(1), 143-54.

Singh, R., Kaushik, S., Wang, Y., Xiang, Y., Novak, I., Komatsu, M., Tanaka, K., Cuervo, A. M. and Czaja, M. J. (2009) 'Autophagy regulates lipid metabolism', *Nature,* 458(7242), 1131-5.

Sinka, R., Gillingham, A. K., Kondylis, V. and Munro, S. (2008) 'Golgi coiled-coil proteins contain multiple binding sites for Rab family G proteins', *J Cell Biol,* 183(4), 607-15.

Soldner, F., Laganiere, J., Cheng, A. W., Hockemeyer, D., Gao, Q., Alagappan, R., Khurana, V., Golbe, L. I., Myers, R. H., Lindquist, S., Zhang, L., Guschin, D., Fong, L. K., Vu, B. J., Meng, X., Urnov, F. D., Rebar, E. J., Gregory, P. D., Zhang, H. S. and Jaenisch, R. (2011) 'Generation of isogenic pluripotent stem cells differing exclusively at two early onset Parkinson point mutations', *Cell,* 146(2), 318-31.

Song, W., Wang, F., Lotfi, P., Sardiello, M. and Segatori, L. (2014) '2-Hydroxypropyl-beta-cyclodextrin promotes transcription factor EB-mediated activation of autophagy: implications for therapy', *J Biol Chem,* 289(14), 10211-22.

Soni, K. G., Mardones, G. A., Sougrat, R., Smirnova, E., Jackson, C. L. and Bonifacino, J. S. (2009) 'Coatomer-dependent protein delivery to lipid droplets', *Journal of Cell Science,* 122(11), 1834-1841.

Sousa-Nunes, R., Yee, L. L. and Gould, A. P. (2011) 'Fat cells reactivate quiescent neuroblasts via TOR and glial insulin relays in Drosophila', *Nature,* 471(7339), 508-12.

Southall, T. D., Elliott, D. A. and Brand, A. H. (2008) 'The GAL4 System: A Versatile Toolkit for Gene Expression in Drosophila', *CSH Protoc,* 1(10).

Spang, A. (2008) 'The life cycle of a transport vesicle', *Cell Mol Life Sci,* 65(18), 2781-9.

Sparks, D. L. (2011) 'Alzheimer disease: Statins in the treatment of Alzheimer disease', *Nat Rev Neurol,* 7(12), 662-663.

Spranger, J. W. and Wiedemann, H. R. (1970) 'The genetic mucolipidoses. Diagnosis and differential diagnosis', *Humangenetik,* 9(2), 113-39.

Squier, T. C. (2001) 'Oxidative stress and protein aggregation during biological aging', *Exp Gerontol,* 36(9), 1539-50.

Stefano, G., Renna, L., Hanton, S. L., Chatre, L., Haas, T. A. and Brandizzi, F. (2006) 'ARL1 plays a role in the binding of the GRIP domain of a peripheral matrix protein to the Golgi apparatus in plant cells', *Plant Mol Biol,* 61(3), 431-49.

Stolp, H. B. and Dziegielewska, K. M. (2009) 'Review: Role of developmental inflammation and blood-brain barrier dysfunction in neurodevelopmental and neurodegenerative diseases', *Neuropathol Appl Neurobiol,* 35(2), 132-46.

Stork, T., Bernardos, R. and Freeman, M. R. (2012) 'Analysis of glial cell development and function in Drosophila', *Cold Spring Harb Protoc,* 1(1), 1-17.

Subramani, D. and Alahari, S. K. (2010) 'Integrin-mediated function of Rab GTPases in cancer progression', *Mol Cancer,* 9, 312.

Takahashi, K. and Yamanaka, S. (2006) 'Induction of pluripotent stem cells from mouse embryonic and adult fibroblast cultures by defined factors', *Cell,* 126(4), 663-76.

Tamkun, J. W., Kahn, R. A., Kissinger, M., Brizuela, B. J., Rulka, C., Scott, M. P. and Kennison, J. A. (1991) 'The arflike gene encodes an essential GTP-binding protein in Drosophila', *Proc Natl Acad Sci U S A,* 88(8), 3120-4.

Tamura, A. and Yui, N. (2015) 'beta-Cyclodextrin-threaded Biocleavable Polyrotaxanes Ameliorate Impaired Autophagic Flux in Niemann-Pick Type C Disease', *J Biol Chem,* 24, 636803.

Tarugi, P. and Averna, M. (2011) 'Hypobetalipoproteinemia: genetics, biochemistry, and clinical spectrum', *Adv Clin Chem,* 54, 81-107.

Taylor, J. P., Hardy, J. and Fischbeck, K. H. (2002) 'Toxic Proteins in Neurodegenerative Disease', *Science,* 296(5575), 1991-1995.

Teleman, A. A. (2009) 'Molecular mechanisms of metabolic regulation by insulin in Drosophila', *Biochem J,* 425(1), 13-26.

Tennessen, J. M. and Thummel, C. S. (2011) 'Coordinating growth and maturation - insights from Drosophila', *Curr Biol,* 21(18), 033.

Thomas, P. S., Jr., Fraley, G. S., Damian, V., Woodke, L. B., Zapata, F., Sopher, B. L., Plymate, S. R. and La Spada, A. R. (2006) 'Loss of endogenous androgen receptor protein accelerates motor neuron degeneration and accentuates androgen insensitivity in a mouse model of X-linked spinal and bulbar muscular atrophy', *Hum Mol Genet,* 15(14), 2225-38.

Thompson, L. M. and Marsh, J. L. (2003) 'Invertebrate models of neurologic disease: insights into pathogenesis and therapy', *Curr Neurol Neurosci Rep,* 3(5), 442-8.

Thompson, P. M., Egbufoama, S. and Vawter, M. P. (2003) 'SNAP-25 reduction in the hippocampus of patients with schizophrenia', *Prog Neuropsychopharmacol Biol Psychiatry,* 27(3), 411-7.

Tiede, S., Storch, S., Lubke, T., Henrissat, B., Bargal, R., Raas-Rothschild, A. and Braulke, T. (2005) 'Mucolipidosis II is caused by mutations in GNPTA encoding the alpha/beta GlcNAc-1-phosphotransferase', *Nat Med,* 11(10), 1109-12.

Timson, B. F., Bowlin, B. K., Dudenhoeffer, G. A. and George, J. B. (1985) 'Fiber number, area, and composition of mouse soleus muscle following enlargement', *J Appl Physiol,* 58(2), 619-24.

Tofaris, G. K. (2012) 'Lysosome-dependent pathways as a unifying theme in Parkinson's disease', *Mov Disord,* 27(11), 1364-9.

Torres, I. L., Rosa-Ferreira, C. and Munro, S. (2014) 'The Arf family G protein Arl1 is required for secretory granule biogenesis in Drosophila', *J Cell Sci,* 127(Pt 10), 2151-60.

Trancikova, A., Ramonet, D. and Moore, D. J. (2011) 'Genetic mouse models of neurodegenerative diseases', *Prog Mol Biol Transl Sci,* 100, 419-82.

Turner, B. J. and Talbot, K. (2008) 'Transgenics, toxicity and therapeutics in rodent models of mutant SOD1-mediated familial ALS', *Prog Neurobiol,* 85(1), 94-134.

Turner, M. R., Kiernan, M. C., Leigh, P. N. and Talbot, K. (2009) 'Biomarkers in amyotrophic lateral sclerosis', *Lancet Neurol,* 8(1), 94-109.

Turpin, J. C., Masson, M. and Baumann, N. (1991) 'Clinical aspects of Niemann-Pick type C disease in the adult', *Dev Neurosci,* 13(4-5), 304-6.

Um, J. W., Im, E., Lee, H. J., Min, B., Yoo, L., Yoo, J., Lubbert, H., Stichel-Gunkel, C., Cho, H. S., Yoon, J. B. and Chung, K. C. (2010) 'Parkin directly modulates 26S proteasome activity', *J Neurosci,* 30(35), 11805-14.

Van Valkenburgh, H., Shern, J. F., Sharer, J. D., Zhu, X. and Kahn, R. A. (2001) 'ADP-ribosylation factors (ARFs) and ARF-like 1 (ARL1) have both specific and shared effectors: characterizing ARL1-binding proteins', *J Biol Chem*, 276(25), 22826-37.

Vance, J. E. and Karten, B. (2014) 'Niemann-Pick C Disease and Mobilization of Lysosomal Cholesterol by Cyclodextrin', *J Lipid Res*, 24, 24.

Venken, K. J. and Bellen, H. J. (2012) 'Genome-wide manipulations of Drosophila melanogaster with transposons, Flp recombinase, and PhiC31 integrase', *Methods Mol Biol*, 859, 203-28.

Ventura, P., Presicci, A., Perniola, T., Campa, M. G. and Margari, L. (2006) 'Mental retardation and epilepsy in patients with isolated cerebellar hypoplasia', *J Child Neurol*, 21(9), 776-81.

Vereshchagina, N. and Wilson, C. (2006) 'Cytoplasmic activated protein kinase Akt regulates lipid-droplet accumulation in Drosophila nurse cells', *Development*, 133(23), 4731-5.

Vickers, J. C., King, A. E., Woodhouse, A., Kirkcaldie, M. T., Staal, J. A., McCormack, G. H., Blizzard, C. A., Musgrove, R. E., Mitew, S., Liu, Y., Chuckowree, J. A., Bibari, O. and Dickson, T. C. (2009) 'Axonopathy and cytoskeletal disruption in degenerative diseases of the central nervous system', *Brain Res Bull*, 80(4-5), 217-23.

Vignini, A., Giulietti, A., Nanetti, L., Raffaelli, F., Giusti, L., Mazzanti, L. and Provinciali, L. (2013) 'Alzheimer's disease and diabetes: new insights and unifying therapies', *Curr Diabetes Rev*, 9(3), 218-27.

Vogel, P., Payne, B. J., Read, R., Lee, W. S., Gelfman, C. M. and Kornfeld, S. (2009) 'Comparative pathology of murine mucolipidosis types II and IIIC', *Vet Pathol*, 46(2), 313-24.

Waheed, A., Pohlmann, R., Hasilik, A., von Figura, K., van Elsen, A. and Leroy, J. G. (1982) 'Deficiency of UDP-N-acetylglucosamine: Lysosomal enzyme N-acetylglucosamine-1-phosphotransferase in organs of I-cell patients', *Biochemical and Biophysical Research Communications*, 105(3), 1052-1058.

Walker, D. W., Muffat, J., Rundel, C. and Benzer, S. (2006) 'Overexpression of a Drosophila homolog of apolipoprotein D leads to increased stress resistance and extended lifespan', *Curr Biol*, 16(7), 674-9.

Walther, T. C. and Farese, R. V., Jr. (2012) 'Lipid droplets and cellular lipid metabolism', *Annu Rev Biochem*, 81, 687-714.

Wang, C., Liu, Z. and Huang, X. (2012) 'Rab32 Is Important for Autophagy and Lipid Storage in Drosophila', *PLoS One*, 7(2), e32086.

Wang, J.-W., Beck, E. S. and McCabe, B. D. (2012) 'A Modular Toolset for Recombination Transgenesis and Neurogenetic Analysis of Drosophila', *PLoS One*, 7(7), e42102.

Wang, J.-W., Brent, J. R., Tomlinson, A., Shneider, N. A. and McCabe, B. D. (2011) 'The ALS-associated proteins FUS and TDP-43 function together to affect Drosophila locomotion and life span', *The Journal of Clinical Investigation*, 121(10), 4118-4126.

Wang, L., Schuster, G. U., Hultenby, K., Zhang, Q., Andersson, S. and Gustafsson, J. A. (2002) 'Liver X receptors in the central nervous system: from lipid homeostasis to neuronal degeneration', *Proc Natl Acad Sci U S A*, 99(21), 13878-83.

Wang, T., Lao, U. and Edgar, B. A. (2009) 'TOR-mediated autophagy regulates cell death in Drosophila neurodegenerative disease', *J Cell Biol*, 186(5), 703-11.

Wang, X. and Michaelis, E. K. (2010) 'Selective neuronal vulnerability to oxidative stress in the brain', *Front Aging Neurosci*, 2(12).

Watson, M. R., Lagow, R. D., Xu, K., Zhang, B. and Bonini, N. M. (2008) 'A Drosophila Model for Amyotrophic Lateral Sclerosis Reveals Motor Neuron Damage by Human SOD1', *The Journal of Biological Chemistry,* 283(36), 24972-24981.

White, R. and Kramer-Albers, E. M. (2014) 'Axon-glia interaction and membrane traffic in myelin formation', *Front Cell Neurosci,* 7(284), 6.

Wilder, E. L. (2000) 'Ectopic expression in Drosophila', *Methods Mol Biol,* 137, 9-14.

Wilfling, F., Haas, J. T., Walther, T. C. and Farese, R. V., Jr. (2014) 'Lipid droplet biogenesis', *Curr Opin Cell Biol,* 29, 39-45.

Wine, R. N., McPherson, C. A. and Harry, G. J. (2009) 'IGF-1 and pAKT signaling promote hippocampal CA1 neuronal survival following injury to dentate granule cells', *Neurotox Res,* 16(3), 280-92.

Winter, J. N., Fox, T. E., Kester, M., Jefferson, L. S. and Kimball, S. R. (2010) 'Phosphatidic acid mediates activation of mTORC1 through the ERK signaling pathway', *Am J Physiol Cell Physiol,* 299(2), 28.

Winterstein, C., Trotter, J. and Kramer-Albers, E. M. (2008) 'Distinct endocytic recycling of myelin proteins promotes oligodendroglial membrane remodeling', *J Cell Sci,* 121(Pt 6), 834-42.

Wong, K., Sidransky, E., Verma, A., Mixon, T., Sandberg, G. D., Wakefield, L. K., Morrison, A., Lwin, A., Colegial, C., Allman, J. M. and Schiffmann, R. (2004) 'Neuropathology provides clues to the pathophysiology of Gaucher disease', *Molecular Genetics and Metabolism,* 82(3), 192-207.

Wood, P. L. (2012) 'Lipidomics of Alzheimer's disease: current status', *Alzheimers Res Ther,* 4(1).

Wu, M., Lu, L., Hong, W., and Song, H. (2003) 'Structural basis for recruitment of GRIP domain golgin-245 by small GTPase Arl1', *Nat Struc Mol Bio,* 11, 86-94.

Wymann, M. P. and Schneiter, R. (2008) 'Lipid signalling in disease', *Nat Rev Mol Cell Biol,* 9(2), 162-176.

Xie, H., Hou, S., Jiang, J., Sekutowicz, M., Kelly, J. and Bacskai, B. J. (2013) 'Rapid cell death is preceded by amyloid plaque-mediated oxidative stress', *Proc Natl Acad Sci U S A,* 110(19), 7904-9.

Xie, X. and Auld, V. J. (2011) 'Integrins are necessary for the development and maintenance of the glial layers in the Drosophila peripheral nerve', *Development,* 138(17), 3813-22.

Xie, X., Hu, J., Liu, X., Qin, H., Percival-Smith, A., Rao, Y. and Li, S. S. (2010) 'NIP/DuoxA is essential for Drosophila embryonic development and regulates oxidative stress response', *Int J Biol Sci,* 6(3), 252-67.

Xu, X. and Kim, S. K. (2011) 'The early bird catches the worm: new technologies for the Caenorhabditis elegans toolkit', *Nat Rev Genet,* 12(11), 793-801.

Yancey, P. G., Rodrigueza, W. V., Kilsdonk, E. P. C., Stoudt, G. W., Johnson, W. J., Phillips, M. C. and Rothblat, G. H. (1996) 'Cellular Cholesterol Efflux Mediated by Cyclodextrins: Demonstration of Kinetic Pools and Mechanism of Efflux', *Journal of Biological Chemistry,* 271(27), 16026-16034.

Ye, P., Li, L., Richards, R., DiAugustine, R. and D'Ercole, A. (2002) 'Myelination is altered in insulin-like growth factor-I null mutant mice', *J Neurosci,* 22, 6041 - 6051.

Yoshino, A., Setty, S. R., Poynton, C., Whiteman, E. L., Saint-Pol, A., Burd, C. G., Johannes, L., Holzbaur, E. L., Koval, M., McCaffery, J. M. and Marks, M. S. (2005) 'tGolgin-1 (p230, golgin-245) modulates Shiga-toxin transport to the Golgi and Golgi motility towards the microtubule-organizing centre', *J Cell Sci,* 118(Pt 10), 2279-93.

Zahn, C., Hommel, A., Lu, L., Hong, W., Walther, D. J., Florian, S., Joost, H. G. and Schurmann, A. (2006) 'Knockout of Arfrp1 leads to disruption of ARF-like1 (ARL1) targeting to the trans-Golgi in mouse embryos and HeLa cells', *Mol Membr Biol*, 23(6), 475-85.

Zahn, C., Jaschke, A., Weiske, J., Hommel, A., Hesse, D., Augustin, R., Lu, L., Hong, W., Florian, S., Scheepers, A., Joost, H. G., Huber, O. and Schurmann, A. (2008) 'ADP-ribosylation factor-like GTPase ARFRP1 is required for trans-Golgi to plasma membrane trafficking of E-cadherin', *J Biol Chem*, 283(40), 27179-88.

Zhu, X., Libby, R. T., de Vries, W. N., Smith, R. S., Wright, D. L., Bronson, R. T., Seburn, K. L. and John, S. W. (2012) 'Mutations in a P-type ATPase gene cause axonal degeneration', *PLoS Genet*, 8(8), 9.

Zielasek, J. and Toyka, K. V. (1999) 'Nerve conduction abnormalities and neuromyotonia in genetically engineered mouse models of human hereditary neuropathies', *Ann N Y Acad Sci*, 883, 310-20.

Zimmermann, R., Lass, A., Haemmerle, G. and Zechner, R. (2009) 'Fate of fat: the role of adipose triglyceride lipase in lipolysis', *Biochim Biophys Acta*, 6, 494-500.

Zirzow, G. C., Sanchez, O. A., Murray, G. J., Brady, R. O. and Oldfield, E. H. (1999) 'Delivery, distribution, and neuronal uptake of exogenous mannose-terminal glucocerebrosidase in the intact rat brain', *Neurochem Res*, 24(2), 301-5.

Appendix

Table 1. Lysosomal enzyme activities (nmol/min/ml) in blood sera of wild-type, heterozygote (*nym*/+) and *nym* (*nym/nym*) mouse

Lysosomal enzyme	wild-type (+/+)	*nym*/+	*nym/nym*
β-Hexosaminidase (nmol/min/ml)	86.94±7.32	144.02±7.21	1094.69±68.90
β-Mannosidase (nmol/min/ml)	10.49±0.57	11.88±1.76	29.07±1.84
α-Mannosidase (nmol/min/ml)	50.30±4.12	119.13±7.23	1433.02±144.98
β-Glucoronidase (nmol/min/ml)	6.96±0.54	6.43±1.06	28.88±6.46
β-Galactosidase (nmol/min/ml)	8.13±1.24	6.98±0.93	63.58±7.30
α-Galactosidase (nmol/min/ml)	2.12±0.25	1.90±0.13	2.20±0.13
Glucocerebrosidase (pmol/min/ml)	3.31±0.4	3.36±0.45	3.47±0.28

Table 2. Lysosomal enzyme activities (nmol/mg/h) in brain lysate of wild-type and *nym* (*nym/nym*) mouse

Lysosomal enzyme	wild-type (+/+)	*nym/nym*
β-Hexosaminidase (nmol/mg/h)	1.39±0.19	2.24±0.22
β-Mannosidase (nmol/mg/h)	0.71±0.09	0.70±0.09
α-Mannosidase (nmol/mg/h)	0.47±0.07	0.70±0.02
β-Glucoronidase (nmol/mg/h)	0.54±0.07	0.87±0.05
β-Galactosidase (nmol/mg/h)	1.60±0.24	0.99±0.10
α-Galactosidase (pmol/mg/h)	42.42±11.57	45.34±3.41
Glucocerebrosidase (pmol/mg/h)	16.70±3.96	16.98±5.97

Table 3. List of antibodies

Antibody	manufacturer	species	WB	IF	Catalog No./clone
Lamp1	Abcam	rat	1:200	-	ab25245
Npc2	Santa Cruz	rabbit	1:200	-	H-125
HA	Roche	rat	1:1,000	-	CF10
β-tubulin	Sigma	mouse	1:1,000	-	T8328
kinesin	Cytoskeleton, Inc.	rabbit	1:1,000	-	AKIN01
Akt	Cell Signalling	rabbit	1:1,000	-	4691
pAkt	Cell Signalling	rabbit	1:1,000	-	4060
Calbindin D28k	Swant	rabbit	1:10,000	-	300
myc	Abcam	rabbit	-	1:300	ab39688
GM130	Abcam	mouse	-	1:250	ab52649
PDI	Abcam	mouse	-	1:100	ab2792
GFAP	Sigma	mouse	-	1:400	G3893
repo	Developmental Studies Hybridoma Bank	mouse	-	1:200	8D12
MYHC1	German Collection of Microorganisms and Cell Culture	mouse	-	1:200	B8-F8
MYHC2A	German Collection of Microorganisms and Cell Culture	mouse	-	1:200	SC-71
MYHC2B	German Collection of Microorganisms and Cell Culture	mouse	-	1:100	BF-F3

WB: Westernblot, IF: Immunofluorescence

THE JOURNAL OF BIOLOGICAL CHEMISTRY VOL. 289, NO. 39, pp. 26709–26721, September 26, 2014

A Novel Mouse Model of a Patient Mucolipidosis II Mutation Recapitulates Disease Pathology*

Received for publication, June 5, 2014, and in revised form, July 31, 2014 Published, JBC Papers in Press, August 8, 2014, DOI 10.1074/jbc.M114.586156

Leigh Paton[‡1], Emmanuelle Bitoun[‡1], Janet Kenyon[‡], David A. Priestman[§2], Peter L. Oliver[‡], Benjamin Edwards[‡], Frances M. Platt[§3], and Kay E. Davies[‡4]

From the [‡]Medical Research Council Functional Genomics Unit, Department of Physiology, Anatomy, and Genetics, University of Oxford, South Parks Road, Oxford OX1 3PT, United Kingdom and the [§]Department of Pharmacology, University of Oxford, Mansfield Road, Oxford OX1 3QT, United Kingdom

Background: Mucolipidosis II is a severe lysosomal storage disorder, fatal in childhood and lacking drug treatments.
Results: This novel mouse model of a mucolipidosis II patient mutation recapitulates the human pathology.
Conclusion: Mouse models based on patient mutations are more valuable to study mucolipidosis II than a knock-out of the gene.
Significance: This novel mouse model will be useful for future drug development.

Mucolipidosis II (MLII) is a lysosomal storage disorder caused by loss of *N*-acetylglucosamine-1-phosphotransferase, which tags lysosomal enzymes with a mannose 6-phosphate marker for transport to the lysosome. In MLII, the loss of this marker leads to deficiency of multiple enzymes and non-enzymatic proteins in the lysosome, leading to the storage of multiple substrates. Here we present a novel mouse model of MLII homozygous for a patient mutation in the *GNPTAB* gene. Whereas the current gene knock-out mouse model of MLII lacks some of the characteristic features of the human disease, our novel mouse model more fully recapitulates the human pathology, showing growth retardation, skeletal and facial abnormalities, increased circulating lysosomal enzymatic activities, intracellular lysosomal storage, and reduced life span. Importantly, MLII behavioral deficits are characterized for the first time, including impaired motor function and psychomotor retardation. Histological analysis of the brain revealed progressive neurodegeneration in the cerebellum with severe Purkinje cell loss as the underlying cause of the ataxic gait. In addition, based on the loss of Npc2 (Niemann-Pick type C 2) protein expression in the brain, the mice were treated with 2-hydroxypropyl-β-cyclodextrin, a drug previously reported to rescue Purkinje cell death in a mouse model of Niemann-Pick type C disease. No improvement in brain pathology was observed. This indicates that cerebellar degeneration is not primarily triggered by loss of *Npc2* function. This study emphasizes the value of modeling MLII patient mutations to generate clinically relevant mouse mutants to elucidate the pathogenic molecular pathways of MLII and address their amenability to therapy.

The rare autosomal recessive lysosomal storage disorder MLII[5] (originally called I-cell disease (1)) presents with delayed motor milestones and cognitive impairments, severe skeletal abnormalities, coarse facial features, thickened skin, and early death in the first decade of life due to cardiac and pulmonary failure (2, 3). The disease is caused by the loss of multiple hydrolases in the lysosome due to a defect in their targeting to lysosomes. Waste material in the cell is targeted to the lysosome by the endocytic or autophagic pathways. Here lysosomal enzymes degrade and recycle this waste material. Thus, this mechanism is important for the maintenance of cells and tissues (4). The majority of acid hydrolases are targeted for transport to lysosomes via the presence of a surface mannose 6-phosphate (M6P) marker that is recognized by its cognate receptor (5–9). The protein responsible for the synthesis of the M6P marker is dysfunctional in MLII.

Both MLII-causing *GNPTAB* homozygous and compound heterozygous nonsense and frameshift mutations, leading to premature termination codons, have been described. These result in the total loss of the hexameric ($\alpha_2\beta_2\gamma_2$) GlcNAc-1-phosphotransferase (GNPTA) enzyme activity (10–12). GNPTA catalyzes the first step in the synthesis of the M6P marker. Its subunits are encoded by the genes *GNPTAB* and *GNPTG*. *GNPTAB* encodes an initially enzymatic inactive transmembrane precursor protein (13, 14), which is cleaved by the site-1 protease to release catalytically active α- and β-subunits (15). *GNPTG* encodes the soluble γ-subunits of the GNPTA complex and has been shown to facilitate the recognition process (16).

Loss of GNPTA function leads to missorting and hypersecretion of lysosomal enzymes into the circulation, making them detectable in the blood sera of MLII patients (17). Due to the lack of hydrolases in the lysosomes, their substrates accumulate, leading to lysosomal "storage." Animal models of MLII have been described with the feline model of MLII (18) recapitulating the human disease most closely, including coarse facial features, behavioral dullness, ataxia, and reduced life span (18, 19). *Gnptab*-depleted zebrafish embryos have been engineered using morpholinos and showed skeletal abnormalities, craniofacial defects, and reduced motility. In addition, developmental studies were more accessible with this model, and changes in the expression pattern of chondrogenic factors were shown (20,

* This work was supported by the Medical Research Council.
⌘ *Author's Choice*—Final version full access.
[1] Both authors contributed equally to this work.
[2] Supported by the Mizutani Foundation, Japan.
[3] Recipient of a Royal Society Wolfson Research Merit Award.
[4] To whom correspondence should be addressed. Tel.: 44-1865-285880; Fax: 44-1865-285878; E-mail: kay.davies@dpag.ox.ac.uk.
[5] The abbreviations used are: MLII, mucolipidosis II; NPC, Niemann-Pick type C; M6P, mannose 6-phosphate; GNPTA, GlcNAc-1-phosphotransferase; MEF, mouse embryonic fibroblast; ER, endoplasmic reticulum; GM2, monosialoganglioside 2.

21). A *Gnptab* gene trap mouse model has also been described and is characterized by impaired growth, retinal degeneration, lesions in secretory epithelial cells of exocrine glands, and elevated levels of serum acid hydrolases (22, 23). This mutant presented with a relatively normal life span and did not develop characteristic disease features, such as skeletal and facial abnormalities. Here, we describe a novel mouse model, which was recovered from an *N*-ethyl-*N*-nitrosourea screen, termed Nymphe (*nym*), which carries the previously reported patient mutation Y888X (12). Importantly, the Nymphe mouse (*nym/nym*) recapitulates the major features of the human disease and, for the first time, enables a detailed behavioral characterization of the motor dysfunction and psychomotor retardation. Histological analysis of the brain revealed progressive neurodegeneration of Purkinje neurons in the cerebellum, probably the underlying cause of ataxia. Also, there was complete loss of Npc2 protein expression. Purkinje cell pathology in the Nymphe mouse was treated with 2-hydroxypropyl-β-cyclodextrin, a drug previously reported to delay Purkinje cell loss in a mouse model of NPC disease. This approach did not rescue Purkinje cell loss, indicating that the loss of Npc2 expression in the Nymphe mouse brain is not the primary molecular mechanism triggering Purkinje cell degeneration.

EXPERIMENTAL PROCEDURES

Animals—Animal work was approved by the University of Oxford Ethics Panel and was carried out in accordance with United Kingdom Home Office regulations. The *nym*/*nym* mouse was identified from a phenotype-driven screen of the progeny from Balb/cAnNHsd *N*-ethyl-*N*-nitrosourea mutagenized mice crossed to female C3H/HeNHsd engineered at MRC Harwell. The colony was maintained by back-crossing against C3H/HeNHsd.

Genetic Mapping and Mutation Detection—Mutant mice were initially screened for genome-wide SNP markers between the parental C3H/HeH and BALB/c (*N*-ethyl-*N*-nitrosourea-treated) strains, followed by mapping using additional microsatellite markers to an interval between D10Mit42 and D10Mit178. Further fine mapping was carried out to reduce the critical subchromosomal region to 6 Mb between SNPs 86559223 and 92592980 (NCBI build 37). The *nym* mutation was identified by PCR and direct sequencing of all genes present within this interval, including the coding regions and exon-intron boundaries (primer sequences are available upon request). Analysis of mutant mice was conducted after a minimum of 15 back-crosses, ensuring only the subchromosomal region being contained within the wild-type background. Genotyping for the presence of the *nym* mutation was carried out using the primers *nym* forward (5′-GGAGACGGTGACATACAAAAATCT-3′) and *nym* reverse (5′-CACTGGATGCTCTAAGGAAGATAT-3′) and subsequent digest with MseI because this can cleave when the mutation is present.

RNA Extraction and RT-PCR—Whole brain was dissected from 3-month-old wild type and *nym*/*nym* mice. RNA was extracted using the RNeasy kit (Qiagen). Total RNA was reverse transcribed using Expand reverse transcriptase (Roche Applied Science). Total cDNA and genomic DNA were subjected to semiquantitative analysis. Cycling conditions were as follows: Gnptab, 1 μg of cDNA using 29 cycles; 18 S, 1 μg of cDNA using 16 cycles. Primers used were *Gnptab* forward (5′-GGCCTCAGAGTCAGAAAG-3′), *Gnptab* reverse (5′-CAACGCAAGCATAAAACAGC-3′), 18 S forward (5′-GCGGCTTGGTGACTCTAGAT-3′), and 18 S reverse (5′-CCCTCTCCGGAATCGAAC-3′). Samples were run in duplicates, and the sample loading was normalized by using the 18 S loading control. Blots were analyzed using ImageJ, and bands were quantified.

Plasmid Construction—The full-length cDNA sequence of mouse Gnptab (NM_001004164) was subcloned into pcDNA3 (Invitrogen) in frame with a C-terminal c-Myc tag for expression in mammalian cells. Mutant versions of this construct containing the *nym* mutation were engineered by QuikChange site-directed mutagenesis (Agilent Technologies) according to the manufacturer's instructions (primer sequences available upon request).

Cell Culture, Transfection, and Immunofluorescence—HEK 293 cells and mouse embryonic fibroblasts (MEFs) were cultured in DMEM supplemented with L-glutamine, 10% FBS, and 1% penicillin/streptomycin at 37 °C, 5% CO_2. MEFs were isolated at day 12.5 after terminated mating. Cells were seeded onto poly-L-lysine-coated glass coverslips. pCDNA3-*Gnptab* wild-type and *nym*/*nym* mutant constructs were transfected into HEK 293 cells using Fugene 6 (Roche Applied Science). pEGFP-N1 (Clontech) was used to control for transfection efficiency. For immunocytochemistry, cells were fixed, blocked, and stained for 1 h at room temperature each with primary (Myc (1:200 dilution) from Sigma; GM130 (1:250) from Abcam; protein-disulfide isomerase (1:150) from Abcam) and Alexa Fluor-conjugated secondary antibodies (1:400; Invitrogen). Slides were imaged under a phase-contrast microscope (Leica), and images were captured using the Axiovision software (Axiocam).

Western Blotting—Tissue extracts were prepared in 10 mM Tris-HCl, pH 8, 10 mM NaCl, 1 mM EDTA, pH 8, 1% Triton X-100, and protease inhibitors (Roche Applied Science). Protein concentration of the lysates was determined by a BCA assay (Pierce). After primary antibody (anti-β-tubulin-1 (1:1000) was obtained from Sigma and anti-NPC2 (H-125) (1:100) from Santa Cruz Biotechnology, Inc.) and peroxidase-conjugated secondary antibody (1:5000) incubation (Invitrogen), blots were developed with the ECL kit (GE Healthcare). Band intensity relative to internal controls was analyzed using ImageJ software.

Immunohistochemistry and Histology—For immunohistochemical analysis, the trachea and pancreas were dissected, fixed overnight in 4% paraformaldehyde, and cryoprotected in 30% sucrose, and tissue was embedded in OCT and sectioned. The tissue sections were stained with H&E for histopathological examination. To investigate CNS pathology, mice were transcardially perfused with 4% paraformaldehyde, and brains were dissected and postfixed overnight and cryoprotected in sucrose before embedding in OCT. Slides were blocked for 1 h and incubated overnight at 4 °C with primary antibodies (anti-D28K calbindin (1:10,000) from Swant; anti-GFAP (1:400) from Sigma). Primary antibody staining was visualized using the Vectastain ABC Elite kit (Vector Labs) or Alexa Fluor 488 secondary antibodies (Invitrogen) for immunofluorescence. For luxol fast blue staining, fresh frozen brain sections were incubated at

56 °C overnight in 0.1% luxol fast blue solution (Solvent Blue 38, Sigma). Excess stain was rinsed off with 95% ethyl alcohol followed by distilled water. Slides were differentiated in 0.05% lithium carbonate solution for 2 min, followed by 70% ethyl alcohol for 1 min, and rinsed in distilled water. This step was repeated three times until the gray matter was clear, and the white matter was sharply defined. Periodic acid-Schiff staining was carried out using a periodic acid-Schiff kit (Sigma) as instructed by the manufacturer. Filipin complex (Sigma) was used at a working concentration of 10 μg/ml. Brain sections were incubated for 3 h at room temperature in the dark. Slides were imaged as described above.

Lysosomal Enzyme Assay—Blood sera were collected from adult wild-type ($n = 8$), *nym*/+ ($n = 8$), and *nym/nym* mice ($n = 6$) at 12 weeks of age by severing the jugular vein after CO_2 narcosis. Blood serum was separated by centrifugation and stored at −20 °C until assayed. Activities of β-hexosaminidase were assayed with 5 mM 4-nitrophenyl *N*-acetyl-β-D-glucosaminide (Sigma), β-galactosidase with 5 mM *p*-nitrophenyl-β-D-galactopyranoside (Sigma), β-glucuronidase with 5 mM 4-nitrophenyl β-D-glucuronide (BioChemika), α-mannosidase with 5 mM 4-nitrophenyl α-D-mannopyranoside (Sigma), β-mannosidase with 5 mM 4- nitrophenyl β-D-mannopyranoside (Sigma), α-galactosidase with 5 mM 4-methylumbelliferyl-α-D-galactopyranoside (Sigma), and β-glucocerebrosidase with 5 mM 4-methylumbelliferyl-β-glucoside. Blood sera and brain lysate was incubated with 5 mM substrate at 37 °C for 1 h. Reactions were stopped by the addition of 0.1 M glycine NaOH solution (pH 10.3), and the fluorescence was read at 399 nm. Activities were expressed as nmol of substrate cleaved/mg of protein/h. The specific activities of the wild-type were set to 1, and -fold changes of *nym/nym* are expressed as ratio to the wild-type.

Behavioral Testing—Behavioral testing was carried out on mice at 3, 7, and 11 months of age.

Rotarod—A commercial rotarod device was used (Accelerating model, Ugo Basile, Biological Research Apparatus, Varese, Italy) consisting of a grooved plastic beam 5 cm in diameter. Mice were placed on the beam (revolving at the default 5 rpm), and after 1 min, the rod speed was gradually accelerated to a maximum of 30 rpm over 4 min by electronic control of the motor. Latency to fall in each trial was recorded.

Inverted Screen—A 90-cm^2 screen of wire mesh consisting of 12 mm^2 of 1-mm diameter wire surrounded by a 10-cm-deep wooden frame was used. The mouse was placed in the center of the wire mesh screen and immediately rotated. The screen was maintained 27 cm above a padded surface. Latency of how long the mice remained upside down on the screen was measured, with a maximum score of 180 s.

Spontaneous Alternation Y-maze—Maze testing was carried out as described previously (25).

Catwalk Automated Quantitative Gait Analysis—Abnormalities in gait were assessed using the Noldus Catwalk gait analysis system (26). Mice were allowed to freely transverse the glass walkway while the video camera recorded the paw contact points. The Catwalk software then assigned identities to the respective paw prints recorded, generating a wide range of parameters. The regularity index acts as a measure of generalized coordination (27) by computing whether the mouse footfalls fall within regular step patterns. Gait regularity tests how consistently the mouse takes "normal strides" compared with "abnormal strides." The base of support is the average width between either the front paws or the hind paws.

RESULTS

Gnptab Is the Gene Mutated in the Nymphe Mouse—We isolated the recessive *nym* mouse from a large scale chemical mutagenesis screen that we are exploiting to uncover novel genes and pathways essential for the maintenance of nervous system function. This mutant was selected based on its smaller size and ataxic gait. Haplotype analysis localized the *nym* mutation to a genetic interval of 6 Mb on mouse chromosome 10, between markers *D10Mit42* and *D10Mit178*. PCR and direct sequencing of all 28 protein-coding genes within the interval including exonic regions and exon-intron boundaries revealed a single non-synonymous homozygote point mutation in exon 13 of the *Gnptab* gene. This mutation introduces a T to A substitution at nucleotide 2601 of the cDNA sequence (T2601→A) (Fig. 1*A*) that changes the tyrosine into a premature stop codon at position 867 of the protein sequence (Y867X) within an evolutionarily conserved spacer region 40 residues upstream of the cleavage signal between the α- and β-subunits (Fig. 1*B*). This is predicted to result in the production of a slightly truncated α-subunit (~95% of full length) and a complete lack of the β-subunit. In agreement with the loss of a functional Gnpt enzyme, the counterpart *nym* mutation in the human protein sequence (Y888X) has, in fact, recently been identified in an MLII patient (12). Consistent with nonsense-mediated decay, *Gnptab* transcript levels were reduced by 75% in *nym* mice compared with wild type (Fig. 1*C*). The endoplasmic reticulum (ER) export signal is deleted in the *nym* mutation, and the truncated protein would be expected to remain in the ER; thus, the cellular localization of the mutant protein was investigated. The cytoplasmic domain of the β-subunit contains the (R/K)X(R/K)-type ER export signal and a C-terminal valine, which are both required for cargo-receptor-mediated packaging into COPII vesicles and trafficking of the GNPT precursor protein to the Golgi, where it gets cleaved (28, 29). Subcellular localization of the *nym* Gnpta was monitored in transfected HEK 293 cells. As expected, the wild-type Gnpta protein colocalized with the *cis*-Golgi marker GM130 (Fig. 1*D*, *top*), whereas the *nym* Gnpta protein did not (Fig. 1*D*, *middle*). The *nym* Gnpta protein remained trapped in the ER, as demonstrated by colocalization with protein-disulfide isomerase (Fig. 1*D*, *bottom*, *PDI*), an ER marker. These results confirm that the *nym* mutation indeed leads to a dysfunctional Gnpta enzyme and imply that the *nym* mouse is a novel model of MLII. These findings suggest that truncation mutations present in GNPTAB inhibit ER exit (30).

Growth Retardation and Facial and Skeletal Abnormalities Are Part of the Pathological Features of MLII in the Nymphe Mutant—Prominent features of MLII are growth retardation and facial and skeletal abnormalities (12). Indeed, *nym* mutants remained significantly smaller than wild-type littermates (~60%) throughout life (Fig. 2, *A* and *B*). Facial and skeletal abnormalities were evident from birth, including thickened

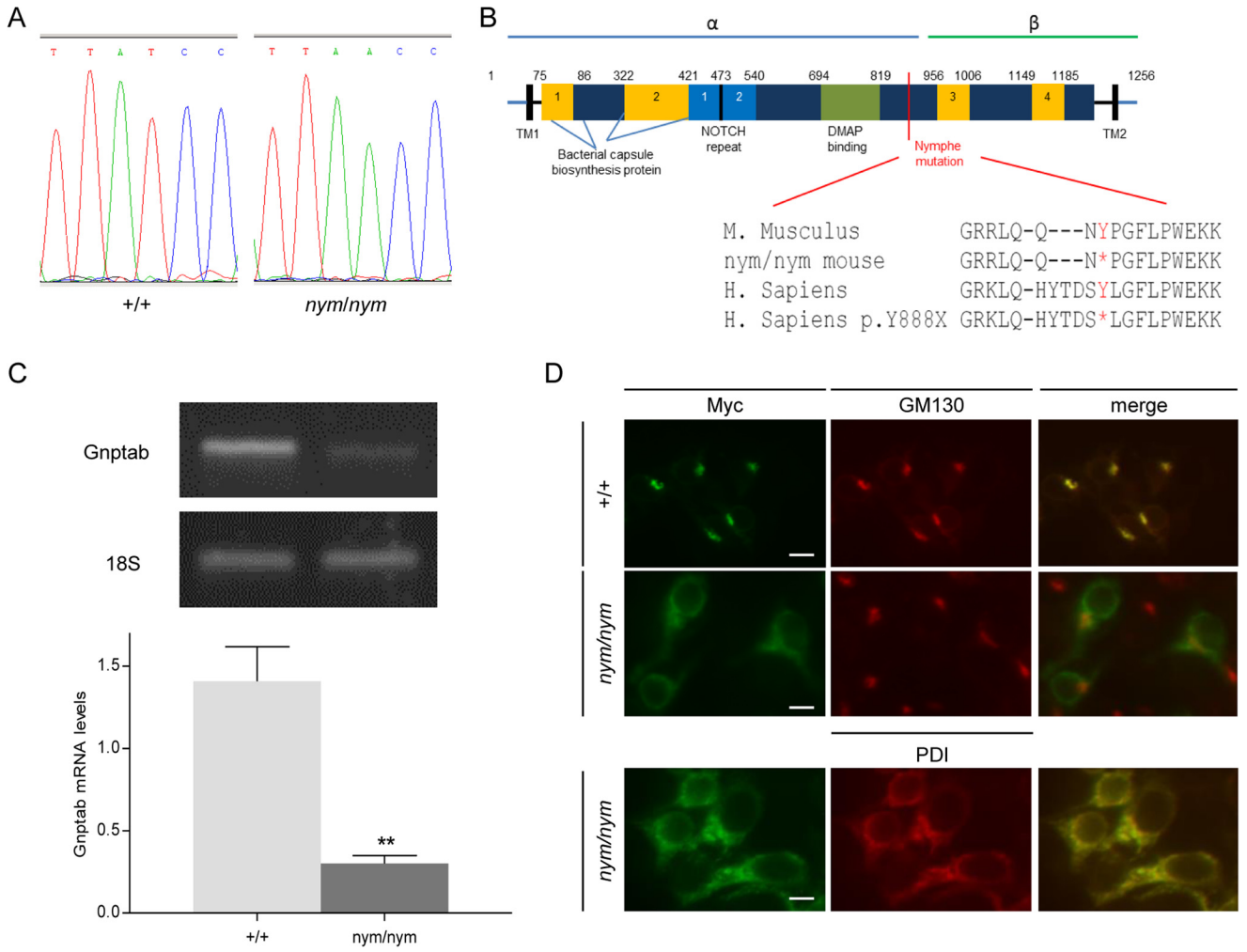

FIGURE 1. ***Gnptab* is the gene mutated in *nym* mutant.** *A*, sequencing of the *Gnptab* locus identified a single nucleotide change resulting in a coding change from a tyrosine residue (TAT) to a premature stop codon (TAA) in the *nym* (*nym/nym*) mouse. *B*, schematic of human GNPTA α/β subunits presenting the location of the *nym* mutation and its conservation from mice to humans (indicated by an *asterisk* in *nym* mutants and for the human (*H. sapiens*) mutation Y888X). The precursor protein is cleaved between Lys-928 and Asp-929 by the site 1 protease to produce two catalytically active α and β subunits. *TM*, transmembrane domain; *aa*, amino acid. This figure is adapted from Ref. 59. *C*, semiquantitative RT-PCR analysis ($n = 4$) reveals that the mRNA is reduced by 75%. Results are expressed as relative levels after normalization for the internal control 18 S. *D*, intracellular localization of wild-type and mutant Gnpta in HEK 293 cells. Cells were fixed and stained with monoclonal antibodies against the Myc tag (*green*), the *cis*-Golgi marker protein GM130 (*red*), or the ER marker protein, protein-disulfide isomerase (*PDI*; *red*). In *merged images*, *yellow* indicates colocalization. *Scale bars*, 15 μm. Values are expressed as mean S.E. (*error bars*) ($n = 8$; *, $p < 0.05$; **, $p < 0.01$).

eyelids and a flat profile with reduced nasal bridge (Fig. 2, *A* and *C*), as well as severe deformities that affect most prominently the back, in particular the spine, identified as kyphosis (Fig. 2*D*). In addition, *nym* mutants had an unusually stiff and thick skin. This presentation indeed resembles closely that of MLII patients with the same characteristic features. *nym* mice also displayed increased mortality compared with controls, and survival fell below 50% by 60 weeks of age (Fig. 2*E*).

Characteristic features of the pathology of MLII, used for the diagnosis of patients, are increased activities of lysosomal hydrolases found in the blood sera and intracellular accumulation of inclusion bodies (31). In the serum of *nym* mice, activities of the lysosomal hydrolases β-hexosaminidase, β-galactosidase, α-mannosidase, and β-mannosidase were increased by 2.5–30-fold compared with wild-type controls (Fig. 3*A*), which is consistent with the values reported in the *Gnptab* knock-out mouse and MLII patients (32). Lysosomal enzyme activities for blood sera in nmol/min/ml can be seen in Table 1. Fibroblasts, secretory organs, and connective tissue have been shown to be severely affected by inclusion bodies in MLII. Hence, we analyzed cytoplasmic inclusions by staining MEFs, pancreatic acinar cells as a sample for secretory tissue and chondrocytes in the cartilage of the trachea as a sample for connective tissue. The characteristic inclusion bodies (indicative of lysosomal storage) were clearly present in embryonic fibroblasts from *nym* mice (Fig. 3*B*). Chondrocytes in the cartilage of the trachea were enlarged, with the cytoplasm filled by inclusion bodies and abundant microvacuoles (Fig. 3*C*, *top*). In contrast, wild-type chondrocytes had low basic cytoplasm, containing a single clear vacuole. In addition *nym* chondrocytes were not affected by fixation-dependent shrinkage as much as wild-type chondrocytes (Fig. 3*C*, *top*). Pancreatic sections showed disorganization of tissue structure, including enlargement of acinar cells by the presence of large vacuoles containing faint granular material (Fig. 3*C*, *bottom*). Similar findings have previously been reported in the *Gnptab* gene trap mouse (22).

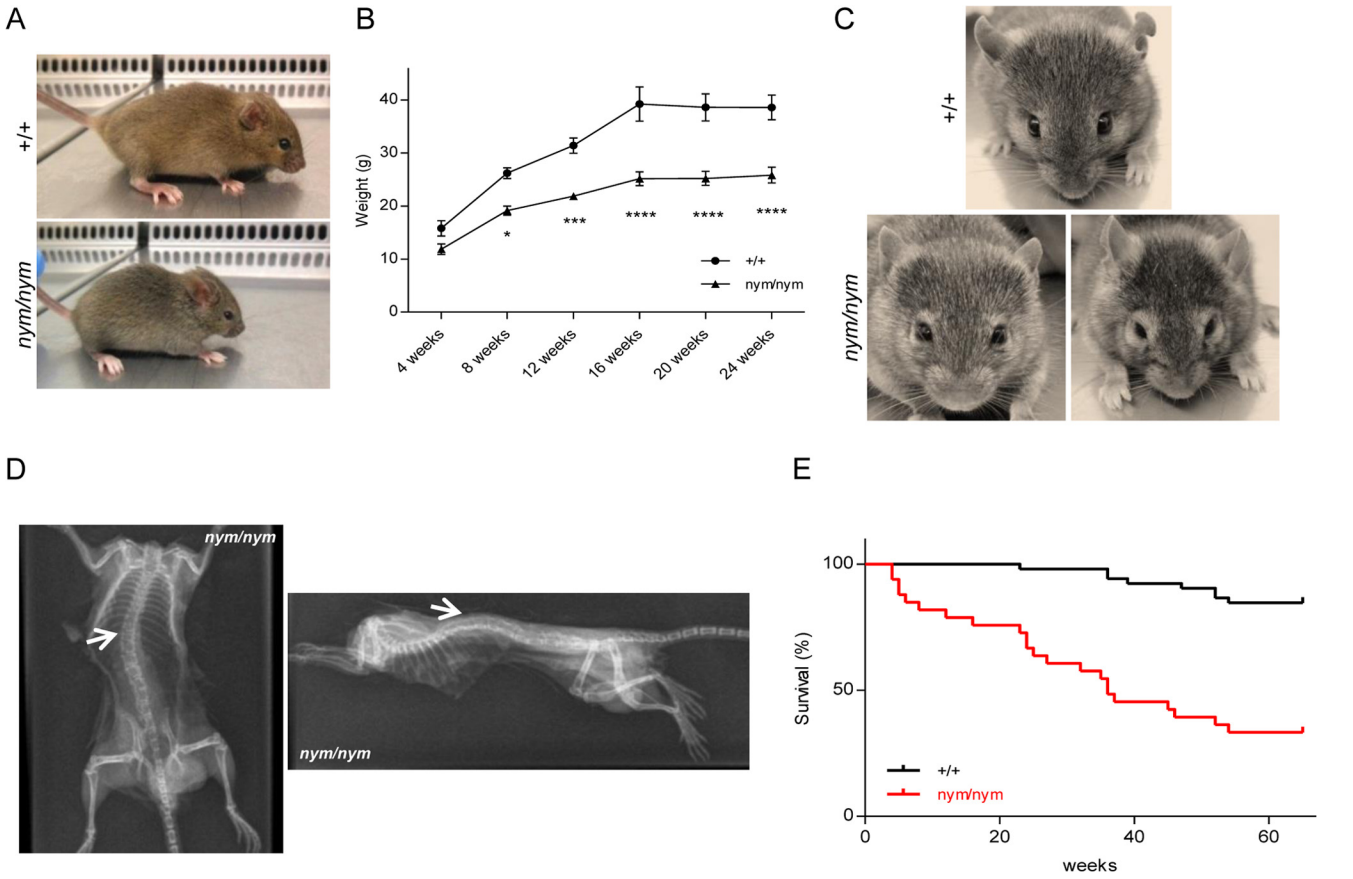

FIGURE 2. **Growth retardation, facial dysmorphism, and reduced life span.** *A*, 1-month-old *nym* (*nym/nym*) mice show reduced body size and skeletal abnormalities (*e.g.* facial dysmorphism and curvature of the spine) in comparison with wild-type (+/+) littermates. *B*, body weight progression of *nym* mice is reduced compared with wild-type littermates. *C*, facial phenotype progresses with age. Particularly evident is the thickening of the eyelids. *D*, whole body exotic dorso-ventral view of the 12-month-old *nym* mouse (*left*) and whole body exotic lateral view of the 12-month-old *nym* mouse (*right*). *White arrows*, abnormal curvature (*left*) and hunched back (*right*). *E*, Kaplan-Meier analysis of wild-type and *nym* mice (+/+, $n = 52$; *nym/nym*, $n = 33$). Values are expressed as mean ± S.E. (*error bars*) ($n = 8$; *, $p < 0.05$; **, $p < 0.01$; ***, $p < 0.001$; ****, $p < 0.0001$).

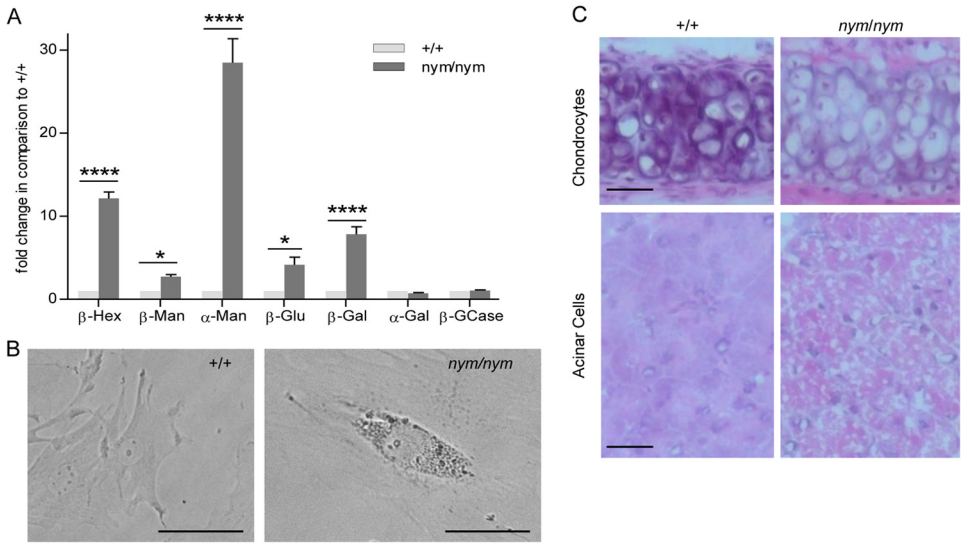

FIGURE 3. **Increased lysosomal enzyme activity in blood sera and inclusion bodies present in mouse fibroblasts, secretory and connective tissue.** *A*, the relative enzymatic activities of the lysosomal hydrolases β-Hexosaminidase (*β-Hex*), β-mannosidase (*β-Man*), α-mannosidase (*α-Man*), β-glucuronidase (*β-Glu*), β-galactosidase (*β-Gal*), α-galactosidase (*α-Gal*), and β-glucocerebrosidase (*β-GCase*) were measured in blood sera of 3-month-old wild-type (+/+) and *nym (nym/nym)* mice. The specific activities of the wild-type were set to 1. Values are expressed as mean ± S.E. (*error bars*) ($n = 8$; *, $p < 0.05$; **, $p < 0.01$; ***, $p < 0.001$; ****, $p < 0.0001$). *B*, light microscopy imaging of MEFs isolated from wild-type and *nym* embryos (E12.5). Accumulation of inclusion bodies present in the *nym* MEFs. *Scale bar*, 40 μm. *C*, *top*, the cytoplasm of hypertrophic chondrocytes is distended by microvacuoles in the *nym* mouse. These inclusions are aggregates of polysaccharides that increase in storage material with age. *Bottom*, marked disorganization of the pancreas in the *nym* mouse with tightly packed cells distended by large vacuoles. *Scale bar*, 50 μm.

TABLE 1
Lysosomal enzyme activities (nmol/min/ml) in blood sera of wild-type, heterozygote (*nym*/+), and *nym* (*nym/nym*) mouse

Lysosomal enzyme	Wild type (+/+)	*nym*/+	*nym/nym*
β-Hexosaminidase (nmol/min/ml)	86.94 ± 7.32	144.02 ± 7.21	1094.69 ± 68.90
β-Mannosidase (nmol/min/ml)	10.49 ± 0.57	11.88 ± 1.76	29.07 ± 1.84
α-Mannosidase (nmol/min/ml)	50.30 ± 4.12	119.13 ± 7.23	1433.02 ± 144.98
β-Glucoronidase (nmol/min/ml)	6.96 ± 0.54	6.43 ± 1.06	28.88 ± 6.46
β-Galactosidase (nmol/min/ml)	8.13 ± 1.24	6.98 ± 0.93	63.58 ± 7.30
α-Galactosidase (nmol/min/ml)	2.12 ± 0.25	1.90 ± 0.13	2.20 ± 0.13
Glucocerebrosidase (pmol/min/ml)	3.31 ± 0.4	3.36 ± 0.45	3.47 ± 0.28

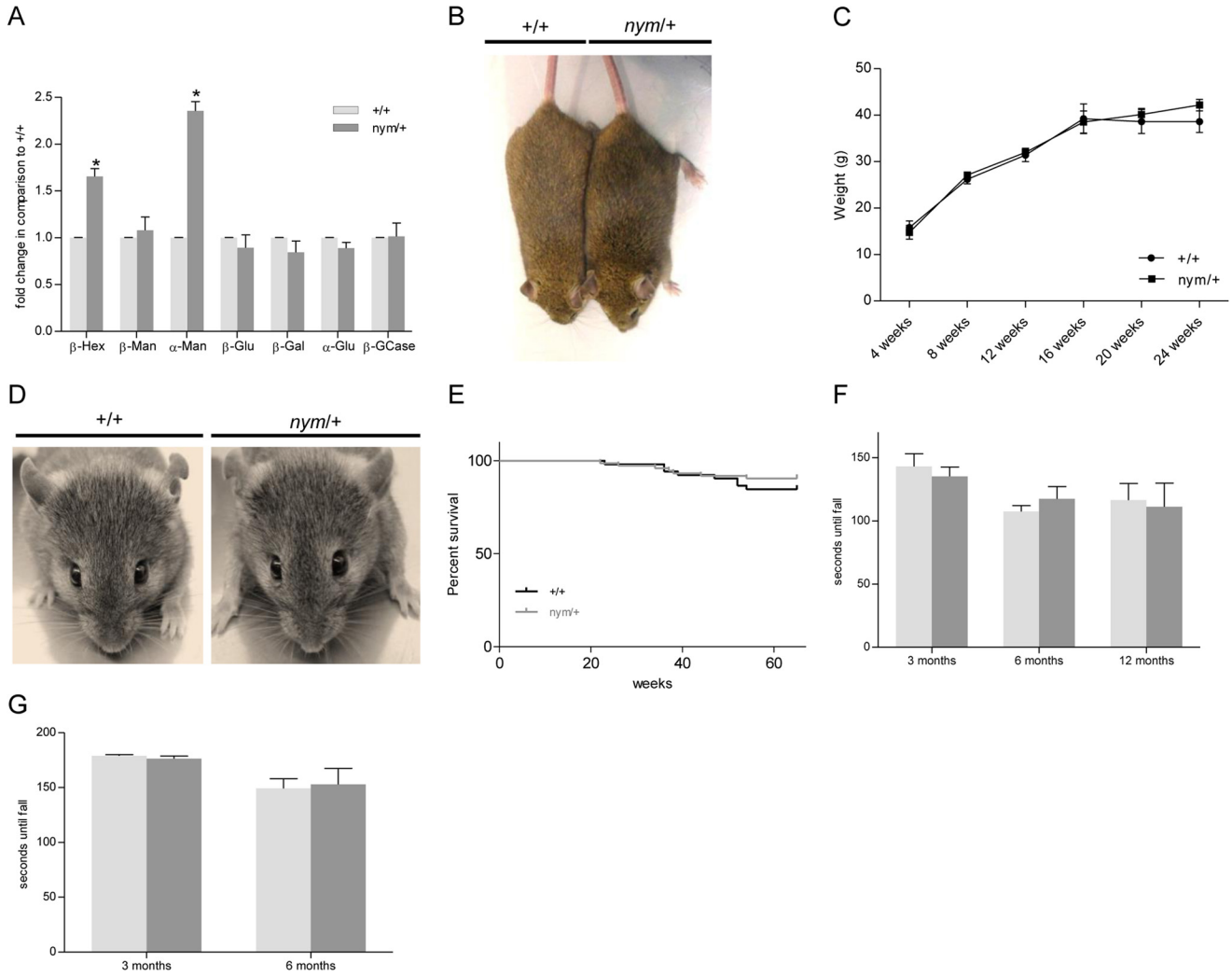

FIGURE 4. **The *nym* heterozygote mouse shows no obvious pathology except for an increase in enzymatic activity similar to carriers of mucolipidosis II.** *A*, the relative enzymatic activities of the lysosomal hydrolases β-Hexosaminidase (*β-Hex*), β-mannosidase (*β-Man*), α-mannosidase (*α-Man*), β-glucuronidase (*β-Glu*), β-galactosidase (*β-Gal*), α-Galactosidase (*α-Gal*), and β-glucocerebrosidase (*β-GCase*) were measured in blood sera of 3-month-old wild-type (+/+) and *nym*/+ mice. The specific activities of the wild type were set to 1. Three-month-old heterozygote (*nym*/+) mice are similar in size to the wild-type (+/+) littermates (*B*), and body weight progression of *nym*/+ mice is not significantly different from that of wild-type mice (*C*). *D*, facial phenotype of the *nym*/+ and wild-type mouse are no different. *E*, Kaplan-Meier analysis of wild-type and *nym*/+ mice (+/+, $n = 52$; *nym*/+, $n = 82$). *nym*/+ mice present with the same motor coordination on the rotarod (*F*) and muscle strength (*G*), which was measured on the inverted screen, as the wild-type littermate. Values are expressed as mean ± S.E. (*error bars*) ($n = 8$; *, $p < 0.05$; **, $p < 0.01$; ***, $p < 0.001$; ****, $p < 0.0001$).

Mating of *nym* mutants was only successful in 9% of breeding pairs, indicating infertility or incapacity of females to carry pups to term. Furthermore, *nym* mutants were born with a reduced frequency of 15% instead of the expected 25% Mendelian frequency, which implies reduced survival *in utero*. An increased frequency of *nym* males also presented with penile prolapse from 3 months of age. Despite a 1.7-fold increase in β-hexosaminidase and 2.4-fold increase in α-mannosidase (Fig. 4*A*) for the heterozygote (*nym*/+) mice in comparison with the wild-type control, no overt phenotype was displayed in the *nym*/+ mice. The *nym*/+ mice were indistinguishable from wild-type controls in fertility, size, body weight progression (Fig. 4, *B* and *C*), facial features (Fig. 4*D*), survival (Fig. 4*E*), motor coordination, and muscle strength (Fig. 4, *F* and *G*).

Our mouse presents molecular and cellular features very similar to those characterizing the human form of MLII. We

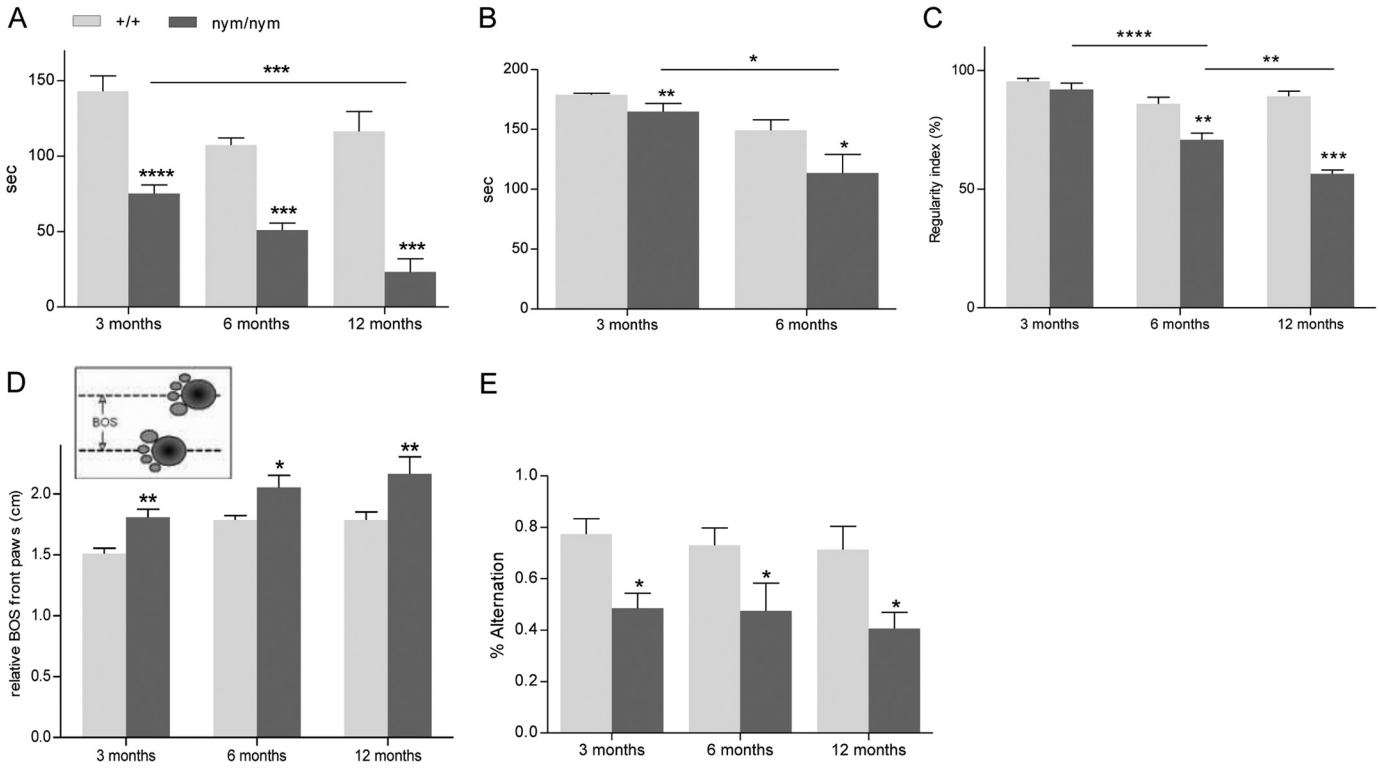

FIGURE 5. **Impairments in motor and cognitive function.** *nym* (*nym/nym*) mice present with reduced motor coordination on the rotarod (*A*) and reduced muscle strength (*B*), which was measured on the inverted screen. *C*, furthermore, gait analysis was conducted via the Noldus Catwalk system, in which most prominently the regularity index was significantly reduced and progressed with age in the *nym* mouse in comparison with the wild-type (+/+) control. *D*, the regularity index was not significant at 3 months; however, the base of support (*BOS*) for the front paws was significantly increased, and this indicates that the front paws are wider apart than in the wild-type control, giving more stability. *E*, percentage of spontaneous alternation in the Y-maze. Values are expressed as mean ± S.E. (*error bars*) ($n = 8$; *, $p < 0.05$; **, $p < 0.01$; ***, $p < 0.001$).

next investigated whether it could mimic the behavioral features as well.

Progressive Neurodegeneration in the Nymphe Mouse—nym mice developed progressive abnormality of gait and showed limb-clasping reflexes from 5 months. Hind limb clasping is an indication of motor imbalance and occurs in various neurodegenerative mouse models (33, 34). Because psychomotor retardation is impaired in MLII patients and is a consequence of slowness in mental activity and locomotion, we first investigated the motor function of the mice using a rotarod and inverted screen to assess motor coordination and strength, respectively. Indeed, the mouse showed reduced muscle strength on the inverted screen test and reduced motor balance and coordination on the rotarod at 3, 6, and 12 months (Fig. 5, *A* and *B*). The rotarod and inverted screen performances also worsened with age, as seen at 6 and 12 months (Fig. 5, *A* and *B*).

Impaired motor strength and coordination was shown with the rotarod and inverted screen; hence, locomotion was subsequently analyzed in more detail by using Noldus Catwalk automated gait analysis (26) to confirm an ataxic gait. A progressive and highly significant reduction of the regularity index, a measure of regular footstep pattern, was observed between 6 and 12 months of age (Fig. 5*C*). Furthermore, the front paw base of support was significantly increased from 3 months of age, indicating reduced stability in the *nym* mice as early as 3 months (Fig. 5*D*).

Because MLII patients have prominent psychomotor retardation with slowness in mental activity, we conducted a preliminary test investigating cognitive deficits in this mouse model. The Y-maze spontaneous alternation task was employed, and it gives a measure of working or short term memory (35). The hippocampus and the frontal cortex have been proposed to be important for these functions (36). In contrast to wild-type mice, which show a high level of performance in this task, *nym* mice just about reach chance levels, which is defined as 50% alternation in choosing an arm at random (Fig. 5*E*). We do not observe a progression of performance with age. These results demonstrate for the first time behavioral deficits in psychomotor performance in a mouse model of MLII, which is a typical finding in patients.

Ataxia typically results from dysfunction of the cerebellum that controls balance and motor coordination; hence, we examined the cerebellum and brain for any gross pathology. The *nym* brain is about 30% smaller than the wild-type brain, including the cerebellum (Fig. 6*A*). We investigated whether the mutant has any defects in the cerebellum structure as well as cell number. Immunohistochemical staining for calbindin showed a substantial loss of Purkinje cells, the main cell output to the cerebellum, in 11-month-old *nym* mice with onset from 7 months (Fig. 6*B*). The Purkinje cell loss and atrophy of brain tissue worsen over time, as seen at 7 months and with about 50% Purkinje cell loss at 11 months (Fig. 6*B*). At 3 months, there is no Purkinje cell loss present; however, we already observe axonal spheroid formation and axonal torpedoes typical of cell atrophy that worsens in severity with age (Fig. 6*C*). Cell death is often accompanied by an inflammatory response and a defect in

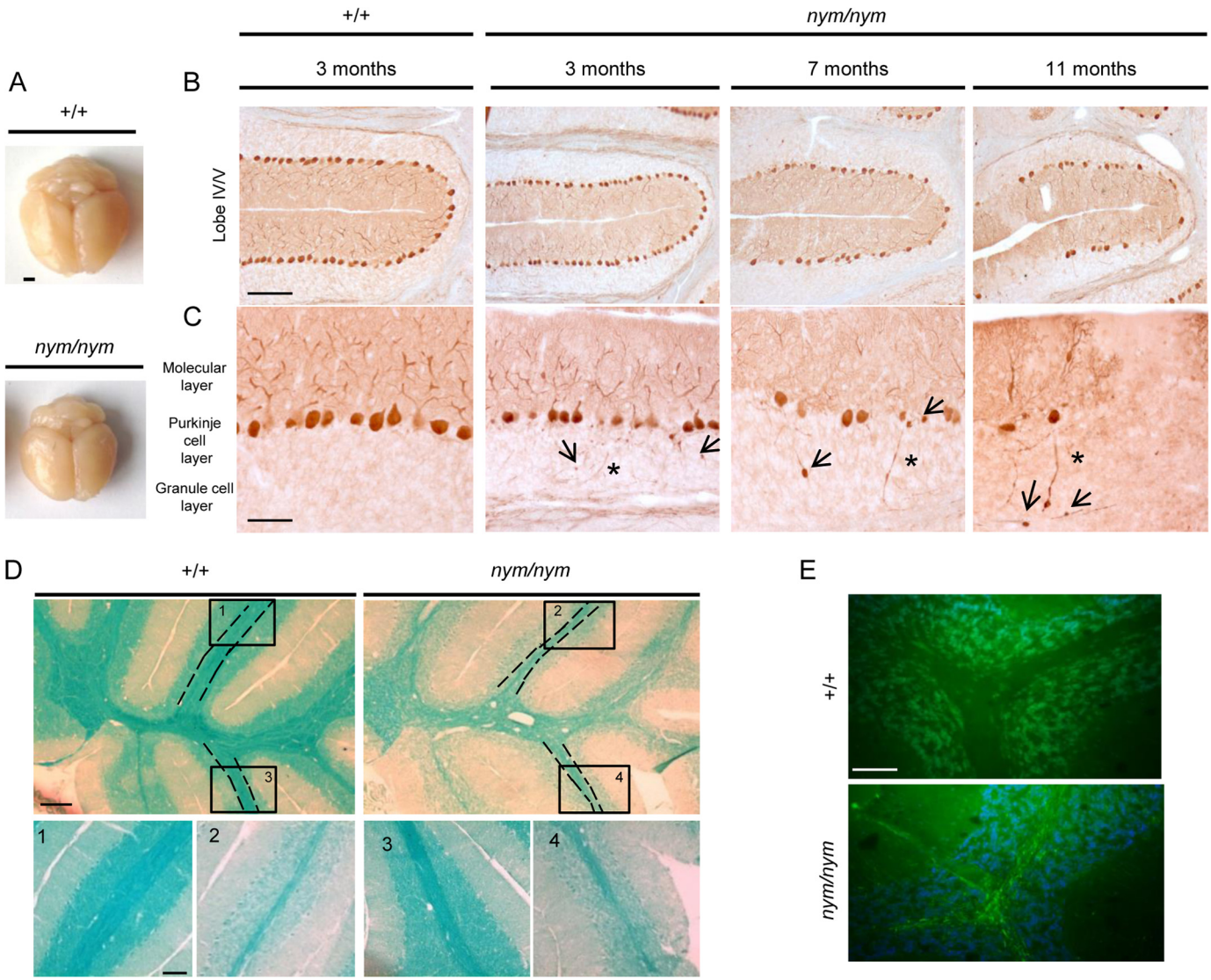

FIGURE 6. **Pathological alterations in the cerebellum.** *A*, the *nym* (*nym/nym*) brain is about 30% smaller than the wild-type (+/+) brain. *Scale bar*, 3 mm. *B*, parasagittal brain sections were immunostained for calbindin. Analysis of PC degeneration in the whole cerebellum in 3-, 7-, and 11-month-old *nym* mice showed progressive PC loss. Lobe IV/V is shown as a representative lobe of the cerebellum. The majority of Purkinje cells in lobe IV/V are still present at 3 months, but only 75% remain at 7 months, and only 40–50% remain at 11 months. *Scale bar*, 100 μm. *C*, higher magnification images of the 3-month-old *nym* brain revealed that axonal spheroids/torpedoes precede Purkinje cell loss. Swelling of Purkinje cell axons (*arrow*) and neuronal torpedoes (*) in the white matter are observed already at 3 months and increase in severity with age. *Scale bars*, 50 μm. *D*, luxol fast blue staining of the cerebellar sections indicates decreased myelination and degeneration of the subcortical white matter in the *nym* mouse. Higher magnification images are shown below in *panels 1–4* (*1* and *3*, +/+; *2* and *4*, nym/nym). *Scale bars*, 200 μm (*top*) and 100 μm (*bottom*). *E*, strong immunoreactivity for glial fibrillary acidic protein (*GFAP*) in the cerebellum of the *nym* mouse brain. *Scale bar*, 50 μm.

myelination. Demyelination of the cerebellum occurred with thinning of the white matter tracts (Fig. 6*D*). The nym mice had a reduced level of lipoprotein, which is the binding partner for the luxol fast blue stain. Inflammatory response was present, as seen by an increase in GFAP immunoreactivity throughout the whole brain of *nym* mice, the most affected tissue being the cerebellum. Astrogliosis was present in the white matter and granular and Purkinje cell layer (Fig. 6*E*).

The activity of lysosomal enzymes was also deregulated in brain homogenates from the *nym* mice. β-Hexosaminidase, α-mannosidase, and β-glucoronidase were increased by 1.5-fold, whereas β-galactosidase was significantly decreased by 30% (Fig. 7*A*). Lysosomal enzyme activities for brain homogenate in nmol/mg/h can be seen in Table 2. Furthermore, we found a loss of expression of the Npc2 protein in the *nym* brain (Fig. 7*B*). Due to this deregulation of lysosomal enzymes, it was of interest to analyze which substrates accumulate in the *nym* brain. Periodic acid-Schiff-stained brain sections revealed increased glycolipid and cholesterol storage in the cerebellum, cortex, and hippocampus (Fig. 7, *C* and *D*). Specifically, the cerebellar molecular layer had increased storage of glycolipids in comparison with the granular layer (Fig. 7*D*, *top*). Large amounts of storage of glycolipids were present in the cortical layers 3–5 and lesser amounts in layers 1 and 2 (Fig. 7*D*, *middle*). Furthermore, the hippocampal layers CA1 and CA3 presented with increased glycolipid storage (Fig. 7*D*, *bottom*). These findings agree with what is observed in NPC mouse models and α-mannosidosis causing GM2 accumulation (37, 38).

Interestingly, the *Npc2* disease mouse model shows a brain pathology very similar to that of the *nym* mouse with Purkinje cell

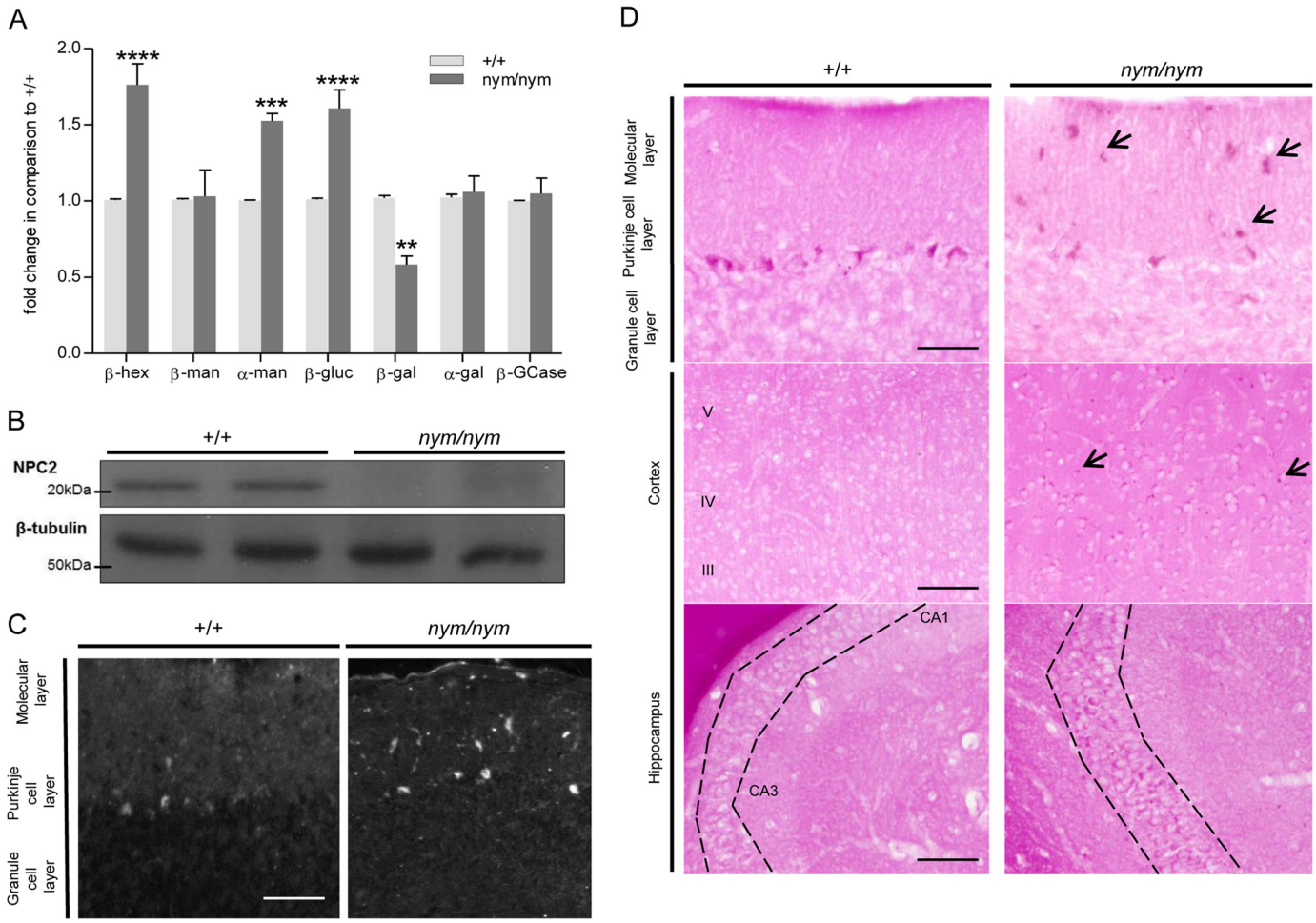

FIGURE 7. **Biochemical alterations in the brain.** *A*, the relative enzyme activities of the lysosomal hydrolases β-hexosaminidase (*β-Hex*), β-mannosidase (*β-Man*), α-mannosidase (*α-Man*), β-glucuronidase (*β-Glu*), β-galactosidase (*β-Gal*), α-galactosidase (*α-Gal*), and β-glucocerebrosidase (*β-GCase*) were measured in whole brain homogenates of wild-type (+/+) and *nym* (*nym/nym*) mice (4 months of age). The specific activities of the wild type were set to 1. Values are expressed as mean ± S.E. (*error bars*) ($n = 4$; *, $p < 0.05$; **, $p < 0.01$; ***, $p < 0.001$; ****, $p < 0.0001$). *B*, representative Western blot showing levels of Npc2 in wild-type and *nym* mice. β-Tubulin was used as a loading control ($n = 4$). *C*, nine-month-old *nym* and wild-type brain sections were stained with filipin for the detection of cholesterol. The molecular layer of the *nym* cerebellum showed increased storage in comparison with the wild-type control. *Scale bar*, 50 μm. *D*, nine-month-old *nym* and wild-type brain sections were stained with periodic acid-Schiff for detection of glycolipids. Increased storage was detected in the cerebellum (*top*, specifically in the molecular layer), the cortex (*middle*, specifically in layers 3–5), and the hippocampus (*bottom*, specifically in layers CA1 and CA3). *Scale bar*, 50 μm.

TABLE 2

Lysosomal enzyme activities (nmol/mg/h) in brain lysate of wild-type and *nym* (*nym/nym*) mouse

Lysosomal enzyme	Wild type (+/+)	*nym/nym*
β-Hexosaminidase (nmol/mg/h)	1.39 ± 0.19	2.24 ± 0.22
β-Mannosidase (nmol/mg/h)	0.71 ± 0.09	0.70 ± 0.09
α-Mannosidase (nmol/mg/h)	0.47 ± 0.07	0.70 ± 0.02
β-Glucoronidase (nmol/mg/h)	0.54 ± 0.07	0.87 ± 0.05
β-Galactosidase (nmol/mg/h)	1.60 ± 0.24	0.99 ± 0.10
α-Galactosidase (pmol/mg/h)	42.42 ± 11.57	45.34 ± 3.41
Glucocerebrosidase (pmol/mg/h)	16.70 ± 3.96	16.98 ± 5.97

degeneration, suggesting that loss of Npc2 function may be a factor driving this aspect of pathogenesis (39, 40). In the NPC disease model, the drug 2-hydroxypropyl-β-cyclodextrin has been reported to delay Purkinje cell loss and is currently in clinical trials for patients with this disorder (41, 42). To test whether dysfunction of the Npc2 pathway is also implicated in the brain pathogenesis of the *nym* mouse, we treated this mutant with 2-hydroxypropyl-β-cyclodextrin for 7 months, when we started seeing Purkinje cell loss. However, we did not see any rescue or delay in the cerebellar pathology at 3 months or at 7 months (Fig. 8, *A–D*), and neither motor improvement was observed at both of these ages (Fig. 8, *E–H*). These findings indicate that the loss of Npc2 function is not the primary pathogenic mechanism that triggers Purkinje cell degeneration in MLII disease.

DISCUSSION

In this study, we describe a novel mouse model of MLII, which carries a premature stop codon mutation previously reported in a patient (12). Importantly, unlike the existing gene knock-out mouse model, it more completely recapitulates the characteristic pathological features observed in patients, including facial and skeletal abnormalities, mislocalization of lysosomal enzymes, abnormal intracellular storage, and also psychomotor retardation, motor dysfunction, and reduced life span (31).

The *nym* mouse resembles closely a recently described knock-in mouse of another MLII human mutation, the G1028X mouse equivalent (43). Both mutations lead to premature stop

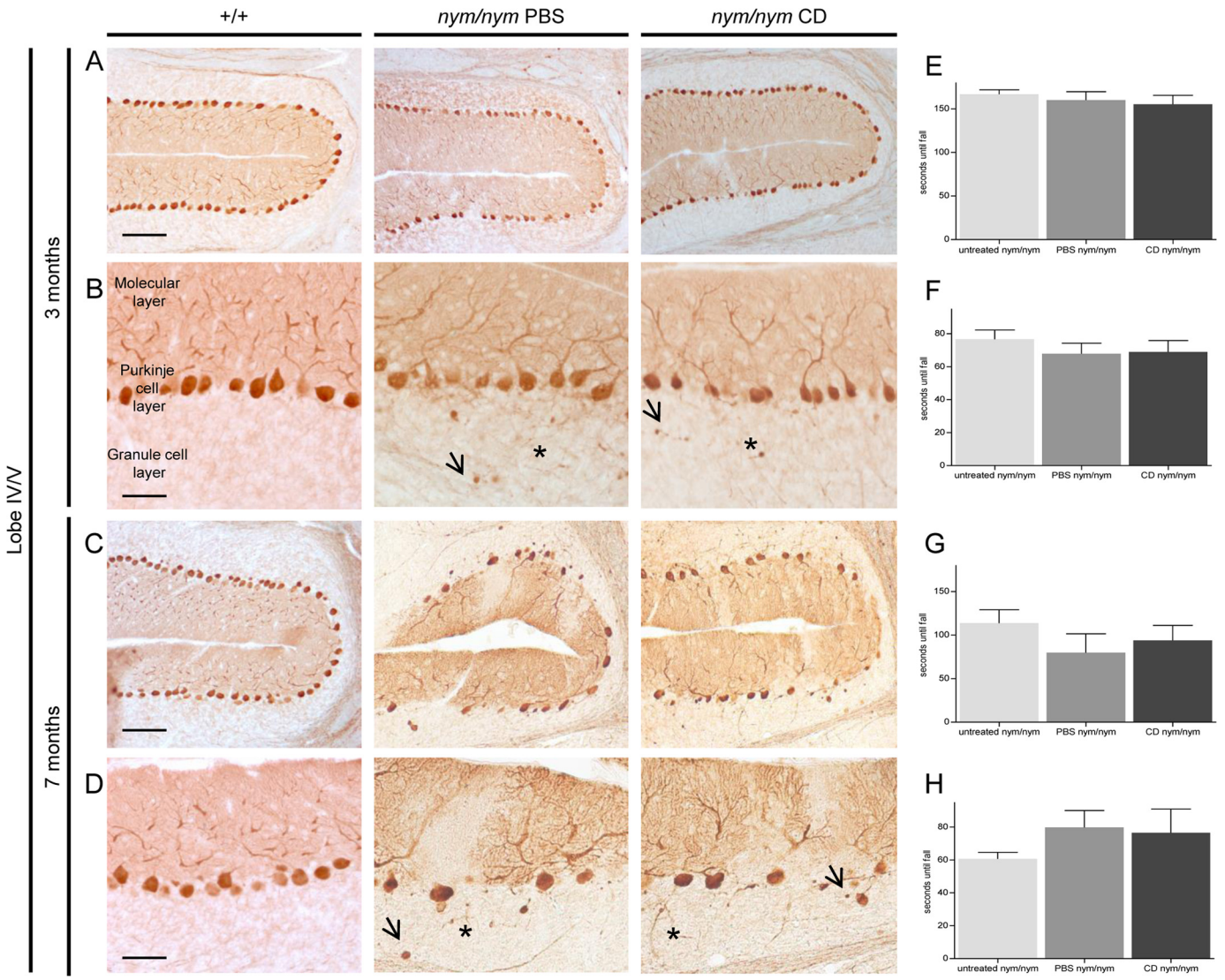

FIGURE 8. **Cyclodextrin does not delay cerebellar pathology and motor impairments.** P7 *nym* (*nym/nym*) mice were injected weekly for 7 months with cyclodextrin (*CD*) at 4000 mg/kg or the vehicle PBS ($n = 7$ in each group). *A*, no PC loss was observed at 3 months, as can be seen in lobe IV/V as a representative lobe of the cerebellum. *Scale bar*, 100 μm. *B*, typical signs of PC degeneration, including swelling of PC dendrites (*arrow*) and axonal torpedoes (*), can be observed. *Scale bars*, 50 μm. *C*, PC loss was observed at 7 months in lobe IV/V as a representation of a lobe of the cerebellum in *nym* PBS- and *nym* CD-treated mice. *Scale bar*, 100 μm. *D*, typical signs of PC degeneration, including swelling of PC dendrites (*arrow*) and axonal torpedoes (*), can be observed. *Scale bars*, 50 μm. *E–H*, 3- and 7-month-old cyclodextrin (*CD*) treated *nym* mice perform the same as PBS and untreated *nym* mice on the inverted screen (3 months (*E*) and 7 months (*G*)) and rotarod (3 months (*F*) and 7 months (*H*)). Values are expressed as mean ± S.E. (*error bars*) ($n = 8$). +/+, wild-type mice.

codons. The *nym* mutation Y867X leads to the production of a slightly truncated α-subunit retaining 95% of the wild-type equivalent and a complete lack of β-subunit, and the knock-in mutation G1028X carries a complete α- and a truncated β-subunit (Fig. 1*B*). Both mutations lead to a loss of the C terminus of the β-subunit that contains a transmembrane domain and ER exit motif (R/K)*X*(R/K). Without the ER exit motif, the protein will reside in the ER and not locate to the Golgi (Fig. 1*D*). This will ultimately lead to a non-functional Gnpta protein because the assembly of α- and β-subunit will not occur because the cleavage of the precursor protein occurs at the Golgi (15), to which the mutant protein will not locate.

Both mutants show several biochemical and clinical features of the disease MLII, including skeletal abnormalities and facial dysmorphisms. A phenotypic comparison of the different MLII mouse models is summarized in Table 3. The *nym* spine presents with a thoracic curve in contrast to the wild-type and the knock-in (Table 3) (44). This might be because the knock-in was analyzed at 4 weeks in comparison with 12 months for the *nym* mouse, in which the phenotype might have progressed. Both mice present with reduced life span; however, the *nym* mouse presents with a survival of ~30% at 60 weeks, whereas the knock-in presents with a 2% survival chance at 60 weeks. We are uncertain about the reason, but it might be because of difference in background strain, husbandry effects, or *n*-numbers. Only 33 *nym* mice were analyzed in terms of survival in comparison with 160 animals for the knock-in (43).

The neurodegenerative phenotype is very similar between the knock-in and the *nym* mouse, both presenting with cerebellar pathology, including progressive Purkinje cell loss, demyelination, inflammation. Due to the lysosomal enzymes not being localized to the lysosomes correctly, these are unable to break

TABLE 3
Comparison of the *nym* mouse with *Gnptab* knock-in and knock-out mouse

MLII model	Murine *nym* mutant	Murine knock-out	Murine knock-in
Mutation	Patient mutation (c.2664C>G) in mouse: c.2601T>A leading to a truncation mutation	*Gnptab* Gene TRAP mouse (22)	Patient mutation (c.3145insC) leading to a protein truncation G1028X (43)
Phenotype	Reduced life span	Normal life span	Reduced life span
	Growth retardation	Growth retardation	Growth retardation
	Skeletal abnormalities	No skeletal abnormalities	Skeletal abnormalities
	Craniofacial defects	No craniofacial defects	Craniofacial defects
	Ataxic gait and reduced muscle strength and motor coordination analyzed by catwalk, rotarod, and inverted screen	No report of ataxic gate	Presented with ataxic gait
	Mental retardation shown by the spontaneous alternation task	No report of behavioral dullness	No report of behavioral dullness
	Inclusion bodies present in fibroblasts	Inclusion bodies present in secretory organs (pancreas) and connective tissue (cartilage)	Inclusion bodies present in fibroblasts
	Not analyzed	Retinal impairments	Retinal impairments

down waste material, and storage of gangliosides and cholesterol occurs in a variety of different brain regions. These have not been reported for the knock-out. Also, the *Gnptab* knock-out mouse does not display all of the clinical features and symptoms of MLII patients that are seen in the cat MLII model, knock-in, and *nym* mice (Table 3) (22, 23). The *Gnptab* knock-out mice have normal presentation of liver, brain, and muscle tissue. However, immunohistochemical analysis of brain sections revealed the presence of age-dependent lesions and reactive microgliosis, and they presented with hind limb-clasping at 4–6 months of age (43). Hence, the *Gnptab* knock-out brain represents a less severe course of disease than observed in *nym* or knock-in mice. Lysosomal enzyme activities in serum show very similar trends in *nym* and knock-in mice but also in the knock-out mouse despite the difference in phenotype. Therefore, missorting of lysosomal enzymes is most probably not causing the difference in phenotype but potentially the residual protein of Gnpta in knock-in and *nym* mice that exerts a potential toxic gain of function. Our results highlight the value of clinically relevant point mutants compared with null models because the null does not present with patient relevant pathology of reduced life span, neurodegeneration, and skeletal and facial abnormalities (Table 3).

Psychomotor retardation is a common pathology in MLII patients; however, neurodegeneration has so far not been reported in MLII patients, except for minimal signs of neuronal and glial involvement (45). Patients die in their first decade of life, in which we would expect Purkinje cell death and early markers of neurodegeneration (*e.g.* inflammation, neuronal torpedoes, and swelling of Purkinje cell axons with formation of spheroids in the granular layer) to be present. No investigations have been conducted so far in MLII patients, but the early markers might be cause for psychomotor retardation and should be investigated further.

A well established link between cerebellar pathology and motor dysfunction has already been made (46) and is supported by many cerebellar mutant mice that have ataxic phenotypes, namely *Lurcher*, *hot-foot*, and *staggerer* (47). In the past decade, the cerebellum has also emerged as an important brain region for the control of higher cognitive functions (48). Connections run from the prefrontal cortex to the cerebellum that confirm involvement in cognitive networks (49). Indeed, reports of cerebellar ataxia and psychomotor retardation segregate in many studies, such as in Cayman cerebellar ataxia (50), isolated cerebellar hypoplasia (51), and lysosomal storage disorders, such as Niemann-Pick type C disease (52). The spontaneous alternation task, which we conducted on the *nym* mice, is a measure of working or short term memory (35), and the hippocampus and the frontal cortex have been argued to be important for these functions (36). Microglial activation was observed in the knock-in mouse in all brain regions. The strongest intensity was observed in the cerebellum, cerebral cortex, hippocampus, and thalamus (43). This could explain why the *nym* mouse underperformed in the spontaneous alternation task. This is the first behavioral observation that these mice not only have motor slowness assessed by rotarod, catwalk, and inverted screen but also cognitive slowness challenged in the alternation task. Behavioral dullness is a hallmark of the human pathology and has been observed in the feline model of MLII but so far has been observed in no other mouse model, which supports the *nym* mouse being a human disease-relevant model (12, 18). Further research will be necessary to confirm the exact brain region of dysfunction via measuring electrical activity in different brain regions to observe abnormalities in long term potentiation, which is known to be involved in memory formation (53).

Targeting efficiency of lysosomal enzymes is cell type- and tissue-specific in human and disease models of MLII (8, 54–56). Storage of glycolipids was observed in certain cell types of the *nym* brain. The M6P pathway is important in targeting the majority of lysosomal hydrolases to the lysosome, so high levels of storage would be anticipated. However, the storage of glycolipids and the pathology in general is not as severe as in single enzyme deficiency models, such as Sandhoff disease, in which greater glycolipid storage is observed and the mice have a greatly attenuated life span (57, 58). This highlights the importance of alternative pathways that can deliver lysosomal hydrolases to the lysosomes and need to be further studied, which is in agreement with the observations of Braulke and co-workers (8, 43). Here, we showed that the loss of mannose 6-phosphate residues in *nym* mice led to a loss of the Npc2 protein that is involved in the lysosomal export of cholesterol and sphingolipids in the *nym* brain. Due to the missorting of Npc2, we conducted a drug trial over 7 months, the age when we observe Purkinje cell death, with 2-hydroxypropyl-β-cyclodextrin. This drug has shown to increase the life span and delay

Purkinje cell loss in Npc2 knock-out mice (41). However, this treatment did not delay Purkinje cell loss or motor impairment, suggesting that the reduced levels of lysosomal Npc2 in MLII is not the primary mechanism that triggers Purkinje cell degeneration. Taken together, our findings in this novel mouse model of MLII suggest that it will be a useful system to better understand pathogenic mechanisms and evaluate modifying therapies of disease.

REFERENCES

1. Leroy, J. G., and Spranger, J. W. (1970) I-cell disease. *N. Engl. J. Med.* **283,** 598–599
2. Leroy, J. G., and Demars, R. I. (1967) Mutant enzymatic and cytological phenotypes in cultured human fibroblasts. *Science* **157,** 804–806
3. Spranger, J. W., and Wiedemann, H. R. (1970) The genetic mucolipidoses. Diagnosis and differential diagnosis. *Humangenetik* **9,** 113–139
4. Cox, T. M., and Cachón-González, M. B. (2012) The cellular pathology of lysosomal diseases. *J. Pathol.* **226,** 241–254
5. Hickman, S., and Neufeld, E. F. (1972) A hypothesis for I-cell disease: defective hydrolases that do not enter lysosomes. *Biochem. Biophys. Res. Commun.* **49,** 992–999
6. Kaplan, A., Fischer, D., Achord, D., and Sly, W. (1977) Phosphohexosyl recognition is a general characteristic of pinocytosis of lysosomal glycosidases by human fibroblasts. *J. Clin. Invest.* **60,** 1088–1093
7. Sleat, D. E., Zheng, H., Qian, M., and Lobel, P. (2006) Identification of sites of mannose 6-phosphorylation on lysosomal proteins. *Mol. Cell Proteomics* **5,** 686–701
8. Braulke, T., and Bonifacino, J. S. (2009) Sorting of lysosomal proteins. *Biochim. Biophys. Acta* **1793,** 605–614
9. Lubke, T., Lobel, P., and Sleat, D. E. (2009) Proteomics of the lysosome. *Biochim. Biophys. Acta* **4,** 625–635
10. Tiede, S., Muschol, N., Reutter, G., Cantz, M., Ullrich, K., and Braulke, T. (2005) Missense mutations in *N*-acetylglucosamine-1-phosphotransferase α/β subunit gene in a patient with mucolipidosis III and a mild clinical phenotype. *Am. J. Med. Genet. A* **137A,** 235–240
11. Kudo, M., and Canfield, W. M. (2006) Structural requirements for efficient processing and activation of recombinant human UDP-*N*-acetylglucosamine:lysosomal-enzyme-*N*-acetylglucosamine-1-phosphotransferase. *J. Biol. Chem.* **281,** 11761–11768
12. Cathey, S. S., Leroy, J. G., Wood, T., Eaves, K., Simensen, R. J., Kudo, M., Stevenson, R. E., and Friez, M. J. (2010) Phenotype and genotype in mucolipidoses II and III α/β: a study of 61 probands. *J. Med. Genet.* **47,** 38–48
13. Kudo, M., Bao, M., D'Souza, A., Ying, F., Pan, H., Roe, B. A., and Canfield, W. M. (2005) The α- and β-subunits of the human UDP-*N*-acetylglucosamine:lysosomal enzyme *N*-acetylglucosamine-1-phosphotransferase [corrected] are encoded by a single cDNA. *J. Biol. Chem.* **280,** 36141–36149
14. Tiede, S., Storch, S., Lübke, T., Henrissat, B., Bargal, R., Raas-Rothschild, A., and Braulke, T. (2005) Mucolipidosis II is caused by mutations in GNPTA encoding the α/β GlcNAc-1-phosphotransferase. *Nat. Med.* **11,** 1109–1112
15. Marschner, K., Kollmann, K., Schweizer, M., Braulke, T., and Pohl, S. (2011) A key enzyme in the biogenesis of lysosomes is a protease that regulates cholesterol metabolism. *Science* **333,** 87–90
16. Raas-Rothschild, A., Cormier-Daire, V., Bao, M., Genin, E., Salomon, R., Brewer, K., Zeigler, M., Mandel, H., Toth, S., Roe, B., Munnich, A., and Canfield, W. M. (2000) Molecular basis of variant pseudo-hurler polydystrophy (mucolipidosis IIIC). *J. Clin. Invest.* **105,** 673–681
17. Wiesmann, U., Vassella, F., and Herschkowitz, N. (1971) "I-cell" disease: leakage of lysosomal enzymes into extracellular fluids. *N. Engl. J. Med.* **285,** 1090–1091
18. Mazrier, H., Van Hoeven, M., Wang, P., Knox, V. W., Aguirre, G. D., Holt, E., Wiemelt, S. P., Sleeper, M. M., Hubler, M., Haskins, M. E., and Giger, U. (2003) Inheritance, biochemical abnormalities, and clinical features of feline mucolipidosis II: the first animal model of human I-cell disease. *J. Hered.* **94,** 363–373
19. Bosshard, N. U., Hubler, M., Arnold, S., Briner, J., Spycher, M. A., Sommerlade, H. J., von Figura, K., and Gitzelmann, R. (1996) Spontaneous mucolipidosis in a cat: an animal model of human I-cell disease. *Vet. Pathol.* **33,** 1–13
20. Flanagan-Steet, H., Sias, C., and Steet, R. (2009) Altered chondrocyte differentiation and extracellular matrix homeostasis in a zebrafish model for mucolipidosis II. *Am. J. Pathol.* **175,** 2063–2075
21. Petrey, A. C., Flanagan-Steet, H., Johnson, S., Fan, X., De la Rosa, M., Haskins, M. E., Nairn, A. V., Moremen, K. W., and Steet, R. (2012) Excessive activity of cathepsin K is associated with cartilage defects in a zebrafish model of mucolipidosis II. *Dis. Model Mech.* **5,** 177–190
22. Gelfman, C. M., Vogel, P., Issa, T. M., Turner, C. A., Lee, W. S., Kornfeld, S., and Rice, D. S. (2007) Mice lacking α/β subunits of GlcNAc-1-phosphotransferase exhibit growth retardation, retinal degeneration, and secretory cell lesions. *Invest. Ophthalmol. Vis. Sci.* **48,** 5221–5228
23. Vogel, P., Payne, B. J., Read, R., Lee, W. S., Gelfman, C. M., and Kornfeld, S. (2009) Comparative pathology of murine mucolipidosis types II and IIIC. *Vet. Pathol.* **46,** 313–324
24. Deleted in proof
25. Barkus, C., Dawson, L. A., Sharp, T., and Bannerman, D. M. (2012) GluN1 hypomorph mice exhibit wide-ranging behavioral alterations. *Genes Brain Behav.* **11,** 342–351
26. Hamers, F. P., Lankhorst, A. J., van Laar, T. J., Veldhuis, W. B., and Gispen, W. H. (2001) Automated quantitative gait analysis during overground locomotion in the rat: its application to spinal cord contusion and transection injuries. *J. Neurotrauma* **18,** 187–201
27. Hamers, F. P., Koopmans, G. C., and Joosten, E. A. (2006) CatWalk-assisted gait analysis in the assessment of spinal cord injury. *J. Neurotrauma* **23,** 537–548
28. Bonifacino, J. S., and Glick, B. S. (2004) The mechanisms of vesicle budding and fusion. *Cell* **116,** 153–166
29. Nufer, O., Guldbrandsen, S., Degen, M., Kappeler, F., Paccaud, J. P., Tani, K., and Hauri, H. P. (2002) Role of cytoplasmic C-terminal amino acids of membrane proteins in ER export. *J. Cell Sci.* **115,** 619–628
30. De Pace, R., Coutinho, M. F., Koch-Nolte, F., Haag, F., Prata, M. J., Alves, S., Braulke, T., and Pohl, S. (2014) Mucolipidosis II-related mutations inhibit the exit from the endoplasmic reticulum and proteolytic cleavage of GlcNAc-1-phosphotransferase precursor protein (GNPTAB). *Hum. Mutat.* **35,** 368–376
31. Kornfeld, S., and Sly, W. S. (2001) I-cell Disease and Pseudo-Hurler Polydystrophy: Disorders of Lysosomal Enzyme Phosphorylation and Localization, *Online Metab. Mol. Bases Inherit. Dis.* 10.1036/ommbid.167
32. Otomo, T., Yamamoto, T., Fujikawa, Y., Shimotsuji, T., and Ozono, K. (2011) Elevated bone turnover in an infantile patient with mucolipidosis II: no association with hyperparathyroidism. *Clin. Pediatr. Endocrinol.* **20,** 7–12
33. Guyenet, S. J., Furrer, S. A., Damian, V. M., Baughan, T. D., La Spada, A. R., and Garden, G. A. (2010) A simple composite phenotype scoring system for evaluating mouse models of cerebellar ataxia. *J. Vis. Exp.* 10.3791/1787
34. Fernagut, P. O., Diguet, E., Bioulac, B., and Tison, F. (2004) MPTP potentiates 3-nitropropionic acid-induced striatal damage in mice: reference to striatonigral degeneration. *Exp. Neurol.* **185,** 47–62
35. Sanderson, D. J., and Bannerman, D. M. (2012) The role of habituation in hippocampus-dependent spatial working memory tasks: evidence from GluA1 AMPA receptor subunit knockout mice. *Hippocampus* **22,** 981–994
36. Goldman-Rakic, P. S. (1987) Circuitry of the frontal association cortex and its relevance to dementia. *Arch. Gerontol. Geriatr.* **6,** 299–309
37. Gondré-Lewis, M. C., McGlynn, R., and Walkley, S. U. (2013) Cholesterol Accumulation in NPC1-deficient neurons is ganglioside dependent. *Curr. Biol.* **13,** 1324–1329
38. Goodman, L. A., Livingston, P. O., and Walkley, S. U. (1991) Ectopic dendrites occur only on cortical pyramidal cells containing elevated GM2 ganglioside in α-mannosidosis. *Proc. Natl. Acad. Sci. U.S.A.* **88,** 11330–11334
39. Higashi, Y., Murayama, S., Pentchev, P. G., and Suzuki, K. (1993) Cerebellar degeneration in the Niemann-Pick type C mouse. *Acta Neuropathol.* **85,** 175–184
40. Tanaka, J., Nakamura, H., and Miyawaki, S. (1988) Cerebellar involvement

in murine sphingomyelinosis: a new model of Niemann-Pick disease. *J. Neuropathol. Exp. Neurol.* **47,** 291–300
41. Davidson, C. D., Ali, N. F., Micsenyi, M. C., Stephney, G., Renault, S., Dobrenis, K., Ory, D. S., Vanier, M. T., and Walkley, S. U. (2009) Chronic cyclodextrin treatment of murine Niemann-Pick C disease ameliorates neuronal cholesterol and glycosphingolipid storage and disease progression. *PLoS One* **4,** e6951
42. Ottinger, E. A., Kao, M. L., Carrillo-Carrasco, N., Yanjanin, N., Shankar, R. K., Janssen, M., Brewster, M., Scott, I., Xu, X., Cradock, J., Terse, P., Dehdashti, S. J., Marugan, J., Zheng, W., Portilla, L., Hubbs, A., Pavan, W. J., Heiss, J., H Vite, C., Walkley, S. U., Ory, D. S., Silber, S. A., Porter, F. D., Austin, C. P., and McKew, J. C. (2014) Collaborative development of 2-hydroxypropyl-β-cyclodextrin for the treatment of Niemann-Pick type C1 disease. *Curr. Top. Med. Chem.* **14,** 330–339
43. Kollmann, K., Damme, M., Markmann, S., Morelle, W., Schweizer, M., Hermans-Borgmeyer, I., Röchert, A. K., Pohl, S., Lübke, T., Michalski, J. C., Käkelä, R., Walkley, S. U., and Braulke, T. (2012) Lysosomal dysfunction causes neurodegeneration in mucolipidosis II "knock-in" mice. *Brain* **135,** 2661–2675
44. Kollmann, K., Pestka, J. M., Kühn, S. C., Schöne, E., Schweizer, M., Karkmann, K., Otomo, T., Catala-Lehnen, P., Failla, A. V., Marshall, R. P., Krause, M., Santer, R., Amling, M., Braulke, T., and Schinke, T. (2013) Decreased bone formation and increased osteoclastogenesis cause bone loss in mucolipidosis II. *EMBO Mol. Med.* **5,** 1871–1886
45. Martin, J. J., Leroy, J. G., Farriaux, J. P., Fontaine, G., Desnick, R. J., and Cabello, A. (1975) I-cell disease (mucolipidosis II): a report on its pathology. *Acta Neuropathol.* **33,** 285–305
46. Ito, M. (2000) Mechanisms of motor learning in the cerebellum. *Brain Res.* **886,** 237–245
47. Lalonde, R., and Strazielle, C. (2001) Motor performance and regional brain metabolism of spontaneous murine mutations with cerebellar atrophy. *Behav. Brain Res.* **125,** 103–108
48. Schmahmann, J. D. (1991) An emerging concept. The cerebellar contribution to higher function. *Arch. Neurol.* **48,** 1178–1187
49. Schmahmann, J. D., and Pandya, D. N. (1997) Anatomic organization of the basilar pontine projections from prefrontal cortices in rhesus monkey. *J. Neurosci.* **17,** 438–458
50. Nystuen, A., Benke, P. J., Merren, J., Stone, E. M., and Sheffield, V. C. (1996) A cerebellar ataxia locus identified by DNA pooling to search for linkage disequilibrium in an isolated population from the Cayman Islands. *Hum. Mol. Genet.* **5,** 525–531
51. Ventura, P., Presicci, A., Perniola, T., Campa, M. G., and Margari, L. (2006) Mental retardation and epilepsy in patients with isolated cerebellar hypoplasia. *J. Child Neurol.* **21,** 776–781
52. Turpin, J. C., Masson, M., and Baumann, N. (1991) Clinical aspects of Niemann-Pick type C disease in the adult. *Dev. Neurosci.* **13,** 304–306
53. Matynia, A., Kushner, S. A., and Silva, A. J. (2002) Genetic approaches to molecular and cellular cognition: a focus on LTP and learning and memory. *Annu. Rev. Genet.* **36,** 687–720
54. Owada, M., and Neufeld, E. F. (1982) Is there a mechanism for introducing acid hydrolases into liver lysosomes that is independent of mannose 6-phosphate recognition? evidence from I-cell disease. *Biochem. Biophys. Res. Commun.* **105,** 814–820
55. Boonen, M., van Meel, E., Oorschot, V., Klumperman, J., and Kornfeld, S. (2011) Vacuolization of mucolipidosis type II mouse exocrine gland cells represents accumulation of autolysosomes. *Mol. Biol. Cell* **22,** 1135–1147
56. Waheed, A., Pohlmann, R., Hasilik, A., von Figura, K., van Elsen, A., and Leroy, J. G. (1982) Deficiency of UDP-*N*-acetylglucosamine: lysosomal enzyme *N*-acetylglucosamine-1-phosphotransferase in organs of I-cell patients. *Biochem. Biophys. Res. Commun.* **105,** 1052–1058
57. Jeyakumar, M., Butters, T. D., Cortina-Borja, M., Hunnam, V., Proia, R. L., Perry, V. H., Dwek, R. A., and Platt, F. M. (1999) Delayed symptom onset and increased life expectancy in Sandhoff disease mice treated with *N*-butyldeoxynojirimycin. *Proc. Natl. Acad. Sci.* **96,** 6388–6393
58. Jeyakumar, M., Thomas, R., Elliot-Smith, E., Smith, D. A., van der Spoel, A. C., d'Azzo, A., Perry, V. H., Butters, T. D., Dwek, R. A., and Platt, F. M. (2003) Central nervous system inflammation is a hallmark of pathogenesis in mouse models of GM1 and GM2 gangliosidosis. *Brain* **126,** 974–987
59. Qian, Y., Flanagan-Steet, H., van Meel, E., Steet, R., and Kornfeld, S. A. (2013) The DMAP interaction domain of UDP-GlcNAc:lysosomal enzyme *N*-acetylglucosamine-1-phosphotransferase is a substrate recognition module. *Proc. Natl. Acad. Sci. U.S.A.* **110,** 10246–10251

Molecular Bases of Disease:

A Novel Mouse Model of a Patient Mucolipidosis II Mutation Recapitulates Disease Pathology

Leigh Paton, Emmanuelle Bitoun, Janet Kenyon, David A. Priestman, Peter L. Oliver, Benjamin Edwards, Frances M. Platt and Kay E. Davies

J. Biol. Chem. 2014, 289:26709-26721.
doi: 10.1074/jbc.M114.586156 originally published online August 8, 2014